LIQUID CRYSTALLINE HYDROGEN-BONDED ROSETTES

This research has been financially supported by Council for Chemical Sciences of the Netherlands organization for Scientific Research (CW-NOW), in the Young Chemist programme (grant number 70098305). The research was carried out at the Supramolecular Chemistry and Technology group (SMCT), MESA$^+$ Institute for Nanotechnology, University of Twente.

Publisher: Wöhrmann Print Service, Zutphen, The Netherlands

Cover design by Mirko Faccini and Alessio Piermattei. Cover pictures: Polarized optical image of a double rosette assembly cooling down from the isotropic phase.

Liquid Crystalline Hydrogen-Bonded Rosettes, Ph.D. thesis, University of Twente, Enschede, The Netherlands
ISBN 978-90-365-2496-4

LIQUID CRYSTALLINE HYDROEGEN-BONDED ROSETTES

PROEFSCHRIFT

ter verkrijging van
de graad van doctor aan de Universiteit Twente,
op gezag van de rector magnificus,
prof.dr. W. H. M. Zijm,
volgens besluit van het College voor Promoties
in het openbaar te verdedigen
op donderdag 3 Mei 2007 om 13.15 uur

door

Alessio Piermattei

Geboren op 5 November 1974
te Roma, Italië

Dit proefschrift is goedgekeurd door:

Promotor:	Prof.dr.ir. D. N. Reinhoudt
Assistent Promotor:	Dr. Mercedes Crego Calama

A person who never made a mistake
never tried anything new.
Albert Einstein

Alla mia famiglia

Contents

Chapter 3

Induction of Liquid Crystallinity by Self Assembled Molecular Boxes

Chapter 4

Supramolecular Chirality in Mesogenic Hydrogen-Bonded Molecular Assemblies

Chapter 5

Self-Organization of Guest Molecules in Mesogenic Self-Assembled Nanocontainers

Chapter 6

Supramolecular Organization of Hydrogen-Bonded Molecular Boxes on Surfaces

Chapter 7

Noncovalent Synthesis of Tetrarosette Assemblies and their Behavior as Liquid Crystalline Materials

Chapter 1

General introduction

Supramolecular chemistry aims to develop complex chemical systems from components interacting by noncovalent intermolecular forces.[1] Through the appropriate manipulation of these forces, supramolecular chemistry has become the chemistry of molecular information. It involves the storage of information at the molecular level and their processing at the supramolecular level by molecular recognition events based on well-defined interaction patterns (hydrogen bonding arrays, sequence of donor acceptor groups, ion coordination, etc.).

Supramolecular chemistry has first focused on preorganization for the design of supramolecular receptors, which are formed by the reciprocal recognition of their molecular components via *self-assembly*.[2] One of the main advantages of using self-assembly is that the formation of the assembled structures is under thermodynamic control, allowing the error-correction of mismatched structures, often giving rise to quantitative yields of the product.[3]

Beyond preorganization lies the design of systems which undergo self-organization, i.e. systems capable of spontaneously generating well-defined, organized and functional supramolecular architectures by self-assembling their components, thus behaving as programmed systems.[4] The self-organization of functional supramolecular entities allows the design of new materials opening new perspectives towards “smart” materials, such as liquid crystals, gels, etc..[5] Supramolecular materials are by nature dynamic and may, in principle, select their constituents in response to external stimuli or

environmental factors. Supramolecular materials thus are instructed, dynamic, and combinatorial and behave as adaptive materials.[6]

In this thesis the noncovalent synthesis of assemblies based on hydrogen bonding and their material properties are described. The presented studies are focused on functional materials in particular liquid crystals which display different properties depending on the applied external conditions. The important role of hydrogen bonding in the self-assembly and self-organization of these liquid crystalline materials and the transfer of the molecular information to the macroscopic level is described.

In Chapter 2 an overview of hydrogen-bonded liquid crystalline materials is given. The concepts and the principles that have recently emerged are discussed and examples are given that illustrate the control over these systems.

Chapters 3 and 4 describe the formation of liquid crystalline phases for achiral and chiral hydrogen-bonded double rosette assemblies, after proper functionalization of the dimelamine building block. The liquid crystalline properties of these assemblies have been studied by polarized optical microscopy, differential scanning calorimetry, and X-ray diffraction.

Chapter 5 describes the complexation of small dye molecules by the chiral liquid crystalline double rosettes described in Chapter 4. The diversity in the nature of the building blocks of these mesogenic assemblies leads to different binding modes for these dye molecules, which affect the macroscopic properties of the supramolecular materials as X-ray diffraction, differential scanning calorimetry and CD spectroscopy demonstrated.

Chapter 6 describes the self-organization of the liquid crystalline double rosette assemblies on solid supports. The influence of different parameters on the self-organization process is studied by atomic force microscopy (AFM) and scanning tunneling microscopy (STM) on different solid supports such as highly pyrolytic graphite and mica.

Chapter 7 describes the noncovalent synthesis of cyanurate-based tetrarosette assemblies. The possible employment of these highly ordered structures as liquid crystalline materials after functionalization with octadecyl chains has been investigated by polarized optical microscopy and differential scanning calorimetry. Moreover, the

study of the noncovalent synthesis of cyanurate-based tetrarosette assemblies is described in which the barbiturate acts as a chaperone inhibiting and correcting the non-productive interactions between the cyanurate and the tetramelamine building blocks. The formation of enantiopure tetrarosette assemblies via amplification of the chirality and the use of chaperones was also investigated by CD spectroscopy.

References

[1] J.-M. Lehn, *Supramolecular Chemistry, Concepts and Perspectives*, VCH, Weinheim, Germany, **1995**.

[2] D. N. Reinhoudt, M. Crego-Calama, *Science* **2002**, *295*, 2403-2407.

[3] G. M. Whitesides, J. P. Mathias, C. T. Seto, *Science* **1991**, *254*, 1312-1319.

[4] J.-M. Lehn, *Angew. Chem. Int. Ed. Engl.* **1990**, *29*, 1304-1319.

[5] T. Kato, N. Mizoshita, K. Kishimoto, *Angew. Chem. Int. Ed.* **2006**, *45*, 38-68.

[6] J.-M. Lehn, *Supramolecular Science: Where It Is and Where It Is Going*, eds. Ungaro R. & Dalcanale E., Kluwer, The Netherlands, **1999**.

Chapter 2

Hydrogen-Bonded Liquid Crystals

Liquid crystals are attractive materials for their dynamic nature. For example, the fact that they can be aligned under external stimuli (e.g. a magnetic or electrical field) leads to practical applications in the optoelectronic field (e.g. display screens). Furthermore, new properties can arise from ordering the mesogenic molecules through noncovalent interactions. In particular, hydrogen bonds can be a tool in the construction and ordering of liquid crystalline materials. In this chapter the most representative examples of hydrogen-bonded liquid crystals are described. The versatility of the hydrogen bonding to obtain new structures and properties is highlighted.

2.1 Liquid Crystals

Liquid crystals (LCs) constitute a class of materials that form a unique state of matter. They are also referred to as the *fourth state of matter*, because they combine solid state properties and properties of liquid. Usually, matter is considered either fully ordered (crystalline) or fully disordered (liquid, gas, and glass). In the crystalline phases, molecules possess orientational order and three-dimensional positional order, while in the amorphous or isotropic phases the molecules lack (long-range) order. In the various liquid crystalline phases or mesophases, the molecules possess some level of orientational order, but with a much lower degree of positional order than in a crystalline solid.

The presence of a liquid crystalline phase is strongly related to the the anisometric shape of the the mesogenic molecules, i.e. either the properties of the constituent parts of the molecules vary (e.g. hydrophobic-hydrophilic or rigid-flexible parts), or their molecular axes have different lengths. This leads to two major subclasses: rod-shaped and disk-shaped molecules. From the first, predominantly nematic phases (only orientation order) and smectic (one dimensional positional order) are obtained. Disk-like molecules give liquid crystals that mainly form nematic and columnar phases (with orientational and two-dimensional positional order).

Liquid crystals are molecular materials, which combine anisotropy with dynamic nature. Their unique character can lead to the fabrication of new dynamically functional materials,[1] and led them to be employed as advanced materials for optoelectronic materials such as display devices. Liquid crystals also have close relationships to biomolecular systems. Cell membranes are constituted of amphiphilic molecules, which possess liquid-crystalline behavior.[2] The design of liquid crystals by using a variety of structures and interactions might lead to widen the applicability of mesomorphic materials.

2.1.1 Classification of mesophases

Liquid crystals can be divided into two main groups depending on how the mesophases are formed: thermotropic and lyotropic liquid crystals.[3] Lyotropic liquid crystals are generally composed of amphiphilic molecules and mesophases are obtained by adding a solvent, which is usually rather polar (e.g. water).[4,5] Upon adding solvent the system changes from crystalline to mesophase and upon further increasing of amount of solvent, it changes into an isotropic liquid. A variety of mesophases is possible in lyotropic liquid crystals depending of the amphiphile, solvent and amount of it used.[1] In contrast, thermotropic liquid crystals exhibit mesophases under specific thermal conditions. Different mesophases can be obtained depending on the shape, symmetry, and degree of long range order of the mesogenic molecules in the liquid crystalline phase (Fig. 2.1).[6]

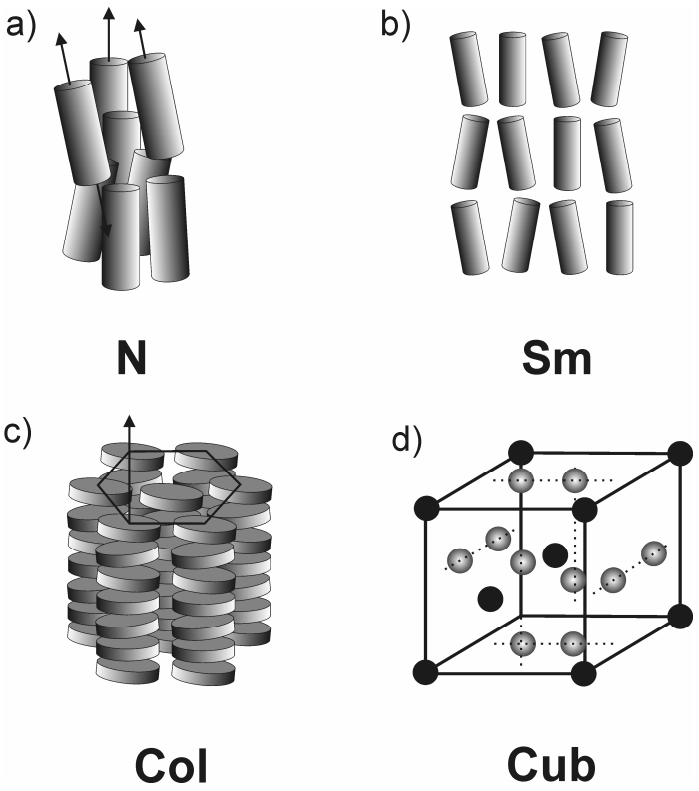

Figure 2.1. *Most common liquid crystalline phases; a) Nematic (N), b) Smectic (Sm), c) Columnar (Col), and d) Cubic (Cub).*

In the nematic phase (N) only orientational order is maintained, while any long range positional order is absent (Fig. 2.1a). The most important phases with long-range positional order are smectic (Sm), columnar (Col) and cubic (Cub) phases (Fig. 2.1). In the smectic phases, generally observed for rod-shaped mesogens, the molecules are ordered into layers (Fig. 2.1b). Depending on the organization of the mesogens into the layer, different smectic phases can be obtained.[6] On the other hand, disk-shaped molecules commonly prefer a columnar organization showing two-dimensional positional order (Fig. 2.1c). The several columnar phases are distinguished by the order within the columns and the order between the columns. Both are indicated in a subscripted suffix. The most common phases are hexagonal (Col_h) and rectangular (Col_r) columnar phases.[7,8]

2.2 Hydrogen-Bonded Liquid Crystals

The use of noncovalent interactions such as π-π interactions, Van der Waals, metal coordination, and hydrogen bonding has been widely exploited in the last years to obtain new structures in the solid state.[9-14] In particular, the use of hydrogen bonding interactions has attracted much attention because of its relevance to a variety of naturally occurring processes, such as recognition and self-assembly of complementary nucleobases that stabilize the double helix of nucleic acids. Its dynamic nature together with its stability (between 10 and 50 kJ/mol), directionality and reversibility makes hydrogen-bonding the perfect candidate for obtaining dynamic functional materials.[15-19]

Liquid crystals are functional materials which properties can be modulated also through noncovalent interactions, in particular by hydrogen bonds. The liquid crystals can be classified by hydrogen bonding according to three types *viz.* liquid crystalline molecular associates between *identical* and *different* components, and polymeric liquid crystals (Fig. 2.2).

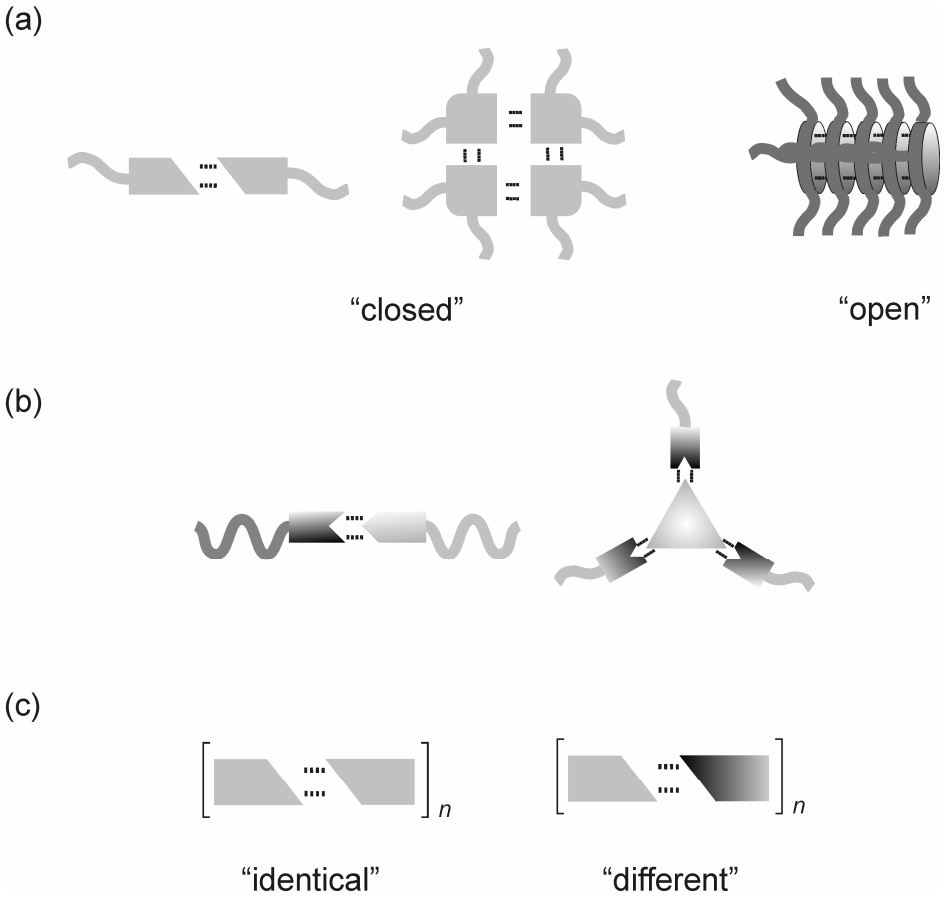

Figure 2.2. *Hydrogen-bonded liquid crystalline materials formed by (a) identical components (closed or open structure), (b) different components, and (c) polymers.*

The first type can be subdivided in hydrogen-bonded liquid crystals that can be formed by closed and well-defined structures or by open structures (ribbon, layer, etc.). Liquid crystals formed by hydrogen-bonded polymers can also be obtained by the association of *identical* and *different* components.

2.2.1 Molecular assemblies of identical molecules

2.2.1.1 Closed structures

2.2.1.1a Thermotropic liquid crystals

Thermotropic liquid crystalline materials can be prepared by the organization of closed structures obtained by hydrogen bonding. For example, pyridone forms a hydrogen-bonded dimer with a closed structure in solution (Fig. 2.3a).[20-22] Upon functionalization of a pyridone unit with dodecyl chains, the dimer **1** forms a hexagonal columnar phase (Col_h) between 88 and 108°C.[22,23] On the other hand, a phthalhydrazide derivative which forms a trimer through similar hydrogen bonding (Fig. 2.3b), shows columnar mesophases between 100 and 270°C depending on the length of the alkyl chains. The type of columnar arrangement is influenced by the length of the alkyl chains. By increasing the length of the chains, the mesophase changes from rectangular columnar mesophases for n= 6 to hexagonal columnar for n= 14.[24]

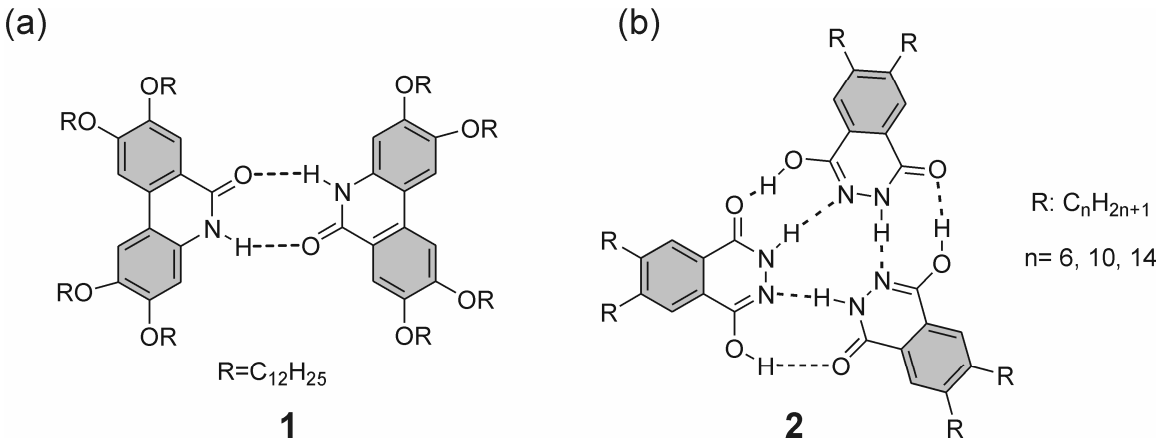

Figure 2.3. *Chemical structures of the hydrogen-bonded (a) pyridone dimer and (b) phthalhydrazide trimer.*

Kato *et al.* have widely used hydrogen bonds for the formation of liquid crystalline materials in order to obtain new functional soft materials by the self-organization of disk-like mesogens.[15,17] They showed that the oligo(glutamic) unit, which is biologically relevant, forms thermotropic hexagonal columnar liquid crystals from 26 to 89°C when it is properly functionalized. This relative low isotropization temperature is due to the

weakness of the hydrogen bonds between the amido groups of the oligo(glutamic) unit.[25]

The authors discovered that the isotropization temperature rises when folic acid, which forms a tetrameric complex in solution,[26] is attached to the oligo(glutamic) unit (compound **3**) (Fig. 2.4). The length of the alkyl chains of the oligo(glutamic) unit of **3** determines the type of mesophase: smectic for n=11 and hexagonal columnar for n=18.[27,28]

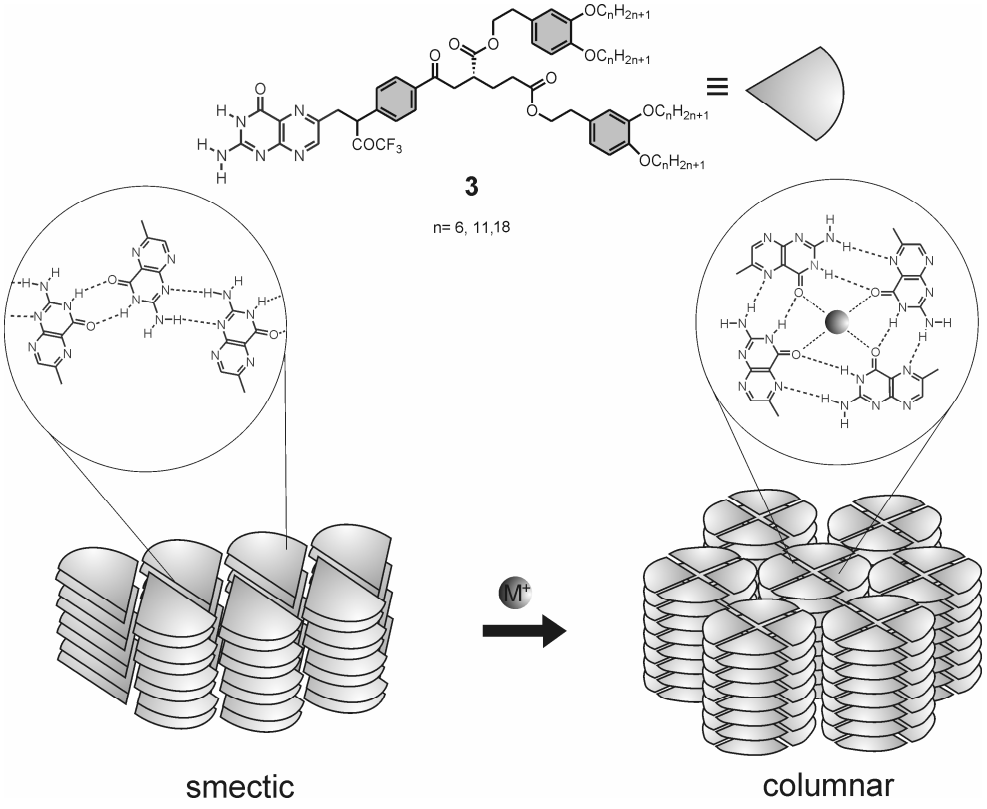

Figure 2.4. *Chemical structure of compound **3**. The presence of an metal ion induces a change in the hydrogen-bonding pattern, as a result of which the ribbon structure changes to a disk structure.*

Due to the noncovalent nature of the hydrogen bonds, the type of organization of **3** in the mesophase can be modulated. The addition of a metal ion induces a change in the hydrogen bonding motif of the folic acid unit, and the mesophase goes from a smectic (phase) to a columnar phase.[27] When a more stable hydrogen-bonded motif is used, as in

the guanine-cytosine DNA base pair, the integrity of the disk-like building blocks is retained.[29]

Percec *et al.* have extensively investigated the formation of thermotropic liquid crystals through the self-assembly of dendritic molecules such as **5** and **6** (Fig. 2.5).[30-36] The apex of the dendrons has different functionalities, such as carboxylic acids or esters, that have the ability to from hydrogen bonds. The rational variations in the number of substituents and the geometry of the functional groups has led to different mesophases in a broad temperature range, going from columnar phases to cubic to micelles (Fig. 2.5).[37-39]

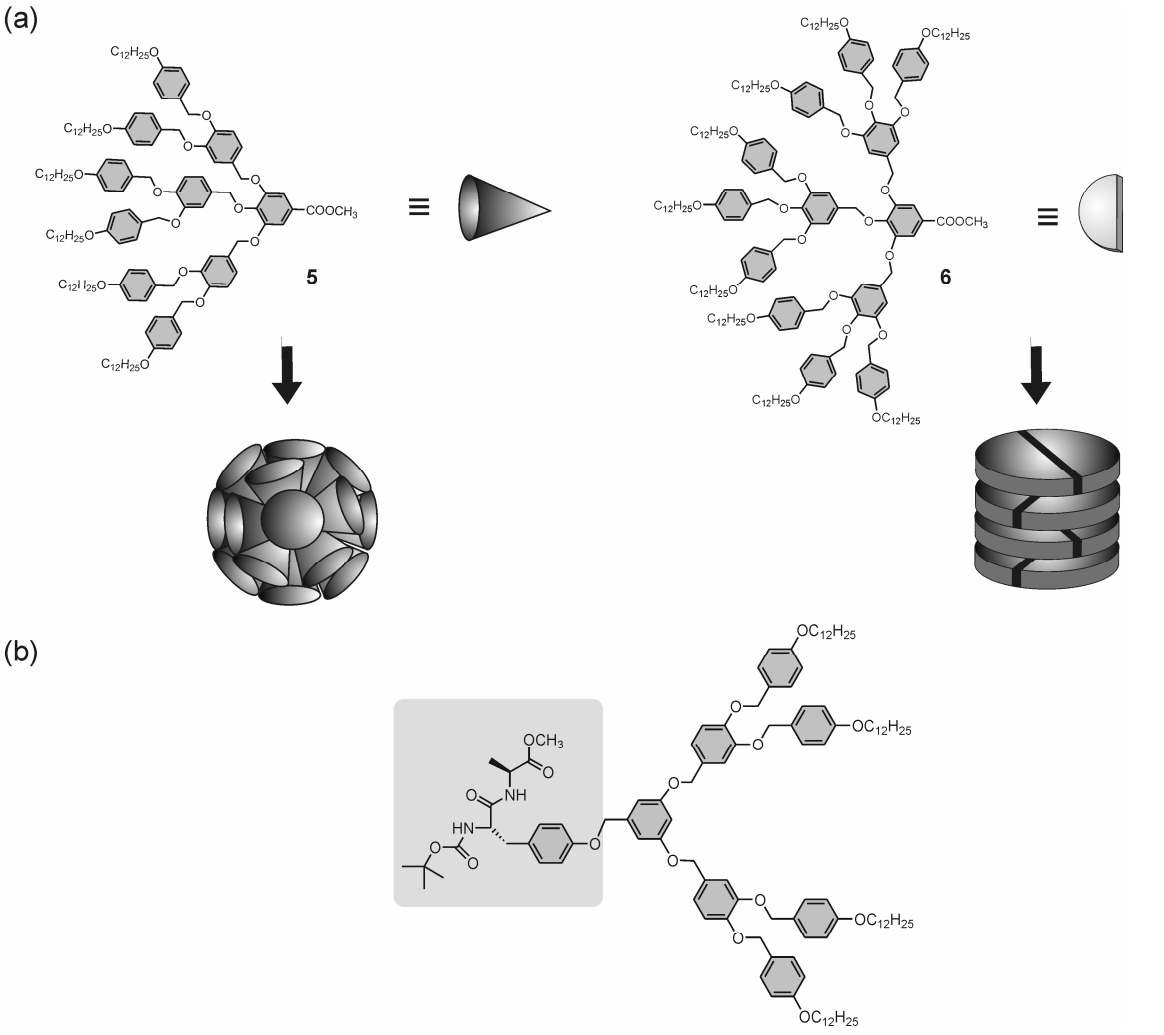

Figure 2.5. *(a) Self-assembly of monodendrons in different arrangements depending on the type of functionalization. (b) Chemical structures of the oligopeptide monodendron.*

The ability to modulate the shape of the dendrons by rational design has allowed the discovery of new organizations, which are typical for metal alloys, opening the route toward photonic bandgap arrays of soft materials.[40,41] Percec and coworkers have demonstrated that the functionalization of the dendron apex with an oligo-peptide (Fig. 2.5b) leads to the formation of pore liquid crystalline materials.[42] By increasing the length of the alkyl chains on the dendrons, the ordering of mesophases increased going from a nematic columnar phase to hexagonal phases. The principles of self-assembly of these new classes of liquid crystals have been analyzed. The stereochemistry of chiral centers and the type of protecting groups on the peptide are the two crucial parameters in the formation of pores with controlled diameter.[43] Furthermore, the modulation of the pore size has been achieved by thermal stimuli.[44] Tschierske and coworkers have used hydrogen bonds to combine incompatible parts in thermotropic liquid crystals.[45-48] Compounds **7**-**9**, which are amphiphilic mesogens having diol moieties (Fig. 2.6), showed very different self-assembly behavior. Compound **7** exhibited a stable thermotropic smectic phase, while rectangular columnar phases were induced for compounds **8** and **9**. The cooperative and dynamic networks of intermolecular hydrogen bonding between the diol groups provided sufficient cohesive energy to inhibit a complete collapse of the molecular order and support the segregation of the incompatible parts, leading to a series of novel mesophases.

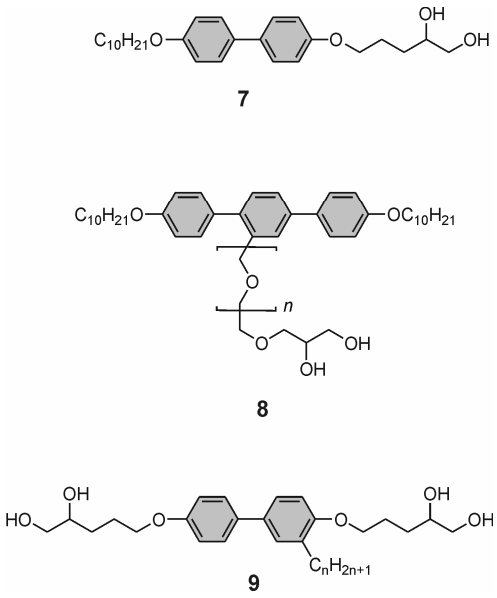

Figure 2.6. *Chemical structures of the diol derivatives **7**, **8** and **9**.*

2.2.1.1b Lyotropic liquid crystals

Biomolecule complexes, such as DNA and RNA, have shown lyotropic liquid-crystalline behavior in water. Interesting examples of biomolecules that show lyotropic liquid crystallinity by association of identical molecules are guanosine and folic acids (Fig. 2.7a).[49-51] These molecules exhibit columnar mesophases due the formation of hydrogen-bonded assemblies in water. Folic acids, in the presence of sodium ions, self-assemble in a tetramer structure that stack in columns showing hexagonal arrangements.[50]

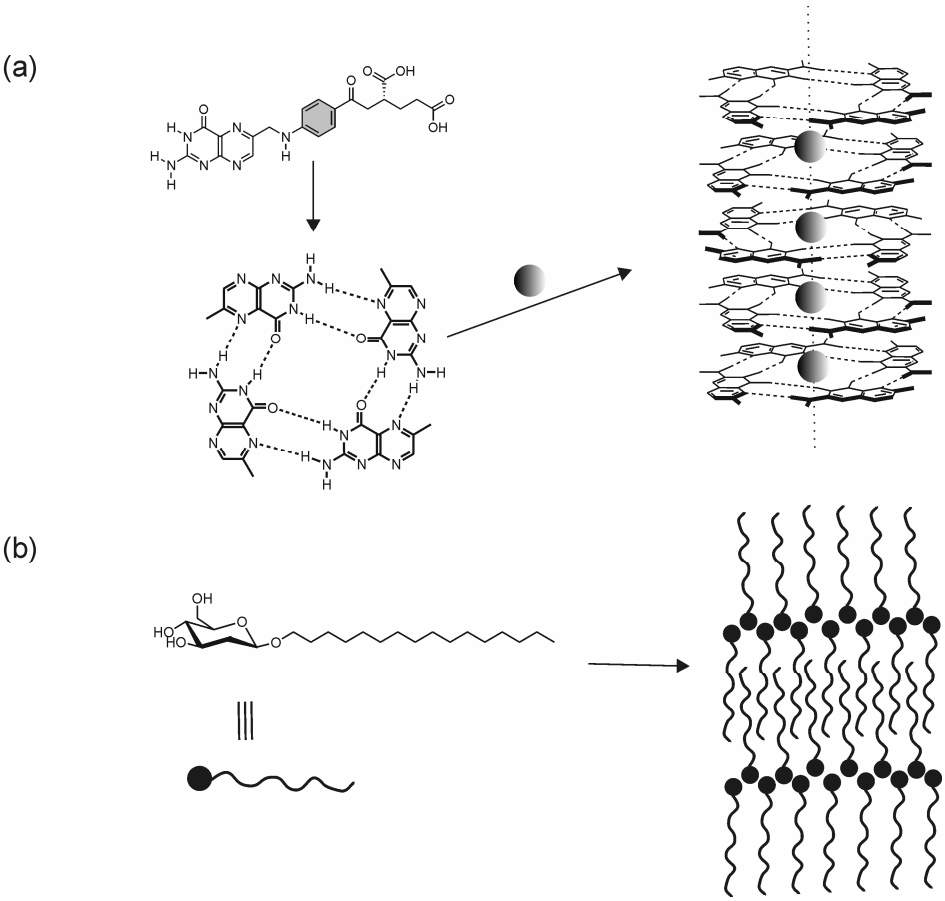

Figure 2.7. *a) Stacking of a folic acid derivatives in aqueous solution. b) Carbohydrates forming a smectic phase in aqueous solution.*

Other molecules, which have also biological importance and show lyotropic mesophases, are carbohydrates and multihydroxylated compounds (Fig. 2.7b).[4,52] Being amphiphilic molecules they present a smectic mesophase where the polar heads form a well-defined hydrogen bonding network, and the hydrophobic tails interdigitate with each other. Increasing the temperate new mesophases can be obtained as in the case of octyl-β-D-galactopyranoside, which also presented columnar and discontinuous phases.[4,52]

2.2.1.2 Open structures

Open structures forming columnar liquid crystals with nanometer order (Fig. 2.2a) have attracted attention for their possible use in optical photovoltaic devices.[53] Formation of columnar structures can be favored when amide groups are used. The

conformation of the amide bond allows stacking of molecules along the stacking direction through the formation of orthogonal hydrogen bonds. Unfortunately, for liquid crystals the number of amide-containing molecules is limited because the intermolecular hydrogen bonding chain often raises the melting temperatures and reduces the liquid crystallinity.[18] Nevertheless, a proper use of amide groups to direct the assembly of a new class of crowded aromatics has been reported.[54] The fine-tuning between steric hindrance and the number of hydrogen bonds allowed those mesogenic molecules to have a liquid crystalline phase between 47°C and 200°C.[55] When the bulkiness of the peripheral groups was increased, the liquid crystalline packing was influenced, going from hexagonal millimeter-scale domains to a distorted hexagonal lattice.

Amide groups have also been employed to stabilize the mesophases of triphenylene molecules.[56,57] The intermolecular hydrogen bonds led to a minor inter-disk distance from 3.32 to 3.18 Å, with consequently an increase of the charge carrier mobility in the triphenylene derivative.[56] Compound **10**, which was obtained by covalent attachment of three triphenylene moieties to a 1,3,5-benzenecarboxamide, gives a discotic hexagonal plastic phase with an isotropization temperature of 208°C (Fig. 2.8).

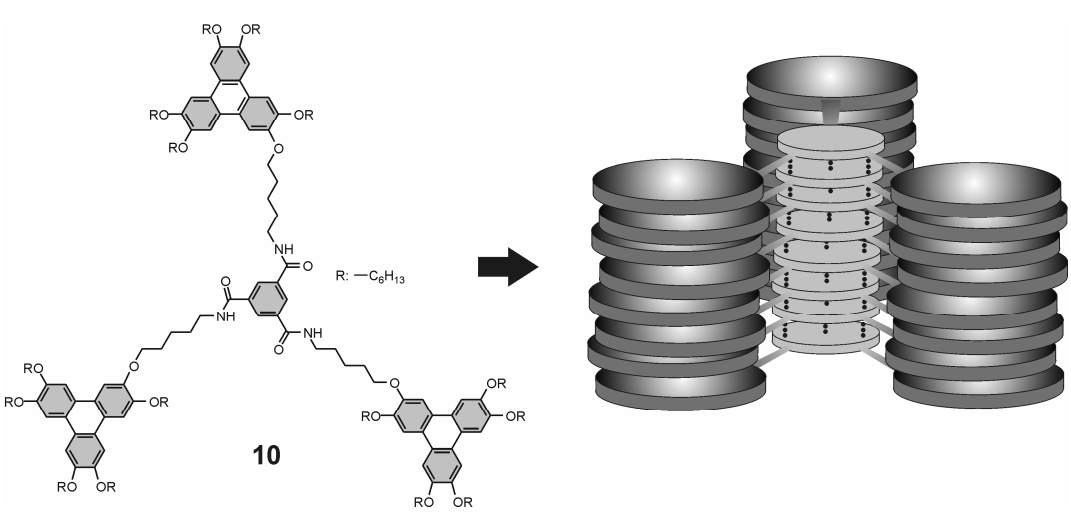

Figure 2.8. *Self-organization of compound **10** in the liquid crystalline phase through hydrogen bonding.*

The formation of hydrogen bonds and π-π interactions in **10** led to a helix-like rotation over 60° allowing a large overlap of triphenylene units with consecutive an increase of the charge carrier mobility.[57]

Meijer et al. also reported the use of 1,3,5-benzenetricarboxamide derivatives in order to promote the formation of columnar aggregates.[58] The intermolecular hydrogen bonds formed by the amide groups were used to direct the stacking, resulting in columnar aggregates with a mesophase between 158-171°C. The functionalization of the 1,3,5-benzenetricarboxamide derivatives with a photopolymerizable group allowed afterwards the manipulation of the columnar aggregates in solution.

Percec and coworkers have reported the preparation of twin-tapered dendritic benzamides **11**, which self-assemble into supramolecular columns generated by an orthogonal hydrogen-bonded dendritic benzamide unit (Fig. 2.9).[59-61] The dendritic benzamides have an unequal length of the alkyl chains. A crystalline phase was observed when the combination of short and long alkyl chains was dissimilar, while a hexagonal columnar phase was observed from 47 to 92°C when the length was the same.[59] Surprising, when the alkyl chains were partially fuorinated the twin-dendritic benzamides **12** changed the mode of self-assembly from single-layer supramolecular columns to an unprecedented bilayered pyramidal supramolecular columns (Fig 2.9). The mesophase for this new class of molecules was columnar hexagonal. The intermolecular hydrogen bonds maintained the columnar stacking, and the segregation between partially fluorinated aliphatic chains was the driving force for the formation of pyramidal columns.[59,60]

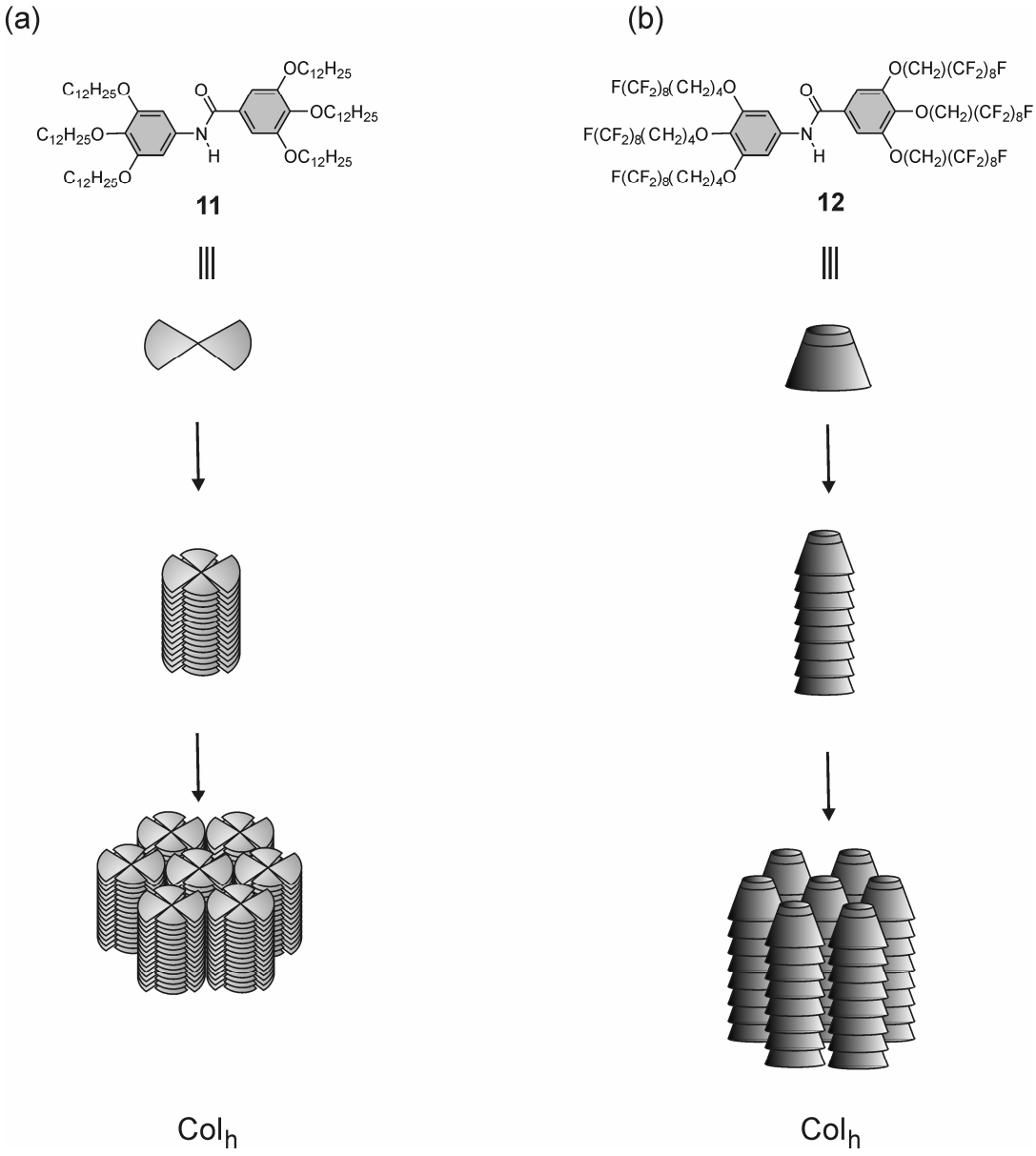

Figure 2.9. *Self-assembly of building blocks based on (a) twin dendrons* ***11*** *into cylindrical columns, (b) fluorinated twin dendrons* ***12*** *into pyramidal columns and their self-organization into hexagonal columnar lattices.*

2.2.1.3 Polymers

Liquid crystallinity in hydrogen-bonded polymers can be achieved using bifunctional monomers through the association of single or multiple hydrogen bonds.[62-67] Meijer and coworkers have reported several hydrogen-bonded polymers through the self-assembly of ureidopyrimidinone derivatives (UPy)[67] and ureidotriazines (UTr)[62] (Fig. 2.10).

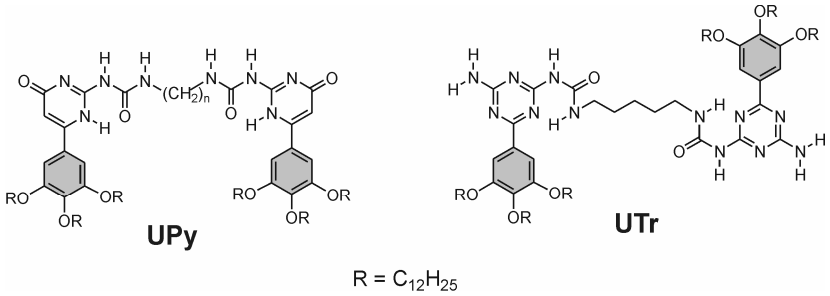

Figure 2.10. *Chemical structures of the monomers based on ureidopyrimidinone (UPy) and ureidotriazines (UTr) derivative, which are used to form hydrogen-bonded polymers.*

The UPy mesogens showed a columnar discotic mesophase where the isotropization temperature depended on the rigidity and length of the spacer between the two receptor sites. The isotropization temperature decreased from 173 to 140°Cwhen the number of carbon atoms in the alkyl spacer was increased. Using a rigid spacer such as a benzyl group increased the isotropization temperature to 247°C.[67]

2.2.2 Supramolecular assemblies consisting of different molecules

2.2.2.1 Closed structures

The first example of rod-shaped closed structures that form liquid crystals by hydrogen bonding between different molecules was reported in 1989.[68-70] The supramolecular liquid crystals obtained by the hydrogen bonding between **13** and **14** showed a mesophase up to 252°C, which is higher than the two single components (Fig. 2.11a).[69] The theory of this type of association in liquid crystalline materials has been studied by Tanaka and co-workers.[71]

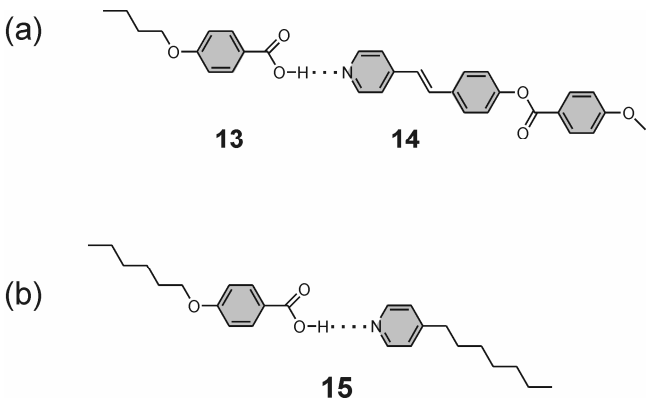

Figure 2.11. *Structure of a hydrogen-bonded mesogen between **13** and **14** (a) and an electrooptically active complex **15** (b).*

Another interesting example of a rod-shaped mesogen is the supramolecular structure **15**. This structure displayed a mesophase at room temperature (Fig. 2.11b), while the two individual building blocks do not show any mesogenic behavior. The hydrogen-bonded complex produced a nematic phase with an electro-optical respons.[72-75]

Rod-shaped mesogens formed by molecular recognition of stilbazole derivatives and ferrocene derivatives with acid functionalities have been described.[76] The delicate balance between the volume occupied by the central core and the flexible chains is responsible for the formation of different mesophases (from smectic to cubic mesophases). Hydrogen-bonded mesogens which do not have a rod shape have been prepared from a variety of components.[68,77] Double[77] and triple[68] hydrogen bonds

were utilized for the formation of those mesogenic assemblies, which have a shape in between rod-like and disk-like.

Disk-like molecules based on the 3:1 hydrogen-bonded complex between the carboxylic acid and imidazole derivatives[78,79] show hexagonal columnar mesophases from 62 to 288°C when the carboxylic acid derivatives are functionalized with long alkyl chains (Fig. 2.12).[78,79]

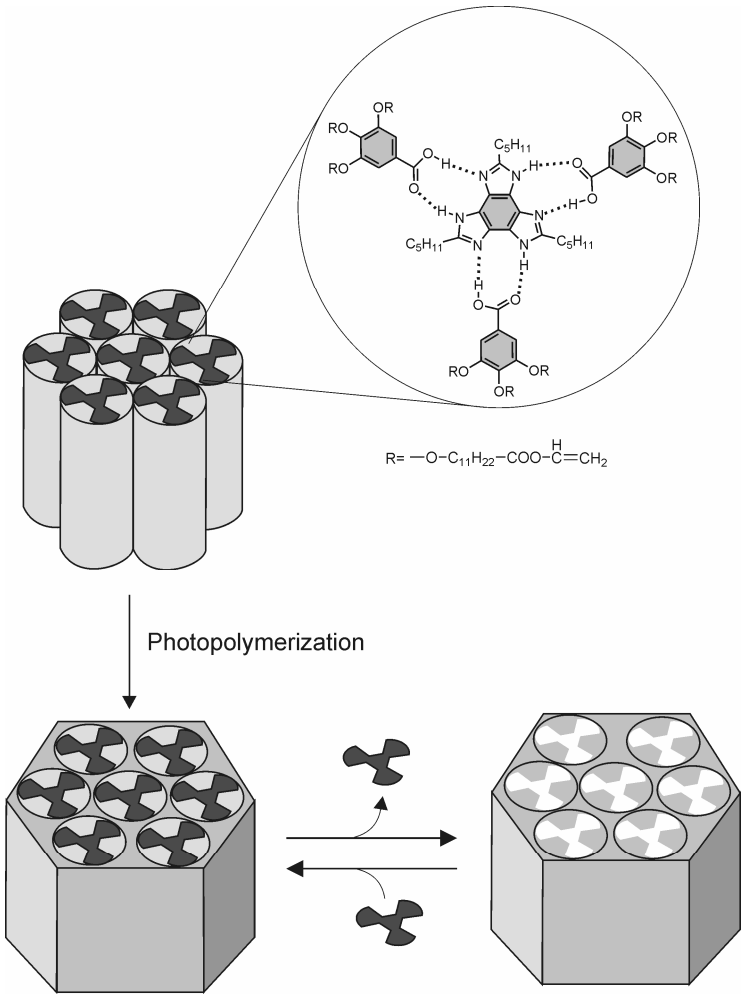

Figure 2.12. *Organic nanoporous materials obtained by using hydrogen-bonded liquid crystalline templates.*

The presence of polymerizable groups in the carboxylic acids allows the formation of ordered nanopores, which show good nitrogen gas permeability after the removal of the imidazole derivative.[78]

Mesogenic assemblies having the V-shape typical for banana mesogens have been prepared by hydrogen bonding between a stilbazole derivative and a carboxylic acid derivative.[80] The hydrogen-bonded banana mesogens showed almost the same thermal behavior of its covalent analog; a smectic polar phase between 93-119°C for the hydrogen-bonded mesogens and between 110-119°C for the covalent analog. The formation of closed structures by hydrogen bonding is not always a favorable process. For example, diazoperylene derivatives show a decrease of the isotropization temperature after complexation with different carboxylic acid derivatives because the hydrogen bonds disturbed the packing of the diazoperylene.[81]

2.2.2.1a Melamine-based mesogens

Melamine derivatives have been widely employed as building blocks for the construction of supramolecular architectures through hydrogen bonding in solution,[82-91] solid state,[92-95] and on solid supports.[96-99] Due to the versatility in forming different hydrogen bonding motifs with barbiturates and cyanuric derivatives,[82,89,100-102] they have been employed also as building blocks for the formation of mesogenic structures.[103-108] The proper functionalization of the melamine with benzyl groups bearing alkoxy chains has led to the formation of columnar liquid crystalline phases when complexed to benzoic acids.[104] The resulting arrangements of the columns in mesophases could be tuned. The complex formed a columnar hexagonal mesophase when the acid was functionalized with one alkyl chain, while a rectangular columnar mesophase was displayed when the acids bore two alkyl chains. The difference in the columnar arrangements could be attributed to an unequal distribution of the alkyl chains around the hydrogen-bonded core in the case of the difunctionalized acid. This led to an ellipsoidal shape of the complex and to a rectangular columnar mesophase. Serrano and coworkers have studied the same kind of system in order to understand how to modulate the columnar packing in hydrogen-bonded liquid crystals. They emphasized the importance of the effective space filling by a sufficient number of peripheral tails in the formation of columnar mesophases.[106] For example when the number of chains was too high, a stable hydrogen-bonded complex could not be formed and consequently no mesophase was observed. Depending on the

type of benzoic acids, the stability and the polymorphism of the liquid crystalline phase vary. For example, in the case of acids with bulky substituents the mesophase of the complex resembled more that of the acid than that of the triazine component.

Proper functionalization of the melamine unit with benzyl groups bearing alkyl chains (**16**) led to the formation of mesogenic hydrogen-bonded rosettes with the barbiturate dye **17** or cyanurate **18** (Fig.2.13a).

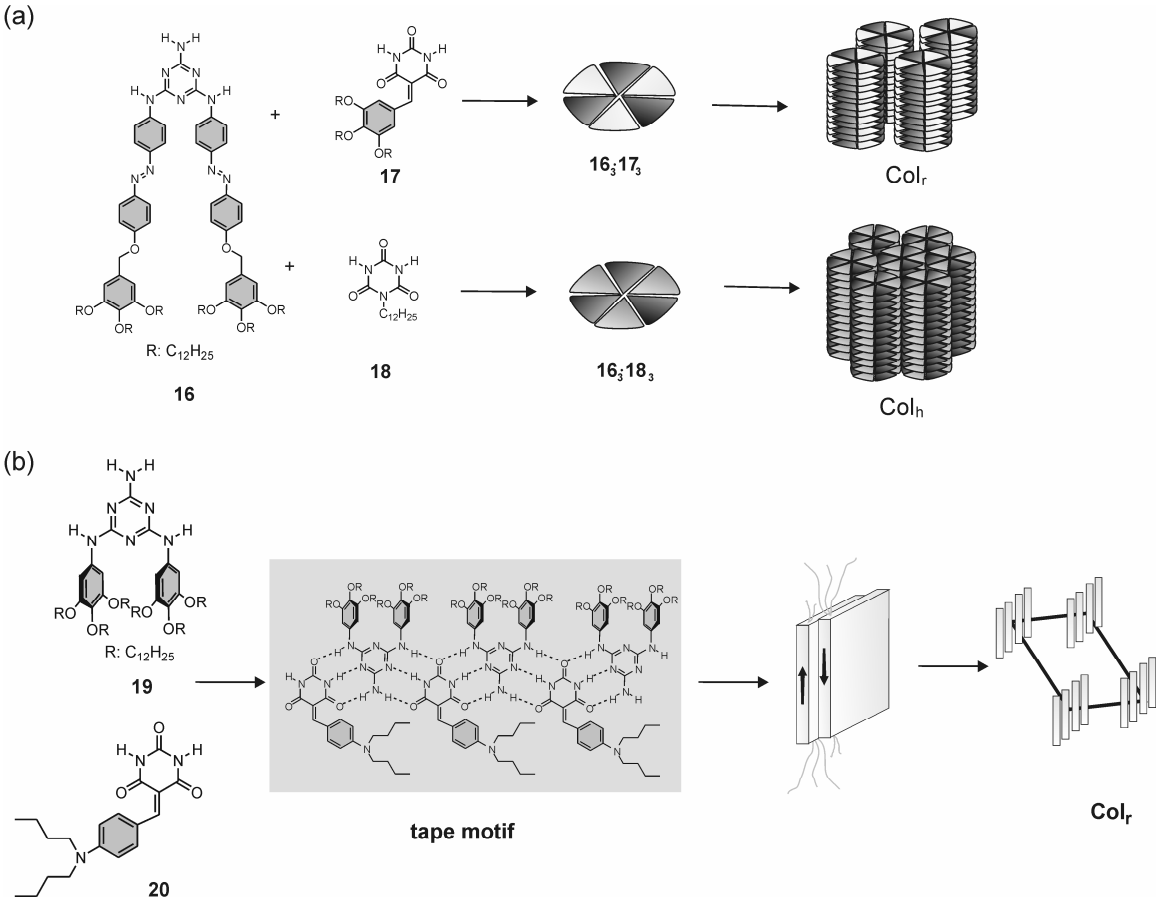

Figure 2.13. *Mesophases obtained by different hydrogen-bonded motives:(a) "rosette" and (b) "tape".*

The rosette assembly $\mathbf{16}_3$•$\mathbf{17}_3$ arranged into a rectangular columnar phase due to the bulkiness of the peripheral groups of **17**. Less steric hindrance in building block **18** led to the formation of a hexagonal columnar phase.[107] The rosette was not formed when more bulky substituents were used as in melamine **19**. The self-assembly of **19** with the barbituric dye **20** led to the formation of a tape motif, which assembles in a rectangular columnar phase (Fig. 2.13b).[108]

2.2.2.2 Polymers

Noncovalent interactions have been recognized to be versatile for the design of functional polymeric materials in building mesogenic polymers.[17,109,110] Dynamic functions, such as phase modulation, can be introduced into polymeric systems by hydrogen bonds. The first example of a mesogenic hydrogen-bonded polymer by hetero-intermolecular hydrogen bonding was reported by Kato and Fréchet in 1989.[69] Since then many types of hydrogen bonded polymers have been prepared having well-defined structures, such as main-chain,[111-117] side-chain,[69,118-124] and network structures.[125,126]

Main chain polymers show different behavior depending on the type of molecules involved in the formation of the polymer itself.[113,115,116] For example, when the length of the spacer in rod-coil copolymer **21** was increased, the mesophase in those polymers changes from cubic (n = 8, 10) to hexagonal (n = 15, 17, 21). The liquid crystallinity was completely suppressed for n = 27 (Fig. 2.14a).[115] The type of spacer between the receptor sites was critical in the formation of the liquid crystalline phase.[113,115,116] Rod-like polymers are formed by the molecular recognition between the mesogenic 5-alkoxyisophthalic acid and different diamines. The complex showed a lamellar phase only when it was formed with flexible amines such as 1,3-propyldiamine. When more rigid amines were used, liquid crystallinity was not observed.

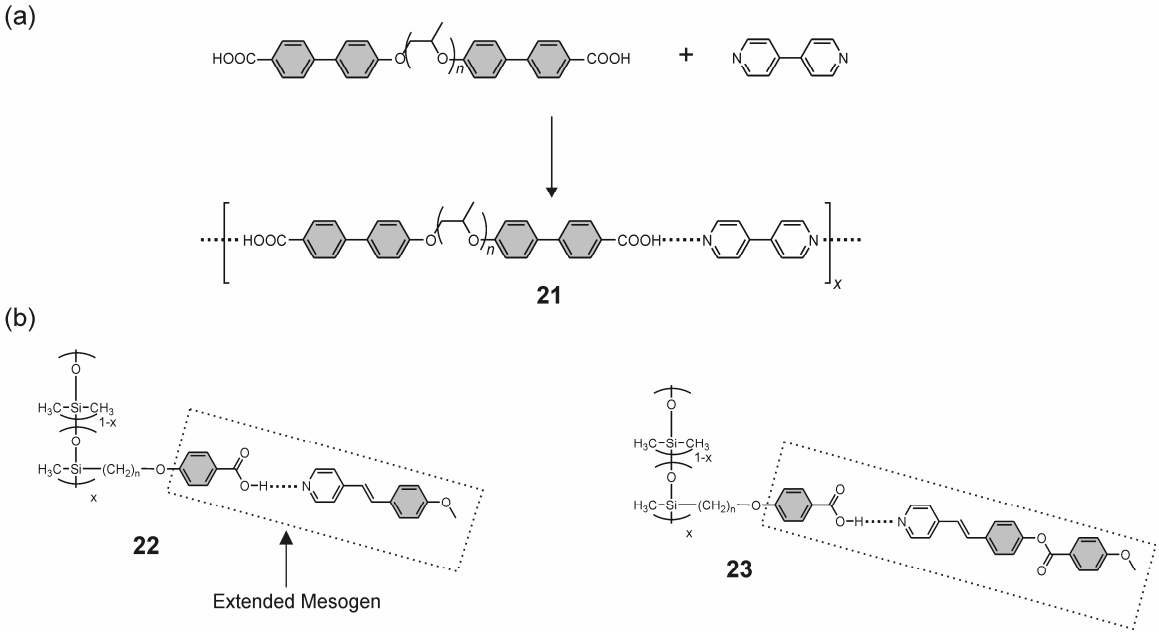

Figure 2.14. *Chemical structures of main-chain rod coil polymer* ***21*** *(a) and side chain polymers* ***22*** *and* ***23*** *(b).*

A variety of hydrogen-bonded side-chain polymers based on polyacrylate and stibazoles have been prepared, showing different types of mesophases.[69, 119, 122-124] Different smectic phases could be obtained just varying the functional group in the stibazoles derivatives (Fig. 2.14b).[124] The hydrogen-bonded polymer based on **22** showed lower isotropization temperatures than those based on **23** ($\Delta T_{\mathbf{23\text{-}22}}$ = 50°C). This is due to the shorter length of the extended mesogen compared to its diameter.

It is well known that hydrogen bonds could showed reversible processes of association and dissociation because of their moderate bonding energies. A new type of dynamic material was obtained through the control of such processes in hydrogen-bonded polymers (Fig. 2.15). Self-assembly of low molecular weight compounds led to the formation of liquid crystalline network polymers.[126] Depending on the type of substitution in the carboxylic acid derivative different mesophases were obtained. A smectic mesophase was displayed by the compound **24** in the presence of **25** (Fig. 2.15a), while **26** formed a nematic phase in the presence of **25** (Fig. 2.15b).

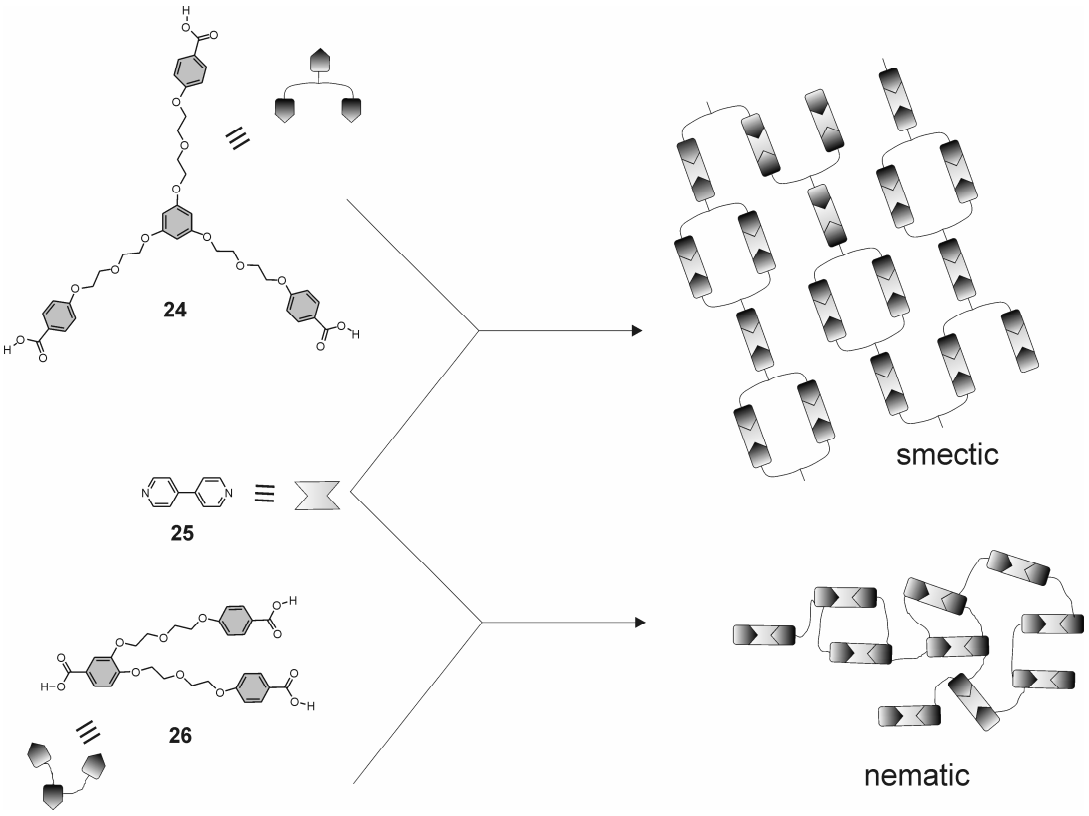

Figure 2.15. *Schematic illustration of the smectic network formed by hydrogen bonding of* ***24*** *and* ***25*** *and nematic network by* ***26*** *and* ***25****.*

2.2.3 Chirality in hydrogen-bonded liquid crystals

The role of supramolecular chemistry in material science is perhaps expressed most impressively in liquid crystals in which slight variations of chiral content can lead to dramatic variation in the properties of the mesophases.[127] The helical sense (twist) of these mesophases is determined not only by intrinsically chiral mesogens but also by the use of dopants which more often than not interact with achiral host LCs to generate chiral phases.[128,129] As in the case of achiral mesophases, the type of chiral mesophases depends on the shape, symmetry and order of the chiral mesogen. Rod-shaped molecules give chiral nematic phases, the so-called cholesteric phase, because it was first observed for cholesterol derivatives. Hydrogen bonding can be a tool for the “synthesis” of chiral mesogenics or for the induction of chirality in achiral LCs. The directional nature can

direct the twist of mesogens along the stacking direction in the formation of a chiral mesophase.

2.2.3.1 Chiral mesogens

Chiral nematic LCs can be prepared from achiral polysiloxanes with 4-alkoxybenzoic acid side chains in combination with optically active *trans*-stilbazole. The chiral properties can be tuned through the ratio of stilbazole to polymer units, as well as by the length of alkyl spacers in the structures.[130] The same principle can be used with small molecules such as benzoic acids.[131] A study of mixtures of benzoic acids and chiral stilbazole derivatives showed that the 1:1 complex actually did not give the largest range of the chiral phase. When 25% of the chiral stilbazole was added the chiral smectic C (SmC*) phase existed from 72 to 124ºC. Thereafter a chiral nematic (cholesteric) phase was observed up to the isotropization point of 138ºC.

The valency of the hydrogen bond donor and acceptor can be varied to produce chiral mesophases.[132] Mixtures of divalent 4,4'-bipyridine with 4-[(*S*)-2-methylbutoxy]benzoic acid in ratios between 1:9 and 4:6 showed LC behavior, but chiral mesophases existed only over a smaller ratio range of components.[133]

Lehn *et al.* have shown the stereospecific formation of helical fibers from diastereomers of tartaric acid functionalized with either uracil or 2,6-diacylamino pyridine. The complementary components, which are not liquid crystals in their pure state, upon mixing formed mesophases in a very broad temperature range, which depended on whether the tartaric acid core is either D, L or meso (Fig. 2.16).[65]

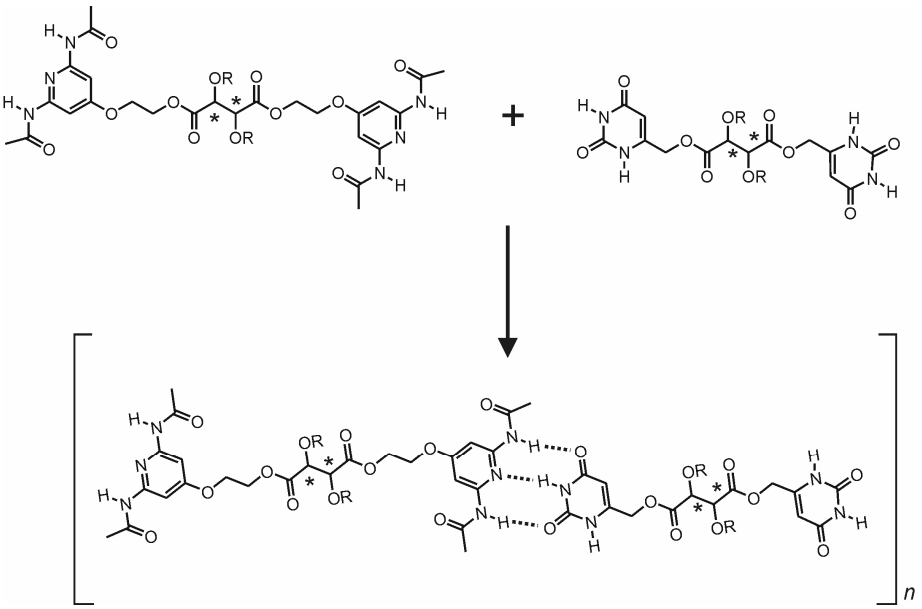

Figure 2.16. *Self-assembly of complementary chiral tartaric acid derivatives to liquid crystalline materials.*

Aminoacid derivatives have been widely used to form chiral liquid crystals.[60,134,135] Kato et al. have reported the use of glutamic acid derivatives as the source of chirality in hydrogen-bonded liquid crystals.[136-139] When a pyrene moiety was attached to the glutamic residue chiral columnar mesophases were displayed through one-dimensional self-assembly of the mesogens.[139] Chiral cubic phases could be induced from the columnar hexagonal phase by addition of metal salts when a folic acid moiety was attached to the glutamic residue.[138] In these compounds, the formation of chiral structures in solution is aided by the addition of sodium cations in chloroform. In dodecane the ions are not necessary for the chiral expression.

Melamine derivatives have been also used in combination with chiral benzoic acids to form chiral disk-shaped structures. These systems were able to form chiral hexagonal columnar phases (Fig. 2.17a).[140] The stabilization of the chiral columnar mesophases is a compromise between the number of peripheral chains and bulkiness of the carboxylic acids. The chirality is transferred from the benzoic acid to the liquid crystalline assembly through the hydrogen bonds. The chiral information can also be transferred from the melamine derivative to the mesophases through the complexation with carboxylic acids (Fig. 2.17b).[141]

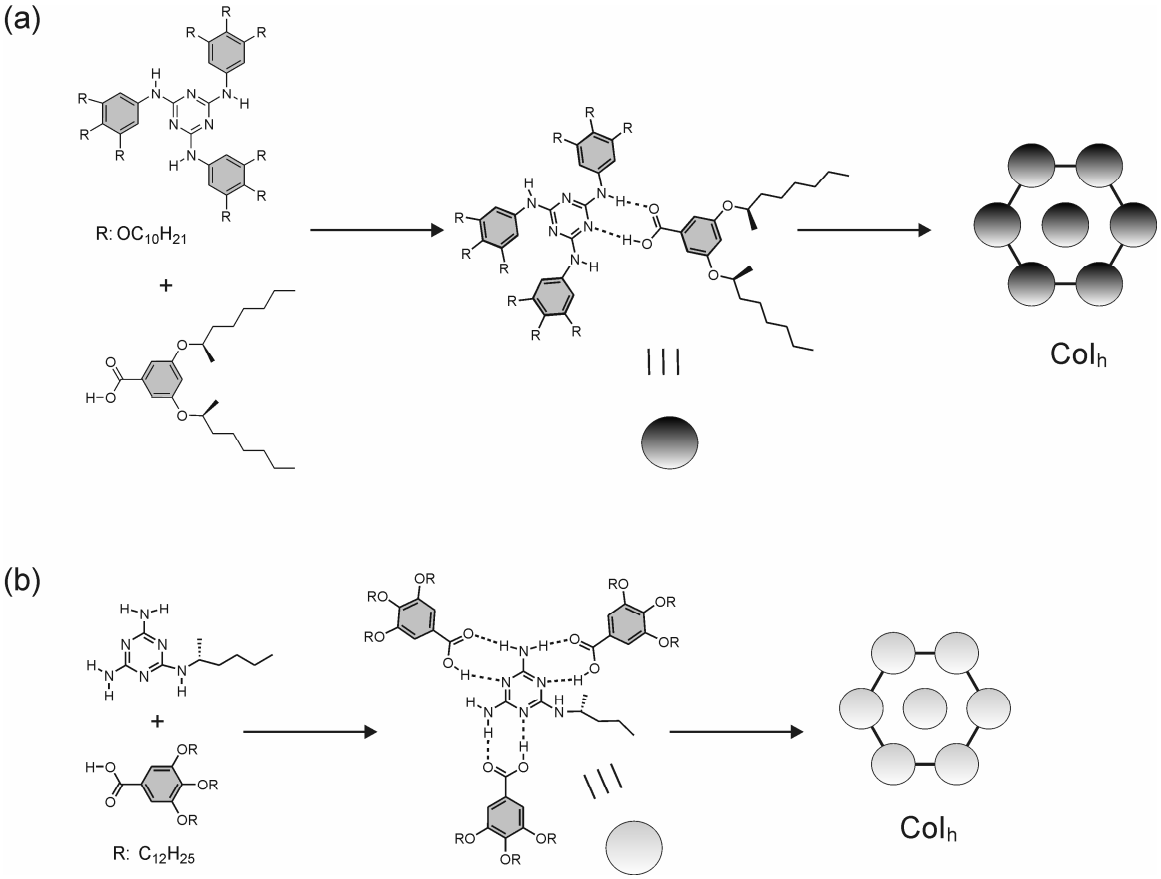

Figure 2.17. *Structures of the chiral mesogen formed by (a) achiral melamine derivative and chiral carboxylic acid and (b) chiral melamine and achiral carboxylic acid. Both mesogenic complexes give a hexagonal columnar mesophase.*

2.2.3.2 Induction of chirality

The induction of chirality in LCs is of interest for the possible application in display technology.[142] Chiral induction can be obtained by the addition of a non-racemic dopant to an achiral mesophase. The chiral superstructure is achieved by the noncovalent interaction of the solvent with the solute, or vice versa when an achiral dopant is introduced into a chiral LC. For achiral C_3-symmetrical trisamides which exhibit discotic liquid crystalline phases, chiral induction has been reported.[143,144] When the compound was dissolved in chiral (*R*)-(-)-2,6-dimethyloctane significant Cotton effects were detected.[145] A chiral disc-like trisamide could also be used as a dopant at concentrations

as low as 2.5% to induce supramolecular chirality in the stacks of achiral compounds (Figure 2.18). However, additional hydrogen bonds in a self-complementary urea unit in the C_3-symmetrical trisamide were unfavorable for chiral induction.

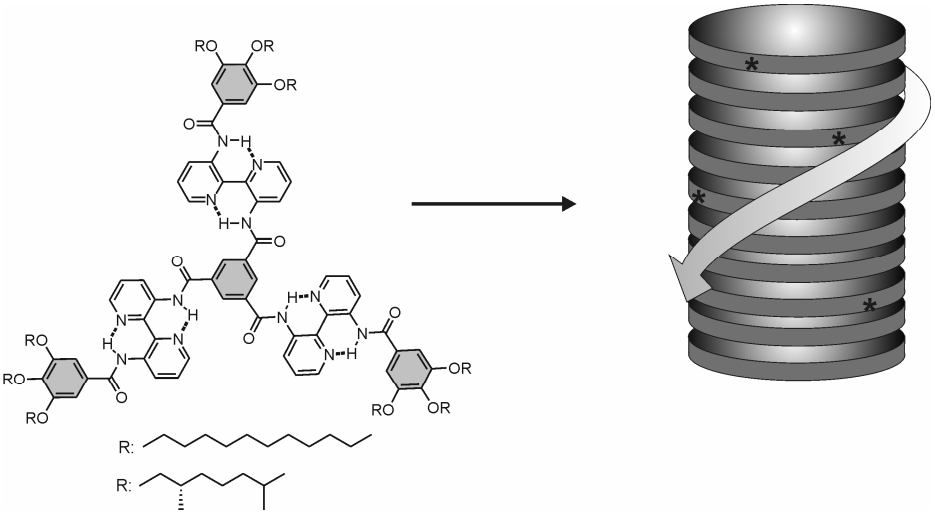

Figure 2.18. *C_3-symmetrical disk-shaped molecules with achiral and chiral side-chains. A small percentage of chiral molecules induces supramolecular chirality in the columns.*

Sierra *et al.* have reported the induction of chirality in hydrogen-bonded disk-like mesogens by the complexation with chiral carboxylic diacids.[146] When the ratio between the mesogenic assembly and the chiral diacid is varied, different phases were formed. For a ratio assembly-diacid of 2:1 a hexagonal columnar phase was obtained, while for a ratio of 1:4 a crystal phase could be seen. Circular dichroism spectroscopy showed that thermodynamically stable chiral mesophases were formed when the ratio between the assembly and the diacid is 2:1. Sierra and co-workers also showed that a chiral columnar arrangement could be obtained with a self-assembled mesogen, formed by a melamine derivative and a series of banana-shaped carboxylic acids (1:3 ratio).[147] The combination of hydrogen bonding and the π-stacking of melamine allow the self-assembled mesogen to form columnar aggregates. The particular shape of the carboxylic acids allows both enantiomeric stacking possibilities: right-handed (P) and left-handed (M). As shown by circular dichroism, the functionalization of the carboxylic acid with chiral alkyl chains led to formation of only one enantiomer, which displayed a rectangular columnar mesophase.

2.2.3.3 Spontaneous chiral resolution

The chiral induction in liquid crystalline phases by achiral molecules[148] can be considered an analogue of chiral induction in crystal phases where only one chiral conformation of achiral molecules is retained during the crystallization process.[149] The first compounds discovered with the ability to have chiral resolution were the "bent-core" or "banana-shaped" mesogens.[150,151] Hydrogen bonds can be used to create bent-core mesogens with the same characteristics as covalent analogs (Fig. 2.19).[80]

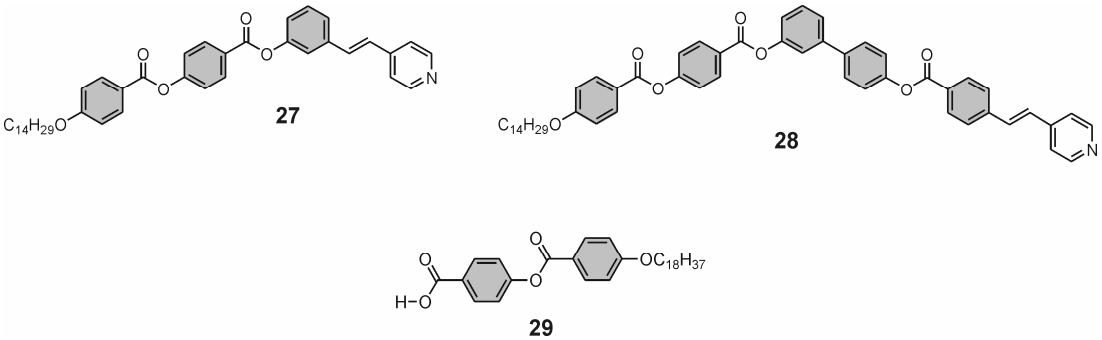

Figure 2.19. *Chemical structures of the hydrogen bonding acceptors **27**, **28**, and hydrogen bond donor **29**. The hydrogen-bonded complexes give a chiral smectic polar phase (SmCP) typical for banana-shape mesogens.*

The formation of the complexes between the calamitic benzoic acid derivative **29** and bent-core molecules functionalized with a pyridyl group (**27** and **28**), neither of which display mesomorphic behavior gave rise to a material which displayed a chiral smectic polar phase (SmCP) mesophase. It is worth to notice that the hydrogen-bonded complex **28•29** exhibited a phase transition from the smectic polar to the isotropic phase at 119 °C. The same phase transition (SmCP-isotropic) temperature is shown by its covalent analog.

Kishikawa *et al.* reported the spontaneous chiral resolution of achiral *N,N'*-bis(3,4,5-trialkoxylphenyl)urea derivatives, which formed disk-like dimers with a columnar liquid crystalline phase from 60 to 188 °C.[152] The presence of urea moiety in the mesogens allowed the formation of hydrogen bonds in one-directional stacking. The hydrogen bonds induced a reduction of the inter-columnar dipole-dipole interaction allowing the formation of a chiral mesophase by achiral molecules. Strigazzi and coworkers reported

achiral nematic-type LCs formed by trans-4-alkylcyclohexane carboxylic acids[153] and 4-n-alkyloxybenzoic acids,[154] which display spontaneous chiral resolution. These molecules form a dimer at low temperatures by hydrogen bonding between acid groups. This dimer dissociated at higher temperatures. The chirality was displayed through the textures cooling from the isotropic phase, the polarized optical images are characteristic of cholesteric rather than nematic phases. The authors suggest that the carboxylic acid, which is anchored on the surface, oligomerizes and generates a chiral super-structure.

2.3 Conclusions and Outlook

Liquid crystals are promising soft materials with dynamic functions because they form ordered and dynamic structures which allow fast response to external stimuli such as magnetic field or light with great importance in the technology field (e.g. screen displays).

In this chapter, a short overview of the development of hydrogen-bonded liquid crystals has given. Depending of the association of identical and different components by hydrogen bonds, different types of liquid crystals, such as columnar, smectic and cubic, can be obtained. It has also been shown that, in order to build highly functional liquid crystals, it is important to design molecules with appropriate chemical structures and to control the process of their self-organization. It is very important to notice that supramolecular assembly through specific molecular interactions and phase segregation are the keys for further structural control over the materials. In particular, hydrogen bonding can be an invaluable tool to form mesogenic molecules with novel shapes and to organize those in order to obtain new functions. Furthermore, hydrogen bonding allows the stabilization and the induction of the chirality in liquid crystalline phases with important consequences for applications in materials science.

The work described in this thesis deals with the role of hydrogen bonds in self-assembled nano-containers, which form achiral and chiral liquid crystalline materials. The dynamic nature of these liquid crystalline materials is exploited through their response to external stimuli such as temperature and surface interactions.

2.4 References:

[1] G. W. Gray, V. Vill, H. W. Spiess, D. Demus, J. W. Goodby, *Physical Properties of Liquid Crystals*, Wiley VCH, New York, **1999**.

[2] G. T. Stewart, *Liq. Cryst.* **2004**, *31*, 443-471.

[3] J. W. Goodby, G. W. Gray, *Handbook of Liquid Crystals, Vol. 1*, Wiley VCH, New York, **1998**.

[4] V. Vill, R. Hashim, *Curr. Opin. Colloid Int.* **2002**, *7*, 395-409.

[5] B. Donnio, *Curr. Opin. Colloid Int.* **2002**, *7*, 371-394.

[6] D. Demus, *Handbook of Liquid Crystals, Vol. 1*, Wiley VCH, New York, **1998**.

[7] I. Dierking, *Textures of Liquid Crystals*, Wiley VCH, Weinheim, **2003**.

[8] P. J. Collins, J. S. Patel, *Handbook of Liquid Crystals Research*, Oxford University Press, New York, **1997**.

[9] J.-M. Lehn, *Supramolecular Chemistry, Concepts and Perspectives*, VCH, Weinheim, Germany, **1995**.

[10] Y. Kobuke, *Struct. Bond.* (Berlin) **2006**, *121*, 49-104.

[11] D. K. Smith, A. R. Hirst, C. S. Love, J. G. Hardy, S. V. Brignell, B. Q. Huang, *Prog. Polym. Sci.* **2005**, *30*, 220-293.

[12] N. M. Sangeetha, U. Maitra, *Chem. Soc. Rev.* **2005**, *34*, 821-836.

[13] S. G. Zhang, *Nat. Biotechnol.* **2003**, *21*, 1171-1178.

[14] C. Tschierske, *Curr. Opin. Colloid Int.* **2002**, *7*, 69-80.

[15] T. Kato, N. Mizoshita, K. Kishimoto, *Angew. Chem. Int. Ed.* **2006**, *45*, 38-68.

[16] C. M. Paleos, D. Tsiourvas, *Liq. Cryst.* **2001**, *28*, 1127-1161.

[17] T. Kato, N. Mizoshita, K. Kanie, *Macromol. Rapid Commun.* **2001**, *22*, 797-814.

[18] T. Kato, *Struct. Bond.* (Berlin) **2000**, *96*, 95-146.

[19] U. Beginn, *Prog. Polym. Sci.* **2003**, *28*, 1049-1105.

[20] M. Simard, D. Su, J. D. Wuest, *J. Am. Chem. Soc.* **1991**, *113*, 4696-4698.

[21] M. Gallant, M. T. P. Viet, J. D. Wuest, *J. Am. Chem. Soc.* **1991**, *113*, 721-723.

[22] Y. Ducharme, J. D. Wuest, *J. Org. Chem.* **1988**, *53*, 5787-5789.

[23] R. Kleppinger, C. P. Lillya, C. Q. Yang, *J. Am. Chem. Soc.* **1997**, *119*, 4097-4102.

[24] M. Suarez, J.-M. Lehn, S. C. Zimmerman, A. Skoulios, B. Heinrich, *J. Am. Chem. Soc.* **1998**, *120*, 9526-9532.

[25] M. Nishii, T. Matsuoka, Y. Kamikawa, T. Kato, *Org. Biomol. Chem.* **2005**, *3*, 875-880.

[26] F. Ciuchi, G. Dinicola, H. Franz, G. Gottarelli, P. Mariani, M. G. P. Bossi, G. P. Spada, *J. Am. Chem. Soc.* **1994**, *116*, 7064-7071.

[27] K. Kanie, T. Yasuda, S. Ujiie, T. Kato, *Chem. Commun.* **2000**, 1899-1900.

[28] K. Kanie, M. Nishii, T. Yasuda, T. Taki, S. Ujiie, T. Kato, *J. Mater. Chem.* **2001**, *11*, 2875-2886.

[29] S. Jin, Y. G. Ma, S. C. Zimmerman, S. Z. D. Cheng, *Chem. Mater.* **2004**, *16*, 2975-2977.

[30] V. Percec, M. N. Holerca, S. Nununelin, J. L. Morrison, M. Glodde, J. Smidrkal, M. Peterca, B. M. Rosen, S. Uchida, V. S. K. Balagurusamy, M. L. Sienkowska, P. A. Heiney, *Chem. Eur. J.* **2006**, *12*, 6216-6241.

[31] V. Percec, M. Glodde, M. Peterca, A. Rapp, I. Schnell, H. W. Spiess, T. K. Bera, Y. Miura, V. S. K. Balagurusamy, E. Aqad, P. A. Heiney, *Chem. Eur. J.* **2006**, *12*, 6298-6314.

[32] Z. Liu, L. Zhu, Z. H. Shen, W. S. Zhou, S. Z. D. Cheng, V. Percec, G. Ungar, *Macromolecules* **2002**, *35*, 9426-9433.

[33] D. J. P. Yeardley, G. Ungar, V. Percec, M. N. Holerca, G. Johansson, *J. Am. Chem. Soc.* **2000**, *122*, 1684-1689.

[34] V. Percec, C. H. Ahn, G. Ungar, D. J. P. Yeardley, M. Möller, S. S. Sheiko, *Nature* **1998**, *391*, 161-164.

[35] S. D. Hudson, H. T. Jung, V. Percec, W. D. Cho, G. Johansson, G. Ungar, V. S. K. Balagurusamy, *Science* **1997**, *278*, 449-452.

[36] V. Percec, *Macromol. Symp.* **1997**, *117*, 267-273.

[37] V. Percec, C. M. Mitchell, W. D. Cho, S. Uchida, M. Glodde, G. Ungar, X. B. Zeng, Y. S. Liu, V. S. K. Balagurusamy, P. A. Heiney, *J. Am. Chem. Soc.* **2004**, *126*, 6078-6094.

[38] V. S. K. Balagurusamy, G. Ungar, V. Percec, G. Johansson, *J. Am. Chem. Soc.* **1997**, *119*, 1539-1555.

[39] V. Percec, P. W. Chu, G. Ungar, J. P. Zhou, *J. Am. Chem. Soc.* **1995**, *117*, 11441-11454.

[40] X. B. Zeng, G. Ungar, Y. S. Liu, V. Percec, S. E. Dulcey, J. K. Hobbs, *Nature* **2004**, *428*, 157-160.

[41] G. Ungar, Y. S. Liu, X. B. Zeng, V. Percec, W. D. Cho, *Science* **2003**, *299*, 1208-1211.

[42] V. Percec, A. E. Dulcey, V. S. K. Balagurusamy, Y. Miura, J. Smidrkal, M. Peterca, S. Nummelin, U. Edlund, S. D. Hudson, P. A. Heiney, D. A. Hu, S. N. Magonov, S. A. Vinogradov, *Nature* **2004**, *430*, 764-768.

[43] V. Percec, A. E. Dulcey, M. Peterca, M. Ilies, S. Nummelin, M. J. Sienkowska, P. A. Heiney, *Proc. Natl. Acad. Sci. U. S. A.* **2006**, *103*, 2518-2523.

[44] V. Percec, M. Peterca, M. J. Sienkowska, M. A. Ilies, E. Aqad, J. Smidrkal, P. A. Heiney, *J. Am. Chem. Soc.* **2006**, *128*, 3324-3334.

[45] B. Chen, U. Baumeister, G. Pelzl, M. K. Das, X. Zeng, G. Ungar, C. Tschierske, *J. Am. Chem. Soc.* **2005**, *127*, 16578-16591.

[46] X. H. Cheng, M. Prehm, M. K. Das, J. Kain, U. Baumeister, S. Diele, D. Leine, A. Blume, C. Tschierske, *J. Am. Chem. Soc.* **2003**, *125*, 10977-10996.

[47] R. Plehnert, J. A. Schroter, C. Tschierske, *J. Mater. Chem.* **1998**, *8*, 2611-2626.

[48] B. Chen, X. B. Zeng, U. Baumeister, G. Ungar, C. Tschierske, *Science* **2005**, *307*, 96-99.

[49] G. Gottarelli, G. P. Spada, *Chem. Rec.* **2004**, *4*, 39-49.

[50] S. Bonazzi, M. M. Demorais, G. Gottarelli, P. Mariani, G. P. Spada, *Angew. Chem. Int. Ed. Engl.* **1993**, *32*, 248-250.

[51] S. Bonazzi, M. Capobianco, M. M. Demorais, A. Garbesi, G. Gottarelli, P. Mariani, M. G. P. Bossi, G. P. Spada, L. Tondelli, *J. Am. Chem. Soc.* **1991**, *113*, 5809-5816.

[52] C. M. Paleos, D. Tsiourvas, *Curr. Opin. Colloid Int.* **2001**, *6*, 257-267.

[53] L. Schmidt-Mende, A. Fechtenkotter, K. Müllen, E. Moons, R. H. Friend, J. D. MacKenzie, *Science* **2001**, *293*, 1119-1122.

[54] M. L. Bushey, T. Q. Nguyen, W. Zhang, D. Horoszewski, C. Nuckolls, *Angew. Chem. Int. Ed.* **2004**, *43*, 5446-5453.

[55] M. L. Bushey, A. Hwang, P. W. Stephens, C. Nuckolls, *J. Am. Chem. Soc.* **2001**, *123*, 8157-8158.

[56] R. I. Gearba, M. Lehmann, J. Levin, D. A. Ivanov, M. H. J. Koch, J. Barbera, M. G. Debije, J. Piris, Y. H. Geerts, *Adv. Mater.* **2003**, *15*, 1614-1618.

[57] I. Paraschiv, M. Giesbers, B. van Lagen, F. C. Grozema, R. D. Abellon, L. D. A. Siebbeles, A. T. M. Marcelis, H. Zuilhof, E. J. R. Sudholter, *Chem. Mater.* **2006**, *18*, 968-974.

[58] M. Masuda, P. Jonkheijm, R. P. Sijbesma, E. W. Meijer, *J. Am. Chem. Soc.* **2003**, *125*, 15935-15940.

[59] V. Percec, C. H. Ahn, T. K. Bera, G. Ungar, D. J. P. Yeardley, *Chem. Eur. J.* **1999**, *5*, 1070-1083.

[60] V. Percec, A. S. E. Dulcey, M. Peterca, M. Ilies, J. Ladislaw, B. M. Rosen, U. Edlund, P. A. Heiney, *Angew. Chem. Int. Ed.* **2005**, *44*, 6516-6521.

[61] V. Percec, M. R. Imam, T. K. Bera, V. S. K. Balagurusamy, M. Peterca, P. A. Heiney, *Angew. Chem. Int. Ed.* **2005**, *44*, 4739-4745.

[62] J. Hirschberg, A. Ramzi, R. P. Sijbesma, E. W. Meijer, *Macromolecules* **2003**, *36*, 1429-1432.

[63] J. Hirschberg, L. Brunsveld, A. Ramzi, J. Vekemans, R. P. Sijbesma, E. W. Meijer, *Nature* **2000**, *407*, 167-170.

[64] J. W. Xu, C. L. Toh, X. M. Liu, S. F. Wang, C. B. He, X. H. Lu, *Macromolecules* **2005**, *38*, 1684-1690.

[65] C. Fouquev, J.-M. Lehn, A. M. Levelut, *Adv. Mater.* **1990**, *2*, 254-257.

[66] R. K. Castellano, C. Nuckolls, S. H. Eichhorn, M. R. Wood, A. J. Lovinger, J. Rebek Jr, *Angew. Chem. Int. Ed.* **1999**, *38*, 2603-2606.

[67] J. Hirschberg, R. A. Koevoets, R. P. Sijbesma, E. W. Meijer, *Chem. Eur. J.* **2003**, *9*, 4222-4231.

[68] M. J. Brienne, J. Gabard, J.-M. Lehn, I. Stibor, *J. Chem. Soc.* **1989**, 1868-1870.

[69] T. Kato, J. M. J. Frèchet, *J. Am. Chem. Soc.* **1989**, *111*, 8533-8534.

[70] T. Kato, J. M. J. Frèchet, *Macromolecules* **1989**, *22*, 3818-3819.

[71] M. Shoji, F. Tanaka, *Macromolecules* **2002**, *35*, 7460-7472.

[72] S. Machida, T. I. Urano, K. Sano, T. Kato, *Langmuir* **1997**, *13*, 576-580.

[73] T. Kato, M. Fukumasa, J. M. J. Frèchet, *Chem. Mater.* **1995**, *7*, 368-372.

[74] T. Kato, T. Uryu, F. Kaneuchi, C. Jin, J. M. J. Frèchet, *Liq. Cryst.* **1993**, *14*, 1311-1317.

[75] M. Fukumasa, T. Kato, T. Uryu, J. M. J. Frèchet, *Chem. Lett.* **1993**, 65-68.

[76] P. Massiot, M. Imperor-Clerc, M. Veber, R. Deschenaux, *Chem. Mater.* **2005**, *17*, 1946-1951.

[77] T. Kato, Y. Kubota, M. Nakano, T. Uryu, *Chem. Lett.* **1995**, 1127-1128.

[78] H. K. Lee, H. Lee, Y. H. Ko, Y. J. Chang, N. K. Oh, W. C. Zin, K. Kim, *Angew. Chem. Int. Ed.* **2001**, *40*, 2669-2671.

[79] A. Kraft, A. Reichert, R. Kleppinger, *Chem. Commun.* **2000**, 1015-1016.

[80] M. Gimeno, M. B. Ros, J. L. Serrano, M. R. de la Fuente, *Angew. Chem. Int. Ed.* **2004**, *43*, 5235-5238.

[81] A. Sautter, C. Thalacker, F. Würthner, *Angew. Chem. Int. Ed.* **2001**, *40*, 4425-4428.

[82] C. T. Seto, J. P. Mathias, G. M. Whitesides, *J. Am. Chem. Soc.* **1993**, *115*, 1321-1329.

[83] C. T. Seto, G. M. Whitesides, *J. Am. Chem. Soc.* **1993**, *115*, 905-916.

[84] D. C. Sherrington, K. A. Taskinen, *Chem. Soc. Rev.* **2001**, *30*, 83-93.

[85] V. Paraschiv, M. Crego-Calama, R. H. Fokkens, C. J. Padberg, P. Timmerman, D. N. Reinhoudt, *J. Org. Chem.* **2001**, *66*, 8297-8301.

[86] L. J. Prins, F. de Jong, P. Timmerman, D. N. Reinhoudt, *Nature* **2000**, *408*, 181-184.

[87] K. A. Jolliffe, P. Timmerman, D. N. Reinhoudt, *Angew. Chem. Int. Ed.* **1999**, *38*, 933-937.

[88] L. J. Prins, P. Timmerman, D. N. Reinhoudt, *Pure Appl. Chem.* **1998**, *70*, 1459-1468.

[89] R. H. Vreekamp, J. P. M. van Duynhoven, M. Hubert, W. Verboom, D. N. Reinhoudt, *Angew. Chem. Int. Ed. Engl.* **1996**, *35*, 1215-1218.

[90] S. Yagai, M. Higashi, T. Karatsu, A. Kitamura, *Chem. Commun.* **2006**, 1500-1502.

[91] M. J. Krische, J.-M. Lehn, *Struct. Bond.* (Berlin) **2000**, *96*, 3-29.

[92] R. Dobrawa, M. Lysetska, P. Ballester, M. Grune, F. Würthner, *Macromolecules* **2005**, *38*, 1315-1325.

[93] S. Yagai, T. Karatsu, A. Kitamura, *Langmuir* **2005**, *21*, 11048-11052.

[94] H. J. van Manen, V. Paraschiv, J. J. Garciá-López, H. Schönherr, S. Zapotoczny, G. J. Vancso, M. Crego-Calama, D. N. Reinhoudt, *Nano Lett.* **2004**, *4*, 441-446.

[95] S. Yagai, T. Iwashima, K. Kishikawa, S. Nakahara, T. Karatsu, A. Kitamura, *Chem. Eur. J.* **2006**, *12*, 3984-3994.

[96] C. Thalacker, A. Miura, S. de Feyter, F. C. de Schryver, F. Würthner, *Org. Biomol. Chem.* **2005**, *3*, 414-422.

[97] H. Schönherr, M. Crego-Calama, G. J. Vancso, D. N. Reinhoudt, *Adv. Mater.* **2004**, *16*, 1416-1420.

[98] H. A. Klok, K. A. Jolliffe, C. L. Schauer, L. J. Prins, J. P. Spatz, M. Möller, P. Timmerman, D. N. Reinhoudt, *J. Am. Chem. Soc.* **1999**, *121*, 7154-7155.

[99] L. M. A. Perdigao, N. R. Champness, P. H. Beton, *Chem. Commun.* **2006**, 538-540.

[100] K. C. Russell, J.-M. Lehn, N. Kyritsakas, A. DeCian, J. Fischer, *New J. Chem.* **1998**, *22*, 123-128.

[101] N. Kimizuka, S. Fujikawa, H. Kuwahara, T. Kunitake, A. Marsh, J.-M. Lehn, *J. Chem. Soc.* **1995**, 2103-2104.

[102] M. Arduini, M. Crego-Calama, P. Timmerman, D. N. Reinhoudt, *J. Org. Chem.* **2003**, *68*, 1097-1106.

[103] D. Goldmann, D. Janietz, C. Schmidt, J. H. Wendorff, *Angew. Chem. Int. Ed.* **2000**, *39*, 1851-1854.

[104] D. Goldman, D. Janietz, C. Schmidt, J. H. Wendorff, *J. Mater. Chem.* **2004**, *14*, 1521-1525.

[105] J. H. Lee, M. J. Han, S. H. Hwang, I. Jang, S. J. Lee, S. H. Yoo, J. Y. Jho, S. Y. Park, *Tetrahedron Lett.* **2005**, *46*, 7143-7146.

[106] J. Barbera, L. Puig, J. L. Serrano, T. Sierra, *Chem. Mater.* **2004**, *16*, 3308-3317.

[107] S. Yagai, T. Nakajima, K. Kishikawa, S. Kohmoto, T. Karatsu, A. Kitamura, *J. Am. Chem. Soc.* **2005**, *127*, 11134-11139.

[108] F. Würthner, S. Yao, B. Heise, C. Tschierske, *Chem. Commun.* **2001**, 2260-2261.

[109] H. M. Keizer, R. P. Sijbesma, *Chem. Soc. Rev.* **2005**, *34*, 226-234.

[110] C. Schmuck, W. Wienand, *Angew. Chem. Int. Ed.* **2001**, *40*, 4363-4369.

[111] T. Gulikkrzywicki, C. Fouquey, J.-M. Lehn, *Proc. Natl. Acad. Sci. U. S. A.* **1993**, *90*, 163-167.

[112] X. H. Lu, C. B. He, A. C. Griffin, *Macromolecules* **2003**, *36*, 5195-5200.

[113] J. W. Xu, C. B. He, K. C. Toh, X. H. Lu, *Macromolecules* **2002**, *35*, 8846-8851.

[114] K. Yamaoka, T. Kaneko, J. P. Gong, Y. Osada, *Macromolecules* **2001**, *34*, 1470-1476.

[115] M. Lee, B. K. Cho, Y. S. Kang, W. C. Zin, *Macromolecules* **1999**, *32*, 8531-8537.

[116] C. Meiners, S. Valiyaveettil, V. Enkelmann, K. Müllen, *J. Mater. Chem.* **1997**, *7*, 2367-2374.

[117] S. Sivakova, J. Wu, C. J. Campo, P. T. Mather, S. J. Rowan, *Chem. Eur. J.* **2005**, *12*, 446-456.

[118] C. O. Osuji, C. Y. Chao, C. K. Ober, E. L. Thomas, *Macromolecules* **2006**, *39*, 3114-3117.

[119] T. Kato, H. Kihara, S. Ujiie, T. Uryu, J. M. J. Frèchet, *Macromolecules* **1996**, *29*, 8734-8739.

[120] O. Ikkala, M. Knaapila, J. Ruokolainen, M. Torkkeli, R. Serimaa, K. Jokela, L. Horsburgh, A. Monkman, G. ten Brinke, *Adv. Mater.* **1999**, *11*, 1206-1210.

[121] T. Kawakami, T. Kato, *Macromolecules* **1998**, *31*, 4475-4479.

[122] T. Kato, J. M. J. Frèchet, *Macromol. Symp.* **1995**, *98*, 311-326.

[123] U. Kumar, J. M. J. Frèchet, T. Kato, S. Ujiie, K. Timura, *Angew. Chem. Int. Ed. Engl.* **1992**, *31*, 1531-1533.

[124] U. Kumar, T. Kato, J. M. J. Frèchet, *J. Am. Chem. Soc.* **1992**, *114*, 6630-6639.

[125] H. Kihara, T. Kato, T. Uryu, J. M. J. Frèchet, *Liq. Cryst.* **1998**, *24*, 413-418.

[126] H. Kihara, T. Kato, T. Uryu, J. M. J. Frèchet, *Chem. Mater.* **1996**, *8*, 961-968.

[127] K. Akagi, G. Piao, S. Kaneko, K. Sakamaki, H. Shirakawa, M. Kyotani, *Science* **1998**, *282*, 1683-1686.

[128] H. S. Kitzerow, C. Bahr, *Chirality in Liquid Crystals*, Springer, New York, **2001**.

[129] R. Eelkema, M. M. Pollard, J. Vicario, N. Katsonis, B. S. Ramon, C. W. M. Bastiaansen, D. J. Broer, B. L. Feringa, *Nature* **2006**, *440*, 163-163.

[130] H. Kihara, T. Kato, T. Uryu, S. Ujiie, U. Kumar, J. M. J. Frèchet, D. W. Bruce, D. J. Price, *Liq. Cryst.* **1996**, *21*, 25-30.

[131] U. Kumar, J. M. J. Frechet, *Adv. Mater.* **1992**, *4*, 665-667.

[132] T. Kato, J. M. J. Frèchet, P. G. Wilson, T. Saito, T. Uryu, A. Fujishima, C. Jin, F. Kaneuchi, *Chem. Mater.* **1993**, *5*, 1094 - 1100.

[133] M. Grunert, R. A. Howie, A. Kaeding, C. T. Imrie, *J. Mater. Chem.* **1997**, *7*, 211-214.

[134] D. Tsiourvas, C. M. Paleos, A. Skoulios, *Chem. Eur. J.* **2003**, *9*, 5250-5258.

[135] G. Proni, G. Gottarelli, P. Mariani, G. P. Spada, *Chem. Eur. J.* **2000**, *6*, 3249-3253.

[136] Y. Kamikawa, T. Kato, H. Onouchi, D. Kashiwagi, K. Maeda, E. Yashima, *J. Polym. Sci., Part A: Polym. Chem.* **2004**, *42*, 4580-4586.

[137] Y. Kamikawa, M. Nishii, T. Kato, *Chem. Eur. J.* **2004**, *10*, 5942-5951.

[138] T. Kato, T. Matsuoka, M. Nishii, Y. Kamikawa, K. Kanie, T. Nishimura, E. Yashima, S. Ujiie, *Angew. Chem. Int. Ed.* **2004**, *43*, 1969-1972.

[139] Y. Kamikawa, T. Kato, *Org. Lett.* **2006**, *8*, 2463-2466.

[140] J. Barbera, L. Puig, P. Romero, J. L. Serrano, T. Sierra, *Chem. Mater.* **2005**, *17*, 3763-3771.

[141] L. Alvarez, J. Barbera, L. Puig, P. Romero, J. L. Serrano, T. Sierra, *J. Mater. Chem.* **2006**, *16*, 3768-3773.

[142] R. Eelkema, B. L. Feringa, *Org. Biomol. Chem.* **2006**, *4*, 3729-3745.

[143] T. Ishi-i, R. Kuwahara, A. Takata, Y. Jeong, K. Sakurai, S. Mataka, *Chem. Eur. J.* **2006**, *12*, 763-776.

[144] J. J. van Gorp, J. Vekemans, E. W. Meijer, *Mol. Cryst. Liq. Cryst.* **2003**, *397*, 491-505.

[145] J. J. van Gorp, J. Vekemans, E. W. Meijer, *J. Am. Chem. Soc.* **2002**, *124*, 14759-14769.

[146] J. Barbera, L. Puig, P. Romero, J. L. Serrano, T. Sierra, *J. Am. Chem. Soc.* **2005**, *127*, 458-464.

[147] J. Barbera, L. Puig, P. Romero, J. L. Serrano, T. Sierra, *J. Am. Chem. Soc.* **2006**, *128*, 4487-4492.

[148] T. Kajitani, H. Masu, S. Kohmoto, M. Yamamoto, K. Yamaguchi, K. Kishikawa, *J. Am. Chem. Soc.* **2005**, *127*, 1124-1125.

[149] I. Azumaya, K. Yamaguchi, I. Okamoto, H. Kagechika, K. Shudo, *J. Am. Chem. Soc.* **1995**, *117*, 9083-9084.

[150] D. M. Walba, E. Korblova, R. F. Shao, J. E. Maclennan, D. R. Link, M. A. Glaser, N. A. Clark, *J. Phys. Org. Chem.* **2000**, *13*, 830-836.

[151] D. M. Walba, E. Korblova, R. Shao, J. E. Maclennan, D. R. Link, M. A. Glaser, N. A. Clark, *Science* **2000**, *288*, 2181-2184.

[152] K. Kishikawa, S. Nakahara, Y. Nishikawa, S. Kohmoto, M. Yamamoto, *J. Am. Chem. Soc.* **2005**, *127*, 2565-2571.

[153] S. I. Torgova, L. Komitov, A. Strigazzi, *Liq. Cryst.* **1998**, *24*, 131-141.

[154] L. A. Karamysheva, I. F. Agafonova, S. I. Torgova, B. A. Umanskii, A. Strigazzi, *Mol. Cryst. Liq. Cryst.* **2001**, *364*, 547-556.

Chapter 3

Induction of Liquid Crystallinity by Self-Assembled Molecular Boxes*

In this chapter, liquid crystalline materials based on the self-organization of self-assembled molecular boxes are described. Double rosette assemblies $\mathbf{1b}_3$•$(DEB)_6$ *(DEB = diethylbarbituric acid) and* $\mathbf{1b}_3$•$(BuCYA)_6$ *(BuCYA = butylcyanuric acid) are formed spontaneously through the formation of 36 hydrogen bonds by mixing calix[4]arene dimelamine* ***1b*** *with either two equivalents of DEB or BuCYA in apolar solvents. The liquid crystalline phases for these assemblies have been determined by polarized optical microscopy (POM), differential scanning calorimetry (DSC) and X-ray diffraction (XRD). The double rosette assemblies organize in a columnar fashion in the liquid crystalline phase, showing a remarkable thermal stability considering their non-covalent nature.*

---

* Part of this chapter has been published: A. Piermattei, M. Giesbers, A. T. M. Marcelis, E. Mendes, S. J. Picken, M. Crego Calama, D. N. Reinhoudt *Angew. Chem. Int. Ed.* **2006**, *45*, 7543-7546

3.1 Introduction

The self-assembly of small molecular building blocks into supramolecular aggregates by noncovalent interactions has been extensively used for the formation of nanometer-scale structures.[1] Their self-organization into highly ordered nanoarchitectures requires the use of well-defined structures with high thermodynamic stability.[2] Hydrogen bonding is one of the tools to construct such structures due to their directional and dynamic nature[3] and their capability for error correction.[4] A variety of liquid crystalline materials[5,6] have been prepared by self-assembly via hydrogen bond formation.[7,8] Rod-like[9-12] and disk-like[13-21] low molecular weight complexes and polymers[22,23] with side-chain,[9,24,25] main-chain,[26-28] network and host-guest[26, 29-31] combination or single building blocks[20,32-34] have been reported. The shape of mesogenic molecules is one of the factors that determine packing and order in the liquid crystalline phases. Recently, unconventional shapes such as bananas,[35] dendrons,[36-40] cones,[6] shuttlecocks,[6] rod-dendrons,[6] and rings[6] have been reported. The self-assembly of these unconventional mesogenic "supramolecules" has produced supramolecular liquid crystals with new phases.[41] To the best of our knowledge, there are no examples in the literature that report hydrogen-bonded 3D nano objects formed by different building blocks, with the capability to form liquid crystals. In this chapter we report the first example of a liquid crystalline material based on the self-organization of self-assembled molecular boxes.

3.2. Formation of Double Rosette Assemblies

Earlier studies have shown that hydrogen-bonded double rosettes assemblies $\mathbf{1}_3$•$(BAR)_6$/$\mathbf{1}_3$•$(CYA)_6$ are spontaneously formed by mixing calix[4]arene dimelamine **1** with 2 equivalents of barbiturates (BAR) or cyanurates (CYA) in apolar solvents, such as chloroform, benzene and toluene (Fig. 3.1).[42,43] The assembly formation is driven by the formation of 36 complementary hydrogen bonds between the donor-acceptor-donor (DAD) array of the calix[4]arene dimelamine and acceptor-donor-acceptor (ADA) array of the barbiturate/cyanurate building blocks.

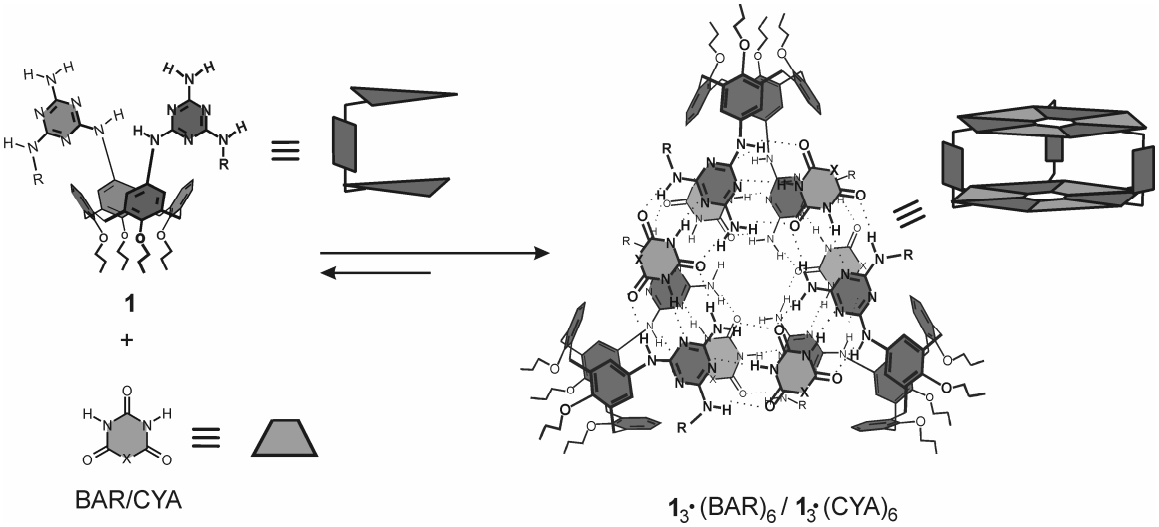

Figure 3.1. *Schematic representation of the molecular building blocks and their self-assembly into double rosettes* $\mathbf{1}_3$•*(BAR)*$_6$/$\mathbf{1}_3$•*(CYA)*$_6$.

These assemblies can exist in three different isomeric forms with D_3-, C_{3h}- and C_s-symmetry (Fig. 3.2).[44] The assemblies with D_3-symmetry, which is the predominant isomer, are chiral due to the staggered (antiparallel) orientation of the two melamine fragments, leading to a twist of the two different rosette planes, which can either adopt a clockwise ((*P*)-isomer) or counterclockwise ((*M*)-isomer) conformation. In both C_{3h}- and C_s-isomers, the two melamine fragments adopt an eclipsed (parallel) orientation and are therefore achiral. The difference between these isomers is the 180^o rotation of one of the calix[4]arene dimelamines in the case of the C_s-isomer.

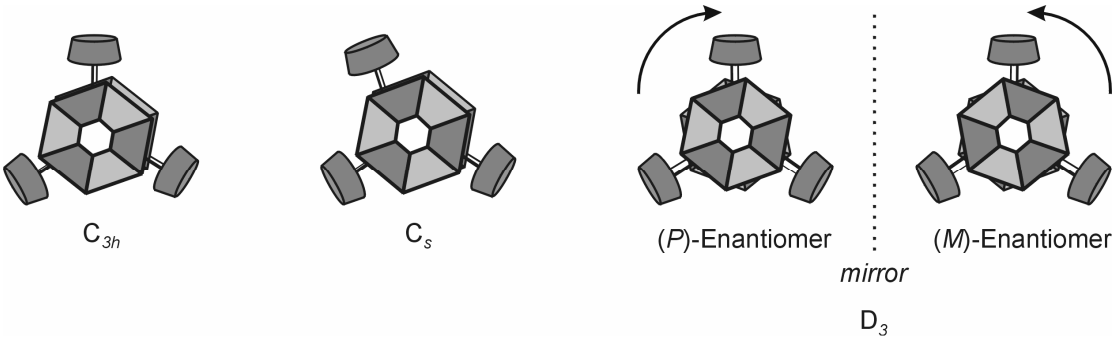

Figure 3.2. *Schematic representation of the possible isomers with* C_{3h}*-,* C_s*-, and* D_3*-symmetry. Both the (P)- and (M)-enantiomers of the* D_3*-symmetrical isomer are depicted.*

3.3 Characterization of Double Rosette Assemblies

Double rosette assemblies can conveniently be characterized by ^{1}H NMR spectroscopy.[42] Titration experiments have proven the 1:2 stoichiometry and the strong cooperativity of the assembly process. Upon formation of the assembly the diagnostic signals of the imide NH protons of BAR/CYA are observed between δ = 13 and 16 ppm. The number of signals in this region indicates the isomeric form of the assembly. For the D_3- and C_{3h}-isomers only two different signals are observed, while six different signals are observed for the assembly with C_s-symmetry.

The D_3-isomer is the most common, and in the absence of an another center of chirality, it is formed as a racemic mixture of both (*P*)- and (*M*)-enantiomers. However, upon introduction of chiral centers in one of the molecular components of the assembly (calix[4]arene dimelamines or barbiturate/cyanurate), only one of the two possible diastereoisomers is formed with a diastereomeric excess (*d.e.*) up to 96%.[45,46] When chiral cyanurates are used the sense of the twist of the melamine fragments is dictated by the stereochemistry of the chiral center in the cyanurates, *i.e*. a cyanurate bearing a chiral center with (*R*)-stereochemistry leads only to the formation of, for example, the (*P*)-diastereomer, while the (*S*)-isomer then leads only to the (*M*)-diastereomer. These chiral (*P*)- and (*M*)-assemblies are highly circular-dichroism (CD) active due to the asymmetric arrangement of the different chromophores within the rigid structure and therefore this characterization technique is of tremendous value.

Another characterization technique is MALDI-TOF mass spectrometry after Ag^+ labelling.[47,48] This is an extremely mild technique and provides a nondestructive way to generate charged assemblies based on the high affinity of Ag^+ for (two) cooperative π-donors, cyano or crown-ether functionalities.

Finally, X-ray crystallography provides evidence for the existence of double rosette assemblies in the solid state. The crystal structure of $\mathbf{1}_3$•$(DEB)_6$ shows that the two single rosette planes are neatly stacked on top of each other, with an interatomic distance of 3.2-3.5 Å (Fig. 3.3). Furthermore, it shows that the calix[4]arene units are fixed in a *pinched* cone conformation, the only conformation that allows simultaneous participation of the calix[4]arene units in both the upper and the lower rosette motifs.

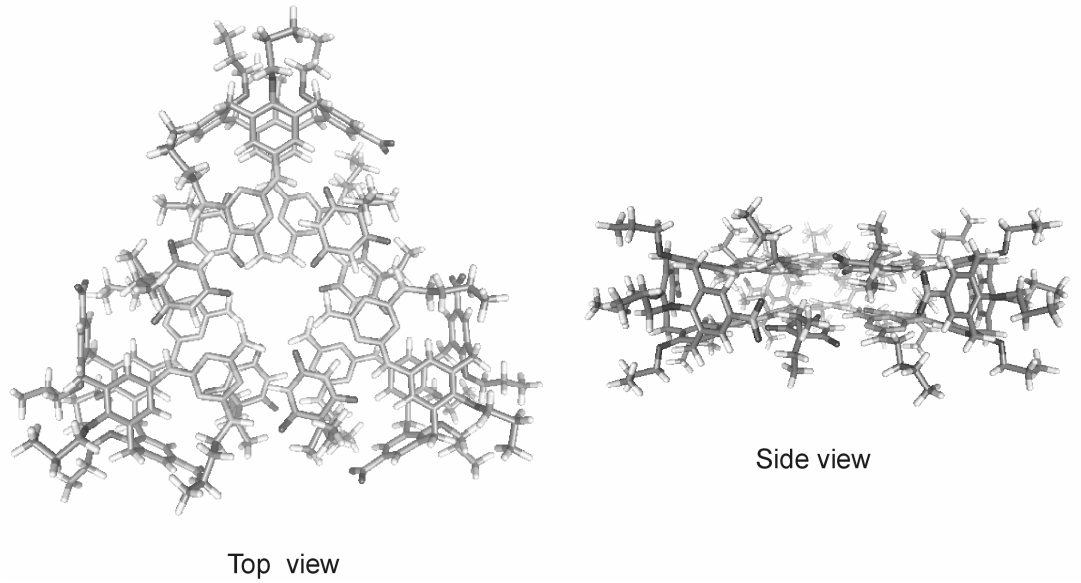

Figure 3.3. *Top and side view of the X-ray crystal structure of assembly* $\mathbf{1}_3$*•(DEB)*$_6$.

3.4. Results and Discussion

With the aim of inducing a liquid crystalline phase in double rosette hydrogen-bonded assemblies, octadecyl chains were introduced on the melamine moieties of the calix[4]arene skeleton (**1**).[5] The long alkyl chains in the dimelamine calix[4]arene **1b** are connected to the melamine moieties to avoid interference with the network of hydrogen bonds that holds the double rosette together.[49] Different assemblies were synthesized mixing the dimelamine **1b** and barbiturates (BAR) or cyanurates (CYA) (Chart 3.1).

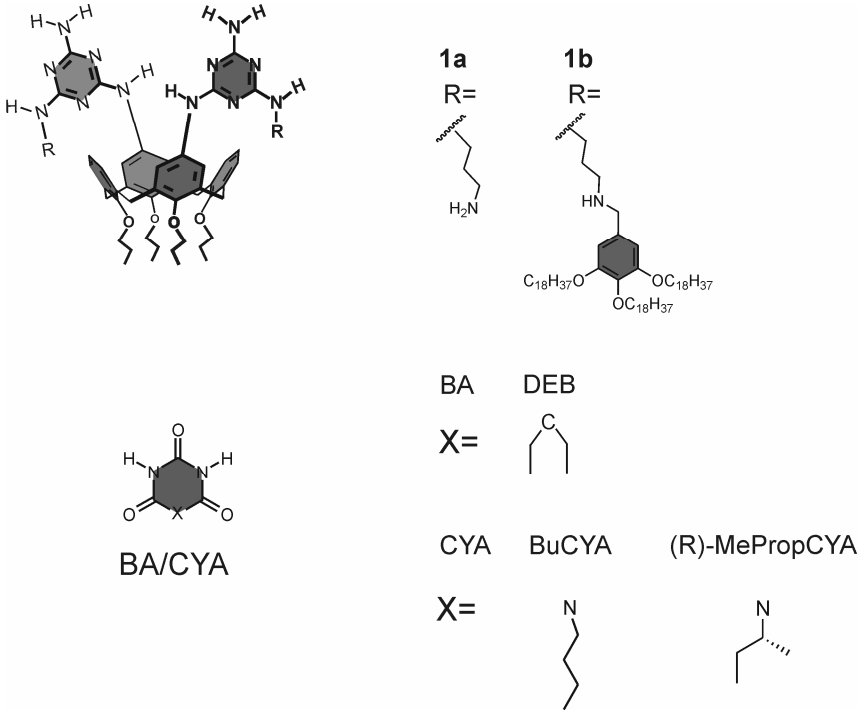

Chart 3.1. *Molecular structures of dimelamines **1** and BAR/CYA.*

3.4.1 Synthesis

Calix[4]arene dimelamine **1b** was obtained by the coupling reaction between the calix[4]arene **1a** and **2**, which were synthesized following literature procedures (Scheme 3.1).[37,50]

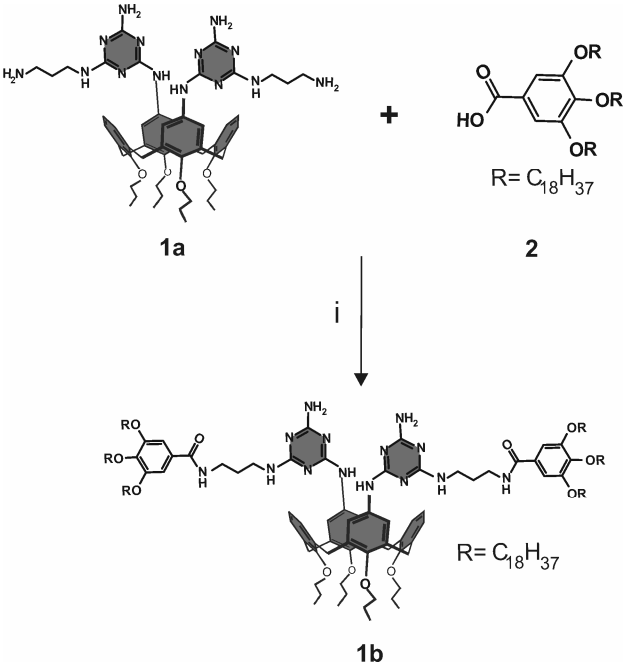

Scheme 3.1. *Synthesis of the dimelamine calix[4]arene* ***1b****: i. HBTU, DIPEA, CH_2Cl_2/DMF*

3.4.2 Liquid crystalline phase characterization

The formation of the self-assembled mesogens was confirmed by ^{1}H NMR spectroscopy in solution (Fig. 3.4). The hydrogen-bonded imide $NH_{(a-b)}$ proton signals of DEB and BuCYA around 15-14 ppm are diagnostic for the formation of the assemblies due to the fact that these protons are strongly shifted downfield upon hydrogen bond formation ($\delta_{NH,freeDEB}$=8.40 ppm; $\delta_{NH,freeBuCYA}$=11.2 ppm).[42]

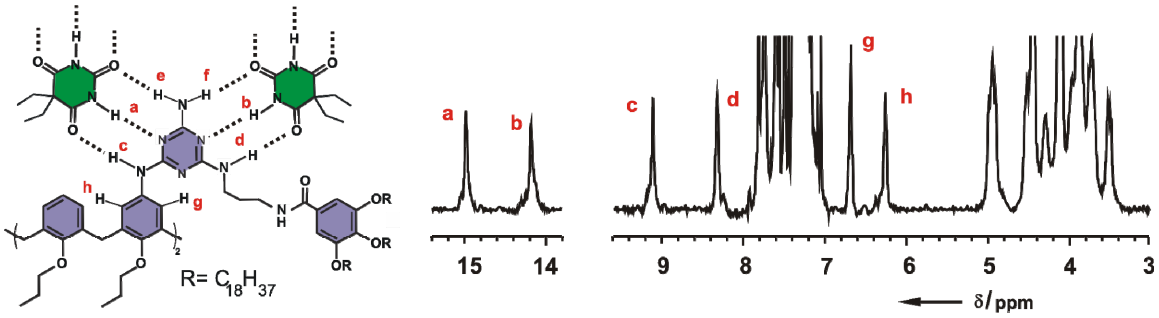

Figure 3.4. *Parts of ^{1}H NMR spectrum (400 MHz) of* ***1b***$_3$*•(DEB)$_6$ (1mM). The spectrum was recorded at 298 K in toluene-d_8.*

The thermal behavior of the assembly and of the isolated components has been determined by polarized optical microscopy (POM), and differential scanning calorimetry (DSC) (Table 1).

Table1. *Thermal properties of* ***1b*** *and the double rosettes* ***1b***$_3$*•(DEB)*$_6$*/****1b***$_3$*•(BuCYA)*$_6$*.*

Compound				Phase Transition[a]			
1b	Cr	17	(59.8)	Iso			
1b$_3$•(DEB)$_6$	Col$_x$	16	(18.7)	Col$_h$	173	(35.0)	Iso
1b$_3$•(BuCYA)$_6$	Cr	31	(167.5)	Col$_h$	233	(70.1)	Iso

[a] Phase transition temperatures (°C) and enthalpy changes (kJ mol^{-1} in parentheses)

Cr: crystalline; Col$_x$: unidentified columnar phase; Col$_h$: hexagonal columnar phase; Iso: isotropic

The DSC shows two transition peaks for each assembly, **1b**$_3$•(DEB)$_6$ and **1b**$_3$•(BuCYA)$_6$ in the thermogram. For **1b**$_3$•(DEB)$_6$ the first phase transition at lower temperature is attributed to a reversible transition between an unidentified columnar phase (Col$_x$) and the hexagonal columnar phase (Col$_h$). However, between these two phases no changes in the optical textures and X-ray diffractograms were observed. In the case of the **1b**$_3$•(BuCYA)$_6$, the first transition is attributed to a crystal-liquid crystalline transition (Col$_h$). The second transition at higher temperature is due to the liquid crystalline-isotropic phase transition for both double rosette assemblies. The thermotropic hexagonal columnar LC phase (from 16°C to 173°C for **1b**$_3$•(DEB)$_6$, and from 31°C to 233°C for **1b**$_3$•(BuCYA)$_6$) is exhibited by the two assemblies over a wide temperature range. This indicates a remarkable thermal stability of the liquid crystalline phase considering the dimensions (1.2 nm height, 3.3 nm width) and the noncovalent nature (twelve DAD•ADA interactions) of the double rosette assembly.[42] For the building block **1b**, the DSC shows only one phase transition peak in the thermogram. This phase transition is attributed to the crystalline-isotropic transition based on polarized optical microscopy which shows its crystalline phase as spherulite texture. It is remarkable that the liquid crystalline phase is observed for the double rosette assemblies even though none of the isolated building blocks is mesogenic.

To exclude thermal degradation of the double rosette assemblies during the heating process circular dichroism (CD) studies on thin layers were performed (data not shown) with an optically active assembly **1b**$_3$•((R)-MePropCYA)$_6$.[51,52] Optically active double rosette assemblies (with (*P*)- or (*M*)- helicity) exhibit a very strong induced CD signal at wavelengths between 250-350 nm,[52] due to the dissymmetric arrangement of the many chromophoric units within the structure, while the individual building block are hardly CD active. The CD signal does not decrease even after several thermal cycles, an evidence of the high thermal stability of these noncovalent assemblies.

By polarized optical microscopy (POM) the liquid crystalline phase is attributed to a columnar mesophase. A mosaic texture was observed for **1b**$_3$•(DEB)$_6$ and **1b**$_3$•(BuCYA)$_6$ after cooling from the isotropic melt showing birefringent areas, which is a strong indication that the mesophase is columnar (Fig. 3.5).[53]

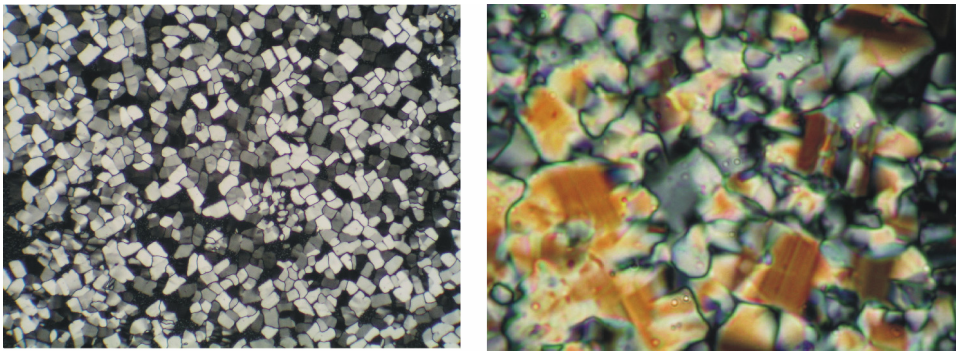

Figure 3.5. *Polarized photomicrographs of* ***1b***$_3$*•(DEB)*$_6$ *at 120 °C (left) and* ***1b***$_3$*•(BuCYA)*$_6$ *at 180 °C (right).*

It is important to notice that the assemblies **1b**$_3$•(DEB)$_6$ and **1b**$_3$•(BuCYA)$_6$ have very different isotropization temperatures ($T_{isoBuCYA}$-T_{isoDEB} = 60°C). Cyanurate derivatives form stronger hydrogen bonds with melamines than barbiturates[52] resulting in the higher thermal stability of the **1b**$_3$•(BuCYA)$_6$. Furthermore, cyanurates have a nitrogen atom with trigonal geometry at position 5 of the heterocycle. As a result the butyl group and the heterocycle are in the same plane. Consequently, the rosette floors with BuCYA can be seen as flat surfaces, leading to good stacking of the double rosette assemblies in the columnar phase. On the other hand, barbiturates have a carbon atom with a tetrahedral

geometry at the 5 position. As molecular simulation studies suggest (Quanta 97, CHARMm 24.0),[54] the ethyl groups point to the top and the bottom of the rosette floor, and this may weaken the interaction between two double rosette assemblies which may also contribute to a lower thermal stability.

The X-ray powder diffraction pattern for the columnar phase of the double rosette assembly **1b**$_3$•(DEB)$_6$ is shown in Figure 3.6. In the small angle region, the relatively sharp reflections of 37.3 Å (1,0,0), 21.9 Å (1,1,0), 19.1 Å (2,0,0) and 14.0 Å (2,1,0) are characteristic of the hexagonal structure. A reflection of 8.4 Å corresponds to the distance between two floors of two different assemblies. In the wide angle region, the diffuse halo of around 4.7 Å is due to the disorder of the terminal alkyl chains, and this is characteristic of the liquid-like arrangement of the aliphatic chains.

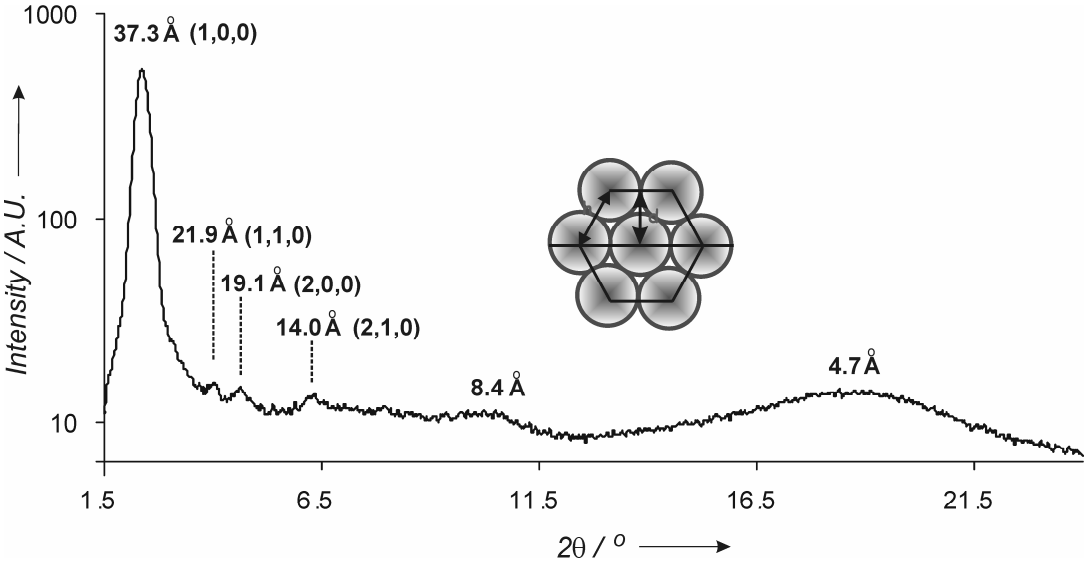

Figure 3.6. *X-ray diffraction intensity versus 2θ of* ***1b***$_3$•*DEB*$_6$ *at 120 °C, and schematic representation of the liquid crystalline hexagonal columnar organization of the double rosette assemblies. Reflections are indexed using Miller indices (hkl)*

The double rosettes pile up in an ordered columnar fashion. The driving force is the nanoscale segregation between the two flat rosette motifs and the lipophilic alkyl chains that leads to the formation of the self-assembled columnar double rosettes.[34,55] The intercolumnar distance (h) is 43.0 Å (Figure 3.6).[56] A similar value for this distance was found for same type of assemblies by AFM.[57] Their deposition on highly ordered

pyrolytic graphite (HOPG) showed that the double rosette assemblies self-organize in rodlike structures by face-to-face arrangement. A hierarchical process leads to the formation of the self-assembled double rosettes that assemble into columns, which are able to self-organize into a liquid crystalline phase with a hexagonal columnar morphology, as demonstrated by X-ray diffraction.

The double rosette **1b**$_3$•(BuCYA)$_6$ shows the same X-ray diffraction pattern observed for **1b**$_3$•(DEB)$_6$, which indicates that the side chain groups of these barbituric and cyanuric derivatives do not interfere with the self-organization and packing. This is probably caused by the large dimensions of the rosette core scaffold when compared to the small size of the side groups.[42]

3.5. Conclusions

Herein we have demonstrated that self-assembled molecular boxes **1b**$_3$•(DEB)$_6$ and **1b**$_3$•(BuCYA) are able to form liquid crystals. The strength of the hydrogen bonds and the spatial disposition of the side groups of the barbituric and cyanuric derivative are crucial factors in the stability of the mesophase. The lateral substitution on the building blocks seems not to affect the hierarchical organization of the mesophase. To the best of our knowledge, there are no examples in literature of well-defined hydrogen-bonded structures that show one LC phase over such a wide temperature range.[58] The remarkable thermal stability and the good ordering together with the easy introduction of chemical diversity in these self-assembled receptors[59,60] make them a good platform for nanomaterials.

3.6. Experimental Section

All chemicals were of reagent grade and used without further purification. CH_2Cl_2 was freshly distilled from $CaCl_2$. NMR spectra were recorded on Varian Unity 300 and 400 (^{1}H NMR 300 MHz and 400 MHz) using tetramethylsilane (TMS) or the corresponding residual solvent as internal standard. MALDI-TOF mass spectra were recorded on a PerSpective Biosystem Voyager-De-RP spectrometer. A 337 nm UV nitrogen laser producing 3 ns pulses was used in the linear and reflection mode. A Perkin-

Elmer DSC-7 was used for thermal analysis. DSC measurements were performed on a DSC Piris Series 7 (scanning rate: 10 °C min^{-1}). A polarizing optical microscope Olympus BH-2 equipped with a Mettler FP82HT hot stage was used for visual observation.

The molecular arrangements in different samples were analyzed with an X-ray diffractometer equipped with a home-built capillary oven. Each sample was placed into X-ray capillary with 1.0 mm internal diameter and then the capillary tube placed inside a vertically aligned graphite tube containing a hole transversal to it, allowing the incident X-ray beam to cross freely. The temperature of the graphite tube was controlled by a system formed by a thermo-couple attached to a power supply and it acts as a fast-response online oven ranging from room temperature to 350 ºC. The X-ray measurements were carried out in a Bruker-Nonius D8 diffractometer with a 2-D detector with a sample-to-detector distance set to 10 cm, and spectra were recorded for 1 h. A focused permanent magnetic field of approximately 4 T was applied perpendicular to the capillary allowing for alignment of any liquid crystal phase. CD measurements were conducted on a JASCO J-715 spectropolarimeter using a Mettler FP82HT hot stage. Transparent thin films of a chiral double rosette assemblies were prepared by casting its toluene solutions (conc. = 1 mM) on quartz plates.

Synthesis. The syntheses of the compounds **1a**,[50] **2**,[37] BuCYA[44] and (R)-MePropCYA[61] have been reported previously.

Calix[4]arene bis(3,4,5-tris(*n*-octadecan-1-yloxy)phenyl)dimelamine (1b): A solution of **2** (534 mg, 0.58 mmol), HBTU (238 mg, 0.063 mmol), DIPEA (0.19 mL, 1.10 mmol) and **1a** (255 mg, 0.26 mmol) in CH_2Cl_2 / DMF ratio 4:1 was stirred overnight at room temperature. The solvent was evaporated and the crude residue was solubilized again in CH_2Cl_2. MeOH was added till complete precipitation. The precipitate was filtered off and purified by column chromatography ($CHCl_3$:MeOH:AcOEt = 95:4:1). **1b** was crystallized by $CHCl_3$/MeOH to give a white powder (60%). ^{1}H NMR (300 MHz, $CDCl_3$, 298K) δ=7.48 (br m, 2H, CH_2NHCO), 7.05 (br m, 8H, CO*o*-ArH + *m*-ArH), 6.85 (br m, 2H, *o*-ArH), 6.17 (br m, 4H, *o*-NHAr), 5.30-4.88 (br, 4H, NH), 4.41 and 3.10 (ABq, 8H,

$^2J_{HH}$=12.5 Hz, $ArCH_2Ar$), 3.96 (s m, 18H, OCH_2+$NHCH_2$ + $ArO\underline{CH_2}\text{-}CH_2$), 3.644 (s t, 4H, OCH_2), 3.40 (br m, 8H, $NH\underline{CH_2}$ + $O\underline{CH_2}$-CH2), 2.11 (br m, 4H, NH-CH_2-$\underline{CH_2}$-CH_2-NH), 1.9 (s m, 8H, OCH_2-$\underline{CH_2}$), 1.43 (br, m, 12H, $ArOCH_2$-$\underline{CH_2}$-CH2), 1.25 (s m, 90H, $ArOCH_2$-CH_2-$(\underline{CH_2})_{15}$-CH_3), 1.08 (s t, 6H, OCH_2-CH_2-$\underline{CH_3}$), 0.87 (s t, 24H, $ArOCH_2$-CH_2-$(CH_2)_{15}$-$\underline{CH_3}$ + OCH_2-CH_2-$\underline{CH_3}$). MS (MALDI-TOF): m/z 2774.6 (100) ([M+H^+], Elemental Analysis calcd (%) for $C_{174}H_{294}N_{14}O_{12}$.: C, 75.33; H, 10.68; N, 7.07; found: C, 75.54; H, 10,72; N, 7.11.

Formation of $\mathbf{1b_3}$•(DEB) $_6$, $\mathbf{1b_3}$•$\mathbf{(BuCYA)_6}$, and $\mathbf{1b_3}$•$\mathbf{((R)\text{-}MePropCYA)_6}$: Hydrogen-bonded assemblies $\mathbf{1b}_3$•$(DEB)_6$ and $\mathbf{1b}_3$•$(BuCYA)_6$ were prepared by mixing calix[4]arene dimelamine **1b** with 2 equivalents of DEB or BuCYA in toluene-d_8 for 15 min. After evaporation of the solvent under high-vacuum, the assembly is ready for use.

Assembly $\mathbf{1b_3}$•$\mathbf{(DEB)_6}$: ^{1}H NMR (400 MHz, toluene-d_8, 298 K) δ= 14.64 (s, 6H, H_a), 13.84 (s, 6H, H_b), 8.77 (s, 6H, H_c), 7.99 (s, 6H, H_d), 7.47 (s, 6H, H_g), 7. 40-7.39 (m, 12H, ^3J(H,H)=6.78 Hz, H_e + ArH), 7.25-7.22 (m, 12H, H_f + ArH), 7.15 (s, 12H, *o*-ArH), 7.04 (m, 6H, ^3J(H,H)=6.78 Hz ArH), 6.34 (s, 6H, Hh), 5.92 (s, 6H, CH_2-$\underline{NH}$-CO), 4.65-4.57 (dd, 12H, ^3J(H,H)=13.4 Hz, $ArCH_2Ar$), 4.10 (t, 12H, $ArO\underline{CH_2}$), 3.95 (m, 6H, NH-$\underline{CH_2}$-CH_2), 3.77 (t, 24H, $ArO\underline{CH_2}$), 3.16 (d 6H, ^3J(H,H)=13.4 Hz, $ArCH_2Ar$).

Assembly $\mathbf{1b_3}$•$\mathbf{(BuCYA)_6}$: ^{1}H NMR (400 MHz, toluene-d_8, 298K) δ= 15,13 (s, 6H, H_a), 14,54 (s, 6H, H_b), 9,27 (s, 6H, H_c), 8.28 (s, 6H, H_e), 8.10 (s, 6H, H_f), 7.64 (s, 6H, H_g) 7.39 (d, 6H, ArH), 7.34 (s, 12H, *o*-ArH), 7.29 (d, 6H, ^3J(H,H)=7.04 Hz, ArH), 7.09 (t, 6H, ArH), 7.04 (m, 6H, ^3J(H,H)=7.04 Hz, ArH), 6.71 (s, 6H, CH_2-$\underline{NH}$-CO), 6.34 (s, 6H, H_h), 4.65-4.57 (dd, 12H, ^3J(H,H)=14.17 Hz $ArCH_2Ar$), 4.12 (t, 12H, $ArO\underline{CH_2}$), 3.85 (t, 24H, $ArO\underline{CH_2}$), 3.34-3.16 (dd 12H, ^3J(H,H)=14.17 Hz, $ArCH_2Ar$).

Assembly $\mathbf{1b_3}$•$\mathbf{((R)\text{-}MePropCYA)_6}$: ^{1}H NMR (400 MHz, toluene-d_8, 298K) δ= 15,19 (s, 6H, H_a), 14,04 (s, 6H, H_b), 9,17 (s, 6H, H_c), 8.09 (s, 6H, H_e), 8.02 (s, 6H, H_f), 7.69 (s, 6H, H_g) 7.49 (d, 6H, ^3J(H,H)=6.87 Hz, ArH), 7.35 (d, 6H, ^3J(H,H)=6.87 Hz, ArH), 7.20 (s, 12H, *o*-ArH), 6.35 (s, 6H, H_h),6.04 (s, 6H, CH_2-$\underline{NH}$-CO), 5.07 (q, 6H, N-$\underline{CH}$-CH_2CH_3) 4.69-4.64 (dd, 12H, ^3J(H,H)=10.72 Hz, $ArCH_2Ar$), 4.15 (t, 12H, $ArO\underline{CH_2}$), 3.37-3.26 (dd 12H, ^3J(H,H)=14.50 Hz, $ArCH_2Ar$).

3.7 References and Notes

[1] J.-M. Lehn, *Supramolecular Chemistry, Concepts and Perspectives*, VCH, Weinheim, Germany, **1995**.

[2] D. N. Reinhoudt, *Supramolecular Materials and Technologies*, Wiley & Sons, Chichester, **1999**.

[3] L. J. Prins, D. N. Reinhoudt, P. Timmerman, *Angew. Chem. Int. Ed.* **2001**, *40*, 2383-2426.

[4] D. N. Reinhoudt, M. Crego-Calama, *Science* **2002**, *295*, 2403-2407.

[5] D. Demus, J. W. Goodby, G. W. Gray, H. W. Spiess, V. Vill, *Handbook of Liquid Crystals*, VCH, Chichester, **1998**.

[6] N. M. K. K. Takashi Kato, *Angew. Chem. Int. Ed.* **2006**, *45*, 38-68.

[7] T. Kato, *Struct. Bond.* (Berlin) **2000**, *96*, 95-146.

[8] C. M. Paleos, D. Tsiourvas, *Liq. Cryst.* **2001**, *28*, 1127-1161.

[9] G. Floudas, P. Papadopoulos, H. A. Klok, G. W. M. Vandermeulen, J. Rodriguez-Hernandez, *Macromolecules* **2003**, *36*, 3673-3683.

[10] T. Kato, J. M. J. Frèchet, P. G. Wilson, T. Saito, T. Uryu, A. Fujishima, C. Jin, F. Kaneuchi, *Chem. Mater.* **1993**, *5*, 1094-1100.

[11] C. A. Schalley, *Adv. Mater.* **1999**, *11*, 1535-1537.

[12] J. W. Xu, C. L. Toh, X. M. Liu, S. F. Wang, C. B. He, X. H. Lu, *Macromolecules* **2005**, *38*, 1684-1690.

[13] T. Kato, T. Matsuoka, M. Nishii, Y. Kamikawa, K. Kanie, T. Nishimura, E. Yashima, S. Ujiie, *Angew. Chem. Int. Ed.* **2004**, *43*, 1969-1972.

[14] S. Jin, Y. G. Ma, S. C. Zimmerman, S. Z. D. Cheng, *Chem. Mater.* **2004**, *16*, 2975-2977.

[15] Q. Miao, T. Q. Nguyen, T. Someya, G. B. Blanchet, C. Nuckolls, *J. Am. Chem. Soc.* **2003**, *125*, 10284-10287.

[16] A. Sautter, C. Thalacker, F. Wurthner, *Angew. Chem. Int. Ed.* **2001**, *40*, 4425-4428.

[17] J. van Gestel, A. R. A. Palmans, B. Titulaer, J. Vekemans, E. W. Meijer, *J. Am. Chem. Soc.* **2005**, *127*, 5490-5494.

[18] M. Suarez, J.-M. Lehn, S. C. Zimmerman, A. Skoulios, B. Heinrich, *J. Am. Chem. Soc.* **1998**, *120*, 9526-9532.

[19] G. Proni, G. P. Spada, G. Gottarelli, F. Ciuchi, P. Mariani, *Chirality* **1998**, *10*, 734-741.

[20] S. Bonazzi, M. M. Demorais, G. Gottarelli, P. Mariani, G. P. Spada, *Angew. Chem. Int. Ed.* **1993**, *32*, 248-250.

[21] J. Barberá, L. Puig, P. Romero, J. L. Serrano, T. Sierra, *J. Am. Chem. Soc.* **2005**, *127*, 458-464.

[22] K. Kanie, M. Nishii, T. Yasuda, T. Taki, S. Ujiie, T. Kato, *J. Mater. Chem.* **2001**, *11*, 2875-2886.

[23] A. Ciferri, *Liq. Cryst.* **2004**, *31*, 1487-1493.

[24] G. Ambrozic, J. Mavri, M. Zigon, *Macrom. Chem. Phys.* **2002**, *203*, 439-447.

[25] M. Ikeda, T. Nobori, M. Schmutz, J.-M. Lehn, *Chem. Eur. J.* **2005**, *11*, 662-668.

[26] J. Barbera, M. Bardaji, J. Jimenez, A. Laguna, M. P. Martinez, L. Oriol, J. L. Serrano, I. Zaragozano, *J. Am. Chem. Soc.* **2005**, *127*, 8994-9002.

[27] L. Brunsveld, E. W. Meijer, R. B. Prince, J. S. Moore, *J. Am. Chem. Soc.* **2001**, *123*, 7978-7984.

[28] J. Hirschberg, R. A. Koevoets, R. P. Sijbesma, E. W. Meijer, *Chem. Eur. J.* **2003**, *9*, 4222-4231.

[29] S. Yagai, T. Nakajima, K. Kishikawa, S. Kohmoto, T. Karatsu, A. Kitamura, *J. Am. Chem. Soc.* **2005**, *127*, 11134-11139.

[30] J. Barberá, L. Puig, J. L. Serrano, T. Sierra, *Chem. Mater.* **2004**, *16*, 3308-3317.

[31] L. J. Prins, C. Thalacker, F. Würthner, P. Timmerman, D. N. Reinhoudt, *Proc. Natl. Acad. Sci. U. S. A.* **2001**, *98*, 10042-10045.

[32] T. Giorgi, S. Lena, P. Mariani, M. A. Cremonini, S. Masiero, S. Pieraccini, J. P. Rabe, P. Samori, G. P. Spada, G. Gottarelli, *J. Am. Chem. Soc.* **2003**, *125*, 14741-14749.

[33] F. Ciuchi, G. Dinicola, H. Franz, G. Gottarelli, P. Mariani, M. G. P. Bossi, G. P. Spada, *J. Am. Chem. Soc.* **1994**, *116*, 7064-7071.

[34] M. Nishii, T. Matsuoka, Y. Kamikawa, T. Kato, *Org. Biomol. Chem.* **2005**, *3*, 875-880.

[35] D. M. Walba, E. Korblova, R. Shao, J. E. Maclennan, D. R. Link, M. A. Glaser, N. A. Clark, *Science* **2000**, *288*, 2181-2184.

[36] V. S. K. Balagurusamy, G. Ungar, V. Percec, G. Johansson, *J. Am. Chem. Soc.* **1997**, *119*, 1539-1555.

[37] V. Percec, C. H. Ahn, T. K. Bera, G. Ungar, D. J. P. Yeardley, *Chem. Eur. J.* **1999**, *5*, 1070-1083.

[38] V. Percec, W. D. Cho, P. E. Mosier, G. Ungar, D. J. P. Yeardley, *J. Am. Chem. Soc.* **1998**, *120*, 11061-11070.

[39] V. Percec, M. Glodde, T. K. Bera, Y. Miura, I. Shiyanovskaya, K. D. Singer, V. S. K. Balagurusamy, P. A. Heiney, I. Schnell, A. Rapp, H. W. Spiess, S. D. Hudson, H. Duan, *Nature* **2002**, *419*, 384-387.

[40] G. Ungar, Y. Liu, X. Zeng, V. Percec, W.-D. Cho, *Science* **2003**, *299*, 1208-1211.

[41] V. Percec, M. Peterca, M. J. Sienkowska, M. A. Ilies, E. Aqad, J. Smidrkal, P. A. Heiney, *J. Am. Chem. Soc.* **2006**, *128*, 3324-3334.

[42] P. Timmerman, R. H. Vreekamp, R. Hulst, W. Verboom, D. N. Reinhoudt, K. Rissanen, K. A. Udachin, J. Ripmeester, *Chem. Eur. J.* **1997**, *3*, 1823-1832.

[43] R. H. Vreekamp, J. P. M. van Duynhoven, M. Hubert, W. Verboom, D. N. Reinhoudt, *Angew. Chem. Int. Ed.* **1996**, *35*, 1215-1218.

[44] L. J. Prins, K. A. Jolliffe, R. Hulst, P. Timmerman, D. N. Reinhoudt, *J. Am. Chem. Soc.* **2000**, *122*, 3617-3627.

[45] L. J. Prins, J. Huskens, F. de Jong, P. Timmerman, D. N. Reinhoudt, *Nature* **1999**, *398*, 498-502.

[46] L. J. Prins, R. Hulst, P. Timmerman, D. N. Reinhoudt, *Chem. Eur. J.* **2002**, *8*, 2288-2301.

[47] K. A. Jolliffe, P. Timmerman, D. N. Reinhoudt, *Angew. Chem. Int. Ed.* **1999**, *38*, 933-937.

[48] P. Timmerman, K. A. Jolliffe, M. Crego-Calama, J. L. Weidmann, L. J. Prins, F. Cardullo, B. H. M. Snellink-Rüel, R. H. Fokkens, N. M. M. Nibbering, S. Shinkai, D. N. Reinhoudt, *Chem. Eur. J.* **2000**, *6*, 4104-4115.

[49] H. J. van Manen, V. Paraschiv, J. J. Garciá-López, H. Schönherr, S. Zapotoczny, G. J. Vancso, M. Crego-Calama, D. N. Reinhoudt, *Nano Lett.* **2004**, *4*, 441-446.

[50] J. Kerckhoffs, M. Crego-Calama, I. Luyten, P. Timmerman, D. N. Reinhoudt, *Org. Lett.* **2000**, *2*, 4121-4124.

[51] V. Paraschiv, M. Crego-Calama, R. H. Fokkens, C. J. Padberg, P. Timmerman, D. N. Reinhoudt, *J. Org. Chem.* **2001**, *66*, 8297-8301.

[52] A. G. Bielejewska, C. E. Marjo, L. J. Prins, P. Timmerman, F. de Jong, D. N. Reinhoudt, *J. Am. Chem. Soc.* **2001**, *123*, 7518-7533.

[53] M. L. Bushey, T. Q. Nguyen, C. Nuckolls, *J. Am. Chem. Soc.* **2003**, *125*, 8264-8269.

[54] M. G. J. ten Cate, J. Huskens, M. Crego-Calama, D. N. Reinhoudt, *Chem. Eur. J.* **2004**, *10*, 3632-3639.

[55] T. Kato, *Science* **2002**, *295*, 2414-2418.

[56] The intercolumnar distance is calculated by the formula $h=d/\cos(\pi/6)$, where d is the reflection (1,0,0), corresponding to the distance between two double rosette layers.

[57] H. A. Klok, K. A. Jolliffe, C. L. Schauer, L. J. Prins, J. P. Spatz, M. Möller, P. Timmerman, D. N. Reinhoudt, *J. Am. Chem. Soc.* **1999**, *121*, 7154-7155.

[58] I. Paraschiv, M. Giesbers, B. vanLagen, F. C. Grozema, R. D. Abellon, L. D. A. Siebbeles, A. T. M. Marcelis, H. Zuilhof, E. J. R. Sudhölter, *Chem. Mater.* **2006**, *18*, 968-974.

[59] M. A. Mateos-Timoneda, M. Crego-Calama, D. N. Reinhoudt, *Supramol. Chem.* **2005**, *17*, 67-79.

[60] J. M. C. A. Kerckhoffs, F. W. B. van Leeuwen, A. L. Spek, H. Kooijman, M. Crego-Calama, D. N. Reinhoudt, *Angew. Chem. Int. Ed.* **2003**, *42*, 5717-5722.

[61] J. M. C. A. Kerckhoffs, M. G. J. ten Cate, M. A. Mateos-Timoneda, F. W. B. van Leeuwen, B. Snellink-Ruël, A. L. Spek, H. Kooijman, M. Crego-Calama, D. N. Reinhoudt, *J. Am. Chem. Soc.* **2005**, *127*, 12697-12708.

Chapter 4

Supramolecular Chirality in Mesogenic Hydrogen-Bonded Molecular Assemblies

In this chapter the supramolecular chirality of mesogenic double rosette assemblies in solution and the liquid crystalline state is described. The chirality of the double rosettes in solution is transferred to the liquid crystalline state, as demonstrated by circular dichroism measurements. In the mesophase different orientations of the columns along the stacking direction are obtained depending on the nature of the building blocks of the assembly. Formation of a gel phase is described for double rosettes.

4.1 Introduction

Chirality in liquid crystals[1] is a topic that attracts a great deal of interest in materials science due to the possibility of achieving highly organized functional supramolecular organizations. Chiral helical organizations provide a way to achieve properties, such as nonlinear optics[2,3] and selective reflection of light,[4, 5] that result from a preferred direction i.e. the helical axis. Columnar mesophases are good candidates for the new generation of functional materials through a helical arrangement of these structured materials using a two-fold organization process. First, a preferred direction is defined within the columns. Second, twisting the columns to a given sense dictated by the chirality defined at the molecular level,[6-12] introducing properties that originate from a helical organization.

The formation of columnar mesophases is usually achieved by self-assembly of disk-like mesogens through the use of noncovalent interactions, in particular hydrogen bonding and π-π interactions.[13-18] The combination of these two interactions has led to the formation of new functional liquid crystalline materials.[19,20] In particular hydrogen bonds have a predominant role in the formation of liquid crystalline materials through their employment in the "synthesis" of new dynamic mesogenic compounds[21-25] able to form columnar aggregates with different properties.[26-28] Furthermore, hydrogen bonds through their directionality can be used to transfer the chirality from the mesogenic molecules to columnar organization.[29,30] In Chapter 3 the liquid crystallinity for achiral hydrogen-bonded 3D nano-objects is described, where the assemblies aggregate in a hexagonal columnar mesophase. This organization is due to the microsegration between the polar core of the assembly and the lipophilic character at the periphery (Chapter 3). This chapter deals with chiral hydrogen-bonded nano-objects that aggregate in a chiral columnar fashion showing liquid crystalline behavior and gel formation depending on the conditions, such as temperature and concentration. The bulkiness of the functional groups on the building blocks (barbiturates and cyanurates) of the assembly is responsible for the double rosette formation and consequently for the mesophase. The strength of the hydrogen bonds is responsible for the column orientation in the mesophase. The transfer

of the chirality from the molecular level to the liquid crystalline phase is investigated by circular dichroism.

4.2. Constitutional Isomers of Assemblies 1_3•$(BAR)_6$/1_3•$(CYA)_6$

Double rosette assemblies $\mathbf{1}_3$•$(BAR)_6$/$\mathbf{1}_3$•$(CYA)_6$ are formed from calix[4]arene **1** and barbiturates (BAR) or cyanurates (CYA) by self-assembly in apolar solvents. The assemblies are composed of two flat rosette motifs that are covalently connected via calix[4]arene moieties (Fig. 4.1). In general, depending of the substitution on the building blocks, three constitutionally different isomers either with D_3-, C_{3h}-, or C_s-symmetry can be obtained (see Chapter 3).

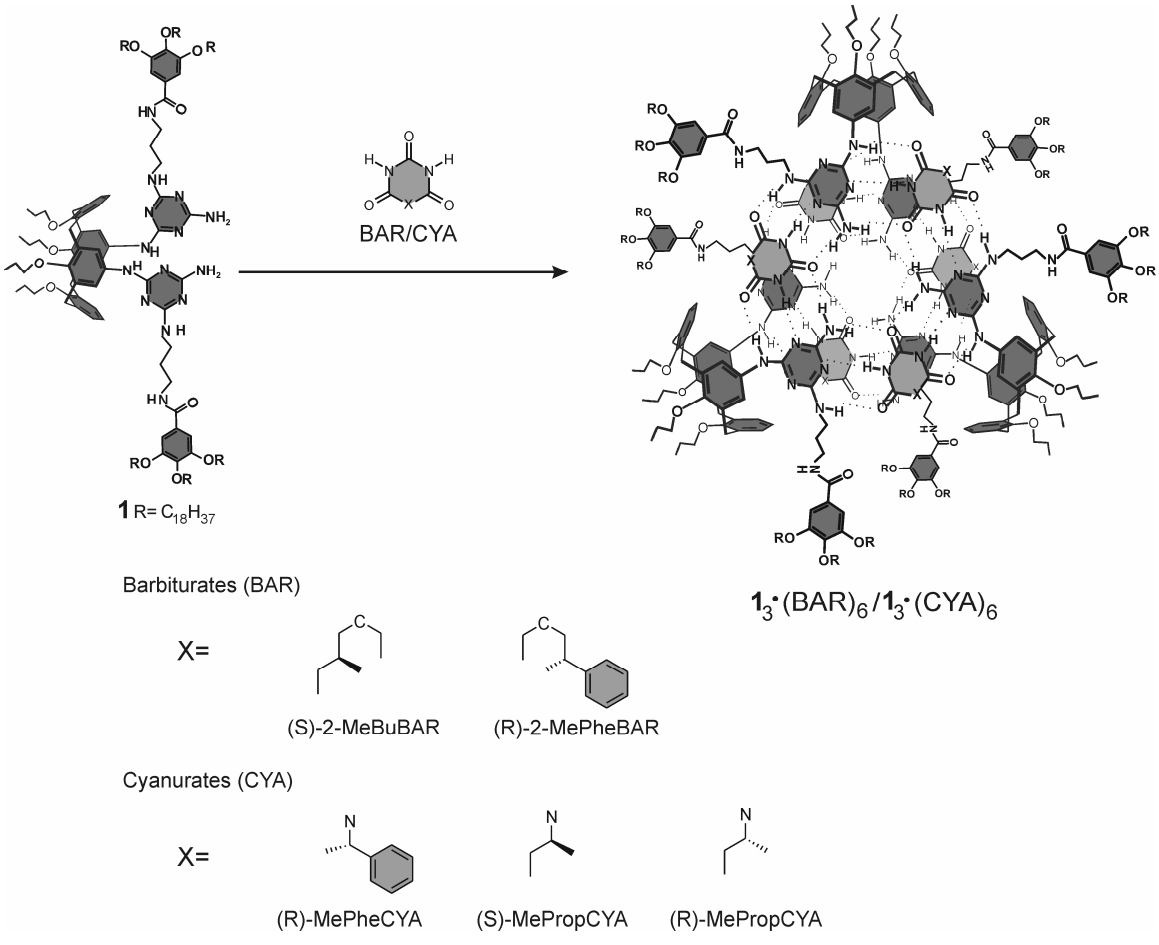

Figure 4.1. *Molecular structure of the double rosettes* $\mathbf{1_3}$•$(BAR)_6$/$\mathbf{1_3}$•$(CYA)_6$

In the D_3-isomer the two melamine fragments of **1** are in a staggered orientation with respect to each other. Since the orientation can be clockwise (P) or counterclockwise (M), this causes the assembly to be chiral (Fig. 4.2). The D_3-isomer is formed as a racemic mixture of (*M*)- and (*P*)-enantiomers when **1** and BAR/CYA are achiral. Assemblies with a single handedness are formed when either **1** or BAR/CYA contains chiral center.[31] The C_{3h}- and C_s-isomers, in which the two melamine fragments of **1** are in an eclipsed orientation, have a plane of symmetry and are therefore achiral (Fig. 4.2). The C_{3h}- and C_s-isomers differ in the sense that the C_s-isomer lacks a C_3-axis, because of a 180° rotation of one of the dimelamines **1** (see Chapter 3).

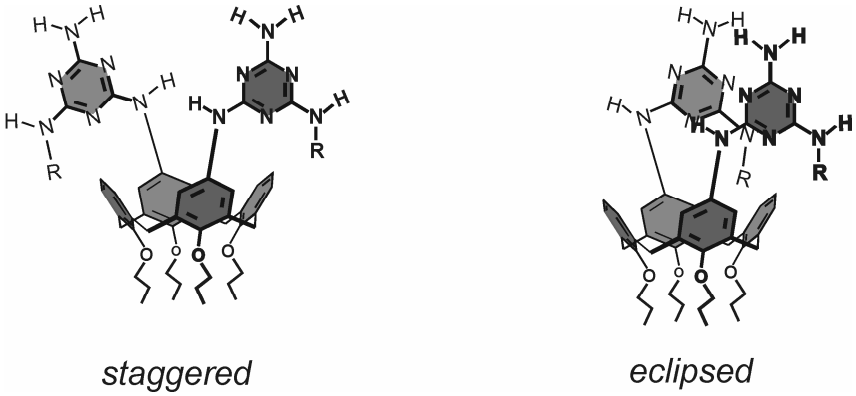

Figure 4.2. *Staggered and eclipsed orientation of the two melamine fragments of calix[4]arene dimelamine **1**.*

4.3 Results and Discussion

In Chapter 3 the liquid crystal behavior of achiral double rosettes having long alkyl chains on the substituted calix[4]arene **1** was discussed. These achiral double rosettes organize in a columnar fashion in the mesophase with a remarkable thermal stability taking into account their noncovalent nature. Here, chiral double rosettes were prepared in order to produce chiral liquid crystals. With the aim of controlling the chiral self-assembly and self-organization of the double rosettes in the mesophase, structural variations within the building blocks have been introduced in the chiral barbiturates and cyanurates. For this reason, double rosette assemblies containing dimelamine calix[4]arene **1** and either barbiturate derivates (S)-2-MeBuBAR and (R)-2-MePheBAR,

or cyanurate derivates, (S)-MePropCYA, (R)-MePropCYA and (R)-MePheCYA have been prepared (Fig. 4.1).

4.3.1 Synthesis

Dimelamine calix[4]arene derivative **1**, (R)-2-MePheBAR, (R)-MePropCYA, (S)-MePropCYA, and (R)-MePheCYA were synthesized following literature procedures.[19, 32, 33] Chiral barbiturate (S-2-MeBuBAR) was prepared in two steps. In the first step, the alkylation of diethyl ethylmalonate with (S)-(+)-bromo-2-methylbutane in dry THF yields compound (S)-**4**. In the second step, the ring closure of (S)-**4** with urea in the presence of sodium ethoxide gave (S)-2-MeBuBAR in overall yield of 14% (Scheme 4.1).

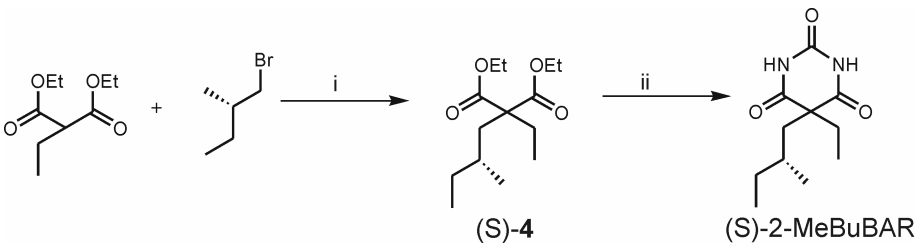

Scheme 4.1*. Synthesis of the barbituric derivative (S)-2-MeBuBAR: i. NaH, dry THF; ii. urea, NaOEt, ethanol.*

4.3.2 Liquid crystallinity

The formation of double rosette assemblies $\mathbf{1}_3$•((S)-2-MeBuBAR)$_6$, $\mathbf{1}_3$•((S)-MePropCYA)$_6$, $\mathbf{1}_3$•((R)-MePropCYA)$_6$, and $\mathbf{1}_3$•((R)-MePheCYA)$_6$ was confirmed by ^{1}H NMR in solution. Surprisingly, the double rosette assembly was not formed when (R)-2-MePheBAR was employed as the building block. The bulky phenyl group in the β-position at the C-5 atom in the barbituric ring may interfere with the formation of the rosette motif. The complete induction of the supramolecular chirality for the assemblies $\mathbf{1}_3$•(S-2-MeBuBAR)$_6$, $\mathbf{1}_3$•((S)-MePropCYA)$_6$, $\mathbf{1}_3$•((R)-MePropCYA)$_6$ and $\mathbf{1}_3$•((R)-MePheCYA)$_6$ was confirmed by circular dichroism (CD) spectroscopy (Fig. 4.3). As mentioned before, the introduction of chiral centers in one of the molecular components of the assemblies (in this case the barbiturate and cyanurate) leads to the formation of only one diasteroisomer with a diastereomeric excess (*d.e.*) up to 96%.[31,33]

The CD signal from 275-350 nm for the double rosette assemblies (1.0 mM, toluene) was due to the asymmetric arrangement of the chromophores in the assemblies. The intensity for the double rosette $\mathbf{1}_3$•((S)-2-MeBuBAR)$_6$ (Figure 4.3, curve a) was lower because the stereocenter is the β-position. CD activity is due to asymmetric arrangement of the chromophores in the assembly. This arrangement is induced by the stereocenters in the double rosette. If the stereocenter is far from the double rosette core, its influence is less pronounced with a consequent decrease of the intensity of the CD signal.[34] The CD intensity is also related to the number of chromophore units in the double rosette assemblies.[33] The latter explains the higher intensity of the CD signals of the phenyl-containing double rosette $\mathbf{1}_3$•((R)-MePheCYA)$_6$ compared to $\mathbf{1}_3$•((R)-MePropCYA)$_6$.

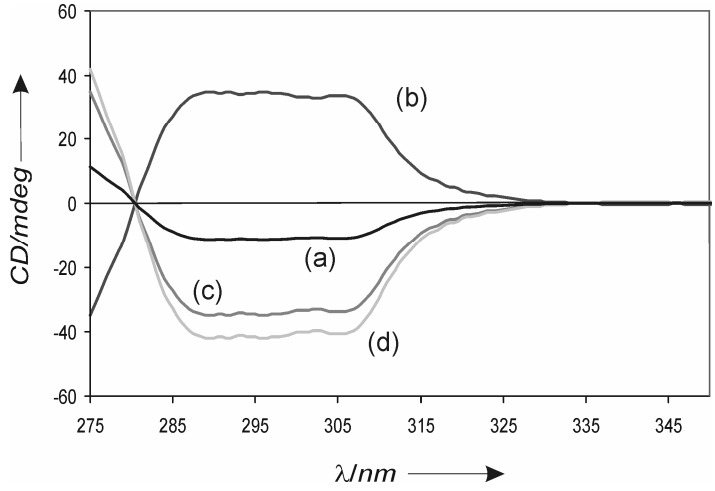

Figure 4.3. *CD spectra for the double rosette assemblies (a)* $\mathbf{1}_3$*•((S)-2-MeBuBAR)$_6$*, (b)* $\mathbf{1}_3$*•((S)-MePropCYA)$_6$*, (c)* $\mathbf{1}_3$*•((R)-MePropCYA)$_6$*, and (d)* $\mathbf{1}_3$*•((R)-MePheCYA)$_6$*. All spectra were recorded in toluene at a 1.0 mM concentration.*

The sign of the CD signal is related to the twist of the melamine fragments, which is dictated by the stereochemistry in the barbiturates and cyanurates. For example, in the case of the double rosette $\mathbf{1}_3$•((S)-MePropCYA)$_6$, the (S)-stereochemistry of the cyanurate leads to the (*M*)-diastereoisomer (Fig. 4.3, curve b), while the (R)-stereochemistry gives the (*P*)-diastereoisomer (Fig. 4.3, curve c), leading to a mirror image of the CD signal.

The thermal behavior of the double rosette assemblies has been determined by polarized optical microscopy (POM) and differential scanning calorimetry (DSC). Based

on polarized optical microscopy the liquid crystalline phase is attributed to a columnar mesophase. For $\mathbf{1}_3$•((S)-2-MeBuBAR)$_6$, $\mathbf{1}_3$•((R)-MePropCYA)$_6$ and $\mathbf{1}_3$•((S)-MePropCYA)$_6$ after cooling from the isotropic melt, a mosaic texture was observed showing birefringent areas, which is a strong indication that the mesophase is columnar (Fig. 4.4 a, b and c), as described in Chapter 3.

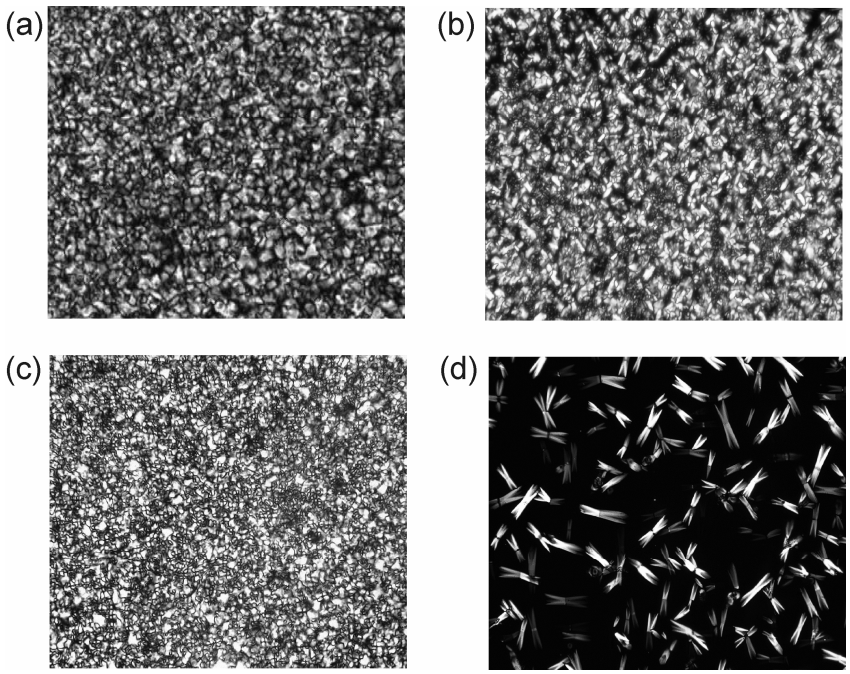

Figure 4.4. *Polarized optical microscopy images of the double rosettes (a) $\mathbf{1}_3$•(S-2-MeBuBAR)$_6$ at 130 °C, (b) $\mathbf{1}_3$•((R)-MePropCYA)$_6$ at 135 °C, (c) $\mathbf{1}_3$•((S)-MePropCYA)$_6$ at 135°C, and (d) $\mathbf{1}_3$•((R)-MePheCYA)$_6$ at 150°C.*

On the other hand, $\mathbf{1}_3$•(R-MePheCYA)$_6$ displays a crystalline phase after cooling from the isotropic state (Fig. 4.4d). The image shows isolated features, typical for crystal phases. Instead for liquid crystalline phases, the features are uniformly spread for the whole sample.[35]

The DSC thermogram of $\mathbf{1}_3$•(MePheCYA)$_6$ shows two transition peaks. The first transition is attributed to a crystal-crystal transition (Cr) by the high value of the enthalpy change (156 kJ mol^{-1}) (Table 1).[36]

Table 4.1: *Thermal properties of the double rosette* ***1***$_3$*•(R-MePheCYA)*$_6$*,* ***1***$_3$*•(S-2-MeBuBAR)*$_6$*,* ***1***$_3$*•((R)-MePropCYA)*$_6$*, and* ***1***$_3$*•((S)-MePropCYA)*$_6$*.*

Compound	Phase Transition[a]						
1$_3$•((R)-MePheCYA)$_6$	Cr	25	(156.5)	Cr	176	(54.1)	Iso
1$_3$•((S)-2-MeBuBAR)$_6$	Col_x	29	(12.7)	Col_h	146	(24.2)	Iso
1$_3$•((R)-MePropCYA)$_6$	Col_x	11	(0.30)	Col_h	157	(59.2)	Iso
1$_3$•((S)-MePropCYA)$_6$	Col_x	12	(0.32)	Col_h	156	(57.3)	Iso

[a] Phase transition temperatures (°C) and enthalpy changes (kJ mol^{-1} in parentheses)
Cr: crystalline; Col_x: unidentified columnar phase; Col_h: hexagonal columnar phase; Iso: isotropic

The second phase transition at higher temperature is due to a crystal-isotropic phase change, as demonstrated by POM. The presence of a crystalline phase for this assembly can be attributed to the phenyl group in the α-position with respect to the nitrogen atom in the 5-position of the cyanuric acid ring (Fig. 4.1). Probably, the packing of the double rosettes in the solid state can be stabilized by additional π-π interactions between phenyl groups of adjacent double rosettes as the high isotropization temperature suggests (Table 4.1). On the other hand, the assemblies **1**$_3$•((S)-2-MeBuBAR)$_6$, **1**$_3$•((S)-MePropCYA)$_6$, and **1**$_3$•((R)-MePropCYA)$_6$ showed liquid crystalline behavior (Table 4.1). The DSC showed two transition peaks for each assembly, **1**$_3$•(S-2-MeBuBAR)$_6$, **1**$_3$•((S)-MePropCYA)$_6$, and **1**$_3$•((R)-MePropCYA)$_6$. The first phase transitions at lower temperature were attributed to a reversible transition between an unidentified columnar phase (Col_x) and the hexagonal columnar phase (Col_h). However, differences between these two phases in the optical textures and X-ray diffractograms were not observed. The second transitions at higher temperature were due to the liquid crystalline-isotropic phase transition for the three double rosette assemblies.

As described in Chapter 3 for the achiral double rosettes, the thermotropic hexagonal columnar LC phase (29-146°C for **1**$_3$•(S-2-MeBuBAR)$_6$, 11-157°C for **1**$_3$•((R)-MePropCYA)$_6$, and 12-156°C for **1**$_3$•((S)-MePropCYA)$_6$) is exhibited over a wide temperature range by these three assemblies. This indicates a remarkable thermal stability

of the liquid crystalline phase considering the dimensions (1.2 nm height and 3.3 nm width)[37] and the noncovalent nature (twelve DAD•ADA interactions; D,A= hydrogen bond donor and acceptor, respectively) of the double rosette assembly. A small difference in isotropization temperature is observed (ΔT_{iso}= T_{isoCYA}-T_{isoBAR}= 10-11 °C) between the assemblies with barbiturate and cyanurate, which is very different from the achiral assemblies (ΔT_{iso}=60 °C) studied in Chapter 3. The difference in isotropization temperature can be attributed to the different strength of the hydrogen bonds between melamine and cyanurate (K_a= (2.2 ± 0.8) × 10^3 M^{-1} in $CDCl_3$) compared to barbiturate (K_a= (1.0 ± 0.1) × 10^2 M^{-1} in $CDCl_3$) in the assemblies. Simulations (Quanta 97, CHARMm 24.0) suggest that in the **1**$_3$•((R)-MePropCYA)$_6$ and **1**$_3$•((S)-MePropCYA)$_6$, the methyl groups of the cyanuric derivatives point out of the top floor of the assembly.[34] This may weaken the stacking interaction between these double rosettes when they stack in the mesophase. This effect might explain the difference in isotropization temperatures when compared to the achiral cyanurates the functional groups of which are in the plane of the double rosette floor, as observed in Chapter 3.

The X-ray powder diffraction pattern for the columnar phase of the double rosette assembly **1**$_3$•(S-2-MeBuBAR)$_6$ is shown in Figure 4.5a. In the small angle region, the relatively sharp reflections at 36.2 Å (1,0,0), 21.9 Å (1,1,0), 19.1 Å (2,0,0) and 11.5 Å (0,3,0) are characteristic of the hexagonal structure ($a= b\sqrt{3}$, where a and b are the lattice parameters). A reflection at 5.7 Å (0,0,1) corresponds to the distance between two floors of two different assemblies. In the wide angle region, the diffuse halo of around 4.8 Å is due to the disorder of the terminal alkyl chains. This is characteristic of the liquid-like arrangement of the aliphatic chains.

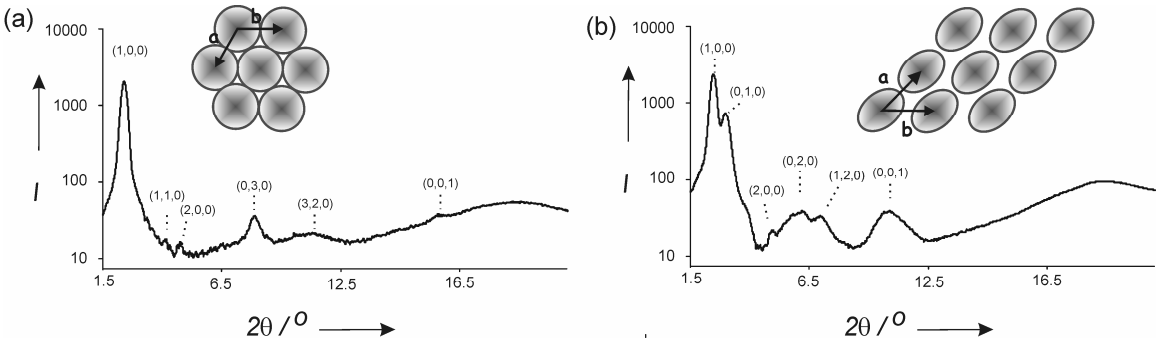

Figure 4.5. *X-ray diffraction intensity versus 2θ of (a)* $\mathbf{1}_3$*•(S-2-MeBuBAR)*$_6$ *at 120 °C, (b)* $\mathbf{1}_3$*•((S)-MePropCYA)*$_6$*, and schematic representation of their liquid crystalline hexagonal columnar organization. Reflections are indexed using Miller indices (hkl).*

Thus it can be concluded that the double rosettes stack in a columnar fashion. Probably the driving force is the nanoscale segregation between the two flat rosette motifs and the lipophilic alkyl chains that lead to the formation of the self-assembled columnar double rosettes, as mentioned in Chapter 3. The inter-columnar distance (*a*) is 42.0 Å (Fig. 4.5).[38]

The double rosette $\mathbf{1}_3$•((S)-MePropCYA)$_6$, as well as its enantiomer $\mathbf{1}_3$•((R)-MePropCYA)$_6$, organize in a columnar mesophase as shown by the X-ray diffraction pattern shown in Figure 4.5b. In the small angle region of the diffractogram, relatively sharp peaks appear corresponding of the reflection of 35.1 Å (1,0,0), 29.0 Å (0,1,0), 17.4 Å (2,0,0), 13.9 Å (0,2,0), and 12.0 Å (1,2,0). This set of reflections, is characteristic for pseudo-hexagonal ($a \approx b\sqrt{3}$) columnar phases where the columns are tilted by 30° with respect to the stacking direction. For the double rosette $\mathbf{1}_3$•((S)-MePropCYA)$_6$, the reflection of 8.8 Å (0,0,1) corresponds the distance between two floors of two different assemblies. In the wide angle region, the diffused halo of around 4.7 Å is due to the disorder of the terminal alkyl chains. The two double rosettes $\mathbf{1}_3$•((S)-2-MeBuBAR)$_6$ and $\mathbf{1}_3$•((R)-MePropCYA)$_6$ arrange in the same manner (hexagonal columnar) in the liquid crystalline phase. The difference is only in the orientation of the columns, i.e. perpendicular and tilted (30°) to the stacking direction in case of $\mathbf{1}_3$•(S-2-MeBuBAR)$_6$ and $\mathbf{1}_3$•((S)-MePropCYA)$_6$, respectively (Fig. 4.6).

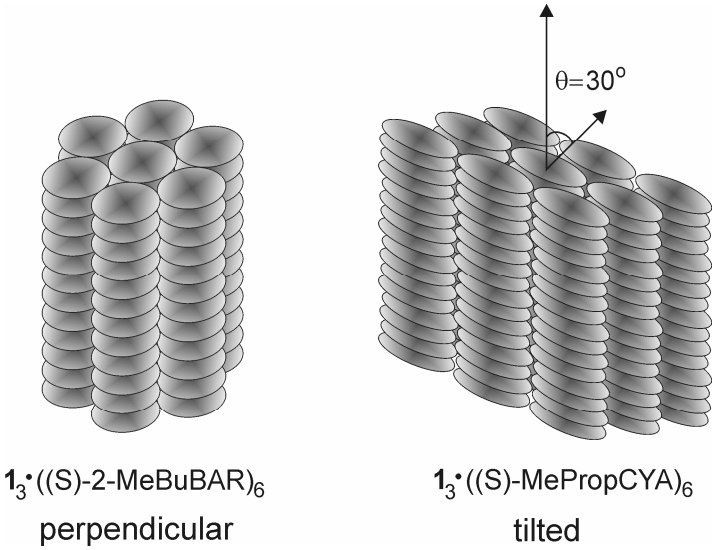

Figure 4.6. *Schematic representation of the orientation of the chiral mesogenic double rosettes in the liquid crystalline phase: perpendicular,* ***1***$_3$*•((S)-2-MeBuBAR)*$_6$*, and tilted,* ***1***$_3$*•((R)-MePropCYA)*$_6$*, to the column stacking direction*

As molecular simulation studies have suggested, the difference may be due to the orientation of the double rosette floors with cyanurates.[39] In these assemblies the hydrogen-bonded floors are not completely parallel to each other but they are convex due to the strong hydrogen bonds between the melamine and the cyanurate. Probably this leads to a tilting of the columns in the mesophase. Nevertheless, it is important to notice that the hydrogen bonds not only enable the formation of the mesogenic achiral double rosette, but they influence the spatial configuration of the double rosette, which determines the orientation of mesogenic molecules in the columns, and consequently the characteristics of the mesophase.

4.3.3 Circular dichroism in the liquid crystalline phase

To study the thermal stability of the mesogenic chiral double rosette assemblies **1**$_3$•((S)-2-MeBuBAR)$_6$, **1**$_3$•((R)-MePropCYA)$_6$, and **1**$_3$•((S)-MePropCYA)$_6$ in the liquid crystalline phase, and the induction of chirality from the single component (double rosette) to the mesophase, circular dichroism (CD) experiments were carried out. These experiments were performed on neat samples both at the temperature of the mesophases and of the isotropic state. The cells were allowed to cool avoiding external mechanical

stress. Linear dichroism effects were eliminated by averaging several CD spectra (recorded at different film positions rotated around the light beam). The CD spectra of the mesophases (Col_h) exhibited significant bands that correspond to absorption bands in the UV spectrum (Fig. 4.7).

The CD spectra of **1**$_3$•((S)-2-MeBuBAR)$_6$ and **1**$_3$•((R)-MePropCYA)$_6$ in the mesophase show a negative exciton splitting, whereas the CD spectrum of **1**$_3$•((S)-MePropCYA)$_6$ shows a positive exciton splitting (Fig. 4.7).

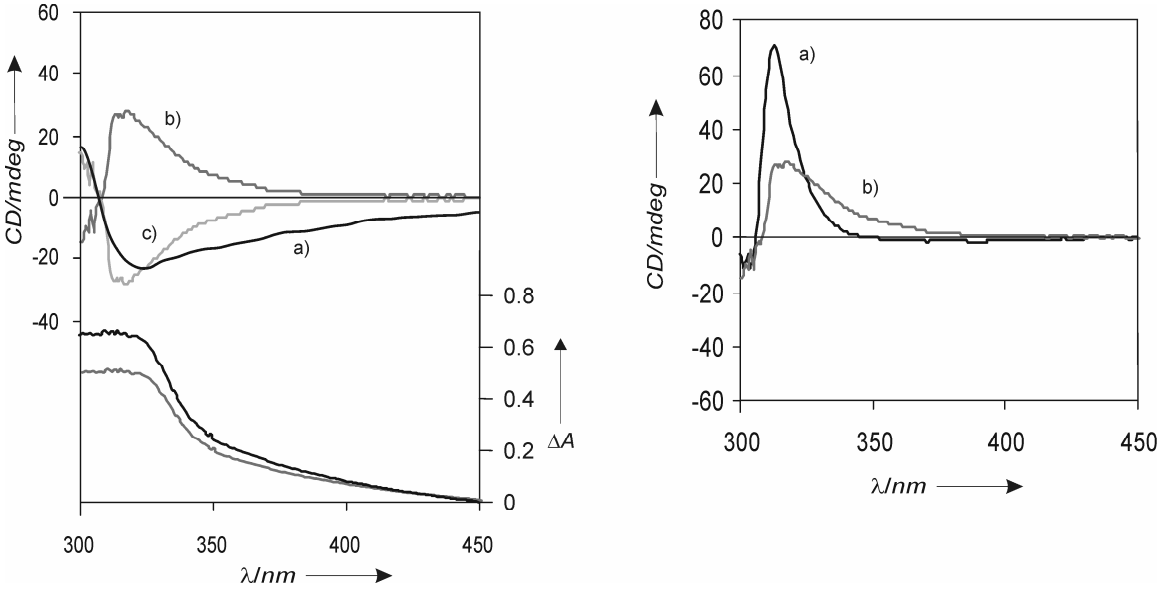

Figure 4.7. *Left image: CD (top) and UV-vis (bottom) spectra of the mesogenic double rosettes a)* ***1***$_3$*•(S-2-MeBuBAR)$_6$, b)* ***1***$_3$*•((S)-MePropCYA)$_6$ and c)* ***1***$_3$*•((R)-MePropCYA)$_6$. Right image: CD spectra for* ***1***$_3$*•((S)-MePropCYA)$_6$ in a) isotropic state and b) liquid crystalline state.*

These signals are centered at the wavelength of π-π* transition of the chromophores. In the spectrum a Cotton effect is visible, corresponding to a shoulder in each of the UV spectra at 325 nm (Fig. 4.7). The results confirm the existence of a helical arrangement within the columns. The (*P*)- or (*M*)-helicity of the columns in the mesophase is determined by the handedness of the double rosette itself, which depends of the stereochemistry of the chiral center (see also Section 4.2.2). For example, the double rosette **1**$_3$•((S)-MePropCYA)$_6$ has (*M*)-helicity that is reflected in the same handedness in the mesophase (Fig. 4.7). It is worth to note that these CD signals are also found for the double rosette in the isotropic state (Fig. 4.7). This indicates a large thermal stability of

double rosettes. This is a remarkable result taking into account that generally for supramolecular chiral systems in the isotropic state no CD signal is present.[29,30,40] On the other hand, the double rosette is intact with a signal of higher intensity than in the mesophase state, probably due to the optimal conformation of the chromophores in the isotropic state.

4.3.4 Self-assembled gels

Supramolecular columnar aggregates are usually associated with the formation of macroscopic gels by low mass molecules in different solvents.[41,42] Here, a gel phase is described for the chiral double rosettes $\mathbf{1}_3$•((R)-MePropCYA)$_6$ and $\mathbf{1}_3$•((S)-MePropCYA)$_6$ in n-alkane solvents such as tetradecane, dodecane, and octane. Generally the formation of supramolecular gels is associated with the stacking of relatively small molecules which have great tendency to aggregate through solvophobic interactions.[17,43,44] Therefore the presence of a supramolecular gel is remarkable taking into account the nanometer dimensions of the double rosette (1.2 nm height and 3.3 nm width) and the molecular weight (~ 10000 g mol^{-1}).

The gels were made in a vial by dissolving the double rosettes in the hot apolar solvents and subsequent cooling. The double rosette was considered in the gel state when no gravitational flow was observed after turning of the vials (Fig 4.8b).

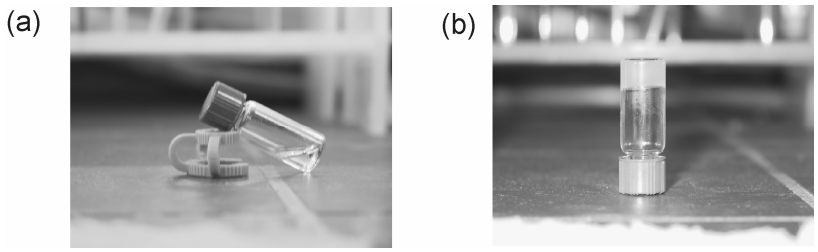

Figure 4.8. *Pictures of the double rosette $\mathbf{1}_3$•((R)-MePropCYA)$_6$ in a) liquid state and b) gel state.*

By this method minimum gel forming concentrations were determined. Depending on the number of the carbon atoms in the solvent, the minimum concentration varied for the double rosettes, going from 47.5 mg/mL (5.0 mM) for tetradecane (n= 14) to 142.5 mg/mL (15.0 mM) for octane (n= 8). It is important to note that only in the case of the

chiral double rosettes the formation of a gel was obtained, whereas neither the achiral double rosettes nor the single building blocks led to the formation of a gel phase. The explanation is still unclear,[44] but it might be due to how the solvent interacts with the surface of the gel fibers.[43] Unfortunately, the characterization of the gel morphology by transmission electron microscopy (TEM) and scanning electron microscopy (SEM) was impossible due to the nature of the solvents that did not allow a good resolution of the fibers. However, the formation of columns in the liquid crystalline state (see section 4.2.2) and the fiber organization on solid support (Chapter 6) are good indications of fiber formation for the double rosette assemblies $\mathbf{1}_3$•((R)-MePropCYA)$_6$ and $\mathbf{1}_3$•((S)-MePropCYA)$_6$. Another proof for the fiber formation in the gel state comes from ^{1}H NMR spectra in deuterated dodecane at 10 mM. As expected the signals of the double rosette assembly $\mathbf{1}_3$•((S)-MePropCYA)$_6$ in the gel state are hardly visible because the assembly is in an aggregated state.[45] When the temperature is increased at 80°C, the typical signals for the hydrogen-bonded double rosette are displayed in the ^{1}H NMR spectrum, indicating the dissolution of the fibers.

The presence of the double rosettes $\mathbf{1a}_3$•((R)-MePropCYA)$_6$ and $\mathbf{1a}_3$•((S)-MePropCYA)$_6$ in the gel was confirmed by CD measurements. In the case of $\mathbf{1}_3$•((R)-MePropCYA)$_6$, the CD absorptions from 290-350 nm in the gel phase is typical for the double rosette assemblies (Fig. 4.9 curve a).[33] Variable-temperature CD performed on a 10.0 mM gel of $\mathbf{1}_3$•((R)-MePropCYA)$_6$ showed that the intensity of the CD signal increased upon heating of the sample, going from a gel to a solution (Fig. 4.9 right). The CD signal intensity observed in solution was higher than in the gel phase due to the optimal conformation of the chromophores in the assemblies. By variable-temperature CD measurements and plotting the CD maximum absorption at a wavelength of 307 nm as a function of the temperature, a value of 65 °C was obtained for T_{gs}. This is the temperature at which the gel turns into a solution (Fig. 4.9).

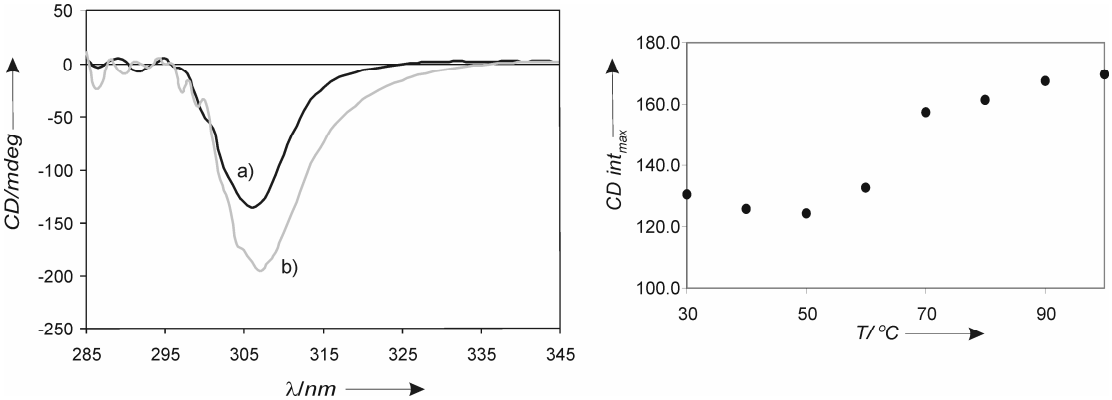

Figure 4.9. *Left image: CD spectra of the double rosette* $\mathbf{1}_3$*•((R)-MePropCYA)*$_6$ *in the a) gel state and b) liquid state. Right image: graph of the CD maximum absorption for* $\mathbf{1}_3$*•((R)-MePropCYA)*$_6$ *(*λ*=307 nm) vs temperature. All spectra were recorded in dodecane at 10.0 mM concentration.*

4.4. Conclusions

The liquid crystallinity of the chiral double rosette assemblies $\mathbf{1}_3$•(S-2-MeBuBAR)$_6$, $\mathbf{1}_3$•((R)-MePropCYA)$_6$ and $\mathbf{1}_3$•((S)-MePropCYA)$_6$ has been demonstrated. The functional groups on the periphery of the double rosettes are responsible for the formation and the physical properties of the assemblies. The stacking direction in the liquid crystalline state strongly depends on the nature of the constituents of the double rosette assembly, pointing out the importance of the noncovalent interactions in the self-organization of the double rosette in the liquid crystalline state. CD spectroscopy revealed that the helicity of the assembly is retained in the columnar organization. The supramolecular chirality is transferred from the molecular level (assembly) to the macroscopic level (mesophase). Surprisingly, the chiral double rosettes $\mathbf{1}_3$•((R)-MePropCYA)$_6$ and $\mathbf{1}_3$•((S)-MePropCYA)$_6$ exhibit a gel phase in n-alkane solvents, which has not been observed for the individual building blocks and the achiral rosettes.

4.5. Experimental Section

THF was freshly distilled from Na/benzophenone, and CH_2Cl_2 from $CaCl_2$. All chemicals were of reagent grade and used without further purification. Flash column chromatography was performed using silica gel (SiO_2, E. Merck, 0.040-0.063 mm, 230-400 mesh). NMR spectra were recorded on a Varian Unity 300 and 400 (^{1}H NMR 300 MHz and 400 MHz) using tetramethylsilane (TMS) or the corresponding residual solvent signal as internal standard. FAB-MS spectra were recorded on a Finningan MAT 90 spectrometer with m-nitrobenzyl alcohol (NBA) as a matrix. CD spectra were recorded on a JASCO J-715 spectropolarimeter. A Perkin-Elmer DSC-7 was used for thermal analysis. DSC measurements were performed on a DSC Piris Series 7 (scanning rate: 10 °C min^{-1}). A polarizing optical microscope Olympus BH-2 equipped with a Mettler FP82HT hot stage was used for visual observation.

The molecular arrangements in different samples were analyzed with an X-ray diffractometer equipped with a home-built capillary oven. Each sample was placed into an X-ray capillary with 1.0 mm internal diameter and then the capillary tube was placed inside a vertically aligned graphite tube containing a hole transversal to it, allowing the incident X-ray beam to cross freely. The temperature of the graphite tube was controlled by a system formed by a thermo-couple attached to a power supply and it acts as a fast-response online oven ranging from room temperature to 350 ºC. The X-ray measurements were carried out in a Bruker-Nonius D8 diffractomenter with a 2-D detector with a sample to detector distance set to 10 cm and spectra were recorded for 1 h. A focused permanent magnetic field of approximately 4 T was applied perpendicular to the capillary allowing for alignment of any liquid crystal phase. CD measurements were conducted on a JASCO J-715 spectropolarimeter using a Mettler FP82HT hot stage.

Synthesis. The synthesis of compounds **1**,[46] (R)-MePropCYA,[32] (S)-MePropCYA[32] and (R)-MePheCYA[33] has been reported previously.

2-((S)-2-methylbutyl)-2-ethylmalonic acid ester ((S)-4). After trituration with hexane, NaH (60% dispersion in mineral oil, 0.73 g, 18.2 mmol) was suspended in dry THF (140

mL) and the diethylmaolonate (6.8 g, 36.4 mmol) was added dropwise at 0°C. After stirring for 1hr at room temperature (S)-(+)-bromo-2-methylbutane (2.50 g, 16.5 mmol) was added and the mixture was stirred for 30 min at room temperature and subsequently refluxed for 3 days. After evaporation of the solvent, the residue was redissolved in CH_2Cl_2 (150 mL), washed with H_2O (2 x 30 mL) and brine (30 mL), and dried on $MgSO_4$. The solvent was evaporated and the residual diethyl ethylmalonate was removed under vacuum (p=0.1 Torr at T=80°C). Compound (S)-**4** was obtained as a colorless oil (2.50 g, 58.6%). ^{1}H NMR (300 MHz, $CDCl_3$) δ 4.13-415 (q, 4H, O*CH*$_2$CH$_3$), 1.94-1.86 (m, 4H, C*CH*$_2$CH and C*CH*$_2$CH$_3$), 1.72-164 (m, 1H, C**H*), 1.2-1.4 (m, 8H, OCH$_2$CH$_3$, C*H*CH$_2$CH$_3$), 0.82-0.72 (m, 9H, CHCH$_3$CH$_2$*CH*$_3$, C*H*CH$_3$, and CH$_2$*CH*$_3$). ^{13}C NMR (75 MHz, $CDCl_3$) δ 171.35, 170.71,60.42, 60.17, 56.85, 46.4, 30.8, 29.8, 29.1, 20.7, 14.1, 11.6, 8.5. MS (FAB): m/z 258.4([M+H$^+$], calcd 258.4).

5-((S)-2- methylbutyl)-5'-ethylbarbiturate ((S)-2-MeBuBAR). A solution of compound (S)-**4** (1.0 g, 3.8 mmol) in EtOH (15 mL) was dropwise added to a solution of Na (0.28 g, 11.6 mmol) in EtOH (35 mL) at room temperature. After the addition of urea (0.277 g, 4.2 mmol), the mixture was refluxed for 2 days, after wich the solvent was evaporated. The residue was redissolved in water (75 mL), acidified till pH of ~ 2/3 using 6 N HCl, and extracted with CH_2Cl_2 (4 x 40 mL). After drying over $MgSO_4$, the combined organic fractions were evaporated to dryness. The compound SmebBAR was obtained as white solid (0.332 g, 38%) after column chromatography (SiO_2, CH_2Cl_2/MeOH/NH_4OH =90/9.5/0.5). ^{1}H NMR (300 MHz, DMSO-d_6) δ 11.3 (s, 2H, N*H*), 1.9-1.6 (m, 4H, C*CH*$_2$CH and C*CH*$_2$CH$_3$), 1.4-1.1 (m, 2H, C*H*CH$_2$CH$_3$), 1.1-0.9 (m, 2H, C**H*), 0.8-0.6 (m, 9H, CHCH$_3$CH$_2$*CH*$_3$, C*H*CH$_3$, and CH$_2$*CH*$_3$). ^{13}C NMR (75 MHz, DMSO-d_6) δ 172.2, 171.5, 53.5, 47.0, 30.0, 29.7, 20.0, 11.6, 7.7. MS (FAB): m/z 226.3 ([M+H$^+$], calcd 226.3).

Formation of double rosette assemblies. Hydrogen-bonded assemblies were prepared by mixing calix[4]arene **1** with 2 equivalents of (S)-2-MeBuBAR, (S)-MePropCYA, (R)-MePropCYA and (R)-MePheCYA respectively, in toluene-d_8 for 20 min at 100°C. For example, 8.32 mg (0.003 mmol) of **1** and 1.10 mg (0.006 mmol) of (S)-MePropCYA

were dissolved in 5 mL of toluene–d_8, stirred and heated at 100°C till all compounds were dissolved. After evaporation of the solvent under high vacuum, the assembly wasready to use.

Circular dichroism in the liquid crystals state. The prepared double rosette assemblies were placed in between two quartz slides and heated by a hot stage untill the isotropic phase. Afterwards, the CD spectra were recorded cooling down from the isotropic point at a rate of 10 °C/min. The thickness of the film was check qualitatively by multiple UV-vis measurements.

4.6 References and Notes

[1] H. S. Kitzerow, C. Bahr, *Chirality in Liquid Crystals*, Eds. Springer, New York, **2001**.

[2] T. Verbiest, S. van Elshocht, A. Persoons, C. Nuckolls, K. E. Phillips, T. J. Katz, *Langmuir* **2001**, *17*, 4685-4687.

[3] T. Verbiest, S. van Elshocht, M. Kauranen, L. Hellemans, J. Snauwaert, C. Nuckolls, T. J. Katz, A. Persoons, *Science* **1998**, *282*, 913-915.

[4] V. A. Mallia, N. Tamaoki, *Chem. Mater.* **2003**, *15*, 3237-3239.

[5] N. Tamaoki, *Adv. Mater.* **2001**, *13*, 1135-1147.

[6] Y. Kamikawa, T. Kato, *Org. Lett.* **2006**, *8*, 2463-2466.

[7] M. Nishii, T. Matsuoka, Y. Kamikawa, T. Kato, *Org. Biomol. Chem.* **2005**, *3*, 875-880.

[8] R. K. Castellano, C. Nuckolls, J. Rebek, *J. Am. Chem. Soc.* **1999**, *121*, 11156-11163.

[9] C. Nuckolls, T. J. Katz, G. Katz, P. J. Collings, L. Castellanos, *J. Am. Chem. Soc.* **1999**, *121*, 79-88.

[10] C. Nuckolls, T. J. Katz, *J. Am. Chem. Soc.* **1998**, *120*, 9541-9544.

[11] J. Barberá, L. Puig, P. Romero, J. L. Serrano, T. Sierra, *J. Am. Chem. Soc.* **2006**, *128*, 4487-4492.

[12] L. Brunsveld, B. G. G. Lohmeijer, J. Vekemans, E. W. Meijer, *Chem. Commun.* **2000**, 2305-2306.

[13] Y. Kamikawa, M. Nishii, T. Kato, *Chem. Eur. J.* **2004**, *10*, 5942-5951.

[14] M. L. Bushey, T. Q. Nguyen, W. Zhang, D. Horoszewski, C. Nuckolls, *Angew. Chem. Int. Ed.* **2004**, *43*, 5446-5453.

[15] I. Paraschiv, M. Giesbers, B. van Lagen, F. C. Grozema, R. D. Abellon, L. D. A. Siebbeles, A. T. M. Marcelis, H. Zuilhof, E. J. R. Sudhölter, *Chem. Mater.* **2006**, *18*, 968-974.

[16] M. Masuda, P. Jonkheijm, R. P. Sijbesma, E. W. Meijer, *J. Am. Chem. Soc.* **2003**, *125*, 15935-15940.

[17] J. J. van Gorp, J. Vekemans, E. W. Meijer, *J. Am. Chem. Soc.* **2002**, *124*, 14759-14769.

[18] V. Percec, M. R. Imam, T. K. Bera, V. S. K. Balagurusamy, M. Peterca, P. A. Heiney, *Angew. Chem. Int. Ed.* **2005**, *44*, 4739-4745.

[19] T. Kato, N. Mizoshita, K. Kanie, *Macromol. Rapid Commun.* **2001**, *22*, 797-814.

[20] T. Kato, N. Mizoshita, K. Kishimoto, *Angew. Chem. Int. Ed.* **2006**, *45*, 38-68.

[21] K. Kanie, T. Yasuda, S. Ujiie, T. Kato, *Chem. Commun.* **2000**, 1899-1900.

[22] C. Fouquev, J.-M. Lehn, A. M. Levelut, *Adv. Mater.* **1990**, *2*, 254-257.

[23] T. Kato, *Struct. Bond.* (Berlin) **2000**, *96*, 95-146.

[24] U. Beginn, *Prog. Polym. Sci.* **2003**, *28*, 1049-1105.

[25] J. Barberá, L. Puig, J. L. Serrano, T. Sierra, *Chem. Mater.* **2004**, *16*, 3308-3317.

[26] V. Percec, C. H. Ahn, G. Ungar, D. J. P. Yeardley, M. Moller, S. S. Sheiko, *Nature* **1998**, *391*, 161-164.

[27] G. Ungar, Y. S. Liu, X. B. Zeng, V. Percec, W. D. Cho, *Science* **2003**, *299*, 1208-1211.

[28] V. Percec, A. E. Dulcey, V. S. K. Balagurusamy, Y. Miura, J. Smidrkal, M. Peterca, S. Nummelin, U. Edlund, S. D. Hudson, P. A. Heiney, D. A. Hu, S. N. Magonov, S. A. Vinogradov, *Nature* **2004**, *430*, 764-768.

[29] J. Barberá, L. Puig, P. Romero, J. L. Serrano, T. Sierra, *Chem. Mater.* **2005**, *17*, 3763-3771.

[30] L. Alvarez, J. Barberá, L. Puig, P. Romero, J. L. Serrano, T. Sierra, *J. Mater. Chem.* **2006**, *16*, 3768-3773.

[31] L. J. Prins, J. Huskens, F. de Jong, P. Timmerman, D. N. Reinhoudt, *Nature* **1999**, *398*, 498-502.

[32] M. A. Mateos-Timoneda, M. Crego-Calama, D. N. Reinhoudt, *Supramol. Chem.* **2005**, *17*, 67-79.

[33] L. J. Prins, R. Hulst, P. Timmerman, D. N. Reinhoudt, *Chem. Eur. J.* **2002**, *8*, 2288-2301.

[34] M. A. Mateos-Timoneda, *Functional chiral hydrogen-bonded assemblies*, PhD Thesis, Universty of Twente, Enschede The Netherlands, ISBN 90-365-2180-7, **2005**.

[35] D. Demus, *In Handbook of Liquid Crystals, Vol. 1*, Wiley VCH, New York, **1998**.

[36] R. Pucciariello, V. Villani, *Polymer* **2004**, *45*, 2031-2039.

[37] P. Timmerman, R. H. Vreekamp, R. Hulst, W. Verboom, D. N. Reinhoudt, K. Rissanen, K. A. Udachin, J. Ripmeester, *Chem. Eur. J.* **1997**, *3*, 1823-1832.

[38] The intercolumnar distance is calculated by the formula $a=d/\cos(\pi/6)$, where d is the reflection (1,0,0), corresponding to the distance between two double rosette layers.

[39] M. G. J. ten Cate, *Self-assembled receptors based on hydrogen bonds*, PhD Thesis, University of Twente, Enschede The Netherlands, ISBN 90-365-2053-3, **2004**.

[40] T. Kato, T. Matsuoka, M. Nishii, Y. Kamikawa, K. Kanie, T. Nishimura, E. Yashima, S. Ujiie, *Angew. Chem. Int. Ed.* **2004**, *43*, 1969-1972.

[41] N. M. Sangeetha, U. Maitra, *Chem. Soc. Rev.* **2005**, *34*, 821-836.

[42] M. de Loos, B. L. Feringa, J. H. van Esch, *Eur. J. Org. Chem.* **2005**, 3615-3631.

[43] A. Friggeri, C. van der Pol, K. J. C. van Bommel, A. Heeres, M. C. A. Stuart, B. L. Feringa, J. van Esch, *Chem. Eur. J.* **2005**, *11*, 5353-5361.

[44] A. Brizard, R. Oda, I. Huc, *Top. Curr. Chem.* **2005**, 167-218.

[45] S. Yagai, T. Nakajima, K. Kishikawa, S. Kohmoto, T. Karatsu, A. Kitamura, *J. Am. Chem. Soc.* **2005**, *127*, 11134-11139.

[46] The synthesis has been described in Chapter 4

Chapter 5

Self-Organization of Guest Molecules in Mesogenic Self-Assembled Nanocontainers

In this chapter, the complexation of alizarin by mesogenic self-assembled molecular boxes (double rosettes) in solution and in the liquid crystalline state is described. Depending on the nature of the building blocks in the self-assembled system, the alizarin is encapsulated or intercalated. In the liquid crystalline state, the alizarin complexation by the double rosettes leads to highly stable mesophases which, in the case of ***1a***$_3$*•((S)-MePropCYA)*$_6$*, leads to a crystalline phase.*

5.1 Introduction

In the last years soft materials, often classified as functional for their rapid response to external stimuli,[1-4] are attracting a lot of interest for their possible applications in materials science and nanotechnology.[5] For example, new properties can be introduced by establishing order in the soft material.[6]

Liquid crystals (LCs) are ordered soft materials consisting of self-organized molecules and can be potentially used as new functional materials.[7-9] A particular class of liquid crystals, the so-called discotic LCs, has attracted attention for their potential application to 1D mass transport and as optoelectronic nanomaterials.[10-15] The columnar superstructures, formed via aromatic π–π stacking interactions of these disk-like mesogenic molecules, can further organize into larger columns via Van der Waals interactions, which is often accompanied with the formation of elongated fibers.[16-18] The propensity of disk-shaped entities to organize into columnar aggregates strongly depends on the morphology of the disks, including peripheral substituents.[19-21] If the morphology of the disk-shape entities may be changed by means of external stimuli such as the complexation with small molecules,[22,23] and the change is amplified via self-organization,[1,24] functional soft materials are obtained.

In the last decades, supramolecular chemistry has been used to construct and order self-assembled structures through the use of noncovalent interactions such as hydrogen bonding.[1,25] Self-assembly and self-organization are considered the tools for the spontaneous and programmed generation of nanoscale architectures and materials, on the basis of the instruction stored in the building components and of the interactive algorithms that bind these components together.[24,26-28]

In Chapter 3, the liquid crystallinity of self-assembled molecular boxes has been described. The liquid crystallinity is induced by the nano-segregation between the polar core of the assemblies and the lipophilic chains at the periphery. This chapter describes the complexation of alizarin by mesogenic self-assembled molecular boxes in solution and in the liquid crystalline state. In solution, the alizarin shows different complexation modes with the double rosette assembly. This complexation depends strongly on the composition of the assemblies. In the liquid crystalline phase, the different complexation

modes lead to distinct physical properties of the double rosette assemblies in the liquid crystalline phase.

5.2. Results and Discussion

Double rosette assembly **1a**$_3$•((S)-2-MeBuBAR)$_6$ consists of three calix[4]arene dimelamines **1a** and six barbiturates molecules held together through the formation of 36 cooperative hydrogen-bonds (Chart 5.1).[29,30] The hydrogen-bonded assembly can be seen as a nano-container, where the calix[4]arene units are the side walls and the space between the two circular networks (rosettes)[31] limits the encapsulation area. The two rosette motifs that form the bottom and top of the nano-box are formed by complementary hydrogen bonds between melamines and barbiturates. These molecular containers are thermodynamically stable, even at a concentration of 5 μM in apolar solvents.[32] The periphery of the assembly is decorated with long alkyl chains, which promote the liquid crystalline (Chapter 3) behavior of the assembly. The liquid crystalline phase for the chiral double rosette **1a**$_3$•((S)-2-MeBuBAR)$_6$ shows a columnar arrangement of double rosettes.

The doping of liquid crystalline materials with optically active molecules is attracting attention because of the possible application in the field of electro-optical materials.[33] Thus, the complexation of the UV-Vis active molecule alizarin by the mesogenic double rosettes in solution and the mesophase is studied here.

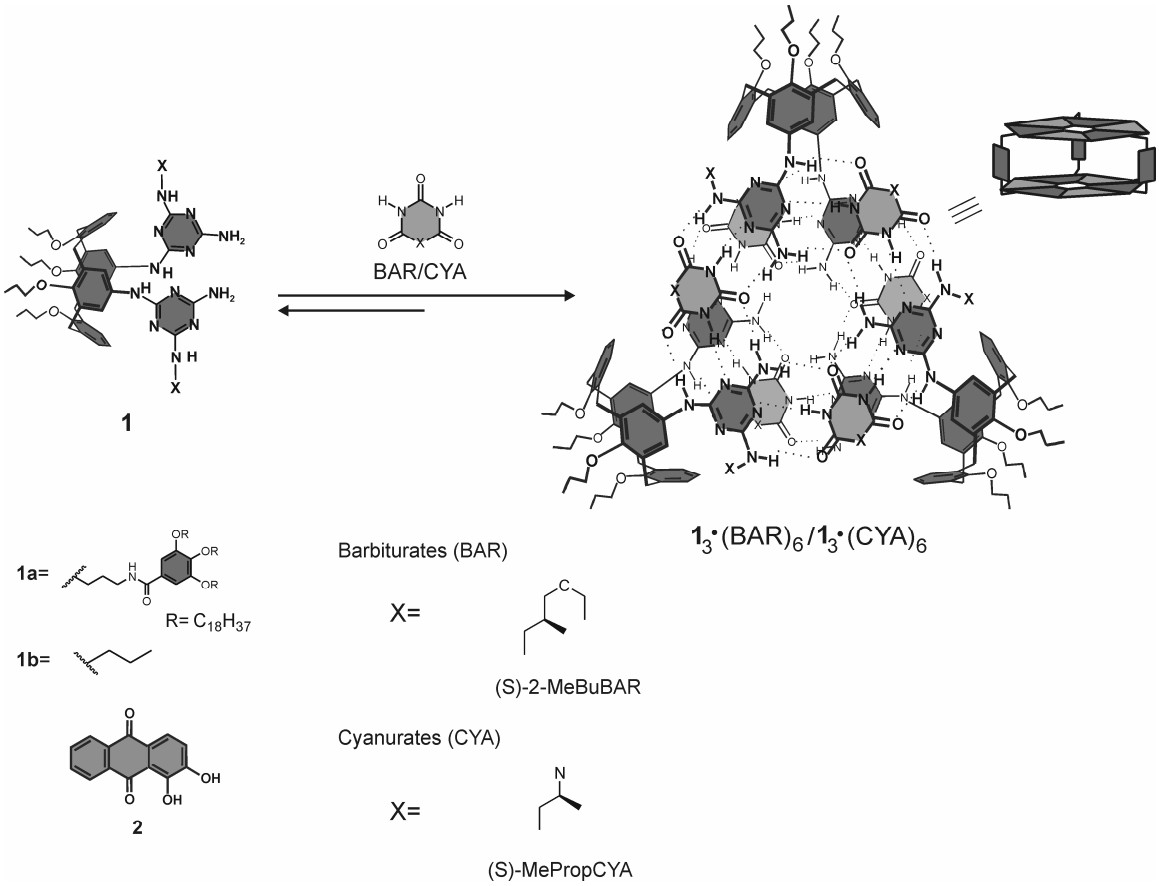

Chart 5.1. *Formation of the hydrogen-bonded assemblies* $\mathbf{1}_3$*•(BAR)*$_6$ *and* $\mathbf{1}_3$*•(CYA)*$_6$ *and molecular structure of the guest molecule* ***2****. The schematic representation of the double rosettes (side view) is also shown.*

5.2.1 Complexation of alizarin by mesogenic double rosette assemblies in solution

^{1}H NMR spectroscopy

Addition of alizarin (**2**, 3 equiv) to the assembly $\mathbf{1a}_3$•((S)-2-MeBuBAR)$_6$ (1.0 mM in toluene-d_8) produced a large shift in the ^{1}H NMR signals for both host and guest molecules (Fig. 5.1). For example, the hydrogen-bonded imide protons of (S)-2-MeBuBAR (Ha and Hb) shows upfield shifts from 14.85 and 14.00 ppm to 14.33 and 13.74 ppm, respectively (Fig. 5.1). Furthermore, the majority of the signals of the guest molecules are upfield shifted by ≥ 3 ppm indicating the encapsulation of **2** (this part of the ^{1}H NMR not shown). The integration of the ^{1}H NMR signals indicates a 3:1 ratio for the complexation of **2** by $\mathbf{1a}_3$•((S)-2-MeBuBAR)$_6$. On the other hand, the downfield shift

(from 6.2 ppm to 10.30 ppm) observed for the hydroxyl proton Hn of **2** indicates the formation of an intermolecular hydrogen bond between this proton and the carbonyl group of the adjacent alizarin guest molecule.

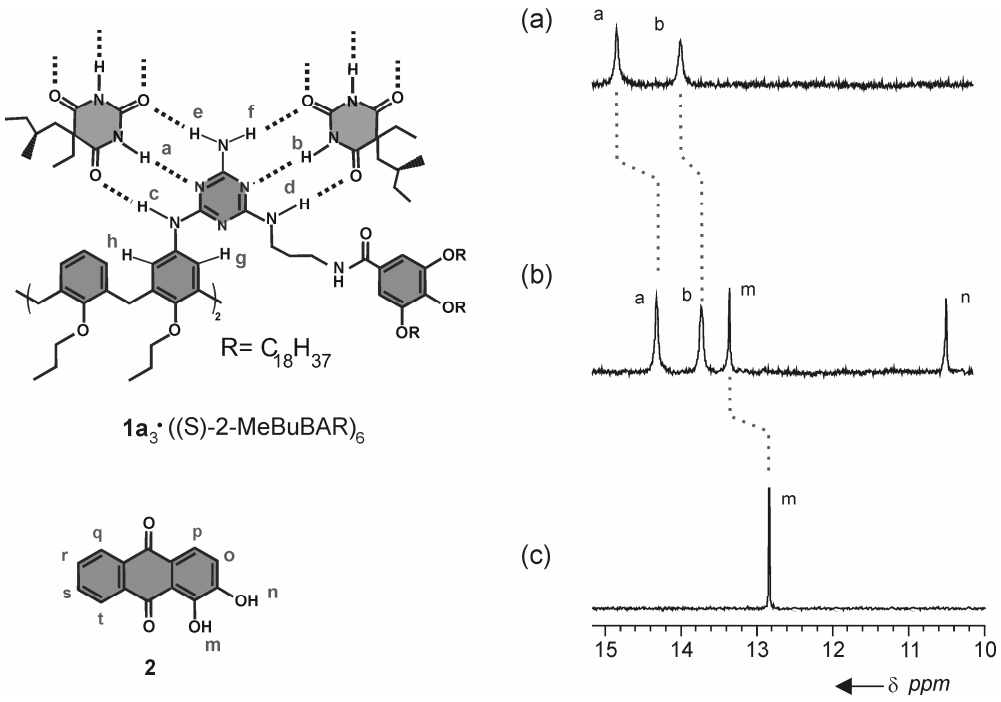

Figure 5.1. *Parts of the ^{1}H NMR spectra (400 MHz) of (a) double rosette assembly* ***1a***$_3$*•((S)-2-MeBuBAR)*$_6$*, (b) complex* ***1a***$_3$*•((S)-2-MeBuBAR)*$_6$*•****2***$_3$*, and (c) alizarin* ***2****. Spectra were taken in toluene-*d_8 *at room temperature.*

This type of encapsulation has been observed previously for non-liquid crystalline hydrogen-bonded double rosettes.[34] Thus, it can be concluded that the alizarin forms a self-assembled trimer between the two rosette floors of a mesogenic assembly resulting in the complex **1a**$_3$•((S)-2-MeBuBAR)$_6$•**2**$_3$ (Fig 5.2).

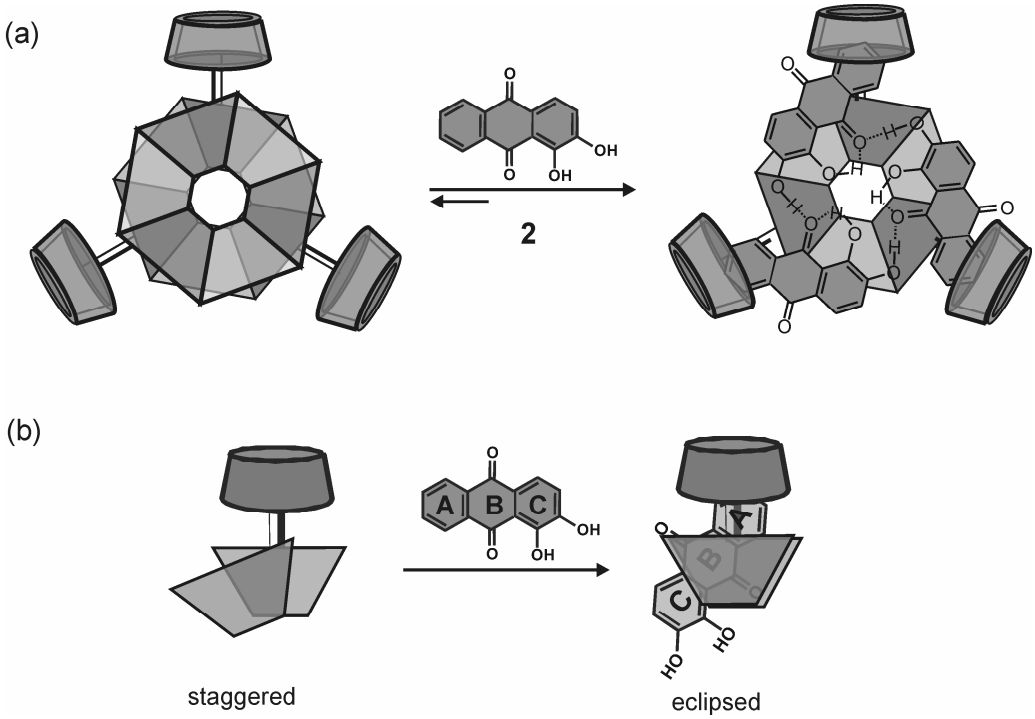

Figure 5.2. *(a) The complexation of the alizarin trimer in the double rosette cavity (only the bottom floor of the rosette is shown in the case of the complexation for clarity) and (b) schematic representation of the change of the calix[4]arene melamine orientation due to the complexation of alizarin in the double rosette assemblies.*

The X-ray studies performed with the non-liquid crystalline double rosettes revealed clearly that the encapsulation of three molecules (trimer) of alizarin **2** exists also in the solid state.[34] These studies showed also that the two melamines of each calix[4]arene adopt an *eclipsed* orientation upon alizarin complexation, while in absence of the guest these melamines are in a *staggered* orientation (Fig. 5.2b). The electron deficient aromatic ring of **2** (ring B, Fig. 5.2b) is stacked between the two relatively electron-poor rings of the melamine units with a slight offset of the face-to-face arrangement.

The possible release of the alizarin from the mesogenic double rosette $\mathbf{1a}_3$•((S)-2-MeBuBAR)$_6$ by adding cyanuric derivatives has been studied.[34] The higher strength of the hydrogen bonds between the melamines and cyanurates compared to barbiturates as reflected by the association constants (K_a= 2.2 ± 0.8 × 10^3 M^{-1} in $CDCl_3$ for melamine-cyanurate and K_a= 1.0 ± 0.1 × 10^2 M^{-1} in $CDCl_3$ for melamine-barbiturate) allows an exchange reaction, where the barbiturates are substituted for the cyanurates derivatives in

the hydrogen-bonded assembly.[35] This exchange can lead to the release of the guest molecules through a conformational change of the assemblies. Therefore, six equivalents of the cyanuric acid derivative (S)-MePropCYA were added to the double rosette **1a**$_3$•((S)-2-MeBuBAR)$_6$. The ^{1}H NMR spectrum shows the formation of assembly **1a**$_3$•((S)-MePropCYA)$_6$ and the release of the alizarin (confirmed also by CD experiments, see below). Additionally, other signals corresponding to a new complex are also seen in the ^{1}H NMR spectrum (Fig. 5.3).[36]

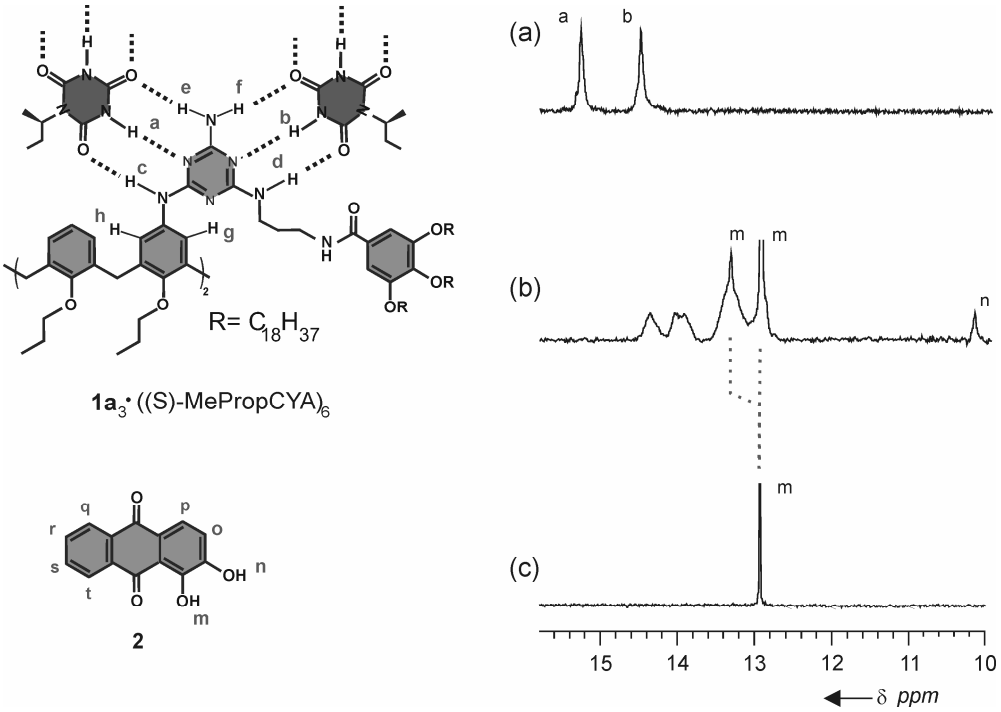

Figure 5.3. *Parts of the ^{1}H NMR spectra (400 MHz) of the double rosette assembly* ***1a***$_3$*•((S)-MePropCYA)$_6$ (a), complex* ***1a***$_3$*•((S)-MePropCYA)$_6$ with 3 equiv of alizarin (b), and alizarin* ***2*** *(c). Spectra were taken in toluene-*d_8 *at room temperature.*

The first evidence of the new complex formation is the upfield shifting and splitting of the hydrogen-bonded imide protons signals of (S)-MePropCYA (Ha and Hb) (Fig. 5.3b). The number of proton signals for Ha and Hb is related to the symmetry of the assembly. Double rosettes with *D*$_3$-symmetry display two signals for Ha and Hb in the ^{1}H NMR spectrum (Fig. 5.3a). However, a change in the symmetry of the assembly can lead to a different number of signals for these protons. The symmetry change can be induced by a change in the number of guest molecules and in the complexation mode.[34,37]

The downfield shift of protons Hm (from 12.95 ppm to 13.30 ppm) and Hn (from 6.2 ppm to 10.30 ppm) of **2** (Fig 5.3) could indicate the encapsulation of **2** by the double rosette **1a**$_3$•((S)-MePropCYA)$_6$ because similar shifts were found for the complex **1a**$_3$•((S)-2-MeBuBAR)$_6$•**2**$_3$. Nevertheless, the integration of the Hn signal of **2** indicates that only two molecules would be encapsulated in the double rosette **1a**$_3$•((S)-MePropCYA)$_6$. This could explain the breaking of the D_3-symmetry and the consequently higher number of hydrogen-bonded $NH_{(S)\text{-MePropCYA}}$-proton signals (Fig. 5.3b). 2D ^{1}H NMR (COSY) experiments were carried out to assign all alizarin protons to confirm this possibility. If the encapsulation occurs then protons Hr, Hs, and Ht of **2** (Fig 5.3) should shift upfield due the partial inclusion of the unsubstituted electron-rich ring of **2** (ring A, Fig. 5.2) in the calix[4]arene cone.[34] Nevertheless, the 2D ^{1}H NMR spectrum did not show any shift of those signals, indicating then that the alizarin is not encapsulated. Therefore, the increase of the number of signals for the protons Ha and Hb is probably due to the complexation of **2** outside of the rosette box, i.e. on top and bottom of the double rosette floors (*exo*-complexation) (see also CD experiments below). The similarity with the encapsulation proton spectrum suggests that the alizarin is *intercalated* between the floors of two different double rosettes. Other groups have also observed a similar intercalation mode upon addition of antraquinone derivatives to guanine quartets-based receptors.[38]

The *exo*-complexation of alizarin has never been observed before for other cyanurate-based double rosettes. One of the reasons for the intercalation of alizarin could be the presence of large aggregates.[21] To confirm this possibility DOSY[39] experiments were carried out (1.0 mM, toluene-d_8). The diffusion constants revealed that the double rosette **1a**$_3$•((S)-MePropCYA)$_6$ form aggregates, and that the addition of alizarin produced even larger aggregates. As a control experiment, assembly **1b**$_3$•((S)-MePropCYA)$_6$, which has short alkyl chains on the melamine units, was prepared. This assembly does not display aggregation under the same experimental conditions. Furthermore, no complexation (or aggregation) was found for **1b**$_3$•((S)-MePropCYA)$_6$ upon addition of 3 equivalents of **2**. Therefore, it seems that aggregation is necessary for the intercalation of alizarin by cyanurate-based double rosettes. Possibly, the alizarin enforces the interactions between the mesogenic double rosettes **1a**$_3$•((S)-MePropCYA)$_6$ allowing a better stacking between

the double rosettes through the interdigitation of the long alkyl chains at the periphery of the assembly. The driving force for the formation of the complex can be the minimization of π-π repulsive interactions between the melamine units and the B-ring of **2** (Fig. 5.2).[40,41] Variable temperature ^{1}H NMR experiments showed that the assemblies are thermodynamically stable until 80 °C.

UV-vis spectroscopy

Alizarin has a maximum absorption peak at a wavelength of 419 nm in toluene (Fig. 5.4). Thus, in order to gain more insight about the encapsulation/intercalation of **2** by double rosette **1a**$_3$•((S)-2-MeBuBAR)$_6$ and **1a**$_3$•((S)-MePropCYA)$_6$, the complexation of **2** was followed by UV-vis spectroscopy.[40]

As established by ^{1}H NMR spectroscopy, the addition of 3 equivalents of **2** to the double rosette **1a**$_3$•((S)-2-MeBuBAR)$_6$ leads to the encapsulation of alizarin. The UV-vis spectrum of **1a**$_3$•((S)-2-MeBuBAR)$_6$ (1.0 mM in toluene and dodecane) in the presence of 3 equivalents of alizarin showed a maximum absorption peak at 432 nm (Fig. 5.4).[40] Probably, the shift of the maximum absorption in the UV-vis spectrum (from 419 to 432 nm) is due to the π-π interaction between the electron-deficient rosette motif and the electron-rich rings (A and C Fig. 5.2) of alizarin. A charge-transfer complex may be formed between the alizarin and the double rosette, as suggested by the change of the color from yellow (alizarin) to red (complex).

Analogously, the addition of 3 equivalents of **2** to **1a**$_3$•((S)-MePropCYA)$_6$ (1.0 mM in toluene and dodecane) produced a color change from yellow to red, indicating also the possible formation of a charge-transfer complex. The UV-vis spectrum of this solution showed also a maximum absorption peak at 432 nm (Fig. 5.4).

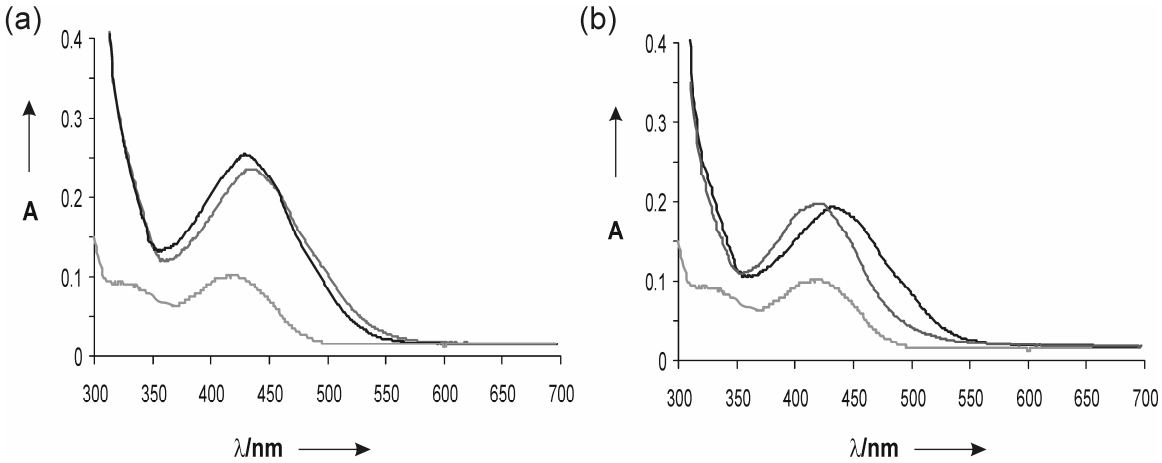

Figure 5.4. *(a) UV-vis absorption spectra for double rosette assembly* ***1a***$_3$*•((S)-MePropCYA)*$_6$*•****2***$_3$ *(black line),* ***1a***$_3$*•((S)-2-MeBuBAR)*$_6$*•****2***$_3$ *(grey) at concentration 1.0 mM, and* ***2*** *(light grey) at 3.0 mM in toluene; (b) UV-vis spectra for* ***1a***$_3$*•((S)-MePropCYA)*$_6$ *with 3 equiv of alizarin in dodecane (black line), in chloroform (grey line)at 1.0 mM, and for* ***2*** *(light grey) at 3.0 mM. All spectra were recorded in 0.01mm cuvette path length.*

Thus, the values of the maximum absorption for both complexes **1a**$_3$•((S)-2-MeBuBAR)$_6$•**2**$_3$ and **2**∩**1a**$_3$•((S)-MePropCYA)$_6$ are very similar which indicates a comparable stacked geometry, i.e. the alizarin is encapsulated between two rosette floors of the same assembly **1a**$_3$•((S)-2-MeBuBAR)$_6$, and intercalated between different assemblies **1a**$_3$•((S)-MePropCYA)$_6$.

In chloroform, only the absorption peak of free alizarin was observed in the UV-vis spectrum of **1a**$_3$•((S)-MePropCYA)$_6$ (Fig. 5.4), indicating that this double rosette does not complex alizarin. Chloroform is a solvent in which solvophobic interactions between aromatic groups and alkyl chains are much weaker than in toluene and dodecane, thus the formation of aggregates is more difficult than in toluene and dodecane.

In conclusion, these UV-vis studies confirm that the presence of double rosette aggregates is necessary for the *exo*-complexation of the alizarin as demonstrated also by DOSY experiments.

Circular dichroism spectroscopy

Circular dichroism (CD) measurements have confirmed the intercalation of alizarin molecules between two floors of different chiral double rosettes assemblies.[42] The CD

spectrum of the double rosette **1a**$_3$•((S)-MePropCYA)$_6$ (1.0 mM in toluene) showed a typical signal for *(M)*-helicity in the 275-325 nm region (Fig. 5.5a) due to the exciton coupling between chromophores in the core of the assembly **1a**$_3$•((S)-MePropCYA)$_6$.[43] The CD spectrum of the solution containing the chiral double rosette **1a**$_3$•((S)-MePropCYA)$_6$ changed completely upon addition of 3 equivalents of alizarin (Fig 5.5b). The CD spectrum showed a bisignate Cotton effect with a negative peak at 373 nm and a positive peak at 432 nm (Fig. 5.5).[44]

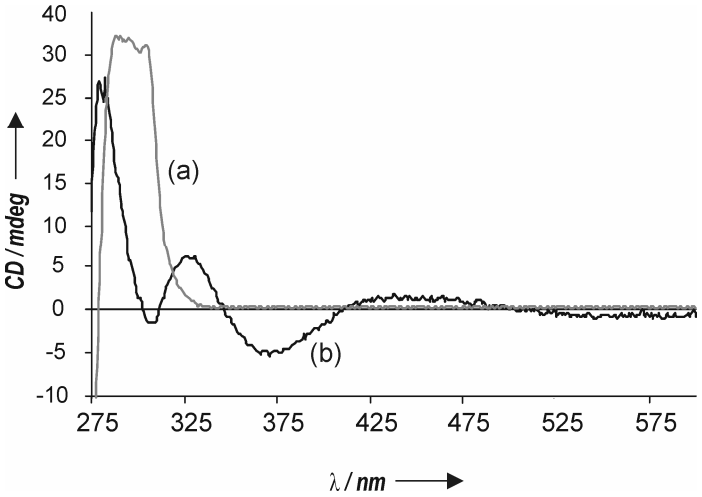

Figure 5.5. *Circular dichroism spectra of (a)* ***1a***$_3$*•((S)-MePropCYA)*$_6$ *and (b)* ***2***$\cap$***1a***$_3$*•((S)-MePropCYA)*$_6$ *at room temperature in toluene. All spectra were recorded at 1.0 mM and 0.01mm cuvette path length.*

Alizarin is a small achiral molecule and does not have an intrinsic CD spectrum and the double rosette **1a**$_3$•((S)-MePropCYA)$_6$ does not present CD signals in the wavelength region of 350-450 nm. Therefore, the observed CD spectrum (Fig 5.5b) is attributed to a chiral environment felt by the alizarin chromophores.[45] If the alizarin is placed on the top and bottom of the double rosette floors, it will be immersed in the chiral environment produced by the double rosette inducing a CD signal for **2** in the 350-450 nm region.[46] This signal rules out a groove binding mode[47] (where the alizarin would be placed on the side of the double rosette assemblies) (Fig. 5.6) because in this binding mode the alizarin would not feel the chiral environment since the stereocenters of the assembly would be too far from the guest molecules (Chapter 4).

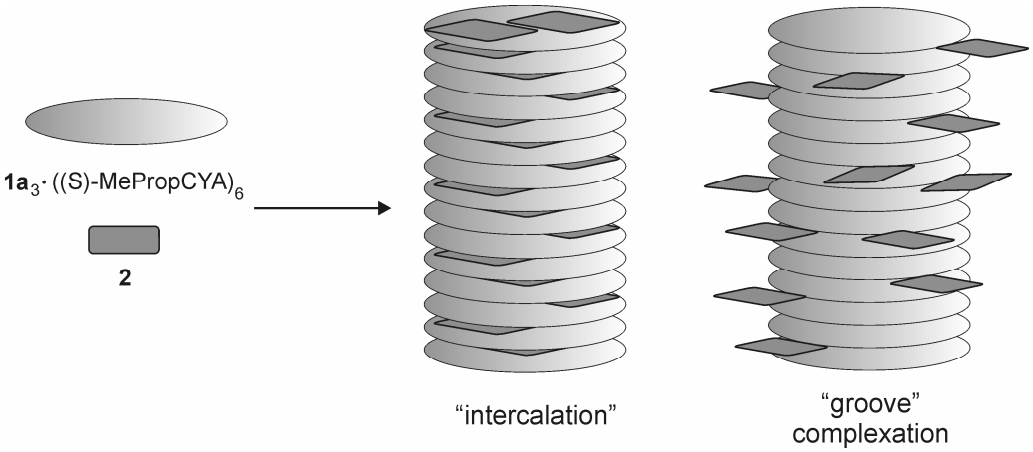

Figure 5.6. *Schematic representation of the possible binding modes of double rosette* ***1a***$_3$*•((S)-MePropCYA)*$_6$.

In summary, we have shown a novel complexation mode of alizarin by the mesogenic double rosette **1a**$_3$•((S)-MePropCYA)$_6$. The aggregation of **1a**$_3$•((S)-MePropCYA)$_6$ in toluene and dodecane enables the intercalation of alizarin between two adjacent double rosettes.

5.2.2 Complexation of alizarin by double rosettes in the liquid crystalline phase

In Chapter 4 of this thesis the liquid crystallinity of assemblies **1a**$_3$•((S)-2-MeBuBAR)$_6$ and **1a**$_3$•((S)-MePropCYA)$_6$ (Chart 5.1) has been discussed. These assemblies showed a columnar liquid crystalline phase for a wide range of temperatures, where the columns are arranged in hexagonal and pseudohexagonal fashion for **1a**$_3$•((S)-2-MeBuBAR)$_6$ and **1a**$_3$•((S)-MePropCYA)$_6$ respectively. They differ also in the columnar alignment along the z-direction in the liquid crystalline phase. In the case of **1a**$_3$•((S)-2-MeBuBAR)$_6$, the columns are parallel to this direction while for **1a**$_3$•((S)-MePropCYA)$_6$ the columns are tilted by an angle of 30° with respect to the stacking direction. [35]

Here the complexation of alizarin **2** by the double rosettes **1a**$_3$•((S)-2-MeBuBAR)$_6$ and **1a**$_3$•((S)-MePropCYA)$_6$ in the liquid crystalline state is studied.

Three equivalents of alizarin were added to a solution of **1a**$_3$•((S)-2-MeBuBAR)$_6$ in toluene. The yellow solution was stirred until the color change to red, which indicates

complexation (see Section 5.2.1). The liquid crystalline behavior of complex **1a**$_3$•((S)-2-MeBuBAR)$_6$•**2**$_3$ was analyzed by different techniques, such as polarized optical microscopy (POM), differential scanning calorimetry (DSC) and X-ray powder diffraction (XRD). The formation of **1a**$_3$•((S)-2-MeBuBAR)$_6$•**2**$_3$ in the liquid crystalline phase was previously demonstrated by CD spectroscopy (see Section 5.2.3). The POM studies showed a mosaic texture for **1a**$_3$•((S)-2-MeBuBAR)$_6$•**2**$_3$ upon cooling down from the isotropic phase. This texture indicates a columnar arrangement of the double rosettes in the mesophase (Fig. 5.7).

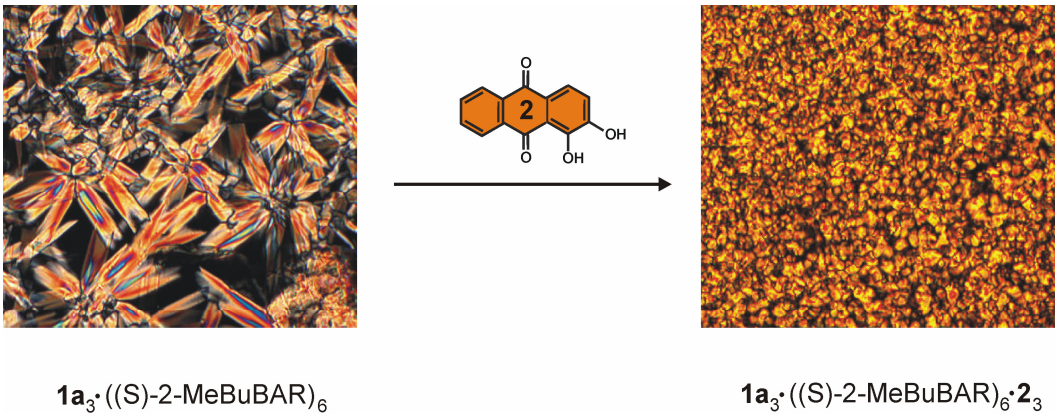

Figure 5.7. *Polarized optical microscopy images of* ***1a***$_3$*•((S)-2-MeBuBAR)*$_6$ *before and after the addition of alizarin at 130 °C.*

DSC showed only one phase transition for the complex **1a**$_3$•((S)-2-MeBuBAR)$_6$•**2**$_3$ at 177°C which corresponds to the liquid crystalline-isotropic phase transition (Table 5.1).

Table 5.1: *Thermal properties of the double rosette* ***1a***$_3$*•((S)-2-MeBuBAR)$_6$,* ***1a***$_3$*•((S)-2-MeBuBAR)$_6$•**2**$_3$,* ***1a***$_3$*•((S)-MePropCYA)$_6$, and* ***2***∩***1a***$_3$*•((S)-MePropCYA)$_6$.*

Compound	Phase Transition[a]						
1a$_3$•((S)-2-MeBuBAR)$_6$	Col_x	29	(12.7)	Col_h	146	(24.2)	Iso
1a$_3$•((S)-2-MeBuBAR)$_6$•**2**$_3$				Col_h	177	(7.5)	Iso
1a$_3$•((S)-MePropCYA)$_6$	Col_x	11	(0.30)	Col_h	157	(59.2)	Iso
2∩**1a**$_3$•((S)-MePropCYA)$_6$	Cr	28	(52.3)	Cr	227	(153.1)	Iso

[a] Phase transition temperatures (°C) and enthalpy changes (kJ mol^{-1} in parentheses)
Cr: crystalline; Col_x: unidentified columnar phase; Col_h: hexagonal columnar phase; Iso: isotropic

The complex **1a**$_3$•((S)-2-MeBuBAR)$_6$•**2**$_3$ has a higher isotropization temperature compared to the double rosette **1a**$_3$•((S)-2-MeBuBAR)$_6$ (ΔT_{Iso} = 31°C), thus the encapsulation of alizarin leads to a more stable mesophase (for **1a**$_3$•((S)-2-MeBuBAR)$_6$•**2**$_3$ than for **1a**$_3$•((S)-2-MeBuBAR)$_6$). It is worth to note the remarkable thermal stability of the assembly **1a**$_3$•((S)-2-MeBuBAR)$_6$•**2**$_3$, considering that the self-assembled complex is held by only noncovalent interactions such as π-π interactions and hydrogen bonds. The higher isotropization temperature for the complex **1a**$_3$•((S)-2-MeBuBAR)$_6$•**2**$_3$ may be attributed to a better stacking of the double rosettes in the columnar phase due to the expansion of its cavity after the accommodation of the alizarin trimers (see section 5.2.1). An indication of the cavity expansion is given by the change of the double rosette column inter-distance from 5.7 Å to 7.0 Å for **1a**$_3$•((S)-2-MeBuBAR)$_6$ and **1a**$_3$•((S)-2-MeBuBAR)$_6$•**2**$_3$ respectively, as demonstrated by X-ray powder diffraction measurements (Table 5.2). Probably this conformational change leads to a different spatial disposition of the functional groups at the periphery of the assembly which otherwise could weaken the stacking interactions as described in Chapter 3.

Table 5.2: *X-ray powder diffraction data for the double rosette* ***1a***$_3$*•((S)-2-MeBuBAR)*$_6$*,* ***1a***$_3$*•((S)-2-MeBuBAR)*$_6$*•****2***$_3$*,* ***1a***$_3$*•((S)-MePropCYA)*$_6$ *and* ***2*∩*1a***$_3$*•((S)-MePropCYA)*$_6$*.*

Compound	*T* (°C)	phase	Lattice constant (Å)	d_{obs} (Å)	d_{calc} (Å)	*hkl*
1a$_3$•((S)-2-MeBuBAR)$_6$	130	Col_{ho}	*a* = 42.0 *c*=5.7	36.2 21.9 19.08 4.8 (br)	36.2 21.9 19.1	100 110 200
1a$_3$•((S)-2-MeBuBAR)$_6$•**2**$_3$	120	Col_{ho}	*a* = 41.8 *c*=7.0	40.3 24.2 4.6 (br)	40.4 24.2	100 110
1a$_3$•((S)-MePropCYA)$_6$	145	Col_{ho}	*a* = 41.0 b = 38.0 *c* = 8.8	35.06 28.97 17.41 13.90 12.00	35.06 28.97 17.41 13.90 12.00	110 010 200 0200 120
2∩**1a**$_3$•((S)-MePropCYA)$_6$	195	Cr_{orth}	*a* = 44.0 b = 38.0 *c* = 5.1	43.9 37.8 28.9 14.6 11.1	44.0 38.0 28.8 14.7 11.1	100 010 110 300 030

Furthermore, the XRD analysis revealed a hexagonal columnar mesophase (Col_{ho}) for the complex **1a**$_3$•((S)-2-MeBuBAR)$_6$•**2**$_3$ (Table 5.2). The presence of sharp peaks in the low-angle region with a reciprocal spacing ratio of 1:√3 is characteristic of hexagonal columnar arrangement, as explained in Chapter 3. The inter-columnar distance is 41.8 Å, which is in agreement with the values found for mesogenic double rosette assemblies **1a**$_3$•((S)-2-MeBuBAR)$_6$ and **1a**$_3$•((S)-MePropCYA)$_6$ (Table 5.2). In summary, the encapsulation of three alizarin molecules stabilizes the mesophases of the double rosette **1a**$_3$•((S)-2-MeBuBAR)$_6$, while the hexagonal columnar arrangement is not disturbed by the encapsulation.

To investigate the influence of the intercalation of alizarin in the columns of the liquid crystalline double rosette **1a**$_3$•((S)-MePropCYA)$_6$ in the mesophases, the complex

2∩**1a**$_3$•((S)-MePropCYA)$_6$ was prepared. Three equivalents of alizarin were added to a solution of **1a**$_3$•((S)-MePropCYA)$_6$ in toluene, which turned red indicating the formation of the complex. After the intercalation of alizarin was confirmed by CD spectroscopy in the solid state (see Section 5.2.3), the thermal behavior of **2**∩**1a**$_3$•((S)-MePropCYA)$_6$ was investigated by POM, DSC, and XRD.

The DSC measurements showed that the double rosette **1a**$_3$•((S)-MePropCYA)$_6$ does not present a liquid crystalline phase when the alizarin is intercalated. The high enthalpy change value (153 kJmol^{-1}) for **2**∩**1a**$_3$•((S)-MePropCYA)$_6$ is typical for a crystalline-isotropic phase transition (Table 5.1). The enthalpy change values for the liquid crystalline-isotropic phase transitions are generally smaller than crystalline-isotropic phase transitions due to the lower ordering in liquid crystalline phases compared to crystalline phases. Probably, the intercalation of alizarin freezes the mobility of double rosettes **1a**$_3$•((S)-MePropCYA)$_6$ resulting in the crystallization of **2**∩**1a**$_3$•((S)-MePropCYA)$_6$ as emphasized by the huge difference between the isotropization temperatures of **2**∩**1a**$_3$•((S)-MePropCYA)$_6$ and **1a**$_3$•((S)-MePropCYA)$_6$ (ΔT_{Iso} = 51°C) (Table 5.1).

The POM image of **2**∩**1a**$_3$•((S)-MePropCYA)$_6$ showed yellow birefringent features, when the sample was cooled down slowly from the isotropic state, indicating a columnar arrangement of the double rosette in the crystalline state (Fig. 5.8).

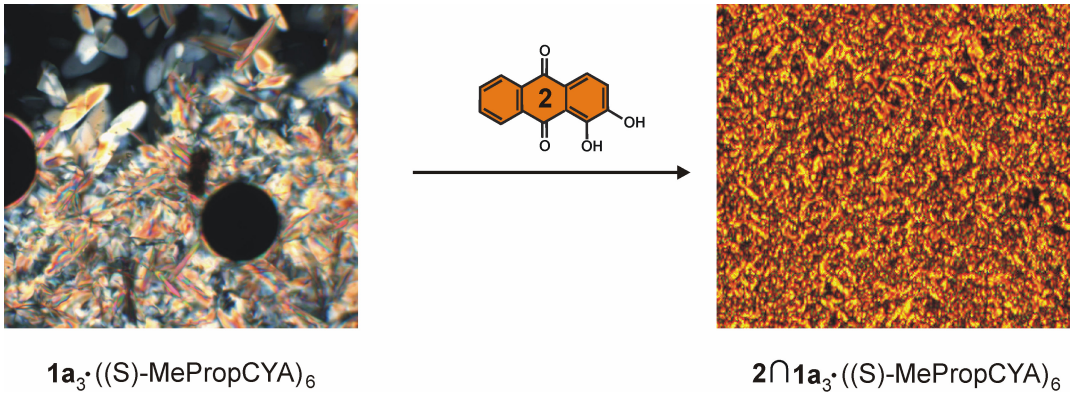

Figure 5.8. *Polarized optical microscopy images of the double rosette* ***1a***$_3$*•((S)-MePropCYA)*$_6$ *before (140 °C) and after intercalation of* ***2*** *(200°C).*

The formation of a crystalline phase for **2**∩**1a**$_3$•((S)-MePropCYA)$_6$ was also confirmed by XRD measurements (Table 5.2). The high number of reflections in the X-ray powder diffractogram is characteristic of crystalline phases. This phase is identified by the presence of a set of low-angle maxima related to a two-dimensional (2D) array of columns. The spacing can be indexed in a 2D orthorhombic lattice (C_{orth}), and the lattice constants are shown in Table 5.2. The double rosettes are still tilted by 30° with respect to the stacking direction of the columns as shown in the case of **1a**$_3$•((S)-MePropCYA)$_6$. The inter-distance between the double rosettes changes from 8.8 Å to 5.1 Å, for **1a**$_3$•((S)-MePropCYA)$_6$, and **2**∩**1a**$_3$•((S)-MePropCYA)$_6$, respectively. The intercalation of alizarin diminishes the inter-assembly distance, as a result the mobility between the columns decreases leading to the crystalline phase.[22]

5.2.3 CD spectroscopy in the liquid crystalline state

As mentioned in Chapter 4, double rosette assemblies **1a**$_3$•((S)-2-MeBuBAR)$_6$ and **1a**$_3$•((S)-MePropCYA)$_6$ have *D*$_3$-symmetry where the two melamine rings of each calix[4]arene are in antiparallel orientation with respect to each other.[48] Due to the presence of a chiral center on the barbituric and cyanuric derivatives only one diastereomer ((*P*)- or (*M*)-) is formed. This property enables the study of the chiral arrangement of the double rosettes in the liquid crystalline state by CD. Thus, the different binding modes of alizarin by the mesogenic double rosettes in the liquid crystalline state were studied by CD spectroscopy. The experiments were performed on the corresponding neat samples both at the temperature of the mesophases and in the isotropic state. The double rosette **1a**$_3$•((S)-2-MeBuBAR)$_6$ in the liquid crystalline state has a helical arrangement within the columns (Chapter 4) (Fig. 6.9, curve a). The negative sign in the CD curve is typical for double rosettes bearing chiral barbiturate derivatives with (S)-stereochemistry (Chart 5.1).[43] Upon direct addition of the alizarin to the liquid crystal **1a**$_3$•((S)-2-MeBuBAR)$_6$ the CD signal in the 310-450 nm region disappeared (Fig. 5.9, curve b). The loss of optical activity for the double rosette assembly is an indication of the encapsulation of alizarin in the double rosette **1a**$_3$•((S)-2-MeBuBAR)$_6$. The encapsulation of the alizarin trimer breaks the *D*$_3$-symmetry of the

assembly **1a**$_3$•((S)-2-MeBuBAR)$_6$ leading to the formation of the complex **1a**$_3$•((S)-2-MeBuBAR)$_6$•**2**$_3$ with C_{3h}-symmetry, which presents a horizontal plane that renders the assembly almost CD silent.[40] This change in symmetry implies a change of the two melamines rings of each calix[4]arene **1a** from the staggered conformation in the empty receptors to an eclipsed conformation in the complex (Fig. 5.2).[34]

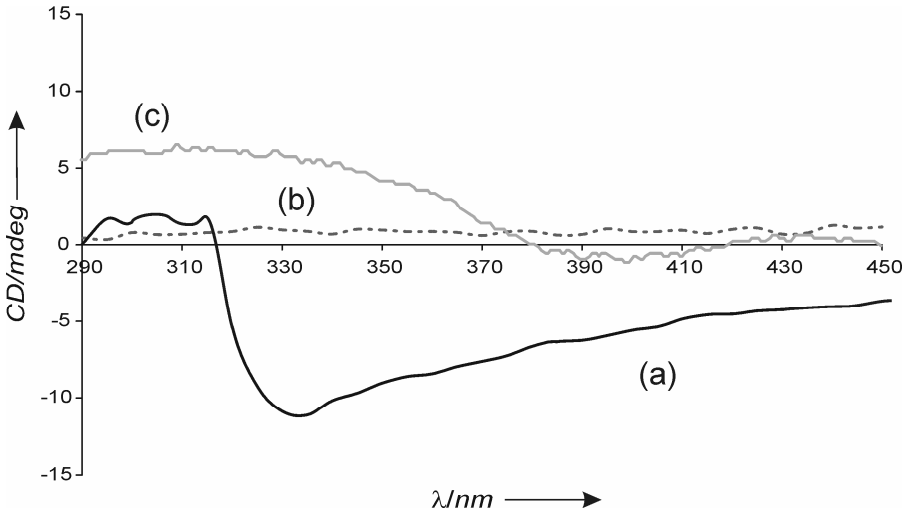

Figure 5.9. *Circular dichroism spectra for double rosette assemblies; (a)* ***1a***$_3$*•((S)-2-MeBuBAR)*$_6$ *at 130°C, (b)* ***1a***$_3$*•((S)-2-MeBuBAR)*$_6$*•****2***$_3$ *at 130°C and (c)* ***1a***$_3$*•((S)-MePropCYA)*$_6$ *in the presence of alizarin at 180°C. All CD spectra were recorded from the same sample cooling down from the isotropic phase.*

As demonstrated before, the addition of cyanurate derivatives leads to the release of alizarin from the double rosette cavity in solution. To study the possible release of the alizarin from the double rosette in the mesophase, (S)-MePropCYA was added to the complex **1a**$_3$•((S)-2-MeBuBAR)$_6$•**2**$_3$. A CD signal is recorded in the region 290-350 nm (Fig. 5.9, curve c). The positive sign in the CD curve is typical for double rosettes with (S)-cyanurate (Chart 5.1), indicating that exchange between the (S)-2-MeBuBAR and (S)-MePropCYA has occurred. Therefore, the recovery of the optical activity for double rosette assembly **1a**$_3$•((S)-MePropCYA)$_6$ suggests that the alizarin is released from the double rosette cavity.[43] The intercalation of the alizarin between the columns of **1a**$_3$•((S)-MePropCYA)$_6$ was confirmed recording a spectrum from 290-600 nm (Fig 5.10). A bisignate Cotton effect with a negative peak at 390 nm and a positive peak at 435 nm was observed (Fig 5.10).[49] The shape of the CD spectrum for the complex

2∩**1a**$_3$•((S)-MePropCYA)$_6$ is similar to the CD spectrum recorded in solution (Fig. 5.5). The observed CD spectrum (Fig 5.10) is probably the result of the chiral environment felt by the alizarin chromophores,[45] which induce a CD signal for **2** in the region of 350-450 nm.[46]

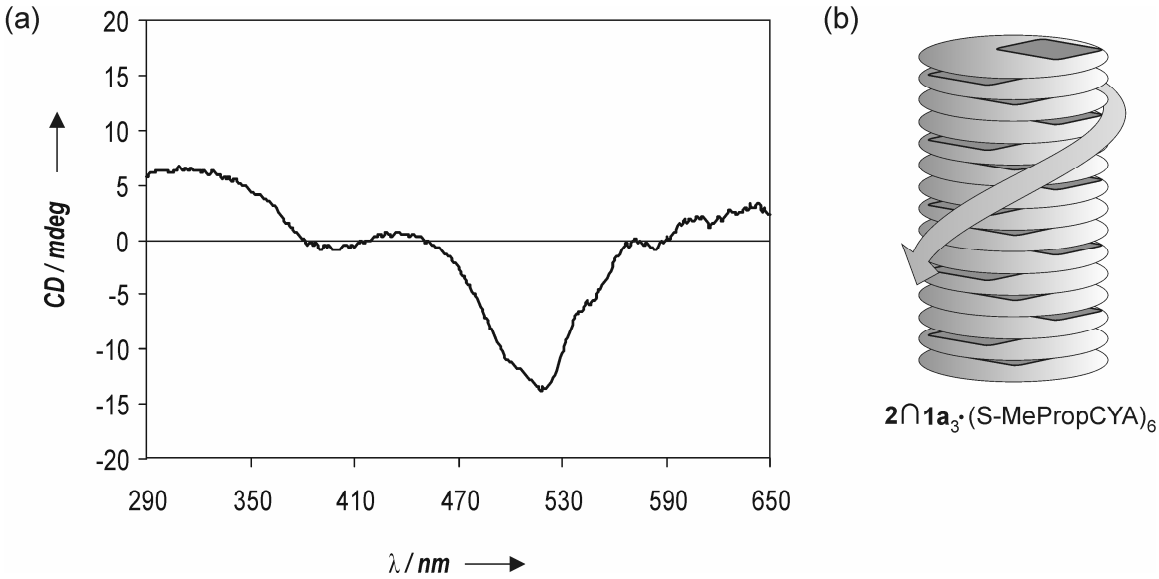

Figure 5.10. *(a) CD spectrum for the complex* ***2***∩***1a***$_3$•*((S)-MePropCYA)*$_6$ *on quartz plates at 175°C after cooling down from the isotropic phase and (b) schematic representation of the chiral columnar arrangement for* ***2***∩***1a***$_3$•*((S)-MePropCYA)*$_6$.

The direct exchange of building blocks in the solid state points out two important aspects: the response to external stimuli for the mesogenic double rosettes and the modulation of the optical activity. The introduction of perturbations to the system, such as the addition of small molecules, has led to a major change at the macroscopic level (e.g. crystal phase). This points out the importance of self-assembly and self-organization to obtain new materials. The control and the ability to *write* the optical activity in the solid state (**1a**$_3$•((S)-2-MeBuBAR)$_6$, CD active), to *eras*e it (**1a**$_3$•((S)-2-MeBuBAR)$_6$•**2**$_3$, CD silent), and *rewrite* it (**1a**$_3$•((S)-MePropCYA)$_6$, CD active) have been demonstrated (Fig 5.11).

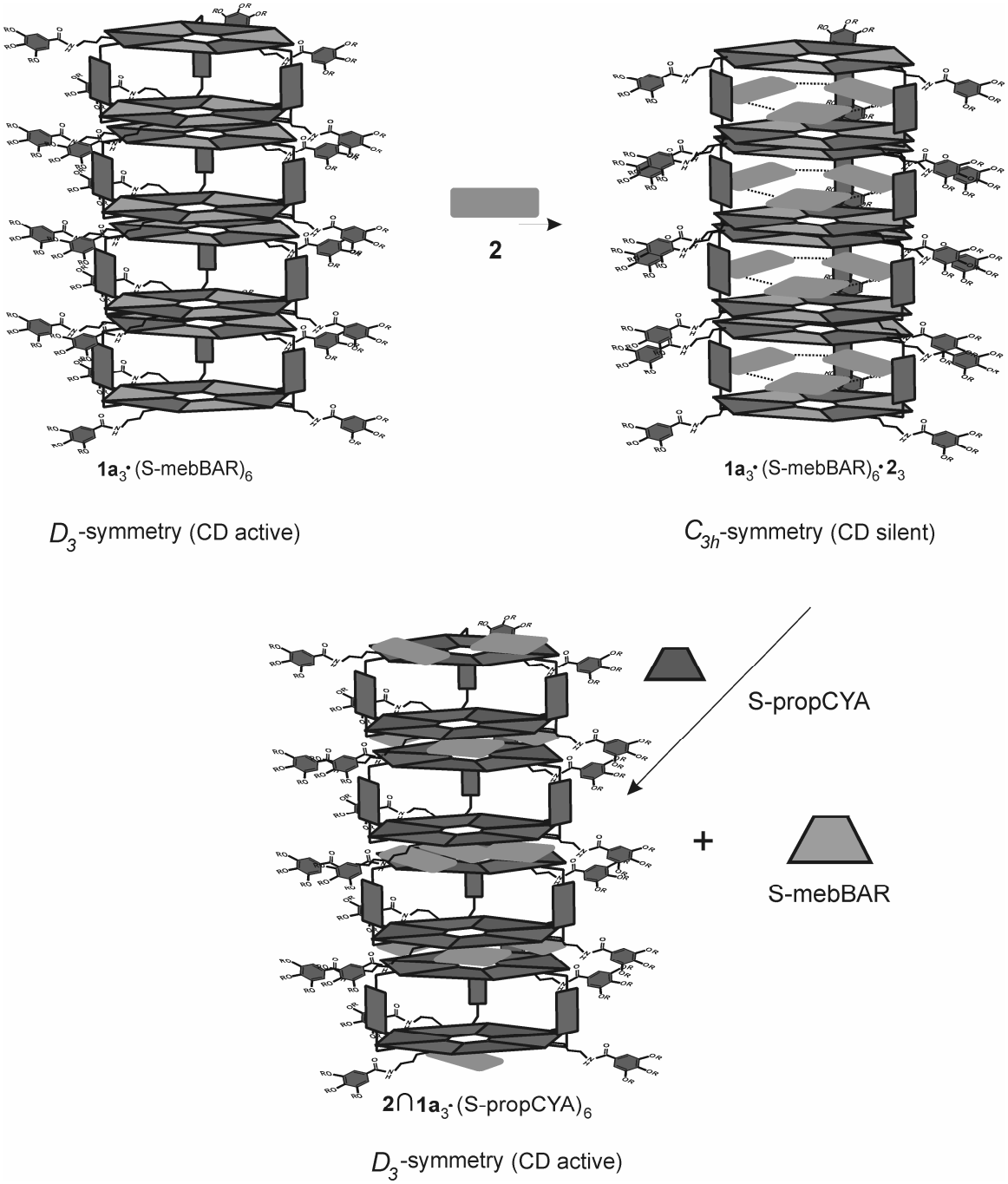

Figure 5.11. *Schematic representation of the direct exchange of the building blocks in the double rosettes* ***1a***$_3$*•((S)-2-MeBuBAR)*$_6$ *and* ***1a***$_3$*•((S)-2-MeBuBAR)*$_6$*•****2***$_3$*. The corresponding symmetries and CD activities are also given.*

5.3. Conclusions

In this chapter, the different complexation modes of alizarin by mesogenic double rosettes **1a**$_3$•((S)-2-MeBuBAR)$_6$ and **1a**$_3$•((S)-MePropCYA)$_6$ have been demonstrated. The alizarin was encapsulated in the cavity of the double rosette **1a**$_3$•((S)-2-MeBuBAR)$_6$ and intercalated between the floors of the double rosettes **1a**$_3$•((S)-MePropCYA)$_6$. In the liquid crystalline state, alizarin complexation led to high thermal stability of the double rosettes mesophases. In the case of **1a**$_3$•((S)-MePropCYA)$_6$, the enhancement in stability is so high that leads to a crystalline phase.

The dynamic behavior of these double rosette assemblies is shown by their ability to adapt rapidly to external stimuli. Different complexation modes can be obtained by direct and selective exchange of the guest molecules and the assembly building blocks, which allows also the modulation of optical activity in the liquid crystalline state.

5.4. Experimental Section

THF was freshly distilled from Na/benzophenone, and CH_2Cl_2 from $CaCl_2$. All chemicals were of reagent grade and used without further purification. NMR spectra were recorded on a Varian Unity 300 (^{1}H NMR 300 MHz) using tetramethylsilane (TMS) or the corresponding residual solvent signal as internal standard. FAB-MS spectra were recorded on a Finningan MAT 90 spectrometer with m-nitrobenzyl alcohol (NBA) as a matrix. CD spectra were recorded on a JASCO J-715 spectropolarimeter. A Perkin-Elmer DSC-7 was used for thermal analysis. DSC measurements were performed on a DSC Piris Series 7 (scanning rate: 10 °C min^{-1}). A polarizing optical microscope Olympus BH-2 equipped with a Mettler FP82HT hot stage was used for visual observation. UV-Vis measurements were carried out on a Varian Cary 3E UV-spectrophotometer.

The molecular arrangements in different samples were analyzed with an X-ray diffractometer equipped with a home-built capillary oven. Each sample was placed into X-ray capillary with 1.0 mm internal diameter and then the capillary tube placed inside a vertically aligned graphite tube containing a hole transversal to it, allowing the incident X-ray beam to cross freely. The temperature of the graphite tube was controlled by a

system formed by a thermo-couple attached to a power supply and it acts as a fast-response online oven ranging from room temperature to 350 ºC. The X-ray measurements were carried out in a Bruker-Nonius D8 diffractomenter with a 2-D detector with a sample to detector distance set to 10 cm and spectra were recorded for 1 hr. A focused permanent magnetic field of approximately 4T was applied perpendicular to the capillary allowing for alignment of any liquid crystal phase. CD measurements were conducted on a JASCO J-715 spectropolarimeter using a Mettler FP82HT hot stage.

Synthesis. The synthesis of compounds **1a**,[50] **1b**,[29] (S)-2-MeBuBAR,[51] (S)-MePropCYA[52] has been reported previously.

Formation of double rosette assemblies. Hydrogen-bonded assemblies were prepared by mixing calix[4]arene **1a** or **1b** with two equivalents of (S)-2-MeBuBAR or (S)-MePropCYA respectively, in toluene-d_8 for 20 min at 100°C. For example, 8.3 mg (0.0030 mmol) of **1** and 1.10 mg (0.0060 mmol) of (S)-MePropCYA were dissolved in 5 mL of toluene–d_8, stirred and heated at 100°C until all compounds were dissolved. In case of the complexes formation 3 equivalents of alizarin **2** were added and the mixtures were stirred untill all compound was dissolved. After evaporation of the solvent under high vacuum, the assembly is ready to use.

Circular dichroism in the liquid crystalline state. The prepared double rosette assemblies were placed in between two quartz slides and heated by hot stage until the isotropic phase. The cells were allowed to cool down with no external mechanical stress. Linear dichroism effects were eliminated by averaging several CD spectra (recorded at different film positions rotated around the light beam). The CD spectra were recorded cooling down from the isotropic point at rate of 10 °C/min^{-1}.

5.5 References and Notes

[1] T. Kato, N. Mizoshita, K. Kishimoto, *Angew. Chem. Int. Ed.* **2006**, *45*, 38-68.

[2] J. Elemans, R. Van Hameren, R. J. M. Nolte, A. E. Rowan, *Adv. Mater.* **2006**, *18*, 1251-1266.

[3] G. Ten Brinke, O. Ikkala, *Chem. Rec.* **2004**, *4*, 219-230.

[4] N. M. Sangeetha, U. Maitra, *Chem. Soc. Rev.* **2005**, *34*, 821-836.

[5] I. W. Hamley, *Angew. Chem. Int. Ed.* **2003**, *42*, 1692-1712.

[6] G. M. Whitesides, B. Grzybowski, *Science* **2002**, *295*, 2418-2421.

[7] T. Kato, *Struct. Bond.* (Berlin) **2000**, *96*, 95-146.

[8] V. Percec, A. E. Dulcey, M. Peterca, M. Ilies, S. Nummelin, M. J. Sienkowska, P. A. Heiney, *Proc. Natl. Acad. Sci. U. S. A.* **2006**, *103*, 2518-2523.

[9] B. Chen, X. B. Zeng, U. Baumeister, S. Diele, G. Ungar, C. Tschierske, *Angew. Chem. Int. Ed.* **2004**, *43*, 4621-4625.

[10] V. Percec, M. Glodde, T. K. Bera, Y. Miura, I. Shiyanovskaya, K. D. Singer, V. S. K. Balagurusamy, P. A. Heiney, I. Schnell, A. Rapp, H. W. Spiess, S. D. Hudson, H. Duan, *Nature* **2002**, *419*, 384-387.

[11] W. Pisula, M. Kastler, D. Wasserfallen, M. Mondeshki, J. Piris, I. Schnell, K. Müllen, *Chem. Mater.* **2006**, *18*, 3634-3640.

[12] N. Sakai, Y. Kamikawa, M. Nishii, T. Matsuoka, T. Kato, S. Matile, *J. Am. Chem. Soc.* **2006**, *128*, 2218-2219.

[13] W. Pisula, M. Kastler, D. Wasserfallen, J. W. F. Robertson, F. Nolde, C. Kohl, K. Müllen, *Angew. Chem. Int. Ed.* **2006**, *45*, 819-823.

[14] J. Piris, M. G. Debije, N. Stutzmann, B. W. Laursen, W. Pisula, M. D. Watson, T. Bjornholm, K. Müllen, J. M. Warman, *Adv. Funct. Mater.* **2004**, *14*, 1053-1061.

[15] M. Yoshio, T. Mukai, H. Ohno, T. Kato, *J. Am. Chem. Soc.* **2004**, *126*, 994-995.

[16] J. J. van Gorp, J. Vekemans, E. W. Meijer, *J. Am. Chem. Soc.* **2002**, *124*, 14759-14769.

[17] T. Ishi-i, T. Hirayama, K. Murakami, H. Tashiro, T. Thiemann, K. Kubo, A. Mori, S. Yamasaki, T. Akao, A. Tsuboyama, T. Mukaide, K. Ueno, S. Mataka, *Langmuir* **2005**, *21*, 1261-1268.

[18] N. Ashkenasy, W. S. Horne, M. R. Ghadiri, *Small* **2006**, *2*, 99-102.

[19] S. Yagai, T. Nakajima, K. Kishikawa, S. Kohmoto, T. Karatsu, A. Kitamura, *J. Am. Chem. Soc.* **2005**, *127*, 11134-11139.

[20] D. Wasserfallen, I. Fischbach, N. Chebotareva, M. Kastler, W. Pisula, F. Jäckel, M. D. Watson, I. Schnell, J. P. Rabe, H. W. Spiess, K. Müllen, *Adv. Funct. Mater.* **2005**, *15*, 1585-1594.

[21] J. P. Gallivan, G. B. Schuster, *J. Org. Chem.* **1995**, *60*, 2423-2429.

[22] P. H. J. Kouwer, W. F. Jager, W. J. Mijs, S. J. Picken, *J. Mater. Chem.* **2003**, *13*, 458-469.

[23] P. H. J. Kouwer, O. van den Berg, W. F. Jager, W. J. Mijs, S. J. Picken, *Macromolecules* **2002**, *35*, 2576-2582.

[24] J. J. D. de Jong, L. N. Lucas, R. M. Kellogg, J. H. van Esch, B. L. Feringa, *Science* **2004**, *304*, 278-281.

[25] L. J. Prins, D. N. Reinhoudt, P. Timmerman, *Angew. Chem. Int. Ed.* **2001**, *40*, 2383-2426.

[26] M. Suarez, J.-M. Lehn, S. C. Zimmerman, A. Skoulios, B. Heinrich, *J. Am. Chem. Soc.* **1998**, *120*, 9526-9532.

[27] P. H. J. Kouwer, W. F. Jager, W. J. Mijs, S. J. Picken, *Macromolecules* **2002**, *35*, 4322-4329.

[28] H. Hofmeier, U. S. Schubert, *Chem. Commun.* **2005**, 2423-2432.

[29] P. Timmerman, R. H. Vreekamp, R. Hulst, W. Verboom, D. N. Reinhoudt, K. Rissanen, K. A. Udachin, J. Ripmeester, *Chem. Eur. J.* **1997**, *3*, 1823-1832.

[30] R. H. Vreekamp, J. P. M. van Duynhoven, M. Hubert, W. Verboom, D. N. Reinhoudt, *Angew. Chem. Int. Ed.* **1996**, *35*, 1215-1218.

[31] C. T. Seto, G. M. Whitesides, *J. Am. Chem. Soc.* **1993**, *115*, 905-916.

[32] L. J. Prins, C. Thalacker, F. Würthner, P. Timmerman, D. N. Reinhoudt, *Proc. Natl. Acad. Sci. U. S. A.* **2001**, *98*, 10042-10045.

[33] V. Percec, M. Glodde, T. K. Bera, Y. Miura, I. Shiyanovskaya, K. D. Singer, V. S. K. Balagurusamy, P. A. Heiney, I. Schnell, A. Rapp, H. W. Spiess, S. D. Hudson, H. Duan, *Nature* **2002**, *419*, 862-862.

[34] J. M. C. A. Kerckhoffs, F. W. B. van Leeuwen, A. L. Spek, H. Kooijman, M. Crego-Calama, D. N. Reinhoudt, *Angew. Chem. Int. Ed.* **2003**, *42*, 5717-5722.

[35] A. G. Bielejewska, C. E. Marjo, L. J. Prins, P. Timmerman, F. de Jong, D. N. Reinhoudt, *J. Am. Chem. Soc.* **2001**, *123*, 7518-7533.

[36] The association constants for formation of these complexes could not be readily determined since the stoichiometry is not exactly known.

[37] M. G. J. ten Cate, D. N. Reinhoudt, M. Crego-Calama, *J. Org. Chem.* **2005**, *70*, 8443-8453.

[38] M. A. Read, S. Neidle, *Biochemistry* **2000**, *39*, 13422-13432.

[39] D. Wu, A. Chen, C. S. Johnson Jr, *J. Magn. Reson.* **1995**, *115*, 260-264.

[40] J. M. C. A. Kerckhoffs, M. G. J. ten Cate, M. A. Mateos-Timoneda, F. W. B. van Leeuwen, B. Snellink-Ruël, A. L. Spek, H. Kooijman, M. Crego-Calama, D. N. Reinhoudt, *J. Am. Chem. Soc.* **2005**, *127*, 12697-12708.

[41] The Hunter-Sanders' model for π-π stacking is used to explain the complex formation. In the model, the σ-framework and the π-electrons are considered separately. This model shows that the π-σ attractions overcome the π-π repulsion giving the net favorable π-π interactions, which lead to the complex formation.

[42] The CD activity for the chiral double rosette assemblies comes from the asymmetrical arrangement of the chromophores units in the assembly.

[43] L. J. Prins, J. Huskens, F. de Jong, P. Timmerman, D. N. Reinhoudt, *Nature* **1999**, *398*, 498-502.

[44] The peaks at 280 and 325 nm are due to the π-π* transition of the chromophores in the assembly.

[45] Y. Kamikawa, T. Kato, *Org. Lett.* **2006**, *8*, 2463-2466.

[46] T. Ishi-i, M. Crego-Calama, P. Timmerman, D. N. Reinhoudt, S. Shinkai, *Angew. Chem. Int. Ed.* **2002**, *41*, 1924-1929.

[47] O. Y. Fedoroff, M. Salazar, H. Han, V. V. Chemeris, S. M. Kerwin, L. H. Hurley, *Biochemistry* **1998**, *37*, 12367-12374.

[48] L. J. Prins, K. A. Jolliffe, R. Hulst, P. Timmerman, D. N. Reinhoudt, *J. Am. Chem. Soc.* **2000**, *122*, 3617-3627.

[49] The CD peak at 530 nm is the result of the exciton coupling between alizarin chromophores as demonstrated by UV-vis measurement (data not shown)

[50] The synthesis of the barbituric and cyanuric derivatives is described in Chapter 4.

[51] The synthesis of the barbituric and cyanuric derivatives is described in Chapter 5.

[52] M. A. Mateos-Timoneda, M. Crego-Calama, D. N. Reinhoudt, *Supramol. Chem.* **2005**, 17, 67-79.

Chapter 6

Supramolecular Organization of Hydrogen-Bonded Molecular Boxes on Surfaces

In this chapter, the investigation of the supramolecular organization of mesogenic double rosettes on surfaces by AFM and STM is described. The self-organization of these assemblies on solid supports was studied by variation of parameters such as the nature of surface, concentration and solvent. The presence of double rosette aggregates in solution at low concentration (25 μM) led to the formation of micrometer-long ordered structures on graphite. The chirality of the double rosettes allowed the organization of these assemblies in ordered structures when deposited onto mica. Moreover, STM measurements allowed the visualization of individual mesogenic double rosettes on HOPG.

6.1 Introduction

The self-assembly of single elements into complex, organized structures via specific intermolecular interactions is the key issue for the realization of molecular devices and well-defined nanometer-scale objects.[1,2] Such programmed structures are commonly found in biological systems such as double stranded DNA.[3] The information encoded at the molecular level guides the organization at the supramolecular level. Several types of noncovalent interactions have been applied to construct complex architectures which may find applications in the field of biology and material science.[4-9] However, the positioning of those complex structures on solid support is not a simple issue. A restricted number of studies show the opportunities and limitations of transferring the objects from solution to a surface in a controlled way.[10-14]

In liquid crystals, the specific properties of the materials are determined by the chemical structure and the supramolecular organization of the building blocks. Their organization in the mesophase, and consequently their properties, can be tailored by noncovalent interactions such as hydrogen bonds.[15-17] In particular, columnar liquid crystalline materials have a high degree of organization in the mesophase leading to possible applications in the optoelectronic field due to their high electron and hole mobility.[18-20] In such applications, it is crucial to control, for example, the column orientation as well as other aspects of thin film morphology. Generally, the constituents of those columns are flat and electron-rich molecules, which can be easily influenced by different parameters when deposited on a solid support from solution.[21-25] However, there are not many studies on the influence of those parameters for mesogens with nanometer dimensions, which have already an intrinsic organization.[26-28]

In Chapter 3 the liquid crystallinity was described of hydrogen-bonded double rosette with nanometer dimensions, obtained by the self-assembly of different components, which displayed hexagonal columnar mesophases for a wide range of temperatures. The driving force for the mesophase formation is the microsegregation between the rigid polar core and the lipophilic alkyl chains attached at the periphery of the assembly. In this chapter the presence in solution of the mesogenic double rosettes and their aggregation at low concentration which has been observed by ^{1}H NMR is reported. The influence of

several parameters (concentration, solvent, etc.) on the self-organization of mesogenic double rosettes on surfaces has been investigated by means of different surface techniques such as atomic force microscopy (AFM) and scanning tunneling microscopy (STM). The self-organization of nonliquid crystalline double rosettes on highly ordered pyrolytic graphite (HOPG) has been also studied by AFM and STM by our group.[6,11,29-31] The rigid structure of those assemblies allowed only rod-like organization. The assemblies followed the main directions of the underlying graphite and they are oriented edge-on[30] or face-on[31] on the surface. The different orientations depended on the nature of the building blocks. In this chapter, a random organization of rod-like structures formed by mesogenic double rosettes on HOPG is described. This different organization of those assemblies is probably due to the dynamic nature of the liquid crystalline double rosettes. A hexagonal organization of these assemblies is also shown by STM.

6.2. Results and Discussion

Dimelamine **1**, BuCYA, (R)-MePropCYA and (S)-MePropCYA (Chart 6.1) have been synthesized following methods previously described.[32,33] The achiral $\mathbf{1}_3$•$(DEB)_6$, $\mathbf{1}_3$•$(BuCYA)_6$ and chiral double rosettes $\mathbf{1}_3$•$((R)\text{-}MePropCYA)_6$, $\mathbf{1}_3$•$((S)\text{-}MePropCYA)_6$ consist of three calix[4]arene dimelamine **1** and six barbiturates or cyanurates held together through the formation of 36 cooperative hydrogen bonds (Chart 6.1).[34,35] The periphery of the self-assembled double rosette is decorated with six phenyl groups, each bearing three octadecyl chains, which are able to promote the self-organization of the double rosette assembly in the liquid crystalline phase.

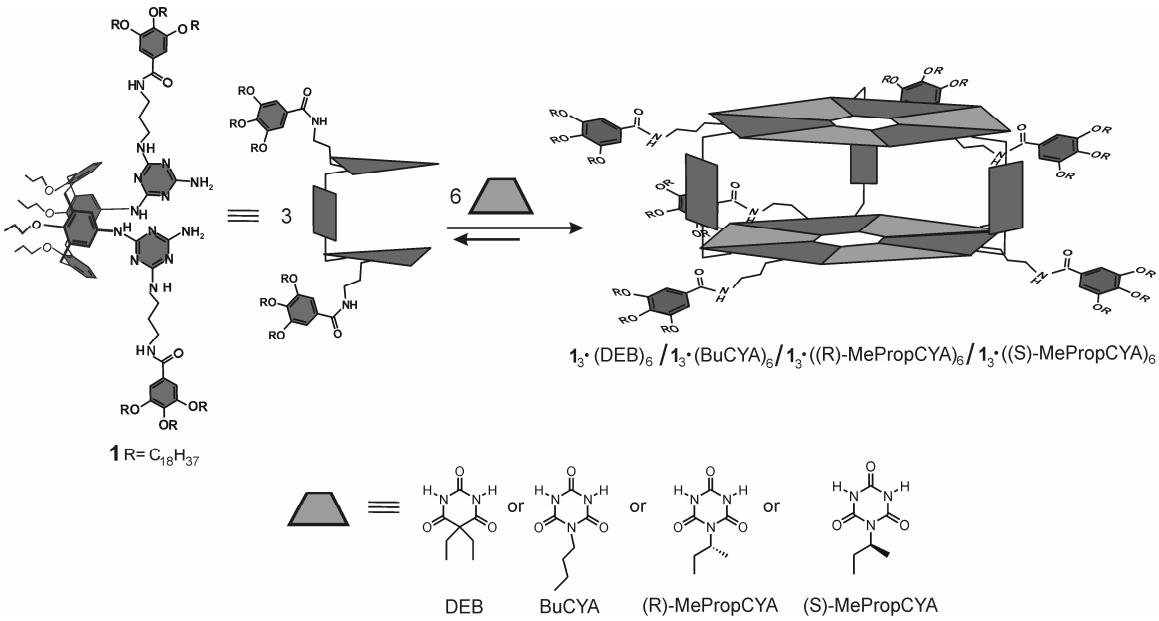

Chart 6.1. *Structural and schematic representation of the dimelamine **1** and barbiturate/cyanurate derivatives, and the corresponding hydrogen-bonded assemblies* $\mathbf{1}_3$*•(DEB)*$_6$*,* $\mathbf{1}_3$*•(BuCYA)*$_6$*,* $\mathbf{1}_3$*•((R)-MePropCYA)*$_6$*, and* $\mathbf{1}_3$*•((S)-MePropCYA)*$_6$*.*

6.2.1. Double rosette aggregation in solution at low concentration

Previously our group has shown by UV-vis studies that double rosette assemblies are thermodynamically stable in solution, even at concentration of 5 μM.[36] Furthermore, in Chapter 5 of this thesis the presence of aggregates of the mesogenic double rosettes in solution at 1.0 mM concentration in apolar solvents (toluene and dodecane) was confirmed by ^{1}H NMR spectroscopy, while in chloroform this aggregation was ruled out. The aggregation of the double rosette **1**$_3$•(BuCYA)$_6$ at low concentration by ^{1}H NMR was investigated, to study whether the pre-organization of mesogenic double rosettes in solution influences the organization on surfaces. Dilution experiments in deuterated toluene showed the presence of the characteristic[34] hydrogen-bonded amide protons around 15-14 ppm for the double rosette **1**$_3$•(BuCYA)$_6$ even at 10.0 μM (Fig. 6.1). The integration of those signals indicated that more than 50% of the assemblies are intact at this concentration.

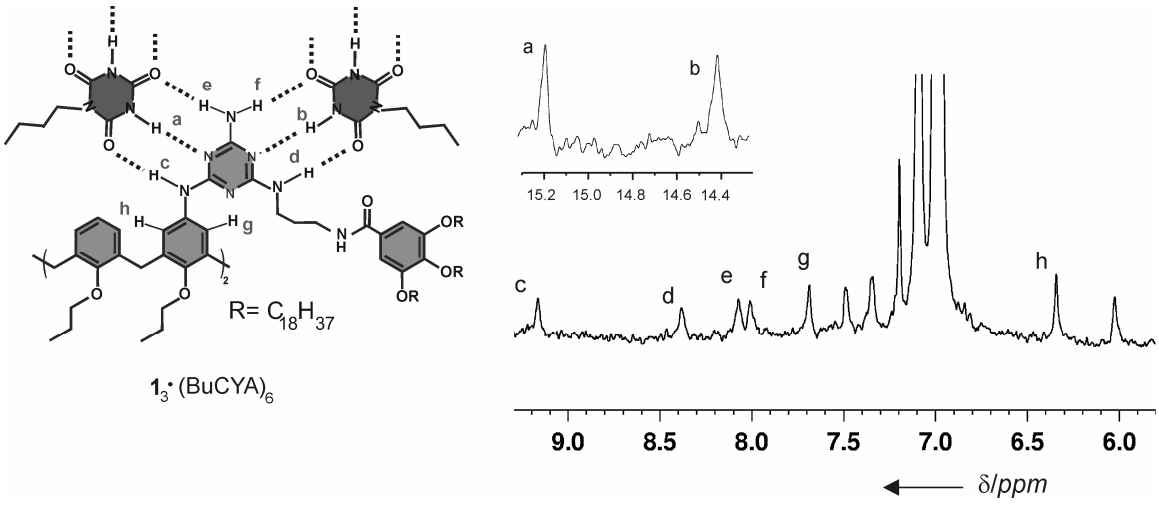

Figure 6.1. *Parts of ^{1}H NMR spectrum (600 MHz) of* ***1***$_3$*•(BuCYA)$_6$ (10 μM). The spectrum was recorded at 298 K in toluene-d_8.*

In dodecane (25.0 μM), the ^{1}H NMR spectrum of the double rosette **1**$_3$•(BuCYA)$_6$ shows broad peaks for the characteristic hydrogen-bonded NH_{BuCYA} protons in the region 15-9 ppm. This indicates the aggregation of double rosette assemblies under these conditions.[37] Probably, dodecane allows better stacking of the double rosettes due to its

more apolar character compared to toluene. Sharp peaks were not visible even at 50°C, indicating the remarkable thermodynamic stability of $\mathbf{1}_3$•(BuCYA)$_6$ aggregates at this concentration.

6.2.2. Double rosettes on HOPG: the effect of the concentration

In order to study the morphology of double rosettes on solid support, solutions of $\mathbf{1}_3$•(DEB)$_6$, $\mathbf{1}_3$•(BuCYA)$_6$, and $\mathbf{1}_3$•((R)-MePropCYA)$_6$ were drop-cast onto freshly cleaved HOPG substrates (10.0 μM in chloroform). The topographic images for the three double rosette assemblies acquired by high resolution tapping mode AFM (TM-AFM) showed the presence of fibers closely packed together in random directions (Fig. 6.2).

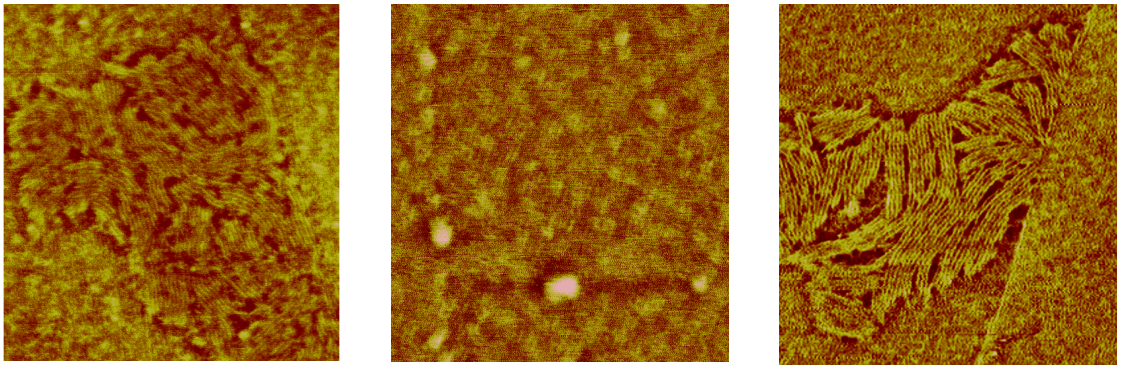

Figure 6.2. *TM-AFM phase images (400 × 400 nm^2) of double rosette assembly $\mathbf{1}_3$•(DEB)$_6$ (left), $\mathbf{1}_3$•(BuCYA)$_6$ (middle) and $\mathbf{1}_3$•((R)-MePropCYA)$_6$ (right) deposited on HOPG from chloroform at 1×10^{-5} M concentration.*

The rod-like structures did not follow the main directions of the HOPG, as it was found earlier for other double rosette assemblies.[11,30] Probably, the interaction between the lipophilic chains and the graphite is strong enough to overcome the interaction between the phenyl groups of the dimelaminecalix[4]arene **1** and the graphite. The latter would lead to rod-like structures that follow the main directions of the underlying graphite.[11] Although the mesogenic double rosettes $\mathbf{1}_3$•(DEB)$_6$, $\mathbf{1}_3$•(BuCYA)$_6$, and $\mathbf{1}_3$•((R)-MePropCYA)$_6$ did not aggregate in chloroform, as described in Chapter 5 of this thesis, at the solid-liquid interface the formation of fibers can be attributed to the nanosegration between the hydrophilic core of the double rosettes and the hydrophobic

alkyl chains. Analysis of the AFM pictures showed that the inter-row distance for the double rosettes $\mathbf{1}_3$•(DEB)$_6$ and $\mathbf{1}_3$•((R)-MePropCYA)$_6$ is 4.5 ± 0.1 nm. This is in good agreement with the inter-column distance found for those assemblies in the LC mesophase (4.3 nm and 4.1 nm, respectively) as described in Chapters 3 and 4. It was not possible to determine the inter-row distance for the double rosette $\mathbf{1}_3$•(BuCYA)$_6$ because the fibers were short and randomly organized. Moreover the random directions of the fibers precludes the determination of the double rosettes orientation through extrapolation of step length at the boundary of the well-oriented rod-like domains.[11,30]

The effect of the concentration of the double rosette assemblies on the thin film packing has been investigated for the assembly $\mathbf{1}_3$•(BuCYA)$_6$. Figure 6.3 shows the AFM pictures of $\mathbf{1}_3$•(BuCYA)$_6$ in chloroform at 1.0 × 10^{-5}, 5.0 × 10^{-6}, and 5.0 × 10^{-7} M concentrations.

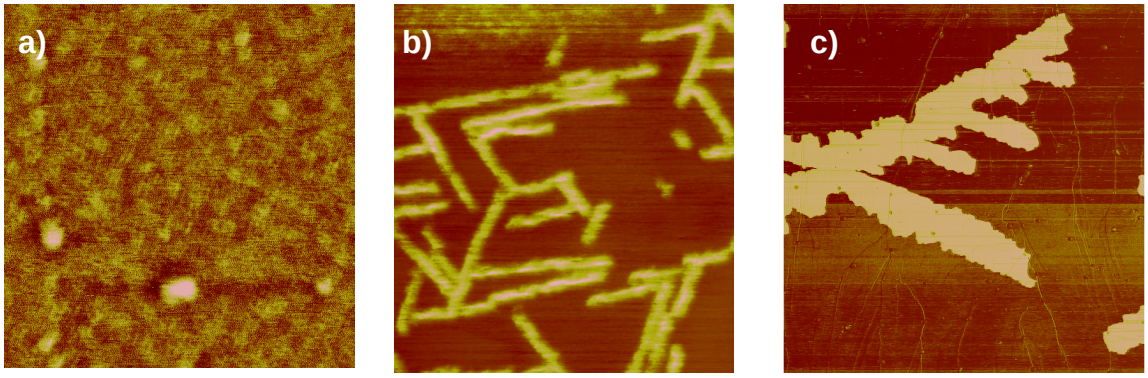

Figure 6.3. *TM-AFM phase images of double rosette assembly* $\mathbf{1}_3$•*(BuCYA)*$_6$ *deposited on HOPG from chloroform: a) 1.0 × 10^{-5} M (image size: 300 × 300 nm^2, b) 5.0 × 10^{-6} M (image size: 200 × 200 nm^2), and c) 5.0 × 10^{-7} M (image size: 15 × 15 μm^2).*

At high concentration, an elevated number of fibers was detected (Fig. 6.3a), but they were short and closely packed together on the surface. As the concentration decreases, the fiber length increased, and isolated stacks of fibers oriented according to the graphite lattice were visible (Fig. 6.3b). Although a constant width of about 18 nm for the fiber was found, the measured lateral dimensions are easily overestimated by several nanometers due to the tip-convolution effects.[38] Therefore, the values of measured heights are a more accurate way to evaluate the orientation of the double rosette on HOPG. The single cylindrical fibers of $\mathbf{1}_3$•(BuCYA)$_6$ had a uniform height of 1.8 nm,

which could correspond to three double rosettes stacked on top of each other in face-on manner (Fig. 6.4). An edge-on orientation of the double rosettes was ruled out because this orientation implies a height ≥ 3.3 nm (Fig. 6.4).[6,31]

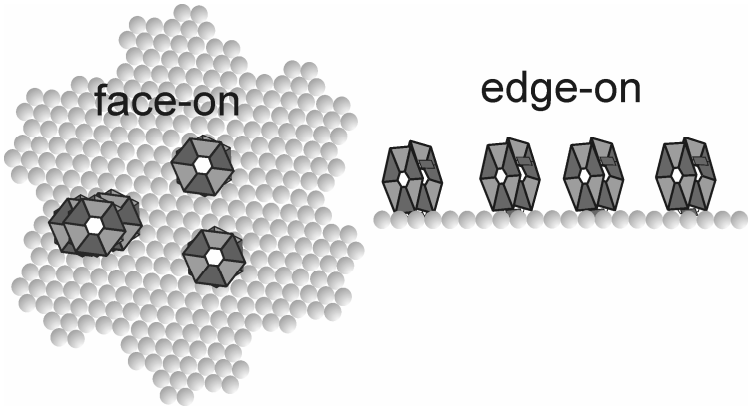

Figure 6.4. *Possible orientations for the mesogenic double rosettes on HOPG.*

Upon lowering the concentration to 5.0×10^{-7} M, the assembly $\mathbf{1}_3$•$(BuCYA)_6$ formed micrometer-long homotropic arrangements typical for hexagonal columnar liquid crystals with the mesogens oriented in a face-on manner when deposited on the surface (Fig. 6.3c).[39] The face-on orientation was confirmed by measuring the height of these features. A value of 0.6 nm was found which is similar to the height found by X-ray diffraction .[35] Thus, at low concentration the double rosette $\mathbf{1}_3$•$(BuCYA)_6$ displayed a higher degree of organization (hexagonal columnar lattice, 2D organization) than at high concentration (fiber, 1D organization). The basic concepts of crystal growth can be applied to explain this growth process. The nucleation sites and the nucleation and growth rates are parameters that can influence the organization of the double rosette on the surface. Generally, the nucleation sites and rate determine the number of fibers in relation to the concentration.[40,41] Instead, the growth process is controlled by diffusion, and hence, at higher concentration, the probability that molecules encounter a nucleation site increases. [40,42] Consequently at high concentration, there are many short fibers on the surface, while at low concentration the fibers are longer, and they can further organize in a 2D arrangement (hexagonal columnar lattice) as shown in Figure 6.3c. Therefore, the concentration can be used to control very easily the type of organization on surfaces.

6.2.3. Double rosettes on HOPG: the effect of the solvent and temperature

Solutions of double rosette $\mathbf{1}_3$•$(BuCYA)_6$ in chloroform, toluene, and tetradecane at 1.0×10^{-6} M concentration were drop-cast on HOPG. Immediately after the deposition, no organization can be seen in the AFM images for the samples in tetradecane and toluene (Fig. 6.5a, b). This is probably due to presence of solvent molecules that make the sample too soft to be imaged. After thermal annealing in a vacuum oven at 60°C overnight, organized structures were revealed by AFM.

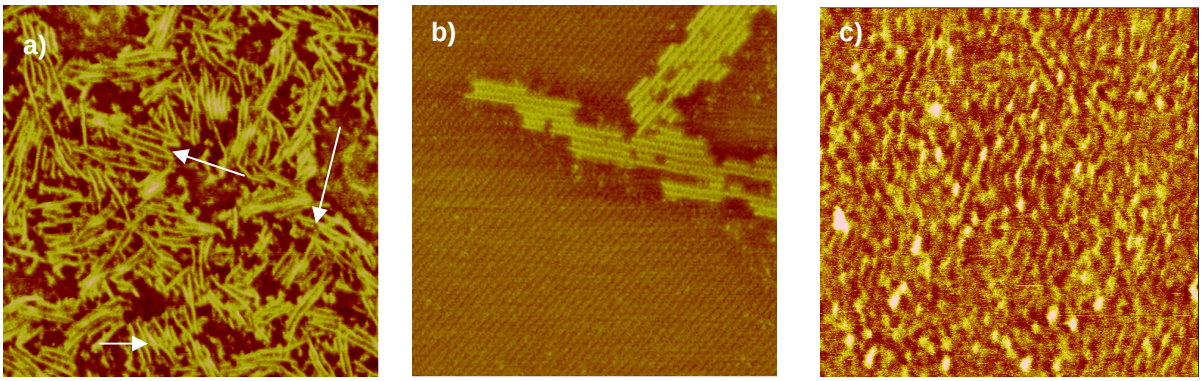

Figure 6.5. *TM-AFM phase images (image size:300 × 300 nm^2) of double rosette assembly* $\mathbf{1}_3$•$(BuCYA)_6$ *(1×10^{-6} M) on HOPG after thermal annealing at 60°C overnight. Deposited from: a) toluene, b) tetradecane, and c) chloroform. White arrows indicate the several points of the samples where the inter-fibers distance was measured.*

The sample in chloroform was annealed at 60°C overnight as well for comparison with the other solvents, even though the structures can be also seen without thermal annealing (Fig. 6.3). This sample shows nanosegration of the double rosettes (Fig. 6.5c) that resembles the TEM pictures for homeotropically aligned liquid crystals.[25,43] Probably, the fiber organization is destroyed by the fast solvent evaporation (see section 6.2.2). Consequently, the double rosette assemblies are organized in small domains where the polar cores of the assembly are fused together surrounded by the lipophilic chains. The sample drop-cast from toluene reflects the opposite situation (Fig. 6.5a). The double rosette $\mathbf{1}_3$•$(BuCYA)_6$ formed bundles randomly oriented on the HOPG. Each bundle is formed by a single layer of double rosettes oriented in a face-on manner as deduced from the height values (0.6 nm). Thus the bundles are formed by fibers, which are formed by

the consecutive alignment of double rosette assemblies. For aligned fibers a distance between two fibers of 7.0 ± 0.2 nm was found (Fig. 6.5a). This value is higher than the inter-column distance found in the liquid crystalline phase, indicating a decrease in the intermolecular interaction between the double rosettes. This decrease is probably due to the competitive interactions between alkyl chains and the graphite which makes the packing weaker than in the mesophase. In tetradecane the double rosette $\mathbf{1}_3$•$(BuCYA)_6$ forms rod-like structures (Fig. 6.5b), similar to the ones observed in previous studies on double rosettes.[30] As it can be observed in Figure 6.5b, multi-layered rods are formed. The height of these features is 1.8 nm corresponding to three double rosette assemblies on top of each other. The inter-row distance of 5.1 ± 0.1 nm indicates that each row is composed by one double rosette oriented in face-on manner. The rods have micrometer dimensions following the lattice of the graphite. The different supramolecular organizations in chloroform, toluene and tetradecane (Fig. 6.6) can be attributed to dewetting phenomena during solvent evaporation.[22,23,44] The boiling temperature of tetradecane is 256°C, which is higher than the boiling temperature of toluene (110°C) and chloroform (68°C).

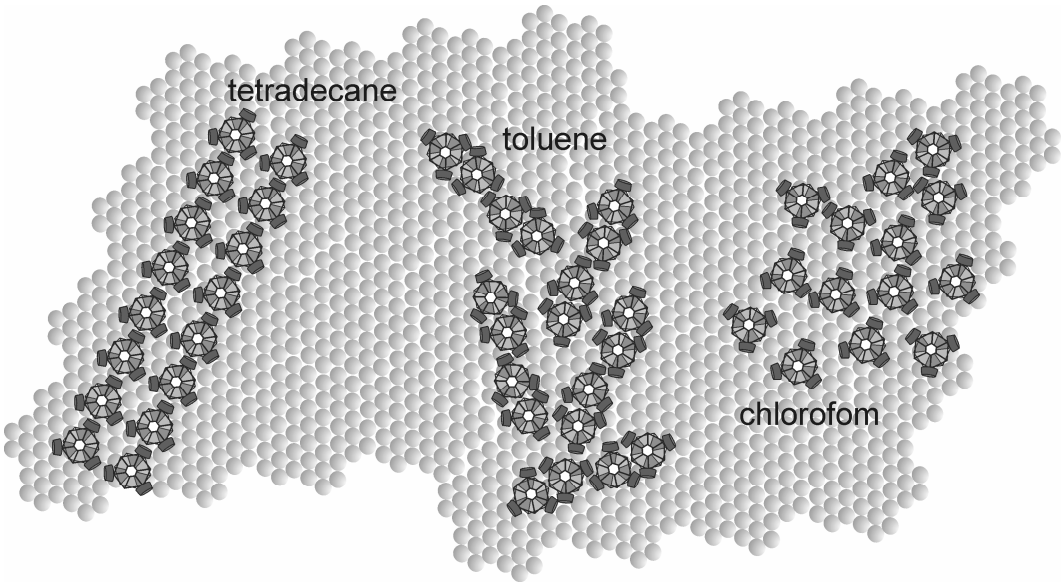

Figure 6.6. *Different organization of the double rosette* $\mathbf{1}_3$•$(BuCYA)_6$ *from tetradecane, toluene, and chloroform.*

The high supramolecular ordering of double rosettes from a tetradecane solution can be ascribed to the formation of aggregates in this solvent as observed for dodecane since they are chemically similar. In toluene, the double rosettes do not form aggregates at 1.0 × 10^{-6} M concentration and the evaporation is faster than for tetradecane. This leads to an alignment of the double rosettes in short bundles of nanometer size (Fig 6.6). Therefore, the slow evaporation rate of the tetradecane allows the double rosettes to be perfectly aligned on the surface. In chloroform, the evaporation of solvent is faster than in toluene. Thus, the dewetting process governs the supramolecular organization.

6.2.4. Double rosettes on mica: the effect of the surface nature

Double rosette **1**$_3$•(BuCYA)$_6$ was deposited on mica from chloroform at (1 × 10^{-5} M). The AFM image shows the formation of globular structures (Fig. 6.7). The formation of these structures can be attributed to the unfavorable interactions between the mesogenic assemblies and the mica surface. Contrary to graphite, the surface of the mica substrate is hydrophilic. On this surface, the double rosettes fuse together to minimize the contact between the hydrophobic alkyl chains and the hydrophilic surface.

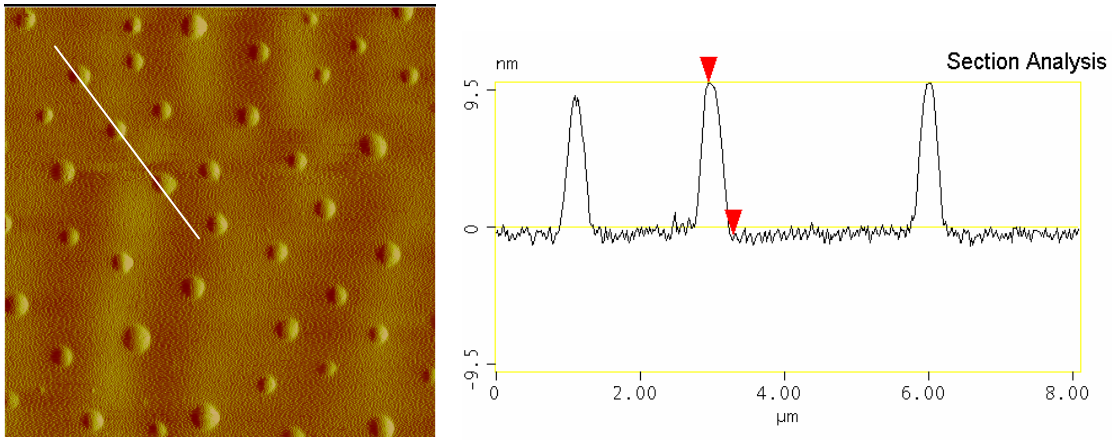

Figure 6.7. *TM-AFM phase images (8.0 × 8.0 µm^2) (left) and the height profile (right) of the double rosette assembly* ***1***$_3$*•(BuCYA)*$_6$ *on mica deposited from chloroform at 1×10^{-5} M concentration.*

The globular structures are quite regular with an average height and width of 10 nm and ~ 200 nm, respectively (Fig 6.7b). The formation of these structures is controlled by sub-micron-scale solvent evaporation dynamics,[45] as highlighted by the globular

structures (Fig. 6.7). On the other hand, when the double rosette $\mathbf{1}_3$•(BuCYA)$_6$ was deposited on mica from toluene, no regular structures or patterns were observed.

For the chiral double rosette $\mathbf{1}_3$•((R)-MePropCYA)$_6$ a regular pattern can be seen upon deposition of a 1.0×10^{-5} M solution in toluene on mica (Fig. 6.8). The organized structures do not show changes in their supramolecular organization even after thermal treatment in vacuum at 60°C overnight, indicating a remarkable thermal stability.

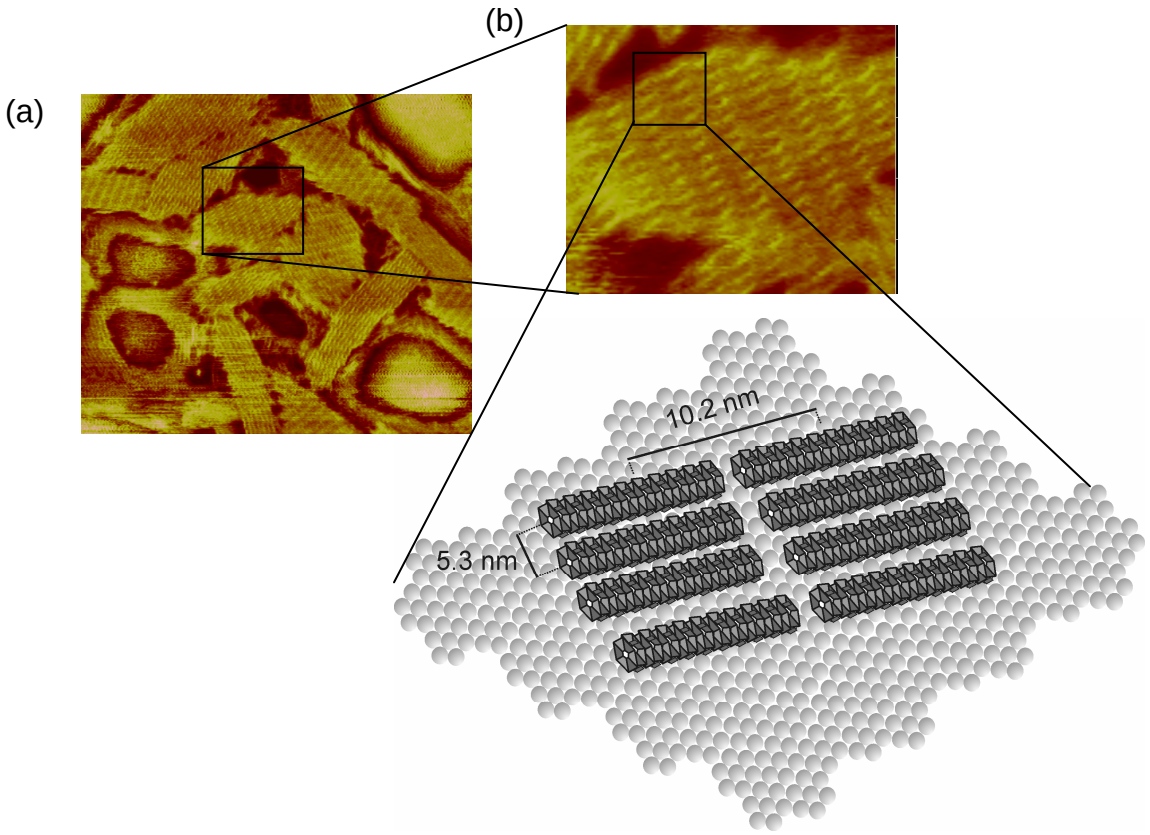

Figure 6.8. *Supramolecular organization of the double rosette assembly* $\mathbf{1}_3$•*((R)-MePropCYA)*$_6$ *on mica; TM-AFM phase images (400 × 400 nm*^{2}*) (a) and schematic representation of the 2D network of the double rosette (b).*

The double rosette assembly $\mathbf{1}_3$•((R)-MePropCYA)$_6$ organized in columns with an inter-column distance of ~10.2 nm (Fig. 6.8b), as measured by AFM. The columns aligned in rows with an inter-row distance of ~5.3 nm indicating a high organization of these structures. The double rosettes $\mathbf{1}_3$•((R)-MePropCYA)$_6$ have a 2D-organization on the mica surface. Considering the dimensions of the double rosette $\mathbf{1}_3$•((R)-MePropCYA)$_6$

(3.3 nm width, 0.8 nm height) obtained by X-ray diffraction in the liquid crystalline state (see Chapter 4) and the X-ray crystal structure for similar assemblies,[35] each bright spot in the AFM image (inset in Figure 6.8a) corresponds to one column of ten double rosettes **1**$_3$•((R)-MePropCYA)$_6$ (Fig. 6.8b). The assemblies have an averaged height of 3.4 nm corresponding to an edge-on orientation. This orientation enables a limited interaction between the hydrophilic surface and the hydrophobic chains. The double rosettes **1**$_3$•(BuCYA)$_6$ and **1**$_3$•((R)-MePropCYA)$_6$ show completely different behavior when deposited onto mica, even though they have the same molecular formula, being the BuCYA and (R)-MePropCYA structural isomers. These assemblies differ only in the presence of a chiral center in (R)-MePropCYA. To investigate the role of the chiral centers in the formation of ordered supramolecular structures on mica, a double rosette solution was prepared with (R)-MePropCYA/(S)-MePropCYA (1:1) (Chart 6.1) and **1**. The resulting solution is a statistical racemic mixture (heteromeric assembly) between the two enantiomers (*M*)-**1**$_3$•((R)-MePropCYA)$_6$ and (*P*)-**1**$_3$•((S)-MePropCYA)$_6$ as demonstrated by ^{1}H NMR spectroscopy. In this case, as for the achiral double rosette **1**$_3$•(BuCYA)$_6$, no regular self-organization was found on mica. Therefore, the supramolecular chirality of optically activity of the double rosette **1**$_3$•((R)-MePropCYA)$_6$ influences the self-organization on surfaces.

6.2.5. Visualization of double rosette assembly on HOPG by STM

It is well known that due to tunneling difficulties, it is difficult to obtain a reliable STM image of an adlayer when the molecules are very large.[46,47] Therefore, the visualization of self-assembled double rosettes which have nanometer size (3.3 nm width, 0.7-1.2 nm height by X-ray data[35]) might be difficult. Previously, the visualization of gold-containing double rosettes has been achieved by STM.[31] It was assumed that the presence of gold atoms facilitates the tunneling through the double rosette assemblies due to the conductive nature of the gold. Consequently it was interesting, to investigate if the presence of the Au atoms was necessary to visualize the double rosettes by STM.

The assembly **1**$_3$•(BuCYA)$_6$ at 1.0×10^{-6} M concentration was deposited on an HOPG surface under a toluene saturated atmosphere. STM data[48] were acquired at ambient

conditions after annealing of the sample at 60°C overnight. The annealing was necessary to allow the complete evaporation of the solvent. It was found that the double rosette $\mathbf{1}_3$•(BuCYA)$_6$, which is oriented face-on (AFM), allows tunneling since the distance between the tip and the substrate is ~1 nm. In Figure 6.9 individual double rosettes are clearly visible. The double rosette $\mathbf{1}_3$•(BuCYA)$_6$ shows a hexagonal organization, which is similar to the one observed by AFM (Section 6.2.2) and in the liquid crystalline state. The hexagonal arrangement is slightly distorted because of the strong interaction between the alkyl chains and the graphite surface, which is typical for discotic liquid crystals absorbed on HOPG.[49] The inter-double rosette distance of 5.8 ± 0.4 nm between the double rosettes $\mathbf{1}_3$•(BuCYA)$_6$ is higher than the inter-column distance found in the liquid crystalline phase. This indicates a decrease in the intermolecular interaction between the double rosettes due to probably the competitive interactions between the alkyl chains and the graphite which makes the packing weaker than in the mesophase. STM measurements were also carried out for the double rosette $\mathbf{1}_3$•(DEB)$_6$ but the STM images did not show any clear organization. Perhaps, the double rosette $\mathbf{1}_3$•(DEB)$_6$ adopts an edge-on orientation, therefore the tunneling through the rosette structures becomes difficult or even impossible due to the high separation between the tip and the substrate (~3 nm).[6,11,30,31]

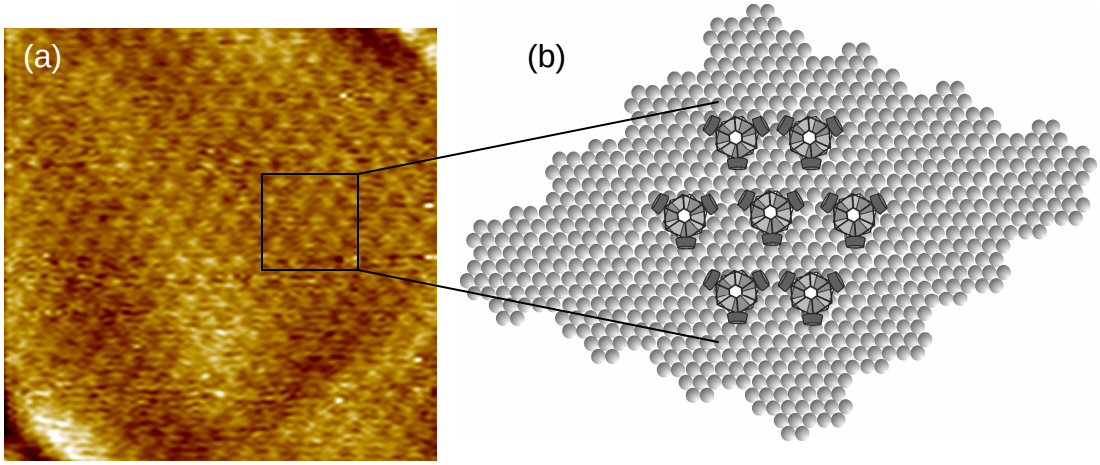

Figure 6.9. *Supramolecular organization of the double rosette assembly* $\mathbf{1}_3$•*(BuCYA)*$_6$*; a) STM images (340 × 340 nm*^{2}*); b) schematic representation of the hexagonal arrangement of the double rosettes on HOPG.*

6.3. Conclusions

The organization of achiral $\mathbf{1}_3$•$(DEB)_6$ and $\mathbf{1}_3$•$(BuCYA)_6$ and chiral $\mathbf{1}_3$•$((R)\text{-}MePropCYA)_6$ double rosettes on HOPG and mica has been investigated by AFM and STM. The mesogenic double rosettes formed ordered rod-like structures on HOPG which did not follow the underlying graphite lattice. Their organization could be controlled by the variation of parameters such as concentration and solvent evaporation rate. The formation of highly organized structures with micrometer size on surfaces couldn be the result of their aggregation in solution, as ^{1}H NMR spectroscopy at low concentration demonstrated. The achiral double rosette $\mathbf{1}_3$•$(BuCYA)_6$ did not show organization on mica, while the chiral double rosette $\mathbf{1}_3$•$((R)\text{-}MePropCYA)_6$ showed 2D-organization, pointing out the importance of chirality in stabilizing the self-organization of the double rosette on surfaces. For the first time STM measurements have been carried out on double rosette assemblies without metals, that might help the tunneling effect through the assembly. The STM images showed that the double rosettes with cyanurates adopted a hexagonal arrangement on HOPG typical for discotic liquid crystals.

6.4 Experimental Section

^{1}H NMR spectra were recorded on Avance II Bruker 600 MHz using a dual inverse ^{1}H/^{13}C HR-MAS probe-head ^{2}H-lock, equipped with Mágic Angle-aligned coil gradient (GRASP II). Zirconia rotors with Teflon PTFE or Kel-F insert were used to obtain a final volume of 12 μL. Residual solvent protons were used as an internal standard and chemical shifts are given relative to tetramethylsilane (TMS). Compound **1**,[50] BuCYA,[32] (R)-MePropCYA[33] and (S)-MePropCYA[33] were prepared according to methods described previously

Formation of assemblies $\mathbf{1}_3$•$(DEB)_6$/$\mathbf{1}_3$•$(BuCYA)_6$/$\mathbf{1}_3$•$((R)\text{-}MePropCYA)_6$/$\mathbf{1}_3$•$((S)\text{-}MePropCYA)_6$. Hydrogen-bonded assemblies $\mathbf{1}_3$•$(DEB)_6$, $\mathbf{1}_3$•$(BuCYA)_6$, and $\mathbf{1}_3$•$((R)\text{-}MePropCYA)_6$ were prepared by mixing calix[4]arene **1** with 2 equivalents of DEB, BuCYA and (R)-MePropCYA respectively, in toluene-d_8 for 20 min at 100°C. For example, 8.32 mg (0.003 mmol) of **1** and 1.10 mg (0.006 mmol) of DEB were dissolved

in 5 mL of toluene–d_8, stirred and heated at 100°C till all compounds were dissolved. After evaporation of the solvent under high-vacuum, the assemblies are ready to use.

AFM measurements. The taping mode (TM)-AFM data were acquired with a Nanoscope III multimode AFM (Veeco Co., Santa Barbara, CA) by using a 10 μm (E) scanner and microfabricated silicon tips/cantilevers (model NCH-W, resonance frequency $\nu_0 \approx$ 320-370 kHz, Nanosensors, Germany). The system was thermally equilibrated over a period of typically 1 to 2 days by operating the AFM in contact mode with false engagement. The rms amplitude of the cantilever (≈ 40 nm) and the amplitude damping (≈ 5%) were minimized to reduce the peak normal forces. Height and phase images were captured using scan rates between 0.75 and ≈ 1 Hz. All data presented here have been subject to a first order plane fit to compensate for sample tilt.

STM measurements. The STM experiments were performed under ambient conditions with a Nanoscope IIIa MultiMode SPM system (Veeco Co., Santa Barbara, CA). STM tips were mechanically cut from a 0.25 mm Pt/Ir wire (80/20) and tested on freshly cleaved HOPG surfaces. All STM images were recorded in the constant current mode under various tunneling conditions (typical tunneling currents 0.5-1.2 nA and tunneling voltages 0.5-1.0 V) and with the sample positively biased. The STM scanner was calibrated using images of clean HOPG using the Scanning Probe Image Processor (SPIP™) software (Image Metrology ApS). Alignment difficulties prevented identification of the lattice directions of the underlying HOPG substrate in the images of molecular over layers. STM images are shown either as unprocessed images (except for background subtraction and a slight low-pass filtering) or processed by the correlation averaging method of the SPIP™ software. In the correlation averaging a template area is defined, and an average is performed over the N (here N = 100) equivalently sized regions in the image that provide the best match (correlation) to this template.

6.5 References and Notes

[1] J.-M. Lehn, *Supramolecular Chemistry, Concepts and Perspectives*, VCH, Weinheim, Germany, **1995**.

[2] D. N. Reinhoudt, *Supramolecular Materials and Technologies*, Wiley & Sons, Chichester, **1999**.

[3] J. D. Watson, F. H. C. Crick, *Nature* **1953**, *171*, 737-738.

[4] G. Gottarelli, E. Mezzina, G. P. Spada, F. Carsughi, G. DiNicola, P. Mariani, A. Sabatucci, S. Bonazzi, *Helv. Chim. Acta* **1996**, *79*, 220-234.

[5] J. Hirschberg, L. Brunsveld, A. Ramzi, J. Vekemans, R. P. Sijbesma, E. W. Meijer, *Nature* **2000**, *407*, 167-170.

[6] H. A. Klok, K. A. Jolliffe, C. L. Schauer, L. J. Prins, J. P. Spatz, M. Moller, P. Timmerman, D. N. Reinhoudt, *J. Am. Chem. Soc.* **1999**, *121*, 7154-7155.

[7] V. Percec, C. H. Ahn, G. Ungar, D. J. P. Yeardley, M. Moller, S. S. Sheiko, *Nature* **1998**, *391*, 161-164.

[8] J. A. Zerkowski, C. T. Seto, D. A. Wierda, G. M. Whitesides, *J. Am. Chem. Soc.* **1990**, *112*, 9025-9026.

[9] E. R. Zubarev, M. U. Pralle, E. D. Sone, S. I. Stupp, *J. Am. Chem. Soc.* **2001**, *123*, 4105-4106.

[10] J. J. van Gorp, J. Vekemans, E. W. Meijer, *J. Am. Chem. Soc.* **2002**, *124*, 14759-14769.

[11] H. Schonherr, V. Paraschiv, S. Zapotoczny, M. Crego-Calama, P. Timmerman, C. W. Frank, G. J. Vancso, D. N. Reinhoudt, *Proc. Natl. Acad. Sci. U. S. A.* **2002**, *99*, 5024-5027.

[12] T. Kawasaki, M. Tokuhiro, N. Kimizuka, T. Kunitake, *J. Am. Chem. Soc.* **2001**, *123*, 6792-6800.

[13] H. Rapaport, H. S. Kim, K. Kjaer, P. B. Howes, S. Cohen, J. Als-Nielsen, M. R. Ghadiri, L. Leiserowitz, M. Lahav, *J. Am. Chem. Soc.* **1999**, *121*, 1186-1191.

[14] P. Jonkheijm, F. J. M. Hoeben, R. Kleppinger, J. van Herrikhuyzen, A. Schenning, E. W. Meijer, *J. Am. Chem. Soc.* **2003**, *125*, 15941-15949.

[15] T. Kato, *Struct. Bond.* (Berlin) **2000**, *96*, 95-146.

[16] T. Kato, N. Mizoshita, K. Kishimoto, *Angew. Chem. Int. Ed.* **2006**, *45*, 38-68.

[17] C. M. Paleos, D. Tsiourvas, *Liq. Cryst.* **2001**, *28*, 1127-1161.

[18] L. Schmidt-Mende, A. Fechtenkotter, K. Mullen, E. Moons, R. H. Friend, J. D. MacKenzie, *Science* **2001**, *293*, 1119-1122.

[19] A. M. van de Craats, J. M. Warman, A. Fechtenkotter, J. D. Brand, M. A. Harbison, K. Mullen, *Adv. Mater.* **1999**, *11*, 1469-1472.

[20] R. I. Gearba, M. Lehmann, J. Levin, D. A. Ivanov, M. H. J. Koch, J. Barbera, M. G. Debije, J. Piris, Y. H. Geerts, *Adv. Mater.* **2003**, *15*, 1614-1618.

[21] T. Q. Nguyen, R. Martel, P. Avouris, M. L. Bushey, L. Brus, C. Nuckolls, *J. Am. Chem. Soc.* **2004**, *126*, 5234-5242.

[22] M. Kastler, W. Pisula, D. Wasserfallen, T. Pakula, K. Mullen, *J. Am. Chem. Soc.* **2005**, *127*, 4286-4296.

[23] V. Palermo, M. Palma, Z. Tomovic, M. D. Watson, K. Mullen, P. Samori, *Synth. Met.* **2004**, *147*, 117-121.

[24] M. Lee, J. W. Kim, S. Peleshanko, K. Larson, Y. S. Yoo, D. Vaknin, S. Markutsya, V. V. Tsukruk, *J. Am. Chem. Soc.* **2002**, *124*, 9121-9128.

[25] H. T. Jung, S. O. Kim, Y. K. Ko, D. K. Yoon, S. D. Hudson, V. Percec, M. N. Holerca, W. D. Cho, P. E. Mosier, *Macromolecules* **2002**, *35*, 3717-3721.

[26] G. D. Sui, M. Micic, Q. Huo, R. M. Leblanc, *Langmuir* **2000**, *16*, 7847-7851.

[27] V. Percec, C. H. Ahn, W. D. Cho, A. M. Jamieson, J. Kim, T. Leman, M. Schmidt, M. Gerle, M. Moller, S. A. Prokhorova, S. S. Sheiko, S. Z. D. Cheng, A. Zhang, G. Ungar, D. J. P. Yeardley, *J. Am. Chem. Soc.* **1998**, *120*, 8619-8631.

[28] K. L. Genson, J. Holzmueller, I. Leshchiner, E. Agina, N. Boiko, V. P. Shibaev, V. V. Tsukruk, *Macromolecules* **2005**, *38*, 8028-8035.

[29] H. Schonherr, M. Crego-Calama, G. J. Vancso, D. N. Reinhoudt, *Adv. Mater.* **2004**, *16*, 1416-1420.

[30] H. J. van Manen, V. Paraschiv, J. J. Garcia-Lopez, H. Schonherr, S. Zapotoczny, G. J. Vancso, M. Crego-Calama, D. N. Reinhoudt, *Nano Lett.* **2004**, *4*, 441-446.

[31] S. Vázquez-Campos, M. Péter, M. Dong, S. Xu, W. Xu, H. Gersen, F. Besenbacher, M. Crego-Calama, D. N. Reinhoudt, *Small* **2006**, *submitted*.

[32] L. J. Prins, R. Hulst, P. Timmerman, D. N. Reinhoudt, *Chem. Eur. J.* **2002**, *8*, 2288-2301.

[33] M. A. Mateos-Timoneda, M. Crego-Calama, D. N. Reinhoudt, *Supramol. Chem.* **2005**, *17*, 67-79.

[34] R. H. Vreekamp, J. P. M. vanDuynhoven, M. Hubert, W. Verboom, D. N. Reinhoudt, *Angew. Chem. Int. Ed.* **1996**, *35*, 1215-1218.

[35] P. Timmerman, R. H. Vreekamp, R. Hulst, W. Verboom, D. N. Reinhoudt, K. Rissanen, K. A. Udachin, J. Ripmeester, *Chem. Eur. J.* **1997**, *3*, 1823-1832.

[36] L. J. Prins, C. Thalacker, F. Wurthner, P. Timmerman, D. N. Reinhoudt, *Proc. Natl. Acad. Sci. U. S. A.* **2001**, *98*, 10042-10045.

[37] S. Yagai, T. Nakajima, K. Kishikawa, S. Kohmoto, T. Karatsu, A. Kitamura, *J. Am. Chem. Soc.* **2005**, *127*, 11134-11139.

[38] C. A. Goss, J. C. Brumfield, E. A. Irene, R. W. Murray, *Langmuir* **1993**, *9*, 2986-2994.

[39] W. Pisula, Z. Tomovic, B. El Hamaoui, M. D. Watson, T. Pakula, K. Mullen, *Adv. Funct. Mater.* **2005**, *15*, 893-904.

[40] J. Lin, D. Zhou, *Eur. Polym. J.* **1999**, *36*, 309-316.

[41] D. N. Petsev, K. Chen, O. Gliko, P. G. Vekilov, *Proc. Natl. Acad. Sci. U. S. A.* **2003**, *100*, 792-796.

[42] O. Galkin, P. G. Vekilov, *J. Am. Chem. Soc.* **2000**, *122*, 156-163.

[43] E. H. Lee, D. K. Yoon, J. M. Jung, S. R. Lee, Y. H. Kim, Y. Kim, G. Kim, H. T. Jung, *Macromolecules* **2005**, *38*, 5152-5157.

[44] V. Palermo, S. Morelli, C. Simpson, K. Mullen, P. Samori, *J. Mater. Chem.* **2006**, *16*, 266-271.

[45] E. Rabani, D. R. Reichman, P. L. Geissler, L. E. Bruns, *Nature* **2003**, *426*, 271-274.

[46] J. Elmans, M. C. Lensen, J. W. Gerritsen, H. van Kempen, S. Speller, R. J. M. Nolte, A. E. Rowan, *Adv. Mater.* **2006**, *16*, 2070-2073.

[47] M. C. Lensen, S. J. T. Van Digenen, S. Speller, R. J. M. Nolte, A. E. Rowan, *Chem. Comm.* **2004**, 762-763.

[48] The STM measurements were carried out at Aarhus University in the Interdisciplinary Nanoscience Center (iNANO).

[49] N. Katsonis, A. Marchenko, D. Fichou, *Synth. Met.* **2004**, *147*, 73-77.

[50] The synthesis is described in Chapter 3.

Chapter 7

Noncovalent Synthesis of Tetrarosette Assemblies and their Behavior as Liquid Crystalline Materials

In this chapter, the noncovalent synthesis of tetrarosette assemblies is described, as well as the formation of liquid crystalline materials by properly functionalized tetrarosettes. The role of barbiturate derivatives as a (chiral) catalytic chaperone in the formation of (optically pure) cyanurate-based tetrarosette assemblies has been studied. The enantioselective synthesis of tetrarosette assemblies was achieved by using substoichiometric amount of chiral barbiturates via amplification of chirality.

7.1 Introduction

The properties of a material depend both on the nature of its constituents and the interactions between them. Therefore the formation of nanometer-size structures with control over the spatial disposition of the molecular components has crucial importance in materials science.[1-3] Self-assembly is well suited to synthesize discrete and well-defined structures through the spontaneous connection of a few (or many) components.[4] The main advantage of self-assembly is that noncovalent bonds are formed spontaneously and reversibly under thermodynamic equilibrium, with the possibility of error correction and without undesired side-products.[5] However, it is expected that the kinetics of formation of noncovalent structures will be no longer fast when the size is ≥ 3 nm and a large number of weak interactions are involved.[6,7]

To direct the noncovalent synthesis of supramolecular assemblies to the desired product, chemists have made use of "helpers" or "templates". In general, a template organizes an assembly of atoms with respect to one or more geometries, in order to achieve a particular linking of atoms. This strategy, also known as template-assisted synthesis, has led to the guest-templated formation of covalent and noncovalent systems,[8-10] self-replicating systems,[11-14] and molecular imprinted polymers,[15] as well as the selection of the best receptor in dynamic combinatorial libraries of receptor.[16,17] Nature uses templates but it also makes use of "helpers", so-called chaperones, to direct the correct folding of polypeptides (proteins).[18] Chaperones are a family of proteins that mediate the correct assembly of other polypeptides, inhibiting incorrect molecular interactions that will generate nonfunctional structures, but they are not themselves components of the final functional structure.[18] Generally, the chaperone stabilizes the metastable conformations of the protein and it is not always attached to it during the whole folding process, while the template has to be present (usually noncovalently) in a specific location during the synthesis to direct the product formation. Surprisingly, the use of molecular chaperones has hardly been exploited for the synthesis of (non)covalent assemblies. The only example found in literature of the use of synthetic chaperones has been recently published by our group.[7] An equimolar amount of molecular chaperone promoted the noncovalent synthesis of a hydrogen-bonded assembly which formation

was unattainable without the chaperone. Later this study was extended to the synthesis of tetrarosette assemblies using *catalytic* chaperones.[19] In this example, a barbiturate derivative acts as catalytic chaperone in the noncovalent synthesis of cyanurate-based tetrarosette assemblies. The barbiturate derivative inhibits the formation of kinetically stable ill-defined assemblies and allows the formation of the tetrarosette assembly.

In this chapter, an extended study of the noncovalent synthesis of hydrogen-bonded assemblies by using chiral and nonchiral barbiturates as a (catalytic) chaperone is described. Using this concept, the enantioselective synthesis of hydrogen-bonded tetrarosette assemblies has been achieved by amplification of chirality. The quantitative formation of the tetrarosette assemblies is obtained by lowering the chiral catalyst concentration to substoichiometric amounts by mixing chiral and nonchiral barbiturates in different ratios. Furthermore, the noncovalent synthesis of hydrogen-bonded tetrarosette assemblies for liquid crystalline materials was attempted.

7.2. Results and Discussion

The tetrarosette $\mathbf{1}_3$•(BAR/*BAR)$_{12}$ consist of fiftheen different components, of which three are tetramelamine calix[4]arene derivatives and tewelve are barbiturate derivatives (BAR/*BAR, BAR= barbiturate derivatives). All these components are held together by 72 hydrogen bonds (Chart 7.1).

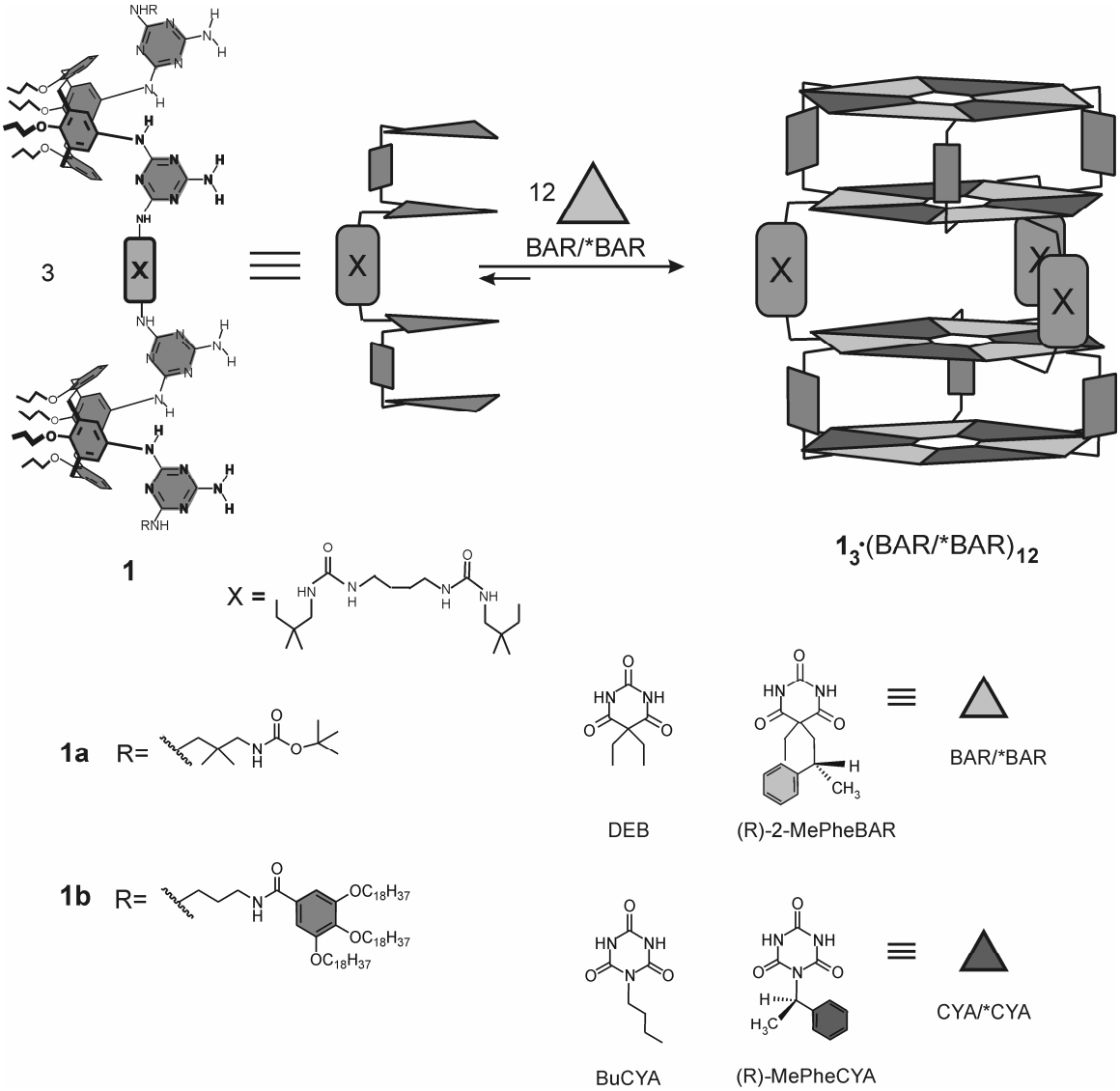

Chart 7.1. *Chemical and schematic representation of the tetramelamine* ***1*** *and barbiturate/cyanurate derivatives, and the corresponding hydrogen-bonded assembly* $\mathbf{1}_3$•*(BAR/*BAR)$_{12}$.*

Similar to double rosette assemblies (see Chapter 4), tetrarosette assemblies can be conveniently characterized by ^{1}H NMR spectroscopy.[20] Upon formation of the assembly $\mathbf{1}_3$•$(DEB)_{12}$, four singlets of equal intensity characteristic of the hydrogen-bonded imide NH protons of DEB were observed in the region between δ = 13 and 16 ppm. Integration of the appropriate signals in the ^{1}H NMR spectrum confirmed the expected 1:4 stoichiometry for assemblies $\mathbf{1}_3$•$(DEB)_{12}$. Tetrarosette assemblies can adopt a large variety of different isomeric structures as result of the staggered (S) or eclipsed (E) orientation of the melamine rings in each rosette layer. Nevertheless, ^{1}H NMR (four signals for the NH protons of DEB) and gas-phase MM calculations have shown the formation of only the SSS-isomer.[21]

In the absence of any source of chirality, this SSS-isomer (D_3-symmetry) exists as a mixture of enantiomers ((*P*)- and (*M*)-enantiomers) due to the staggered orientation of the different melamine rings. However, the introduction of chiral centers in one of the building blocks of the assembly leads to the formation of only one of the two possible diastereomers. Therefore, these assemblies are highly circular dichroism (CD) active. MALDI-TOF mass spectrometry measurements after Ag^+ labeling provided additional evidence for the formation of tetrarosettes.[22,23]

The barbiturate-based tetrarosette assembly $\mathbf{1}_3$•$(DEB)_{12}$ is spontaneously formed in apolar solvents (Chart 7.1), such as chloroform, benzene and toluene,[20] while the formation of cyanurate-based assemblies is a kinetically controlled self-assembly process, which can lead to the formation of ill-defined assemblies. This problem can be overcome using two different approaches: (i) mixing the two building blocks (tetramelamine and cyanurates (1:4 ratio)) in toluene and heating the resulting solution at 100°C for one week (*direct method*) (Fig. 7.1a), and (ii) formation of the assemblies using DEB and subsequent exchange by a cyanuric acid derivative (DEB:cyanuric acid 1:1 ratio) (*exchange method*) (Fig. 7.1b).[7] In this method, the barbiturates are used as molecular chaperones to help the self-assembly process (Fig 7.1b).[19]

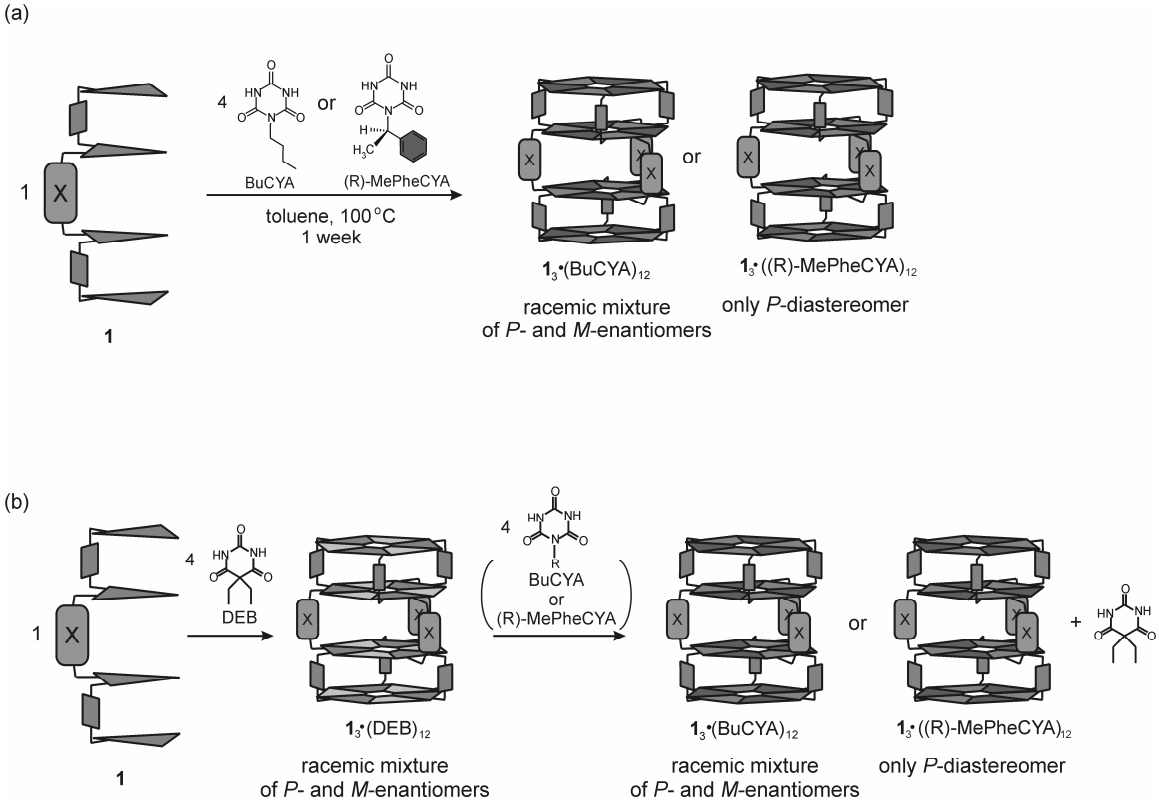

Figure 7.1. *Schematic representation of the direct method (a) and the exchange method (b) for the formation of cyanurate-based tetrarosette assemblies.*

In nanotechnology and materials sciences, the absolute control over the molecular components and their interactions is one of the key issues. In particular in the liquid crystals field this control over the molecular components and the ordering of the resulting structures can lead to new functions for these materials.[24] Here, the noncovalent synthesis of highly ordered tetrarosette assemblies for liquid crystalline materials is described. Additionally and in order to gain more control over their self-organization for further applications, a study on the noncovalent synthesis of these structures is presented.

7.2.1 Synthesis

Tetramelamine **1a**, (R)-2-MePheBAR, BuCYA and (R)-MePheCYA have been synthesized following methods previously described.[25, 26] The tetramelamine **1b** was synthesized via a 4-step synthesis (Scheme 7.1). First, the dimelamine calix[4]arene **2** was mono-protected by reaction with di-*tert*-butyl dicarbonate in anhydrous tetrahydrofuran at room temperature, obtaining the dimelamine calix[4]arene derivative **2a**. The coupling reaction between the dimelamine calix[4]arene **2a** and 1,4-butyl-bis(*p*-nitrophenyl) dicarbamate in dichloromethane resulted in tetramelamine **1c**. The deprotection of **1c** with trifluoroacetic acid at room temperature gave compound **1d**. The final tetramelamine **1b** was obtained by a coupling reaction of **5** with the carboxylic acid **6** in the presence of HBTU.

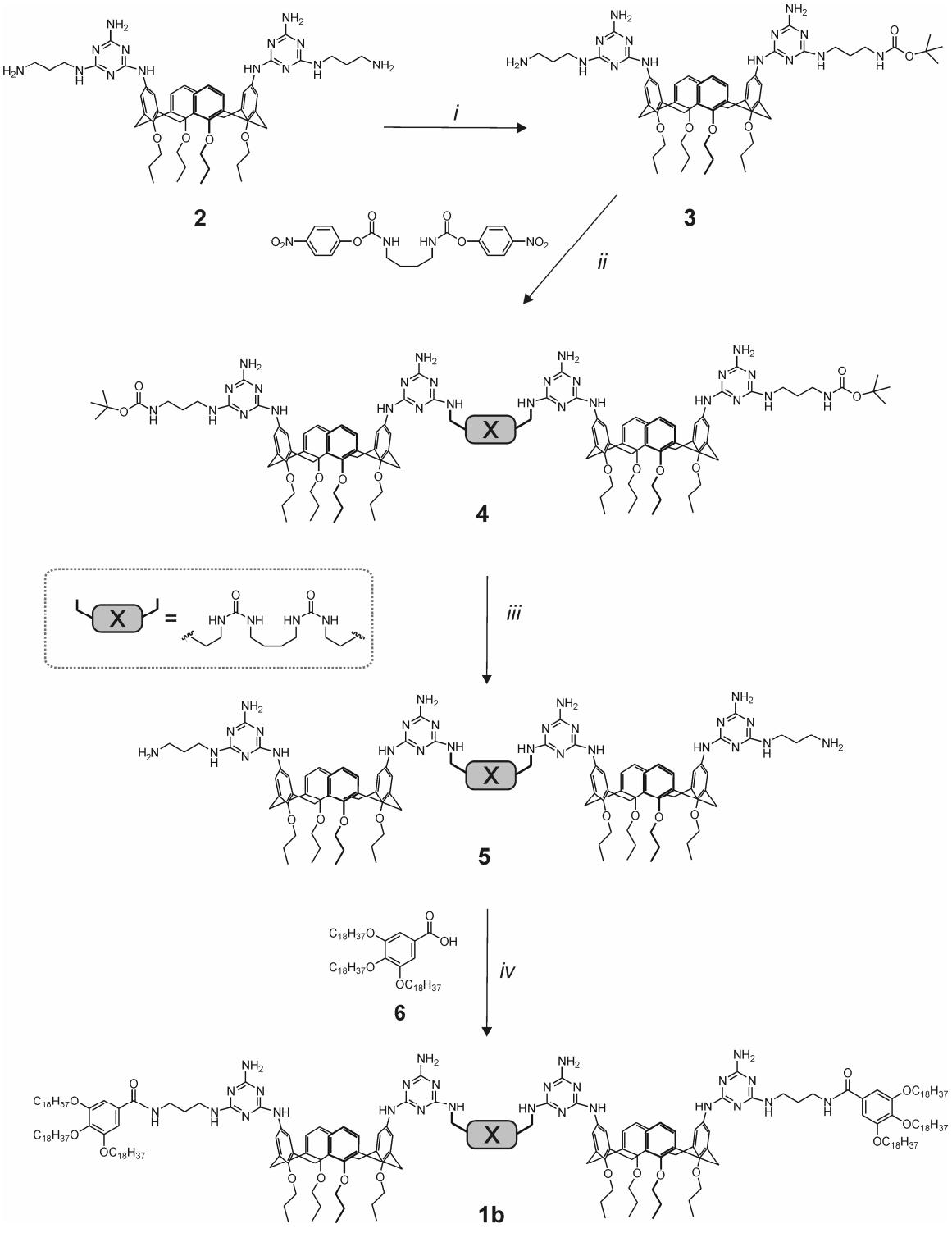

Scheme 7.1. *Synthesis of the tetramelamine* ***1b****: (i) $(Boc)_2O$, THF, r.t; (ii) 1,4-butyl-bis(p-nitrophenyl) dicarbamate, DIPEA, CH_2Cl_2, r.t.; (iii) TFA, CH_2Cl_2, r.t.; (iv) HBTU, DIPEA, CH_2Cl_2/DMF 4:1, r.t.*

7.2.2. Attempts to obtain liquid crystalline materials based on tetrarosette assemblies

In the previous chapters, the liquid crystalline properties of double rosette assemblies have been shown. Here, liquid crystalline materials based on tetrarosette assemblies, which show higher organization compared to double rosettes,[27,28] have been investigated. The high organization of tetrarosettes should allow to obtain liquid crystalline materials with new characteristics since the ordering is one of the requirement to obtain new functions in liquid crystalline materials.[24] Tetramelamine **1b** was synthesized introducing octadecyl chains in order to induce liquid crystallinity in the assembly (Scheme 7.1).[29,30] The long alkyl chains in the tetramelamine **1b** are connected to the melamine moieties to avoid interference with the network of hydrogen bonds that holds the double rosette motifs together.[31] The formation of the self-assembled tetrarosette $\mathbf{1b}_3$•$(DEB)_{12}$ was confirmed by ^{1}H NMR spectroscopy in solution (Fig. 7.2). The ^{1}H NMR spectrum shows the characteristic four signals in the region δ = 15-13 ppm expected for the formation of hydrogen bonds between the NH protons of DEB and the melamine rings of **1b**.

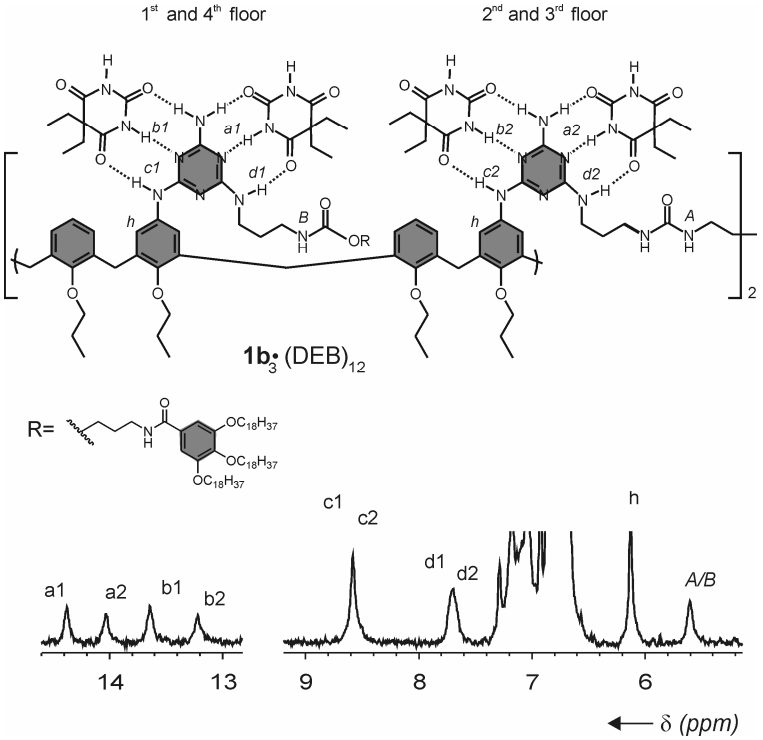

Figure 7.2. *Parts of the ^{1}H NMR spectrum of the tetramelamine **1b**$_3$•(DEB)$_{12}$, recorded at 25°C in toluene-d_8 (400MHz).*

The thermal behavior of the tetramelamine **1b** and the assembly **1b**$_3$•(DEB)$_{12}$ has been investigated by polarized optical microscopy (POM) and differential scanning calorimetry (DSC). Unfortunately, the images obtained by POM did not show any liquid crystalline phase for the single component **1b** or the assembly **1b**$_3$•(DEB)$_{12}$ (Fig 7.3).

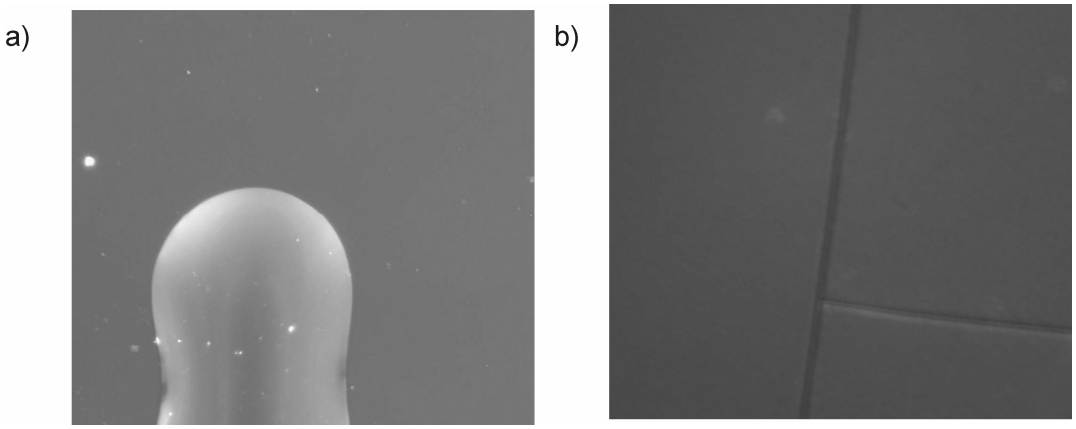

Figure 7.3. *Polarized optical microscopy images for (a) the tetramelamine **1b** at 50°C and (b) tetrarosette **1b**$_3$•(DEB)$_{12}$ at 120°C. The images were taken cooling down form the isotropic phase.*

Cooling down from the isotropic melt, birefringent areas, which are typical for liquid crystalline materials, were not observed. The tetramelamine **1b** and the tetrarosette **1b**$_3$•(DEB)$_{12}$ behaved as glassy materials. The DSC measurements confirmed that both the tetramelamine and the tetrarosette **1b**$_3$•(DEB)$_{12}$ are not liquid crystals because no phase transitions related to a liquid crystalline phase were detected in a range of temperature from -20°C to 300°C. Probably the dimensions of the tetrarosette (3.3 nm width and 3.3 nm height) do not allow the correct interdigitation of the long alkyl chains and consequently the tetrarosette does not self-organize in the molten state.

In the case of cyanurate derivatives BuCYA and (R)-MePheCYA, the tetrarosette assembly was formed neither via the direct method nor the exchange method (see section 7.2). It is possible that the presence of the long alkyl chains stabilizes the ill-defined kinetically stable assembly in such a way that even the chaperone does not help the correct formation of the tetrarosette.

7.2.3 Achiral barbiturate derivates as a catalytic chaperone in the synthesis of tetrarosettes

As described above, highly ordered supramolecular liquid crystals by the self-organization of barbiturate-tetrarosette assemblies could not be achieved. The reasons are the lack of self-organization in the solid state in case of barbiturate-based tetrarosettes and the impossibility to form the assembly in case of cyanurate-based tetrarosettes (see Section 7.2.2). Therefore, it was important to study (in detail) the noncovalent synthesis of non-liquid crystalline cyanurate-based tetrarosettes to obtain information on how to direct the synthesis of large hydrogen-bonded structures and manipulate them through the control of their molecular components.[7,19,28] This could result in valuable information for the fabrication of noncovalent liquid crystalline materials.

Previous studies in our group have shown that the formation of cyanurate-based tetrarosette assemblies is a kinetically controlled self-assembly process.[19] Mixing tetramelamine **1a** with BuCYA (1:4 ratio) in chloroform at room temperature did not result in the expected tetrarosette assembly **1a**$_3$•(BuCYA)$_{12}$. Instead of the characteristic ^{1}H NMR four signals in the region δ = 13-15 ppm expected for the formation of a

tetrarosette, a complex set of proton signals was observed (Fig. 7.4). The mixing process led to the formation of nondefined structures, which displayed high kinetic stability. Only after heating at 100 °C for one week, the ^{1}H NMR showed the formation of the assembly **1a**$_3$•(BuCYA)$_{12}$ (Fig. 7.4b). The high kinetic stability of these ill-defined assemblies was confirmed by CD spectroscopy and gel permeation chromatography (GPC).[19]

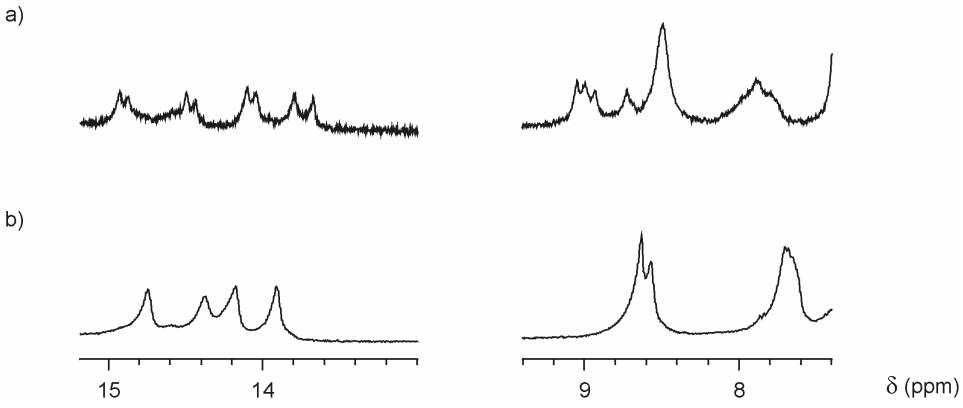

Figure 7.4. *Parts of the ^{1}H NMR spectrum of tetramelamine **1a** and BuCYA (1:4 ratio) (a) immediately after mixing and (b) after 1 week at 100 °C in toluene. The spectra were recorded in $CDCl_3$ at room temperature (300 MHz).*

A solution to overcome the problem of the formation of kinetically stable, ill-defined assemblies is the use of molecular chaperones (Fig. 7.2b). This strategy is widely used in nature for the correct folding of proteins. The 'chaperone' strategy involves the formation of the assembly using a barbiturate derivative (1:4 ratio tetramelamine:barbiturate) and subsequent exchange by cyanuric acid derivatives (1:1 ratio DEB:cyanuric acid).[7] This exchange is possible due to the formation of stronger hydrogen bonds within the melamine:cyanurate pair than the melamine:barbiturate pair.[32]

The noncovalent synthesis of tetrarosette assemblies is also possible using only *catalytic* amounts of chiral/nonchiral barbiturate chaperones.[19] By mixing DEB and **1a** in toluene in a 1:1 ratio (instead of a 4:1 ratio DEB:**1a** as in the sample above) and adding 4 equivalents of the cyanuric derivative (R)-MePheCYA, stirring at 100°C for two 2 h (Fig. 7.5), the formation of the tetrarosette **1a**$_3$•((R)-MePheCYA)$_{12}$ was achieved as ^{1}H NMR spectroscopy demonstrated at room temperature. Whereas in the absence of DEB

the formation of **1a**$_3$•((R)-MePheCYA)$_{12}$ takes place only after one week at 100°C. Chiral cyanuric derivative (R)-MePheCYA was chosen because the formation reaction can be also studied by CD spectroscopy.[33]

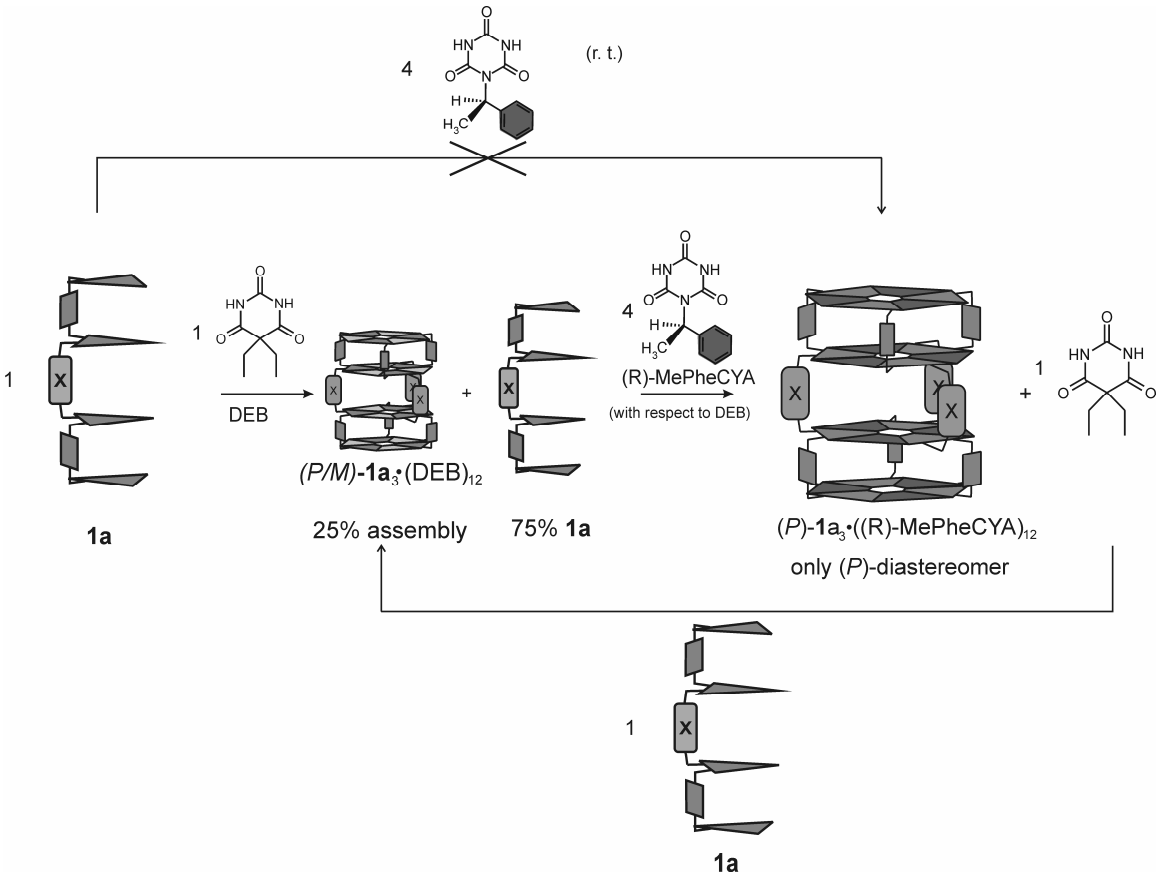

Figure 7.5. *Schematic representation of the formation of cyanurate-based tetrarosette assemblies showing the catalytic chaperone effect by DEB.*

To study in more detail the kinetics of the catalytic effect of the barbiturates, a new experiment was performed where the course of the reaction was monitored in time. Tetramelamine **1a**, DEB, and (R)-MePheCYA were mixed in a 1:1:4 ratio, respectively, in an NMR tube in deuterated toluene. The formation of the assembly (*P*)-**1a**$_3$•((R)-MePheCYA)$_{12}$ was followed by ^{1}H NMR spectroscopy at 100°C recording one spectrum every 10 min for a total of 10 h (Fig. 7.6). The relative intensity of the proton Hc$_{1\text{-}2}$ of the tetrarosette **1a**$_3$•((R)-MePheCYA)$_{12}$ was plotted versus time, showing a trend similar to a

bimolecular reaction (Fig 7.6b). A plateau was reached after 10 h indicating the end of the reaction.

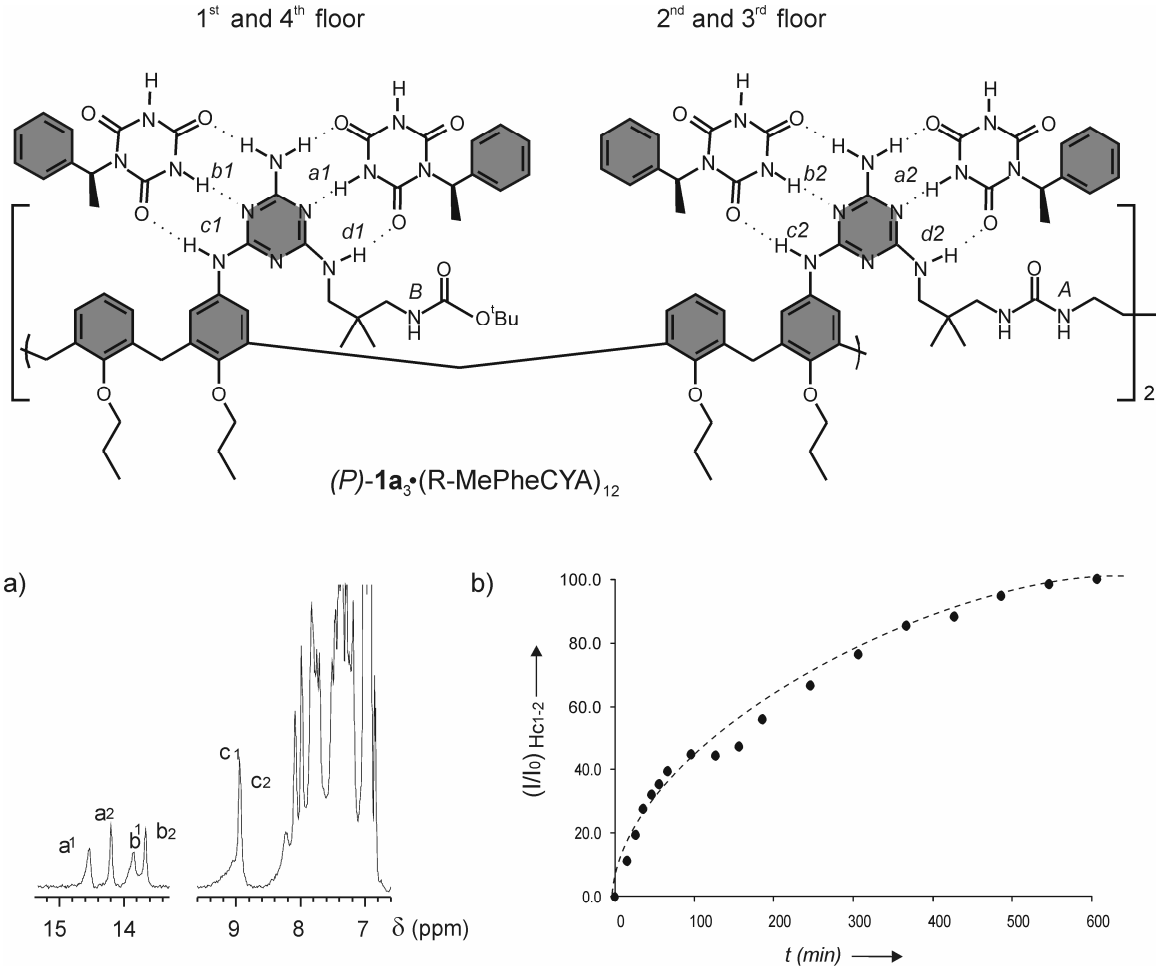

Figure 7.6. *(a) Parts of ^{1}H NMR spectra of the tetrarosette (P)-**1a**$_3$•((R)-MePheCYA)$_{12}$, recorded at 100°C in toleuene-d8 (400MHz); (b) plot of the relative intensity of proton Hc1-2 versus time.*

The ^{1}H NMR studies clearly showed that DEB enhanced the formation rate of the tetrarosette (*P*)-**1a**$_3$•((R)-MePheCYA)$_{12}$ compared to reaction without the barbiturate, which takes place only after one week under the same experimental conditions. Unfortunately, given the complexity of the system, the catalytic effect can be detected only on the overall formation reaction of the tetrarosette assembly and the experimental data can be treated only in qualitative manner.

Other proof of the catalytic effect of the DEB in the noncovalent synthesis of cyanurate-based tetrarosettes comes from the recycling of the catalytic chaperone.[19] After the formation of tetrarosette (*P*)-**1a**$_3$•((R)-MePheCYA)$_{12}$ free DEB is present in solution as demonstrated by ^{1}H NMR spectroscopy. Therefore, the addition of new tetramelamine **1a** (1:1 ratio DEB:**1a**) and (R)-MePheCYA cyanurate (1:4 DEB:cyanurate) respectively leads to the formation of additional amounts of the "correct" assembly (*P*)-**1a**$_3$•((R)-MePheCYA)$_{12}$. The increase in the assembly concentration was demonstrated by CD measurements indicating that the catalyst (chaperone) can be reused. Thus, DEB acts as a catalytic chaperone enhancing the formation rate thus forming the correct tetrarosette assembly from ill-defined kinetically stable assemblies. However, the mechanism of the catalytic chaperone is not clear. Different experiments were carried out to clarify the overall enhancement in the formation rate and the ill-defined assembly formation and inhibition by DEB.

First, the ill-defined assemblies were formed by mixing tetramelamine **1a** and (R)-MePheCYA in 1:4 ratio as shown ^{1}H NMR spectroscopy at 100°C in deuterated toluene. Upon addition of DEB in a catalytic amount (1:4 DEB:cyanurate) the formation of the tetrarosette (*P*)-**1a**$_3$•((R)-MePheCYA)$_{12}$ was observed by ^{1}H NMR spectroscopy. Additional proof for correct formation of the formation of (*P*)-**1a**$_3$•((R)-MePheCYA)$_{12}$ was obtained from CD spectroscopy (Fig. 7.7). First the ill-defined assembly formation was observed for the solution **1a**/(R)-MePheCYA in a 1:4 ratio (Fig. 7.7c), which has a small signal intensity compared to the tetrarosette because of its ill-defined structure. The further addition of DEB led to the complete formation of the tetrarosette assembly (Fig. 7.7d). Thus, the addition of DEB led to the formation of the correct assembly, not only inhibiting the formation of the ill-defined assembly when all the components are added at the same time but also by correcting the errors when the chaperone is added after formation of the "wrong" assemblies (*self-healing*).

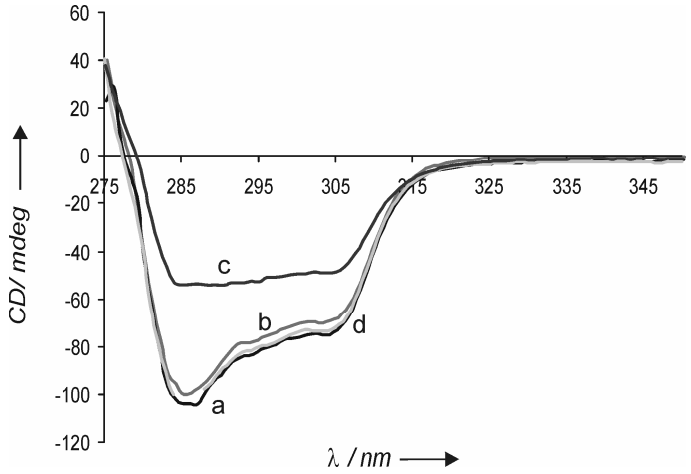

Figure 7.7. *CD spectra of tetramelamine* ***1a***$_3$*•((R)-MePheCYA)*$_{12}$ *recorded in toluene (1.0 mM) after the formation of the tetrarosette assembly by addition of* ***1a****, DEB, (R)-MePheCYA ratio 1:1:4 (a) as powder, (b) as solutions, (c) formation of the ill-defined assembly and (d) after the addition of DEB to ill-defined assembly.*

Furthermore, to exclude that the different solubility of DEB and cyanurate could be one of the causes of the observed catalytic chaperone effect, two different experiments were designed. In the first experiment **1a**, DEB, and (R)-MePheCYA were dissolved individually in toluene-d_8 and mixed in an NMR tube. The formation of the tetrarosette (*P*)-**1a**$_3$•((R)-MePheCYA)$_{12}$ was followed by ^{1}H NMR spectroscopy at 100°C as previously described (Fig. 7.6). In the second experiment the three species tetramelamine **1a**, DEB and (R)-MePheCYA were introduced (as solids) in an NMR tube and the solvent was added later. Immediately there after, the ^{1}H NMR kinetic study was started. Both experiments demonstrated the complete formation of the tetrarosette assembly (*P*)-**1a**$_3$•((R)-MePheCYA)$_{12}$ after 10 h, while in absence of DEB the reaction under the same experimental conditions only took place over a week. Thus, the different solubilities of barbiturates and cyanurates are not responsible for the catalytic effect.

CD spectroscopy also confirmed that the formation of the tetrarosette (*P*)-**1a**$_3$•((R)-MePheCYA)$_{12}$ is not influenced by the solubility of barbiturates and cyanurates (Fig. 7.7). In both cases, i.e. when **1a**, DEB and (R)-MePheCYA in 1:1:4 ratio, were added simultaneously, in solution or as powders, the CD spectra showed tetrarosette formation (Fig. 7.7a,b).

Although the interpretation of the kinetic data is very difficult due to the complexity of the system, the function of the barbiturates as catalyst and molecular chaperone is clearly demonstrated: the addition of the DEB blocks and correct the ill-defined assembly pathway (*chaperone*) and lowers the activation energy of the correct pathway (*catalyst*). Probably, the formation of more labile hydrogen bonds between the pair melamine:barbiturate compare to the pair melamine:cyanurate does not allow the formation and correct the ill-defined species, leading to the formation of the correct assembly.[32]

7.2.4. Asymmetric catalysis in the synthesis of enantiopure tetrarosette assemblies

The development of enantiopure structures is important for new applications of self-assembled systems in nanotechnology and materials sciences. It could be envisioned that one of the possible ways to fabricate them is to make use of enantioselective catalysts.

Ideally, in a catalytic reaction for covalent systems, the amount of catalyst should be low due to its expensiveness. Therefore, it would be very interesting to know if the amount of catalytic chaperone in our system could be reduced. For this purpose the concept of amplification of chirality in noncovalent systems, in which a high enantiomeric or diastereomeric excess (*e.e.* or *d.e.*, respectively) is induced by a small initial amount of chiral bias could be used.[34] In this way, the chiral information carried by the chaperone could be amplified using mixtures of nonchiral/chiral barbiturates (X:Y ratio from 90:10 to 10:90) (Fig 7.8).[19]

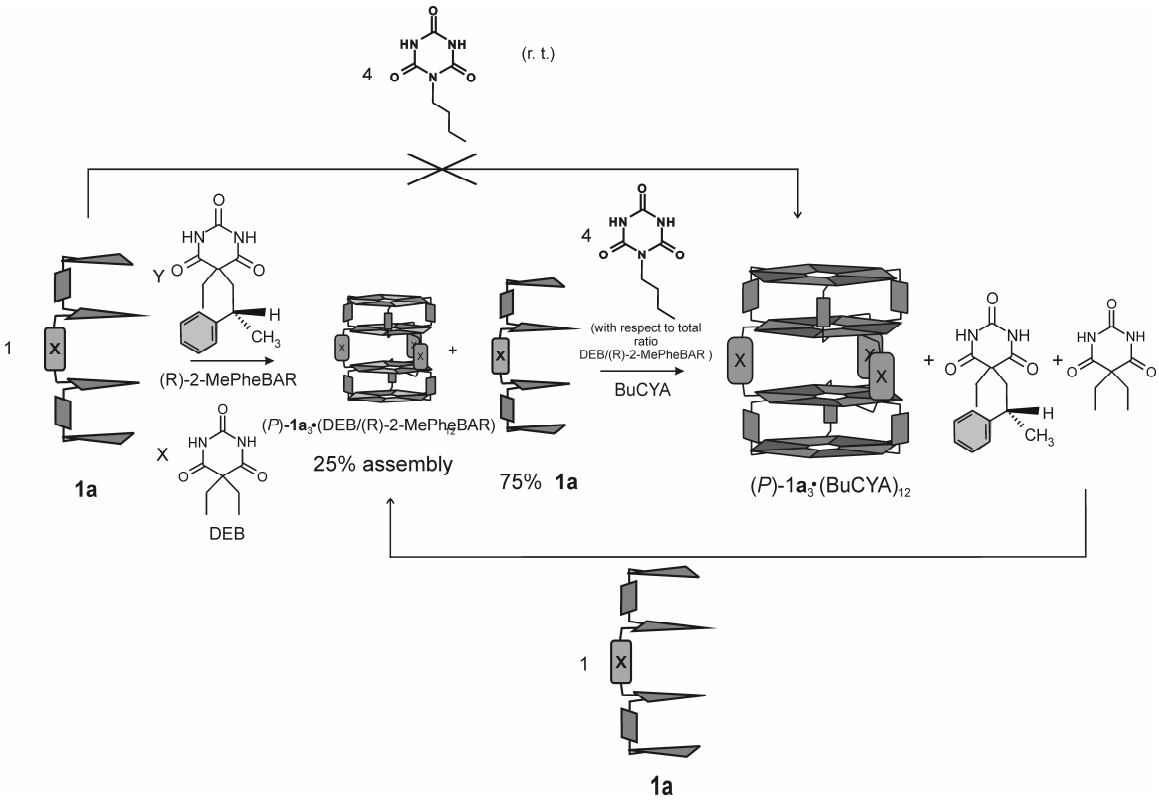

Figure 7.8. *Schematic representation of the enantioselective formation of cyanurate-based tetrarosette assemblies by the amplification of chirality by a catalytic chaperone. Different percentages of DEB/(R)-2-MePheBAR molecules (X/Y=100/0, 90/10, 70/30, 50/50, 30/70, 10/90 and 0/100) were used while the total percentage corresponds to 1 equivalent of barbiturate.*

Solutions of **1a** and DEB in a 1:1 ratio, and solutions of **1a** and (R)-2-MePheBAR in a 1:1 ratio in toluene (0.11 mM) were mixed in ratios ranging from 90:10 to 10: 90. CD spectra were recorded from 275 to 350 nm, showing the formation of the heteromeric assemblies **1a**$_3$•((DEB)$_n$(*P*)-**1a**$_3$•((R)-2-MePheBAR)$_{12-n}$) (n=1-11) (Fig 7.9a).[19,35] The thermodynamic equilibrium was reached almost immediately after the mixing process.[36] From these measurements, the relative CD intensities were related to a calculated 100% value based on the ratio (*P*)-**1a**$_3$•((R)-2-MePheBAR)$_{12}$/**1a**$_3$•(DEB)$_{12}$ and plotted as a function of the molecular fraction of the chiral component (Fig. 7.9b). The plot of the relative CD intensity (measured at 286 nm) as function of the molar ratio of the chiral rosette assembly showed the typical nonlinear behavior resulting from the 'sergeants-and-soldiers' principle, where the achiral units follow the helicity induced by the chiral units. Figure 7.9b clearly shows that in toluene the intensity of the Cotton effect for particular

mixtures is significantly higher than for pure homomeric assembly (*P*)-**1a**$_3$•((R)-2-MePheBAR)$_{12}$.[37]

For example, when a 90:10 mixture of **1a**$_3$•(DEB)$_{12}$ and (*P*)-**1a**$_3$•((R)-2-MePheBAR)$_{12}$ reaches thermodynamic equilibrium, the relative CD intensity has increased from 10% (expected in the case where there is no chiral amplification) to 76%. The nonlinear increase of CD intensity is due to the exchange between the chiral and nonchiral barbiturates within the assemblies, that is to say, to the presence of the heteromeric assemblies **1a**$_3$•((DEB)$_n$(*P*)-**1a**$_3$•((R)-2-MePheBAR)$_{12-n}$) (n=1-11), in which the presence of 1 to 11 chiral centers ((R)-2-MePheBAR) in these assemblies leads to the preferential formation of (*P*)-diastereomer.[38] The addition of BuCYA (1:4 barbiturate:cyanurate) led to a more intense signal in the CD spectrum (Fig. 7.9a), despite the fact the assembly (*P*)-**1a**$_3$•(BuCYA)$_{12}$ no longer contains any chiral center. It can be concluded that the exchange between (R)-2-MePheBAR and BuCYA leads to a quantitative enantioselective formation of assembly (*P*)-**1a**$_3$•(BuCYA)$_{12}$ (0.33 mM) as ^{1}H NMR and CD spectroscopy demonstrated. Plotting the CD intensity for the tetrarosette assembly (*P*)-**1a**$_3$•(BuCYA)$_{12}$ obtained for different ratios of (*P*)-**1a**$_3$•((R)-2-MePheBAR)$_{12}$/**1a**$_3$•(DEB)$_{12}$ as a function of the molecular fraction of the chiral component, it is immediately clear that already when (R)-2-MePheBAR is present only in 50% with respect to DEB, the quantitative formation of the enantiopure assembly (*P*)-**1a**$_3$•(BuCYA)$_{12}$ is obtained (Fig. 7.9c).

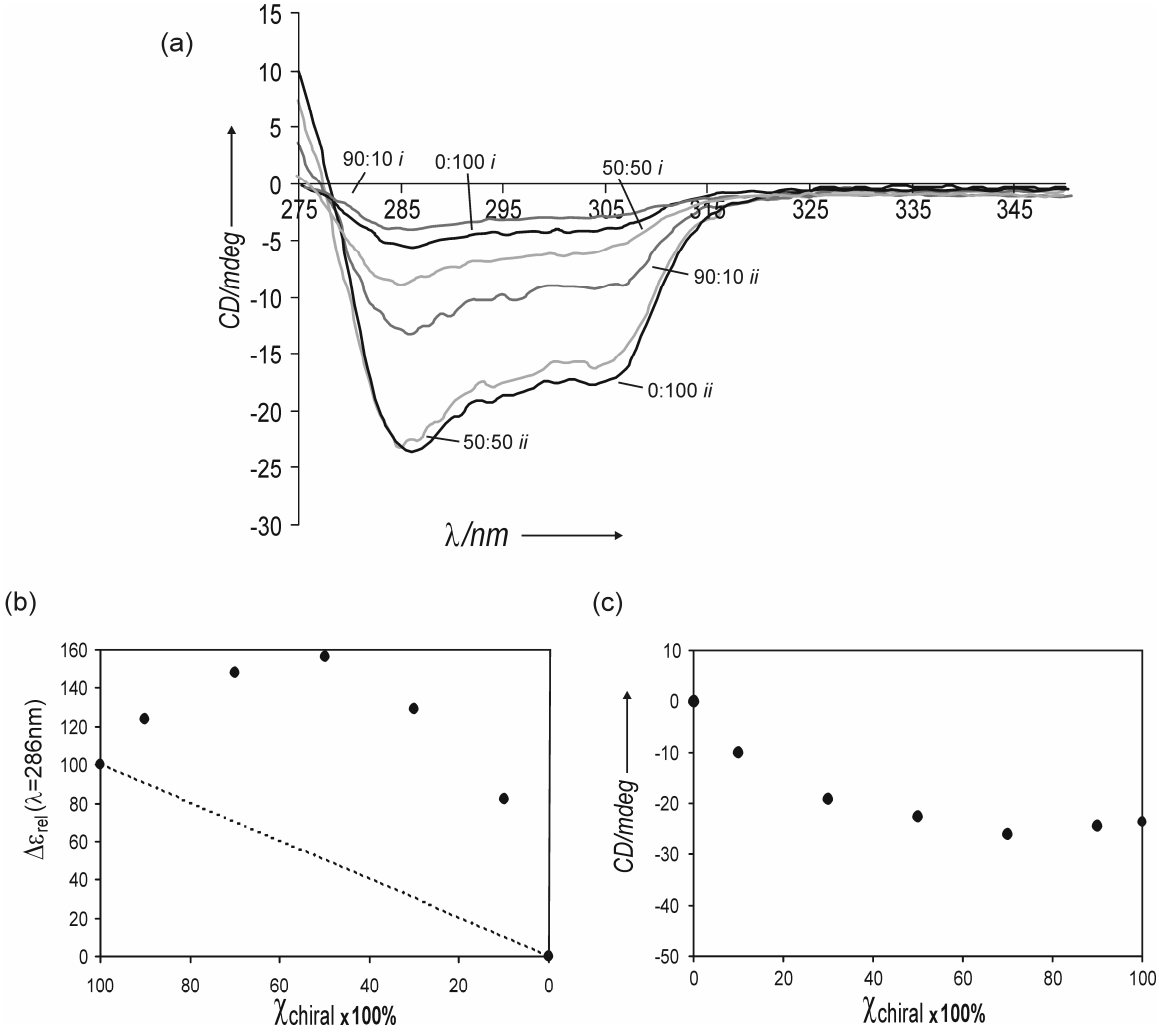

Figure 7.9. *(a) CD spectra of mixtures of (P)-**1a**$_3$•((R)-2-MePheBAR)$_{12}$ and **1a**$_3$•(DEB)$_{12}$ (1:1 **1a**:DEB/(R)-2-MePheBAR) (1.0 mM) before (i) and after (ii) the addition of BuCYA; (b) Plot of the relative CD intensity measured at 286 nm for the mole fraction of chiral assembly (P)-**1a**$_3$•((R)-2-MePheBAR)$_{12}$; (c) Plot of the CD intensity for **1a**$_3$•(BuCYA)$_{12}$ measured at 286 nm versus the mole fraction of chiral assembly (P)-**1a**$_3$•((R)-2-MePheBAR)$_{12}$.*

Thus, it is possible to synthesize enantiopure assemblies using the concept of the amplification of chirality with low concentrations of the catalyst. The concept of a catalytic chaperone is not only valid for the of chiral ((R)-2-MePheBAR) barbiturate but also for the mixtures chiral ((R)-2-MePheBAR) and achiral (DEB) ones, opening new routes to perform reactions by amplifying the chiral information (*asymmetric catalytic noncovalent synthesis*).

7.3. Conclusions

The possible formation of liquid crystalline materials by proper functionalization of barbiturate-based tetrarosette assembly has been investigated. The tetrarosettes do not show any liquid crystalline properties due to dimensions of the tetrarosette (3.0 nm width and 3.0 nm height), which probably do not allow a correct interdigitation of the alkyl chains and the consequent self-organization of these assemblies in the molten state.

The noncovalent synthesis of tetrarosette assemblies by using catalytic chaperones is described. The use of barbiturate derivatives in the formation of cyanurate-based tetrarosette assemblies inhibits (or heals) incorrect interactions between the building blocks (*chaperon*) and enhances the rate of the tetrarosette formation (*catalyst*). Furthermore, the catalyst can be reused as well.

The 'chaperoned' catalytic process displays enantioselectivity when the barbiturate is chiral leading to the formation of the (*P*)-**1a**$_3$•(BuCYA)$_{12}$. By amplification of chirality in the barbiturate-based tetrarosettes, the formation of the enantiopure tetrarosette (*P*)-**1a**$_3$•(BuCYA)$_{12}$ is obtained using substoichiometric amounts of the chiral barbiturates with great implications for further applications in enantioselective noncovalent synthesis. This is the first example in literature of asymmetric catalysis of noncovalent (supramolecular) assemblies.

7.4. Experimental Section

All chemicals were of reagent grade and used without further purification. CH_2Cl_2 was freshly distilled from $CaCl_2$. THF was freshly distilled by Na/benzophenone. NMR spectra were recorded on Varian Unity 300 and 400 (^{1}H NMR 300 MHz and 400 MHz) using tetramethylsilane (TMS) or the corresponding residual solvent as internal standard. MALDI-TOF mass spectra were recorded on a PerSpective Biosystem Voyager-De-RP spectrometer. A 337 nm UV nitrogen laser producing 3 ns pulses was used in the linear and reflection mode. A Perkin-Elmer DSC-7 was used for thermal analysis. CD measurements were conducted on a JASCO J-715 spectropolarimeter. A Perkin-Elmer DSC-7 was used for thermal analysis. DSC measurements were performed on a DSC

Piris Series 7 (scanning rate: 10 °C min^{-1}). A polarizing optical microscope Olympus BH-2 equipped with a Mettler FP82HT hot stage was used for visual observation.

Flash column chromatography was performed using silica gel (SiO_2, E. Merck, 0.040-0.063 mm, 230-240 mesh). All reagents were commercially obtained and used without further purification.

Synthesis. The synthesis of the compounds **2**, **6**, (R)-2-MePheBAR BuCYA and (R)-MePheCYA have been reported previously.[25,26,39]

5-*N*-[4-Amino-6-(3-amino-propylamino)-1,3,5-triazin-2-yl]amino-17-*N*-[4-amino-6-(3-N-Boc-amino-2,2-dimethyl-1,3-propylamino)-1,3,5-triazin-2-yl]amino-25,26,27,28-tetrapropoxycalix[4]arene (3): A solution of di-*tert*-butyl dicarbonate (0.176 g, 0.81 mmol) in THF (63 mL) was added dropwise over 1 hour to a solution of **2** (0.700 g, 0.77 mmol) and DIPEA (0.189 mL, 1.08 mmol) in THF. The reaction mixture was stirred for an additional 60 min and then evaporated to dryness. The residue was redissolved in CH_2Cl_2, washed with NaOH (1 N), H_2O, and brine, and dried over $MgSO_4$. After evaporation of the solvent, the residue was purified by flash column chromatography (SiO_2, 9/1 CH_2Cl_2/CH_3OH-1% NH_4OH) giving **3** as a white solid (310 mg, 38%). ^1H NMR (300 MHz ,$CDCl_3$): δ = 7.48 (br m, 2H, $CH_2\underline{NH}CO$), 7.05 (br m, 8H, CO*o*-ArH + *m*-ArH), 6.17 (br m, 4H, *o*-NHAr), 5.30-4.88 (br, 4H, NH), 4.25 and 3.0 (ABq, 8H, $^2J_{HH}$=12.5 Hz, $ArCH_2Ar$), 3.96 (s m, 4H, $ArO\underline{CH_2}\text{-}CH_2$), 3.644 (s t, 4H, OCH_2), 3.40 (br m, 8H, $NH\underline{CH_2}$ + $O\underline{CH_2}$-CH2), 2.11 (br m, 4H, NH-CH_2-$\underline{CH_2}$-CH_2-NH), 1.9 (s m, 8H, $OCH_2\text{-}\underline{CH_2}$), 1.43 (br, m, 12H, $ArOCH_2\text{-}\underline{CH_2}\text{-}CH_2$), 1.08 (s t, 6H, $OCH_2\text{-}CH_2\text{-}\underline{CH_3}$), 0.87 (s t, 6H, $OCH_2\text{-}CH_2\text{-}\underline{CH_3}$). MS (MALDI-TOF) m/z 1054 (100) ([M + H+], calcd 1055.0). Anal. Calcd for $C_{59}H_{82}O_6N_{14}$: calcd C 65.92, H 7.80, N 17.64; found: C 65.38, H 7.72, N 17.70.

Tetramelamine (4): To a solution of monoBoc-protected dimelamine **3** (189 mg, 0.18 mmol) and DIPEA (70 μL, 0.39 mmol) in CH_2Cl_2 was added instantaneously a solution of 1,4-butyl-bis(*p*-nitrophenyl) dicarbamate (30.7 mg, 0.09 mmol) in CH_2Cl_2, and the reaction was stirred overnight at room temperature. Subsequently, the reaction mixture

was washed with aqueous NaOH (1 N), H_2O, and brine and dried over $MgSO_4$. After removal of the solvent under reduced pressure, the residue was purified by flash column chromatography (SiO_2, CH_2Cl_2/CH_3OH- 1%NH_4OH, 90:10) affording **4** as a white solid (200 mg, 98%). ^{1}H NMR (300 MHz ,$CDCl_3$): δ = 7.4 (br m, 4H, $CH_2\underline{NH}CO$), 7.06 (br m, 16H, CO*o*-ArH + *m*-ArH), 6.17 (br m, 8H, *o*-NHAr), 5.30-4.88 (br, 8H, NH), 4.39 and 3.12 (ABq, 16H, ^2J(H,H)) 13.4 Hz), 4.0-3.9 (s m, 8H, Ar$O\underline{CH_2}$-CH_2), 3.6 (s t, 8H, OCH_2), 3.2 (br m, 16H, $NH\underline{CH_2}$ + $O\underline{CH_2}$-CH_2), 2.11 (br m, 8H, NH-CH_2-$\underline{CH_2}$-CH_2-NH), 1.25 (s, 18H, Boc), 1.05 (t, 12H, ^3J(H,H)= 7.4 Hz), 0.9 (s t, 12H, OCH_2-CH_2-$\underline{CH_3}$) (m, 36H). MS (MALDI-TOF) m/z 2248.0 (100) ([M + 6H+], calcd 2254.0). Anal. Calcd for $C_{124}H_{170}N_{30}O_{14}$•$5CH_3OH$: C 62.99, H 8.05, N 16.44; found: C 62.77, H 7.38, N 16.30

Tetramelamine (5): To a solution of tetramelamine **4** (364 mg, 0.16 mmol) in CH_2Cl_2 TFA was added dropwise (7.24 mL, 100.0 mmol), and the reaction was stirred overnight at room temperature. After removal of the solvent under reduced pressure, the residue was precipitated with ether. The filtrate was washed with ether in order to remove the TFA. The product was used without any further purification. ^{1}H NMR (300 MHz, $CDCl_3$): δ = 7.4 (br m, 4H, $CH_2\underline{NH}CO$), 7.06 (br m, 16H, CO*o*-ArH + *m*-ArH), 6.17 (br m, 8H, *o*-NHAr), 5.30-4.88 (br, 8H, NH), 4.39 and 3.12 (ABq, 16H, ^2J(H,H)) 13.4 Hz), 4.0-3.9 (s m, 8H, Ar$O\underline{CH_2}$-CH_2), 3.6 (s t, 8H, OCH_2), 3.2 (br m, 16H, $NH\underline{CH_2}$ + $O\underline{CH_2}$-CH_2), 2.11 (br m, 8H, NH-CH_2-$\underline{CH_2}$-CH_2-NH), 1.05 (t, 12H, ^3J(H,H)= 7.4 Hz), 0.9 (s t, 12H, OCH_2-CH_2-$\underline{CH_3}$) (m, 36H). MS (MALDI-TOF) m/z 2249.0 (100) ([M + 3H+], calcd 2252.0). Anal. Calcd for $C_{110}H_{148}N_{30}O_{10}$: C 64.43, H 7.27, N 20.49; found: C 64.77, H 7.31, N 20.30;

Tetramelamine (1b): A solution of **6** (230 mg, 0.26 mmol), HBTU (100 mg, 0.26 mmol), DIPEA (0.19 mL, 0.49 mmol) and **5** (230 mg, 0.19 mmol) in CH_2Cl_2 / DMF ratio 4:1 was stirred overnight at room temperature. The solvent was evaporated and the crude residue was solubilized again in CH_2Cl_2. MeOH was added till complete precipitation. The precipitate was filtered off and purified by column chromatography ($CHCl_3$:MeOH:AcOEt = 95:4:1). **1b** was crystallized by $CHCl_3$/MeOH to give a white powder (60%). ^{1}H NMR (300 MHz, $CDCl_3$, 298K) δ=7.48 (br m, 4H, $CH_2\underline{NH}CO$), 7.05

(br m, 16H, CO*o*-ArH + *m*-ArH), 6.85 (br m, 4H, *o*-ArH), 6.17 (br m, 8H, *o*-NHAr), 5.30-4.88 (br, 8H, NH), 4.41 and 3.10 (ABq, 16H, $^2J_{HH}$=12.5 Hz, $ArCH_2Ar$), 3.96 (s m, 32H, OCH_2+$NHCH_2$ + $ArO\underline{CH_2}\text{-}CH_2$), 3.644 (s t, 8H, OCH_2), 3.40 (br m, 16H, $NH\underline{CH_2}$ + $O\underline{CH_2}\text{-}CH_2$), 2.11 (br m, 8H, $NH\text{-}CH_2\text{-}\underline{CH_2}\text{-}CH_2\text{-}NH$), 1.9 (s m, 16H, $OCH_2\text{-}\underline{CH_2}$), 1.43 (br, m, 24H, $ArOCH_2\text{-}\underline{CH_2}\text{-}CH_2$), 1.25 (s m, 90H, $ArOCH_2\text{-}CH_2\text{-}(\underline{CH_2})_{15}\text{-}CH_3$), 1.08 (s t, 12H, $OCH_2\text{-}CH_2\text{-}\underline{CH_3}$), 0.87 (s t, 36H, $ArOCH_2\text{-}CH_2\text{-}(CH_2)_{15}\text{-}\underline{CH_3}$ + $OCH_2\text{-}CH_2\text{-}\underline{CH_3}$). MS (MALDI-TOF): m/z 3866.91 (100) ([$M+H^+$] 3870, Elemental Analysis calcd (%) for $C_{232}H_{372}N_{30}O_{18}\bullet 5CH_3OH$: C, 70.64; H, 9.80; N, 10.43; found: C, 70.54; H, 9,72; N,

Preparation of tetramelamine 1a, barbiturate and cyanurate solutions for the ^{1}H NMR measurements. The solutions of DEB and (R)-MePheCYA were obtained after sonicating at elevated temperatures in toluene-d_8. The tetramelamine **1a** was dissolved at room temperature in toluene-d_8. Typically, 300 μL of a 5.0 mM solution of DEB in toluene-d_8 and 500 μL of a 24.0 mM solution of (R)-MePheCYA were added to 200 μL of 15 mM solution of tetramelamine **1a**. ^{1}H NMR measurements were started as soon as possible after mixing.

7.5 References and Notes

[1] M. L. Bushey, T. Q. Nguyen, W. Zhang, D. Horoszewski, C. Nuckolls, *Angew. Chem. Int. Ed.* **2004**, *43*, 5446-5453.

[2] G. M. Whitesides, B. Grzybowski, *Science* **2002**, *295*, 2418-2421.

[3] Y. N. Xia, G. M. Whitesides, *Annu. Rev. Mater. Sci.* **1998**, *28*, 153-184.

[4] J.-M. Lehn, *Supramolecular Chemistry, Concepts and Perspectives*, VCH, Weinheim, Germany, **1995**.

[5] D. N. Reinhoudt, M. Crego-Calama, *Science* **2002**, *295*, 2403-2407.

[6] J. T. Davis, M. S. Kaucher, F. W. Kotch, M. A. Iezzi, B. C. Clover, K. M. Mullaugh, *Org. Lett.* **2004**, *6*, 4265-4268.

[7] V. Paraschiv, M. Crego-Calama, T. Ishi-i, C. J. Padberg, P. Timmerman, D. N. Reinhoudt, *J. Am. Chem. Soc.* **2002**, *124*, 7638-7639.

[8] H. L. Anderson, J. K. M. Sanders, *Angew. Chem. Int. Ed.* **1990**, *29*, 1400-1403.

[9] Y. Tokunaga, D. M. Rudkevich, J. Santamaria, G. Hilmersson, J. J. Rebek, *Chem. Eur. J.* **1998**, *4*, 1449-1457.

[10] S. Anderson, H. L. Anderson, J. K. M. Sanders, *Acc. Chem. Res.* **1993**, *26*, 469-475.

[11] M. M. Conn, E. A. Wintner, J. J. Rebek, *Angew. Chem. Int. Ed.* **1994**, *33*, 1577-1579.

[12] D. H. Lee, J. R. Granja, J. A. Martinez, K. Severin, M. R. Ghadiri, *Nature* **1996**, *382*, 525-528.

[13] A. Luther, R. Brandsch, G. von Kiedrowski, *Nature* **1998**, *396*, 245-248.

[14] F. Hof, S. L. Craig, C. Nuckolls, J. J. Rebek, *Angew. Chem. Int. Ed.* **2002**, *41*, 1488-1508.

[15] L. Davidson, W. Hayes, *Curr. Org. Chem.* **2002**, *6*, 265-281.

[16] R. L. E. Furlan, S. Otto, J. K. M. Sanders, *Proc. Natl. Acad. Sci. U. S. A.* **2002**, *99*, 4801-4804.

[17] M. Crego-Calama, P. Timmerman, D. N. Reinhoudt, *Angew. Chem. Int. Ed.* **2000**, *39*, 755-758.

[18] R. J. Ellis, S. M. Vandervies, *Annu. Rev. Biochem.* **1991**, *60*, 321-347.

[19] J. M. C. A. Kerckhoffs, M. G. J. ten Cate, M. A. Mateos-Timoneda, F. W. B. van Leeuwen, B. Snellink-Ruël, A. L. Spek, H. Kooijman, M. Crego-Calama, D. N. Reinhoudt, *J. Am. Chem. Soc.* **2005**, *127*, 12697-12708.

[20] K. A. Jolliffe, P. Timmerman, D. N. Reinhoudt, *Angew. Chem. Int. Ed.* **1999**, *38*, 933-937.

[21] M. A. Mateos-Timoneda, J. M. C. A. Kerckhoffs, D. N. Reinhoudt, M. Crego-Calama, *Org. Biomol. Chem.* **2007**, *5*, 447-449.

[22] K. A. Jolliffe, M. Crego-Calama, R. Fokkens, N. M. M. Nibbering, P. Timmerman, D. N. Reinhoudt, *Angew. Chem. Int. Ed.* **1998**, *37*, 1247-1251.

[23] P. Timmerman, K. A. Jolliffe, M. Crego-Calama, J. L. Weidmann, L. J. Prins, F. Cardullo, B. H. M. Snellink-Ruel, R. H. Fokkens, N. M. M. Nibbering, S. Shinkai, D. N. Reinhoudt, *Chem. Eur. J.* **2000**, *6*, 4104-4115.

[24] T. Kato, N. Mizoshita, K. Kishimoto, *Angew. Chem. Int. Ed.* **2006**, *45*, 38-68.

[25] J. M. C. A. Kerckhoffs, M. Crego-Calama, I. Luyten, P. Timmerman, D. N. Reinhoudt, *Org. Lett.* **2000**, *2*, 4121-4124.

[26] L. J. Prins, R. Hulst, P. Timmerman, D. N. Reinhoudt, *Chem. Eur. J.* **2002**, *8*, 2288-2301.

[27] H. Schönherr, M. Crego-Calama, G. J. Vancso, D. N. Reinhoudt, *Adv. Mater.* **2004**, *16*, 1416-1420.

[28] H. Schönherr, V. Paraschiv, S. Zapotoczny, M. Crego-Calama, P. Timmerman, C. W. Frank, G. J. Vancso, D. N. Reinhoudt, *Proc. Natl. Acad. Sci. U. S. A.* **2002**, *99*, 5024-5027.

[29] D. Demus, J. W. Goodby, G. W. Gray, H. W. Spiess, V. Vill*, Handbook of Liquid Crystals*, VCH, Chichester, **1998**.

[30] A. Piermattei, M. Giesbers, A. T. M. Marcelis, E. Mendes, S. J. Picken, M. Crego-Calama, D. N. Reinhoudt, *Angew. Chem. Int. Ed.* **2006**, *45*, 7543–7546.

[31] H. J. van Manen, V. Paraschiv, J. J. Garcia-Lopez, H. Schönherr, S. Zapotoczny, G. J. Vancso, M. Crego-Calama, D. N. Reinhoudt, *Nano Lett.* **2004**, *4*, 441-446.

[32] A. G. Bielejewska, C. E. Marjo, L. J. Prins, P. Timmerman, F. de Jong, D. N. Reinhoudt, *J. Am. Chem. Soc.* **2001**, *123*, 7518-7533.

[33] In the absence of any source of chirality, the tetrarosette assemblies exists as a mixture of enantiomers ((*P*)- and (*M*)-enantiomers) due to the staggered orientation of the different melamine rings. However, the presence chiral centers in one of the building blocks of the assembly such as (R)-MePheCYA, leads to the formation of only one of the two possible diastereomers. Therefore, the assembly (*P*)-1a_3•((R)-MePheCYA)$_{12}$ is highly circular dichroism (CD) active.

[34] B. L. Feringa, R. A. van Delden, *Angew. Chem. Int. Ed.* **1999**, *38*, 3419-3438.

[35] Heteromeric assembly are defined as assemblies where one of the two building blocks i.e. barbiturate is present in the assembly with different functional groups, while homomeric assemblies present only one type of barbiturate.

[36] L. J. Prins, J. Huskens, F. de Jong, P. Timmerman, D. N. Reinhoudt, *Nature* **1999**, *398*, 498-502.

[37] The stronger Cotton effect of the mixtures suggests that for all the assemblies after mixing the $\Delta\varepsilon_\lambda$ (CD intensity at wavelength of maximum absorbance) is not the same as it was assumed for previous studies on these assemblies.

[38] L. J. Prins, P. Timmerman, D. N. Reinhoudt, *J. Am. Chem. Soc.* **2001**, *123*, 10153-10163.

[39] V. Percec, C. H. Ahn, T. K. Bera, G. Ungar, D. J. P. Yeardley, *Chem. Eur. J.* **1999**, *5*, 1070-1083.

Summary

In this thesis different aspects of functional hydrogen-bonded (double and tetrarosette) assemblies are described. The functions were inspired by naturally occurring phenomena such as self-organization, supramolecular chirality, and the correct folding of proteins. The studies presented in this thesis are focused on the synthesis of supramolecular materials by these noncovalent assemblies. The emphasis is on liquid crystals (and gels), which are able to interact with the environment and adapt to it.

Double and tetrarosette assemblies are formed upon mixing calix[4]arene dimelamines and calix[4]arene tetramelamines in apolar solvents with barbiturate and cyanurate derivatives in a 1:2 and 1:4 ratio, respectively. The assembly process is driven by the formation of 36 (double rosette) or 72 (tetrarosette) hydrogen bonds between the complementary hydrogen bonding arrays of different building blocks, leading to assemblies with high thermodynamic stability.

Chapter 2 reviews hydrogen-bonded liquid crystalline materials that have been described in the literature in the past decades. The concepts and the principles for the formation of these materials are discussed, and examples are given that illustrate the control over these systems.

Chapter 3 describes the formation of liquid crystalline materials by hydrogen-bonded double rosettes achieved by the functionalization of the melamine units of the calix[4]arene with octadecyl chains. The liquid crystalline phases of these assemblies have been determined by polarized optical microscopy (POM), differential scanning calorimetry (DSC) and X-ray diffraction (XRD). The double rosette assemblies organized in columnar fashion in the liquid crystalline phase, showing a remarkable thermal stability considering their non-covalent nature. Furthermore, the strength of the hydrogen bonds and the spatial disposition of the side groups of the barbituric and cyanuric derivatives are crucial factors for the stability of the mesophases.

In Chapter 4 the supramolecular chirality of mesogenic double rosette assemblies in solution and the liquid crystalline state is described. The bulkiness and the position of the chiral group of the barbiturate and cyanurate building blocks play an important role in the formation of double rosette assemblies and the liquid crystalline phases. The chirality of the double rosettes in solution was transferred to the liquid crystalline state, as demonstrated by circular dichroism measurements. In the mesophase different arrangements and orientation of the columns along the stacking direction have been obtained depending on the nature of the building blocks of the assembly. Formation of a gel phase is described for these chiral double rosettes in n-alkane solvents.

Chapter 5 describes the complexation of a molecular guest (alizarin) by mesogenic chiral self-assembled double rosettes in solution and in the liquid crystalline state. Alizarin was encapsulated in barbiturate-based assemblies and intercalated between cyanurate-based assemblies. In solution, the presence of aggregates is a necessary requirement for the intercalation of alizarin molecules between the double rosette floors as confirmed by ^{1}H NMR DOSY, UV-Vis and CD experiments. In the liquid crystalline state, the alizarin complexation by the double rosettes led to highly stable mesophases. In case of barbiturate-based assemblies, the complexation did not alter the type of phase, while for cyanurate-based assemblies the complexation led to the formation of a crystalline phase. Furthermore, the in-situ exchange of building blocks in the liquid crystalline state led to the modulation of the optical activity in these assemblies.

In Chapter 6, the investigation by AFM and STM of the supramolecular organization of mesogenic double rosettes on surfaces is described. The self-organization of these assemblies on highly ordered pyrolytic graphite (HOPG) depends on the concentration and polarity of the solvent. For example, the double rosette organization on HOPG went from 1D (fibers) to 2D (hexagonal columnar lattice) order by decreasing the concentration. Furthermore, the presence of double rosette aggregates in solution at low concentration (25 μM) leads to the formation of micrometer-long ordered structures on graphite. The chirality in the double rosettes allowed the organization of these assemblies in ordered structures when deposited onto mica. Moreover, STM measurements allowed the visualization of individual mesogenic double rosette on HOPG.

In Chapter 7 the noncovalent synthesis of cyanurate-based tetrarosettes, in which barbiturate derivatives were employed as a catalytic chaperone, is described. In the noncovalent synthesis of tetrarosette assemblies, the barbiturate acts simultaneously as chaperone inhibiting the formation of kinetically stable ill-defined assemblies and as catalyst accelerating the formation reaction. Furthermore, the enantioselective synthesis of cyanurate-based tetrarosette assemblies was achieved via amplification of chirality by using substoichiometric amounts of chiral barbiturates as a chaperone. Moreover the synthesis of barbiturate-based tetrarosette assemblies have been performed and their liquid crystalline behavior have been studied after the proper functionalization of tetramelamine calix[4]arene with octadecyl chains.

The results presented in this thesis illustrate the ability of well-defined nanometer-size self-assembled structures to form supramolecular materials. The noncovalent nature of the assemblies allows to obtain different materials properties by the simple replacement of one building block with another leading toward the synthesis of responsive materials.

Samenvatting

In dit proefschrift zijn verschillende aspecten van functionele waterstofgebrugde (dubbele en tetrarozet) assemblages beschreven. De functies zijn geïnspireerd op in de natuur voorkomende fenomenen als zelforganisatie, supramoleculaire chiraliteit, en de juiste vouwing van eiwitten. De in dit proefschrift beschreven studies zijn gefocusseerd op de synthese van supramoleculaire materialen door deze niet-covalente assemblages. De nadruk ligt op vloeibare kristallen (en gels), die in staat zijn met hun omgeving interactie te hebben en zich daaraan aan te passen.

Dubbele en tetrarozet assemblages worden gemaakt door calix[4]areen dimelamines en calix[4]areen tetramelamines in apolaire oplosmiddelen te mengen met barbituraten and cyanuraten, in, respectievelijk, een 1:2 en 1:4 verhouding. Het assemblageproces wordt gedreven door de vorming van 36 (dubbele rozet) of 72 (tetrarozet) waterstofbruggen tussen de complementaire waterstofbrug eenheden van verschillende bouwstenen, resulterend in assemblages van thermodynamisch hoge stabiliteit.

Hoofdstuk 2 geeft een overzicht van waterstofgebrugde vloeibaar-kristallÿne materialen die in de afgelopen decennia in de literatuur zijn beschreven. De concepten en principes voor de vorming van deze materialen worden bediscussieerd en er zijn voorbeelden gegeven die de controle over dit soort systemen illustreert.

Hoofdstuk 3 beschrijft de vorming van vloeibaar- kristallÿne materialen door waterstofgebrugde dubbele rozet, verkregen door het functionaliseren van de melamine eenheden van de calix[4]areen met octadecyl alkylketens. De vloeibaar- kristallÿne fase van deze assemblages is gekarakteriseerd met gepolariseerde optische microscopie (POM), differentiële scanning calorimetrie (DSC) en röntgenstraling diffractie (XRD). De dubbele rozet assemblages organiseren zich in kolomachtige structuren in de vloeibaar-kristallijne fase, daarbij een, gezien het niet-covalente karakter, opmerkelijke temperatuur stabiliteit tonend. De kracht van de waterstofbruggen en de ruimtelijke positionering van de zijgroepen van de barbituraten en cyanuraten zijn cruciale factoren in de stabiliteit van de mesofases.

In Hoofdstuk 4 is de de supramoleculaire chiraliteit van de mesogene dubbele rozet structuren in oplossing en in de vloeibaar-kristallijne fase beschreven. De grootte en de positie van de chirale groepen van de barbituraat en cyanuraat bouwstenen speelt een belangrijke rol in de vorming van dubbele rozet structuren en de vloeibaar-kristallijne fase. De chiraliteit van de dubbele rozet in oplossing wordt overgebracht op de vloeibaar-kristallijne fase, bewezen met circulair dichroisme metingen. In de mesofase worden verschillende oriëntaties van de kolommen langs de “stacking”-richting verkregen, afhankelijk van het type bouwsteen dat voor de structuur is gebruikt. Vorming van een gelfase van deze chirale dubbele rozetten in n-alkaan oplosmiddelen wordt ook beschreven.

Hoofdstuk 5 beschrijft het binden van een moleculaire gast (alizarine) door een mesogeen chiraal zelfassemblerend dubbele rozet, in oplossing en in de vloeibaar-kristallijne toestand. De alizarines word gekomplexeerd op barbituraat gevormde structuren en voegen zich daarentegen tussen de rozet eenheden in de op cyanuraat gebaseerde structuren. De aanwezigheid van aggregaten is in oplossing een noodzakelijke vereiste voor de “intercalerende” interactie van alizarine tussen de dubbele rozet vloerdelen, zoals is geconcludeerd aan de hand van 1H NMR DOSY, UV-Vis en CD experimenten. In de vloeibaar-kristallijne fase leidt het binden van de alizarine tot zeer stabiele mesofases. In het geval van de op barbituraat gebaseerde structuren leidt de binding niet tot een verandering van fase, terwijl in het geval van de cyanuraat structuren de binding van alizarine leidt tot de vorming van een kristallijne fase. De *in situ* vervanging van bouwstenen in de vloeibaar-kristallijne toestand leidt tot verandering van de optische activiteit van de structuren.

In Hoofdstuk 6 is de bestudering van de supramoleculaire interactie van mesogene dubbele rozetten met behulp van AFM en STM beschreven. De zelforganisatie van deze structuren op sterk-geordend pyrolitisch grafiet (highly ordered pyrolytic graphite, HOPG) hangt af van de concentratie en van de polariteit van het oplosmiddel. De dubbel rozet organisatie op HOPG gaat bijvoorbeeld van 1D (fibers) naar 2D (hexagonaal kolomachtig rooster) bij afname van de concentratie. De aanwezigheid van dubbel rozet aggregaten in oplossing bij lage concentratie (25 μM) leid tot de vorming van micrometerlange geordende structuren op grafiet. De chiraliteit van de dubbele rozetten

geeft de mogelijkheid om de geordende structuren op het oppervlak van mica te verkrijgen. Met STM is het bovendien mogelijk om individuele mesogene rozetten op de HOPG te visualiseren.

In Hoofdstuk 7 is de niet-covalente synthese van op cyanuraat gebaseerde tetrarozetten beschreven, waarbij barbituraten werden gebruikt als katalytische chaperonnes. In de niet-covalente synthese van tetrarozet structuren functioneert barbituraat zowel als chaperonne, de vorming van foutgedefinieerde structuren voorkomend, en als katalysator, de reactie versnellend. De enantioselectieve synthese van op cyanuraat gebaseerde rozetten is gelukt door versterking van de chiraliteit, gebruikmakend van subequivalente hoeveelheden chirale barbituraat als chaperonne. Verder is ook de synthese van op barbituraat gebaseerde tetrarozetten uitgevoerd en hun vloeibaar-kristallijne gedrag bestudeerd na het benodigde functionaliseren van tetramelamine calix[4]areen met octadecanyl ketens.

Thanks

I really cannot believe that I writing these words, means that I have finished my PhD in Twente. It's a really weird feeling because you know that it's time to leave but also you know that you will miss a lot both under scientifically and personally. As tradition, it's time to thank everybody who has shared these four years with me.

First, I would like to express my gratitude and appreciation to my promotor Prof. David N. Reinhoudt. Thanks David for the opportunity you gave me to be a member of SMCT. Although we have had some friction at the beginning of my PhD, I really appreciate the freedom that you gave me, without that I would not have been able to finish this work. Bedankt voor alles David.

I have to thank my supervisor Mercedes Crego Calama for all the help in these four years and above all when she left me (☹) for the new job. I'm your last PhD and I think you will never forget me after my wonderful speech (Thank you!! Thank you!!) when you left! You gave me a lot of freedom and you supported me during the bad moments. Of course we had some tension and you tried to kill me several times but in the end you have always been there when I needed you. Merce, you were right, we made it!!!

I have to thank some people in Italy, without whom I would never start this adventure, Prof. Paolo Mencarelli Prof. Giancarlo Doddi and Prof. Luigi Mandolini. Grazie mille, mi avete insegnato a lavorare come stare in laboratorio ed essere sempre critico sui risultati che si ottengono. Prof. Mandolini grazie ancora di aver fatto quella telefonata.

During these fours years I had the chance to collaborate with many people. I owe my appreciation to Prof. Flemming Besenbacher and Dr. Mindong Dong from the Interdisciplinary Nanoscience Center (iNANO) at Aarhus University for the STM images. I would like to thank Dr. Eduardo Mendes form Delft University for assisting me with the XRD machine. Mária Péter for her AFM contribution at Chapter 6, the AFM images were always perfect!! I would like to thank Aldrik Velders for helping me with

the NMR machine and for a lot more. Grazie tanto tecnico Aldrik, veramente perché mi hai aiutato tantissimo in tutto anche quando non era tuo il compito. I would like to thank Clemens Padberg for helping with the DSC machine and the optical microscope. Arianna Friggeri, Kjeld van Bommel Davide and Ben Feringa from Groningen University for the great help with the gels in Chapter 4. I have special thanks for the ‘rosette team”. Michel, I cannot say how much I owe you for all the help with the rosette, from the synthesis to the measurements with the CD, thanks to you Chapter 7 is done!! Mattijs, you were right in the end I finished thanks for your tips. I would like to thank all my lab mates during this years, Manon, Henk, Mirko, Juanjio, Marta, Hans, Albert, Xing-Yi, Pinguin, Amela, Dominik, Martine, Moira, Shu Han, Elisabetta, Carmela & Carmela, Laura, Cheng-Chin, Fijs (my favorite mariquita) and I am sorry if I forgot someone.

Thanks also to Marcel de Bruine (Marcelito) for the technical support, everything that I needed you found for me! Richard Egberink for the computer assistance, I will always remember your calling to Acer when my laptop went down. Tieme Stevens (now you can say that I don’t belong anymore to the SMCT) for the help with MS and NMR. I thank Carla, Marieke Slotman and Izabel Katalanc for helping me any time when I needed some administration paper work.

I want to thank Jurriaan, Michel, In Yee and Aldrik for reading and correcting my concept thesis, I hope that you liked it and was it so bad in the end?! Thanks to Aldrik for translating the summary into samenvatting.

Writing a thesis is really stressful process but I was lucky because in room 1717 I had the best mates ever: Christian, I have been so impressed with your order that I still have nightmares! Fernando (Paris is always Paris…), Kim (Christian’s follower), Manon (Christian’s nightmare), Henk (life is like a circle..)

During these years in Enschede, I have met a lot of fantastic people, inside and outside SMCT. Special thanks to those who made my stay in the Netherlands unforgettable, I will remember you for all my life! Juanjio (and Floren) without your spanish lessons I would have never conquered Olga! Mattijs, the octopus, my house is

always open for you. Roberto, the ski weeks were unforgettable! Soco (my dance mate) and Rob (my conga mate) thanks for the fantastic nights in the Three Widows. Xing-Yi and In Yee, I will always remember your Christmas song at my place in Italy! Deborah, grazie per aver portato in Italia il famoso anello! Huib and Rachel, I really loved that day at the mall in Roermond, although I think that Olga enjoyed it more! Thanks to Andrea (vedi di fare il bravo sennò...), Manon (I don't know what to do with myself!), MengLing, Dominiek (the bomb), Albert (trombetta), Alberto, Hans (bierje? I missed you during the borrels), Ignacio, Martine (or Martini), Victoria , Ana (¿que pasa?), Roald (my German friend ☺), Ombretta, Fabio, Francesca (ricorda l'ultimo anno è quello buono!!), Marco, Becky ("I cannot belive it!!!"), Fischer (Becky's cat for its nice present on my jeans☹), Steffen, Itxaro (tu italiano es mejor que mi castellano, seguro..), Alart, Ruben, Cheng-Ching, Riccardo (Riccardino, per gli amici), Laura, Francesca Romana, Cristiano, Charu, La Corbe, La Reinoso, Jurrien (unforgettable flatmate), Kim (thanks your our Aussie lessons), Yanina (and her Caffrey's), Edi e Francesca, Dennis, Janet, Siggi (your cooking was always perfect!), Monique, Oya, Frederik, Richard (Lipperkerkstraat is not the same anymore without you..), Irene (un pranzo 15 piccolissime tapperwears, come si fa!!), l'amica della Reinoso, Shanga, Stinky...I am sure I forgot somebody...

My staying in Enschede would not have been so nice without the Thursday's nights at the Beiaard and il suo famoso "zoccolo duro": Fernado, Lourdes, Olga, Barbara ('te metterei in galera!), Michel, Marina, Bassy (your appetite is unbelievable☺), zia Monica ("bello della zia!", ti chiedo scusa per tutte le volte che ho stancato con i miei discorsi interminabili), Smilio (you have to train more in bending your arm…), Bart Jan (Nino would like to have a glass of water!).

I really loved being here in the Netherlands, although I have complained about the weather, but to Dutch this is a national sport, I found many friends: Michelino, you are like a brother to me when I needed you where always there in my private and work life, muchissima gracias, Marina, tu parli italiano ma anche io posso parlare argentino…"poscio", "plascia", "pisciama"!!! Mirko, Resident Evil 4 rimarrà nella storia di Enschede ma sopratttutto ricordati chi la dura la vince guarda me!! Lourdes, you are a segunda ermana para mí because you have been in all import things of my life here even

in those that you have not realized…☺. Fer, ermano español, I enjoyed your friendship some much that no tengo palabras para expresarlo. La cenas en casa riédonos de todo, lo mejor…Lo mismo que tú con mi familia, yo me siento tambien como si fuera uno de vosotros!! Henk and Marloes, my dutch friends, my personal translators dutch-english, I enjoyed all the moments spent together, overall the parties!!! Zio Tommaso (and Jeanette), sei un calamaro gigante ma anche un grande amico, grazie di tutto.

Michel and Fernando thank you for being my paranimfen. You have been with me throughout these four years that I owe you those 45 min in front of people looking not really clever!!!

In Italy, I have some special friends that I want to thanks because every time I came back, it was like we had never separated. Ciaks, Nevo, Bag, Claudietta, Cristiano, Costa, Paoletta, Massimo, Daniela. Mi avete fatto passare gl'anni dell'uni nel migliore dei modi, grazie tanto.

Papà, mamma, Paolo, Mauro, Alessia grazie per avermi sempre appoggiato anche quando non eravate completamente d'accordo. La scelta di venire è stata sofferta ma soprattutto per te, mamma, è stata scioccante, ma hai visto c'è l'ho fatta a finire. Anche se per alcuni possiamo essere visti come uan famiglia un pò strana, siamo una famiglia e la più bella che ci sia. Vi voglio bene.

Olga, amore mio, lo eres todo para mí. Me has ayudado, apoyado, y siempre me has dado un empujoncito cuando lo necesitaba durante los momentos más difíciles. Tu "energía" me ha dado fuerzas y coraje para llegar hasta el final de esta tesis. Siempre has estado a mi lado, gracias.Tú y yo, juntos, formamos una nueva familia, la nuesta. T'estimo.

Alessio

About the Author

Alessio Piermattei was born in Rome, Italy, on November 05, 1974. He studied chemistry at the University of Rome “La Sapienza” in Rome where he received his degree in February 2002. During his undergraduate training period he worked on template effect on the formation of rotaxane molecules. The work, that was carried out at the Dipartimento di Chimica and IMC-CNR Sezione Meccanismi di Reazione, group of Prof. P. Mencarelli at the University of Rome “La Sapienza”, Italy, resulted in the thesis “Template Effect in the Formation of a Cyclophane containing Bipyridinium Units”. Since October 2002 he joined the Supramolecular Chemistry and Technology Group of Prof. Reinhoudt at the University of Twente, The Netherlands, as PhD candidate. The results of his research are described in this thesis.